

FROM SUPRAMOLECULAR SELECTIVITY TO NANOCAPSULES

by

PRASHANT D. CHOPADE

B. Tech., University of Mumbai. 2005.

AN ABSTRACT OF A DISSERTATION

submitted in partial fulfillment of the requirements for the degree

DOCTOR OF PHILOSOPHY

Department of Chemistry
College of Arts and Sciences

KANSAS STATE UNIVERSITY
Manhattan, Kansas

2012

Abstract

A family of three 2-aminopyrazine derivatives were prepared and co-crystallized with thirty carboxylic acids. Our theoretical charge calculations and experimental results from 90 reactions demonstrated that decreasing the charge on the hydrogen-bond acceptor sites results in a decrease of the *supramolecular yield* (the frequency of occurrence of the desired outcome). However, *synthon crossover* (undesired connectivity) was observed 7/12 times and was unavoidable due to competitive binding sites present in the N-heterocyclic bases chosen.

To avoid synthon crossover, we used a strategy based on *geometric bias*. We utilized hydrogen-bonding two-point contacts and halogen-bonding single-point contacts for supramolecular reactions with the 2-aminopyrazine family of compounds. The desired two-point contact and single-point contact (N \cdots I or N \cdots Br) appeared in 9/9 times even in the presence of other potentially interfering intermolecular interactions. In addition, the role of charge in controlling the presence/absence of proton transfer was also highlighted.

To establish a hierarchy in halogen-bonding interactions we designed and synthesized a library of eight molecules equipped with two different halogen bond donors and combined with variety of halogen-bond acceptors. 11 Halogen-bonded co-crystals were obtained; however, positional disorder of I/Br atoms obscures a complete analysis. This problem was solved by introducing asymmetry in the halogen-bond donor molecules. Finally, successfully demonstrated an unprecedented hierarchy in halogen-bond interactions based on electrostatics.

We developed high-yielding Suzuki-Miyaura coupling reactions of tetraboronic pinacolyl ester cavitand to iodoarenes with a range of functional groups (electron withdrawing/donating group and a heterocycle) that show robustness and versatility, making it a 'launch pad' for the synthesis of many new cavitands in a facile manner. We have also successfully demonstrated cavitand functionalization from tetraaldehyde to tetraoximes using 'solvent assisted grinding', irrespective of the position of the aldehyde.

Finally, we prepared tetra-substituted pyridyl and carboxylic acid cavitands having an ellipsoidal cavity capable of encapsulating asymmetric guest molecules and was subsequently obtained the first of its kind, C_{2v} symmetric molecular capsule with encapsulated asymmetric guest molecule.

FROM SUPRAMOLECULAR SELECTIVITY TO NANOCAPSULES

by

PRASHANT D. CHOPADE

B. Tech., University of Mumbai. 2005.

A DISSERTATION

submitted in partial fulfillment of the requirements for the degree

DOCTOR OF PHILOSOPHY

Department of Chemistry
College of Arts and Sciences

KANSAS STATE UNIVERSITY
Manhattan, Kansas

2012

Approved by:

Major Professor
Prof. Christer B. Aakeröy

Abstract

A family of three 2-aminopyrazine derivatives were prepared and co-crystallized with thirty carboxylic acids. Our theoretical charge calculations and experimental results from 90 reactions demonstrated that decreasing the charge on the hydrogen-bond acceptor sites results in a decrease of the *supramolecular yield* (the frequency of occurrence of the desired outcome). However, *synthon crossover* (undesired connectivity) was observed 7/12 times and was unavoidable due to competitive binding sites present in the N-heterocyclic bases chosen.

To avoid synthon crossover, we used a strategy based on *geometric bias*. We utilized hydrogen-bonding two-point contacts and halogen-bonding single-point contacts for supramolecular reactions with the 2-aminopyrazine family of compounds. The desired two-point contact and single-point contact (N \cdots I or N \cdots Br) appeared in 9/9 times even in the presence of other potentially interfering intermolecular interactions. In addition, the role of charge in controlling the presence/absence of proton transfer was also highlighted.

To establish a hierarchy in halogen-bonding interactions we designed and synthesized a library of eight molecules equipped with two different halogen bond donors and combined with variety of halogen-bond acceptors. 11 Halogen-bonded co-crystals were obtained; however, positional disorder of I/Br atoms obscures a complete analysis. This problem was solved by introducing asymmetry in the halogen-bond donor molecules. Finally, successfully demonstrated an unprecedented hierarchy in halogen-bond interactions based on electrostatics.

We developed high-yielding Suzuki-Miyaura coupling reactions of tetraboronic pinacolyl ester cavitand to iodoarenes with a range of functional groups (electron withdrawing/donating group and a heterocycle) that show robustness and versatility, making it a 'launch pad' for the synthesis of many new cavitands in a facile manner. We have also successfully demonstrated cavitand functionalization from tetraaldehyde to tetraoximes using 'solvent assisted grinding', irrespective of the position of the aldehyde.

Finally, we prepared tetra-substituted pyridyl and carboxylic acid cavitands having an ellipsoidal cavity capable of encapsulating asymmetric guest molecules and was subsequently obtained the first of its kind, C_{2v} symmetric molecular capsule with encapsulated asymmetric guest molecule.

Table of Contents

List of Figures	xii
List of Tables	xx
Acknowledgements.....	xxi
Dedication.....	xxii
Preface.....	xxiii
Chapter 1 - Introduction.....	1
1.1 Covalent vs. supramolecular chemistry?	1
1.2 Crystal engineering.....	3
1.2.1 Hydrogen bonds	5
1.2.2 Halogen bonds	6
1.2.3 Supramolecular synthons	6
1.2.4 Co-crystallization as a tool for understanding intermolecular interactions	8
Chapter 2 - Mapping the binding preferences of 2-aminopyrazines via co-crystallizations	14
2.1 Introduction.....	14
2.2 Experimental.....	18
2.2.1 Synthesis	18
2.2.2.1 Synthesis of 2-amino-5-bromopyrazine, B2 and 2-amino-3,5-dibromopyrazine, B3.....	18
2.2.2 Synthesis of co-crystals and salts.....	19
2.2.2.1 Synthesis of 2-aminopyrazine 4-nitrobenzoic acid (1:2), B1·A11	20
2.2.2.2 Synthesis of 2-aminopyrazinium 3,5-dinitrobenzoate, B1·A14	20
2.2.2.3 Synthesis of 2-aminopyrazine 3-nitrobenzoic acid (1:1), B1·A16	20
2.2.2.4 Synthesis of 2-aminopyrazine succinic acid (1:1), B1·A23	20
2.2.2.5 Synthesis of 2-aminopyrazine glutaric acid (1:1), B1·A24	20
2.2.2.6 Synthesis of 2-aminopyrazine pimelic acid (1:1), B1·A26	21
2.2.2.7 Synthesis of 2-aminopyrazine suberic acid (1:1), B1·A27	21
2.2.2.8 Synthesis of 2-aminopyrazine sebacic acid (1:1), B1·A29.....	21

2.2.2.9 Synthesis of 2-amino-3,5-dibromopyrazine 2,5-dihydroxybenzoic acid (1:1), B3·A7.....	21
2.2.2.10 Synthesis of 2-amino-3,5-dibromopyrazine pentafluorobenzoic acid (1:1), B3·A13.....	21
2.2.2.11 Synthesis of 2-amino-3,5-dibromopyrazine 3,5-dinitrobenzoic acid (1:1), B3·A14.....	21
2.2.2.12 Synthesis of 2-amino-3,5-dibromopyrazine 2,6-difluorobenzoic acid (1:1), B3·A18.....	22
2.2.3 Molecular electrostatic potential charge calculations	22
2.2.4 Single Crystal X-ray Crystallography.....	22
2.3 Results.....	23
2.3.1 Characterization by IR spectroscopy	23
2.3.2 Crystal structures	24
2.3.2.1 Crystal structure of 2-amino-3,5-dibromopyrazine, B3.....	26
2.3.2.2 Crystal structures of B1·A11 and B1·A16.....	27
2.3.2.3 Crystal structure of 2-aminopyrazinium 3,5-dinitrobenzoate, B1·A14.....	27
2.3.2.5 Crystal structure of 2-aminopyrazine succinic acid, B1·A23.....	27
2.3.2.6 Crystal structures of B1·A24, B1·A26, B1·A27 and B1·A29.....	28
2.3.2.10 Crystal structures of B3·A7, B3·A13 and B3·A18.....	29
2.3.2.12 Crystal structure of 2-amino-3,5-dibromopyrazine 3,5-dinitrobenzoic acid, B3·A14.....	29
2.4 Discussion.....	30
2.4.1 Supramolecular yield based on infrared spectroscopy.....	30
2.4.2 Evaluation of donor or acceptor dominance in predicting product formation.....	32
2.4.3 Synthons classification based on crystal structures.....	33
2.4.4 Binding preference of carboxylic acids	36
2.5 Conclusion	36
Chapter 3 - Avoiding 'synthon crossover' in synthetic strategies based on halogen bonds and hydrogen bonds.....	39
3.1 Introduction.....	39
3.2 Experimental.....	44

3.2.1 Synthesis of ligands	44
3.2.1.1 Synthesis of 2,3,5,6-tetrafluoro-4-iodobenzoic acid, IF4BA.....	44
3.2.1.2 Synthesis of 2,3,5,6-tetrafluoro-4-bromobenzoic acid, BrF4BA.....	45
3.2.1.3 Synthesis of 2-aminopyrazine 1,4-diiidotetrafluorobenzene (2:1), B1·DITFB ...	45
3.2.1.4 Synthesis of 2-amino-5-bromopyrazine 1,4-diiidotetrafluorobenzene (2:1), B2·DITFB	46
3.2.1.5 Synthesis of 2-amino-3,5-dibromopyrazine 1,4-diiidotetrafluorobenzene (2:1), B3·DITFB	46
3.2.1.6 Synthesis of 2-aminopyrazinium 2,3,5,6-tetrafluoro-4-iodobenzoate, B1·IF4BA	46
3.2.1.7 Synthesis of 2-aminopyrazinium 2,3,5,6-tetrafluoro-4-bromobenzoate, B1·BrF4BA	46
3.2.1.8 Synthesis of 2-amino-5-bromopyrazine 2,3,5,6-tetrafluoro-4-iodobenzoic acid (1:1), B2·IF4BA.....	46
3.2.1.9 Synthesis of 2-amino-5-bromopyrazine 2,3,5,6-tetrafluoro-4-bromobenzoic acid (1:1), B2·BrF4BA	47
3.2.1.10 Synthesis of 2-amino-3,5-dibromopyrazine 2,3,5,6-tetrafluoro-4-iodobenzoic acid (1:1), B3·IF4BA	47
3.2.1.11 Synthesis of 2-amino-3,5-dibromopyrazine 2,3,5,6-tetrafluoro-4-bromobenzoic acid (1:1), B3·BrF4BA	47
3.3 Results.....	47
3.3.1 Molecular Electrostatic Potential Calculations	49
3.3.2 Crystal structures	49
3.3.2.1 Crystal structure of 2-aminopyrazine 1,4-diiidotetrafluorobenzene, B1·DITFB	49
3.3.2.2 Crystal structure of 2-amino-5-bromopyrazine 1,4-diiidotetrafluorobenzene (2:1), B2·DITFB	50
3.3.2.3 Crystal structure of 2-amino-3,5-dibromopyrazine 1,4-diiidotetrafluorobenzene (2:1), B3·DITFB	51
3.3.2.4 Crystal structure of 2-aminopyrazinium 2,3,5,6-tetrafluoro-4-iodobenzoate, B1·IF4BA	52
3.3.2.5 Crystal structure of 2-aminopyrazinium 2,3,5,6-tetrafluoro-4-bromobenzoate, B1·BrF4BA.....	53

3.3.2.6 Crystal structure of 2-amino-5-bromopyrazine 2,3,5,6-tetrafluoro-4-iodobenzoic acid (1:1), B2·IF4BA	54
3.3.2.7 Synthesis of 2-amino-5-bromopyrazine 2,3,5,6-tetrafluoro-4-bromobenzoic acid (1:1), B2·BrF4BA	55
3.3.2.8 Crystal structure of 2-amino-3,5-dibromopyrazine 2,3,5,6-tetrafluoro-4-iodobenzoic acid (1:1), B3·IF4BA	55
3.3.2.9 Crystal structure of 2-amino-3,5-dibromopyrazine 2,3,5,6-tetrafluoro-4-bromobenzoic acid (1:1), B3·BrF4BA	56
3.4 Discussion	57
3.4.1 Characterization of co-crystals or salts through IR spectroscopy	57
3.4.2 Establishing balance between hydrogen bonding and halogen bonding	58
3.4.3 Secondary hydrogen bonding motifs	62
3.5 Conclusions	62
Chapter 4 - Hierarchical halogen bonding	65
4.1 Introduction	65
4.1.1 Goals	68
4.2 Result and discussion	68
4.2.3 Halogen bonded co-crystals	68
4.3 Conclusions	81
4.4 Experimental	83
4.4.1 Synthesis of halogen bond donors	83
4.4.1.1 Synthesis of 1-bromo-2,3,5,6-tetrafluoro-4-iodobenzene, IF4Br	83
4.4.1.2 Synthesis of 4-bromo-2,2',3,3',5,5',6,6'-octafluoro-4'-iodo-1,1'-biphenyl, IF8Br	84
4.4.1.3 Synthesis of 4-bromo-2,3,5,6-tetrafluorophenyl 2,3,5,6-tetrafluoro-4-iodobenzoate, I	85
4.4.1.4 Synthesis of 2,3,5,6-tetrafluoro-4-iodophenyl 2,3,5,6-tetrafluoro-4-iodobenzoate, II	85
4.4.1.5 Synthesis of 4-bromo-2,3,5,6-tetrafluorophenyl 4-bromo-2,3,5,6-tetrafluorobenzoate, III	86
4.4.1.6 Synthesis of 4-bromo-2,3,5,6-tetrafluorophenyl 2,4,6-trifluoro-3,5-diiodobenzoate, IV	87

4.4.1.7 Synthesis of 4-bromo-2,3,5,6-tetrafluoro-N-(4-iodophenyl)benzamide, V	88
4.4.1.8 Synthesis of N-(4-bromo-2,3,5,6-tetrafluorophenyl)-2,3,5,6-tetrafluoro-4-iodobenzamide, VI.....	89
4.4.2 Synthesis of Co-crystals.....	90
4.4.2.1 Synthesis of 1-bromo-2,3,5,6-tetrafluoro-4-iodobenzene tetramethylpyrazine (1:1), IF4Br·A.....	90
4.4.2.2 Synthesis of 4-bromo-2,2',3,3',5,5',6,6'-octafluoro-4'-iodo-1,1'-biphenyl tetramethylpyrazine (1:1), IF8Br·A	90
4.4.2.3 Synthesis of 1-bromo-2,3,5,6-tetrafluoro-4-iodobenzene tetramethylpyrazine mono-N-oxide (1:1), IF4Br·B.....	90
4.4.2.4 Synthesis of 4-bromo-2,2',3,3',5,5',6,6'-octafluoro-4'-iodo-1,1'-biphenyl tetramethylpyrazine mono-N-oxide (1:1), IF8Br·B.....	90
4.4.2.5 Synthesis of 1-bromo-2,3,5,6-tetrafluoro-4-iodobenzene 4,4'-bipyridine mono N-oxide (1:1), IF4Br·C	91
4.4.2.6 Synthesis of 4-bromo-2,2',3,3',5,5',6,6'-octafluoro-4'-iodo-1,1'-biphenyl 5,6-dimethyl-1-(pyridin-4-ylmethyl)-1H-benzo[d]imidazole (1:1), IF8Br·D	91
4.4.2.7 Synthesis of 4-bromo-2,2',3,3',5,5',6,6'-octafluoro-4'-iodo-1,1'-biphenyl 4-(N-pyrrolidinyl)pyridine (1:1), IF8Br·E.....	91
4.4.2.8 Synthesis of 4-bromo-2,2',3,3',5,5',6,6'-octafluoro-4'-iodo-1,1'-biphenyl 4-(N,N-dimethylamino)pyridine (1:1), IF8Br·F.....	91
4.4.2.9 Synthesis of N-(4-bromo-2,3,5,6-tetrafluorophenyl)-2,3,5,6-tetrafluoro-4-iodobenzamide 1,2-bis(4-pyridyl)ethylene (1:1), VI·G.....	91
4.4.2.10 Synthesis of N-(4-bromo-2,3,5,6-tetrafluorophenyl)-2,3,5,6-tetrafluoro-4-iodobenzamide 1,2-bis(4-pyridyl)ethane (1:1), VI·H.....	92
4.4.2.11 Synthesis of N-(4-bromo-2,3,5,6-tetrafluorophenyl)-2,3,5,6-tetrafluoro-4-iodobenzamide 4,4'-bipyridine (1:1), VI·bipy.....	92
Chapter 5 - Facile functionalization of cavitands	95
5.1 Introduction.....	95
5.1.1 Choice of reaction - Suzuki-Miyaura coupling.....	96
5.1.2 Oxime decorated cavitands	98
5.1.3 Goals	99

5.2 Experimental.....	100
5.2.1 Synthesis	100
5.2.1.1 Synthesis of C-pentylcalix[4]resorcinarene, 1	101
5.2.1.2 Synthesis of C-pentyltetrabromocalix[4]resorcinarene, 2	102
5.2.1.3 Synthesis of C-pentyltetrabromocavitand, 3.....	102
5.2.1.4 Synthesis of C-pentyltetraboronic acid dipinacolyl ester Cavitand, 4.....	103
5.2.1.5 Synthesis of C-pentyltetra(4-methoxyphenyl)cavitand, 5	104
5.2.1.6 Synthesis of C-pentyltetra(4-cyanophenyl)cavitand, 6.....	105
5.2.1.7 Synthesis of C-pentyltetra(3-pyridyl)cavitand, 7.....	106
5.2.1.8 Synthesis of C-pentyltetra(3-bromopyridyl)cavitand, 8	107
5.2.1.9 Synthesis of C-pentyltetraaldehydecavitand, 9.....	107
5.2.1.10 Synthesis of C-pentyltetraaldoximecavitand, 10	108
5.2.1.11 Synthesis of C-pentyltetra(4-phenylformyl)cavitand, 11	109
5.2.1.12 Synthesis of C-pentyltetra(4-phenylaldoxime)cavitand, 12	110
5.2.1.13 Synthesis of C-pentyltetra(3-phenylformyl)cavitand, 13	110
5.2.1.14 Synthesis of C-pentyltetra(3-phenylaldoxime)cavitand, 14	111
5.2.1.15 Synthesis of C-pentyltetramethylresorcin[4]arene, 15	112
5.2.1.16 Synthesis of C-pentyltetramethylcavitand, 16 ³⁰	112
5.2.1.17 Synthesis of C-pentyltetra(bromomethyl)cavitand, 17 ³⁰	113
5.2.1.18 Synthesis of C-pentyltetra(4-formylmethoxyphenyl)cavitand, 18	114
5.2.1.19 Synthesis of C-pentyltetra(4-aldoximemethoxyphenyl)cavitand, 19	114
5.3 Results and discussion	115
5.3.1 Versatile Suzuki-Miyaura coupling protocol for cavitand functionalization.....	115
5.3.2 Oxime decorated cavitands via ‘solvent assisted grinding’	118
5.4 Conclusions.....	122
Chapter 6 - From cavitand co-crystals to molecular capsules	127
6.1 Introduction.....	127
6.1.1 Ethylene bridged cavitands	127
6.1.2 Isothermal titration calorimetry	128
6.1.3 Pyridyl and carboxylic acid functionalized cavitands.....	129
6.1.4 Goals	130

6.2 Experimental.....	131
6.2.1 Synthesis	131
6.2.1.1 Synthesis of C-pentyltetrabromocavitand, 20.....	132
6.2.1.2 Synthesis of C-pentyltetra(3-pyridyl)cavitand, 21.....	132
6.2.1.3 Synthesis of C-pentyltetracarboxylic acid cavitand, 22.....	133
6.2.2 Isothermal Titration Calorimetry (ITC) studies.....	134
6.2.2.1 ITC experiments.....	134
6.2.2.2 ITC data for titration of tetra(3-pyridyl)cavitand 21 into 4-nitrobenzoic acid ...	135
6.2.3 Crystallizations	135
6.2.3.1 C-pentyltetrabromocavitand, 20; C-pentyltetra(3-pyridyl)cavitand, 21	135
6.2.3.2 C-pentyltetra(3-pyridyl)cavitand : 4-nitrobenzoic acid (1:4); 21a.....	136
6.2.3.3 C-pentyltetra(3-pyridyl)cavitand : 3,5-dinitrobenzoic acid (1:2); 21b	136
6.2.3.4 C-pentyltetra(3-pyridyl)cavitand : resorcinol (1:1); 21c.....	136
6.2.3.5 C-pentyltetracarboxylic acid cavitand : 4,4'-bipyridine (1:2); 22a.....	136
6.2.3.6 C-pentyltetracarboxylic acid cavitand : 2-amino-5-bromo-4-chloro-6-methylpyrimidine (1:3); 22b	137
6.3 Results and discussion	137
6.3.1 Multi-component supramolecular assembly in solution	137
6.3.2 Solid-state structures of cavitands.....	141
6.3.2.1 Cavitand co-crystals.....	141
6.3.3.2 Quest for molecular capsules	147
6.3.3.3 Structural analysis of crystal structures	153
6.4 Conclusions.....	154
Appendix A – ¹ H, ¹³ C NMR and HRMS	159

List of Figures

Figure 1.1 Retrosynthetic analysis of Gambierol natural product (total synthesis requires 103 steps). ²	1
Figure 1.2 Schematic representation of synthetic (left) vs. supramolecular chemistry (right).....	2
Figure 1.3 Application of crystal engineering to align molecules in desired fashion for reliable product formation. ⁶	3
Figure 1.4 a) Primary arrangement of chromophore molecules and b) two possible orientations of the pair; type I arrangement gives NLO material and type II arrangement gives non-functional material. ⁷	4
Figure 1.5 Calixarene-based purification of fullerenes from the complex mixture. ¹⁰	5
Figure 1.6 Cartoon representation of DNA helix (left) and hydrogen bonded base pairs (right)...	6
Figure 1.7 General scheme for the formation of halogen bonds.....	6
Figure 1.8 Schematic showing transferable nature of synthons; supermolecules a) and b) contains homomeric synthon, supermolecules b), c) and d) contains heteromeric synthon.	7
Figure 1.9 Some examples of synthons; a) Iodo···iodo, b) acid···acid, c) Iodo···pyridine and d) carboxylic acid···pyridine. ¹⁷	8
Figure 1.10 Recrystallization (right) yields homomeric solids. The co-crystallization process (left) leads to a heteromeric product.	8
Figure 1.11 Schematic of best donor-best acceptor rule from Etter's guidelines.	9
Figure 1.12 Example of supermolecule in binary 1:2 co-crystals of 4,4'-bipyridine and 4-nitrobenzoic acid. ³⁴	10
Figure 1.13 The ternary supermolecule showing the best hydrogen-bond donor binding to the best hydrogen-bond acceptor and the second-best donor binding to the second-best acceptor.	10
Figure 2.1 Examples of a) homomeric and b) heteromeric hydrogen-bond interactions.	15
Figure 2.2 Possible outcomes when a ditopic acceptor molecule is combined with a monotopic donor molecule. Heteromeric products (a), (b) and (c); homomeric products (d) and (e)....	15
Figure 2.3 CSD structural analysis results for combination of carboxylic acid with (a) 2-aminopyridine, and (b) pyridine.....	16

Figure 2.4 Ditopic supramolecular reagents for supramolecular synthesis.	17
Figure 2.5 Postulated homo- and hetero synthons in supramolecular synthesis with 2-aminopyrazine derivatives and carboxylic acids.	17
Figure 2.6 MEP surface calculations of 2-aminopyrazine and brominated analogues thereof. Numbers reflect the charge on the N1 nitrogen atom in each molecule.	22
Figure 2.7 Observed homosynthon in the crystal structure of B3.	26
Figure 2.8 Thermal ellipsoid plots (50% probability level) of (a) B1·A11 and (b) B1·A16.	27
Figure 2.9 The primary synthon in the crystal structure of B1·A14.	27
Figure 2.10 The primary hydrogen bonds in the crystal structure of B1·A23.	28
Figure 2.11 2D network formed in the co-crystal of B1·A23.	28
Figure 2.12 Infinite 1D chains formed in the co-crystal of B1·A24.	28
Figure 2.13 Extended 2D network formed in the co-crystal of B1·A24.	29
Figure 2.14 1:1 co-crystal of B3·A13.	29
Figure 2.15 The primary hydrogen bonds in the crystal structure of B3·A14.	29
Figure 2.16 Potential homo- and hetero synthons in salts and co-crystals based on 2-aminopyrazine derivatives and carboxylic acids.	33
Figure 2.17 Classification of crystal structures obtained from supramolecular reactions between B1-B3 and a variety of acids.	34
Figure 2.18 Binding preferences of carboxylic acids with B1 and B3.	36
Figure 3.1 Examples of commonly occurring supramolecular synthons, a) acid-acid b) amide-amide c) acid-amide d) acid-aminopyridine and e) single-point iodo-N(py).	39
Figure 3.2 Supramolecular assembly from <i>iso</i> -nicotinamide and DITFB. ^{6a}	40
Figure 3.3 Results obtained by combining 2-aminopyrazine derivatives with carboxylic acids. Numbers indicate carboxylic acid binding preference.	41
Figure 3.4 Observed synthons in the CSD database search for (a) co-crystals of substituted pyridines and 1,4-diiodotetrafluorobenzene, (b) substituted 2-aminopyrazine by itself and (c) its extended network.	41
Figure 3.5 Ditopic supramolecular reagents for supramolecular synthesis.	43
Figure 3.6 1D networks formed by postulated hydrogen and halogen bonds (X = I, Br).	43
Figure 3.7 MEP surface calculations of 2-aminopyrazine, B1; 2-amino-5-bromopyrazine, B2 and 2-amino-3,5-dibromopyrazine, B3. Numbers reflect the MEPs on atoms in kJ/mol.	49

Figure 3.8 Thermal ellipsoid plot (50% probability level) and the labeling scheme of the supermolecule B1·DITFB.....	50
Figure 3.9 Infinite 1-D chains produced through a combination of hydrogen- and halogen bonds in the crystal structure of B1·DITFB.....	50
Figure 3.10 Thermal ellipsoid plot (50% probability level) and the labeling scheme of the supermolecule B2·DITFB.....	51
Figure 3.11 1-D motif in the crystal structure of B2·DITFB constructed from HB homosynthons and near-linear N···I halogen bonds (the latter is responsible for the primary assembly of the co-crystal).....	51
Figure 3.12 Thermal ellipsoid plot (50% probability level) and the labeling scheme of the supermolecule B3·DITFB.....	52
Figure 3.13 Part of an infinite chain in the structure of B3·DITFB produced through hydrogen bonds and halogen bonds.....	52
Figure 3.14 Thermal ellipsoid plot (50% probability level) and the labeling scheme of the supermolecule B1·IF4BA.....	53
Figure 3.15 The 1:1 salt of B1·IF4BA. 1-D chain produced through combination of hydrogen and halogen bond.....	53
Figure 3.16 Thermal ellipsoid plot (50% probability level) and the labeling scheme of the supermolecule B1·BrF4BA.....	54
Figure 3.17 The 1:1 salt of B1·BrF4BA. 1-D chain produced through combination of hydrogen and halogen bond.....	54
Figure 3.18 Thermal ellipsoid plot (50% probability level) and the labeling scheme of the supermolecule B2·IF4BA.....	54
Figure 3.19 1-D motif formed in crystal structure of B2·IF4BA. Binary co-crystal formed through hydrogen bond and N···I halogen bond.....	55
Figure 3.20 Thermal ellipsoid plot (50% probability level) and the labeling scheme of the supermolecule B2·BrF4BA.....	55
Figure 3.21 1-D motif formed in crystal structure of B2·BrF4BA. Binary co-crystal formed through hydrogen bond and N···Br halogen bond.....	55
Figure 3.22 Thermal ellipsoid plot (50% probability level) and the labeling scheme of the supermolecule B3·IF4BA.....	56

Figure 3.23 1-D motif formed in crystal structure of B3·IF4BA. Binary co-crystal formed through hydrogen bond and N···Br halogen bond.....	56
Figure 3.24 Thermal ellipsoid plot (50% probability level) and the labeling scheme of the supermolecule B3·BrF4BA.	57
Figure 3.25 1-D motif formed in crystal structure of B3·BrF4BA. Binary co-crystal formed through hydrogen bond and N···Br halogen bond.....	57
Figure 3.26 Interactions observed in crystal structures between DITFB and B1-B3.	59
Figure 3.27 Space filling representation of a portion of the crystal structure of B3·DITFB.....	59
Figure 3.28 Summary of observed synthons in the crystal structures. (X = I/Br, * Including two cases where proton transfer occurred from carboxylic acid to the base B1)	61
Figure 4.1 The best hydrogen-bond donor (oxime group), binds to the best acceptor, while the second-best donor (carboxylic acid) interacts with the second-best acceptor. ¹	65
Figure 4.2 Schematic showing molecular electrostatic potential (MEP) of a) CF ₄ , b) CF ₃ Cl, c) CF ₃ Br, d) CF ₃ I. ^{11a} (Red indicates positive MEP and blue indicating negative MEP)	66
Figure 4.3 Co-crystallization reaction of ditopic halogen-bond donor with a ditopic halogen-bond acceptor.	67
Figure 4.4 Scheme representing existing powerful halogen-bond donor molecules DITFB, DBTFB and target ditopic halogen-bond donor molecule IF4Br.	67
Figure 4.5 Target ditopic halogen bond donor molecules.	68
Figure 4.6 Synthetic scheme for IF4Br.....	69
Figure 4.7 Molecular electrostatic potential charges on activated ditopic halogen bond donor sites based on PM3 semi-empirical calculation.	70
Figure 4.8 Halogen bonded co-crystals of tetramethylpyrazine with a) DITFB and b) I ₂ . ^{18,19}	70
Figure 4.9 1D network formed in IF4Br·A. Structure shows disordered IF4Br halogen bonded to tetramethylpyrazine.....	71
Figure 4.10 1D network formed in IF8Br·A. Structure shows I/Br disorder.	72
Figure 4.11 MEP surfaces of a) pyridine and b) pyridine- <i>N</i> -oxide.	73
Figure 4.12 Co-crystal of DITFB with 4,4'-bipyridine <i>N,N'</i> -dioxide (CSD code – OCOMUO).	73
Figure 4.13 MEP surfaces of a) tetramethylpyrazine mono- <i>N</i> -oxide, B and b) 4,4'-bipyridine mono <i>N</i> -oxide, C.....	74

Figure 4.14 1D network formed in IF ₄ Br·B. Structure shows disordered IF ₄ Br and B. a) Ball and stick model and b) Space filling model.....	75
Figure 4.15 1D halogen bonded network formed in IF ₈ Br·B. Structure shows disordered IF ₈ Br and B.	75
Figure 4.16 1D halogen bonded network formed in IF ₄ Br·C. Structure shows disordered IF ₄ Br.	75
Figure 4.17 Schematic of ditopic asymmetric halogen bond acceptor a) molecular structure of D with MEP charges and b) its MEP surface.	76
Figure 4.18 Halogen bonded network formed in IF ₈ Br·D via C-X _{I/Br} ···N interaction.	76
Figure 4.19 1:1 co-crystal formed by combination of IF ₈ Br with a) 4-(<i>N</i> -pyrrolidinyl)pyridine E and b) 4-(<i>N,N</i> -dimethylamino)pyridine F (Disorder is removed for clarity).....	77
Figure 4.20 An ester bridged halogen-bond donor molecule library.....	78
Figure 4.21 The molecular structure of V (left), ladder formation via C=O···H-N interactions in the crystal structure of V (center) and VI with MEP charges on iodo and bromo XB donor (right).	79
Figure 4.22 2D sheet generated in the crystal structure of VI·bipyethylene via combination of N···I, N···Br and C=O···H-N interactions.	80
Figure 4.23 Zig-zag network formed via a combination of I···N and N-H···N interactions in the structure of IF ₈ Br·bipyethane.....	81
Figure 4.24 2D sheets in the crystal structure of VI·bipy via a combination of N···I, N···Br and C=O···H-N interactions.	81
Figure 4.25 Flow chart summarizing outline of the chapter. Numbers indicate path direction. Green circles represent co-crystallization reaction.	82
Figure 5.1 Schematic representation of molecular capsule formation.....	95
Figure 5.2 Resorcin[4]arene cavitand scaffold with labeled possible adaptable locations.....	96
Figure 5.3 Tetraboronic pinacolyl ester cavitand precursor for a Suzuki-Miyaura reaction.	97
Figure 5.4 Schematic of possible homomeric and heteromeric interactions of oximes.	98
Figure 5.5 Schematic showing tunable nature of oxime group.	99
Figure 5.6 Cartoon representation of oxime decorated cavitand.	99
Figure 5.7 Schematic showing proposed Suzuki-Miyaura coupling protocol with target arenes.	100

Figure 5.8 Schematic representation of; a) shallow, b) deeper and c) deep and more flexible oxime cavitands.	100
Figure 5.9 Synthesis of tetraboronic pinacolyl ester cavitand 4.	116
Figure 5.10 Synthetic route for Suzuki-Miyaura cross coupling reaction of cavitand 4.	117
Figure 5.11 Possible homomeric and heteromeric capsule formation using oximes.....	118
Figure 5.12 Cartoon representation for oxime cavitand synthetic scheme.	119
Figure 5.13 Synthetic scheme for tetraaldoxime cavitand 10. (a) (1) <i>n</i> -BuLi, THF, -78 °C; (2) <i>n</i> -formylmorpholine, -78 °C to rt; (b) NH ₂ OH·HCl, NaOH, DCM, Ethanol, rt.	120
Figure 5.14 Synthetic scheme for tetraphenyl aldoxime cavitand 12 and 14 (R = pentyl). (a) Toluene/Ethanol/ Water, Pd(PPh ₃) ₄ , Na ₂ CO ₃ , Reflux, 72hrs; (b) NH ₂ OH·HCl, NaOH, DCM, Ethanol, rt.....	121
Figure 5.15 Synthesis of deep tetra aldoxime cavitand 19 (R = pentyl) . (a) K ₂ CO ₃ , Acetonitrile (b) NH ₂ OH·HCl, NaOH, DCM, Ethanol, rt.....	122
Figure 5.16 Schematic of developed versatile Suzuki-Miyaura coupling protocol.....	122
Figure 5.17 Tetraaldehyde to tetraaldoxime cavitand synthesis via ‘solvent assisted grinding’.	123
Figure 5.18 Schematic representation of; a) shallow, b) deeper and c) deeper and flexible oxime cavitands.	123
Figure 6.1 Schematic showing (a) methylene bridged cavitand and (b) ethylene bridged cavitand.	128
Figure 6.2 Energy minimized structures of (a) methylene bridged cavitand and (b) ethylene bridged cavitand showing top view with interior cavity dimensions.	128
Figure 6.3 Schematic of commonly occurring a) pyridine-carboxylic acid and b) pyridine-hydroxy synthons.	129
Figure 6.4 Schematic showing carboxylic acid hydrogen-bond with, (a) 4,4'-bipyridine and (b) 2-aminopyrimidine.....	130
Figure 6.5 Ethylene bridged cavitand.	130
Figure 6.6 Target tetrapyridyl cavitand.	131
Figure 6.7 Target tetracarboxylic acid cavitand.	131
Figure 6.8 Proposed multi-component supramolecular assembly in solution.	137
Figure 6.9 (a) ITC titration curve of C-pentyltetra(3-pyridyl)cavitand vs. 4-nitrobenzoic acid; (b) thermodynamic fit parameters.	138

Figure 6.10 (a) Statistical data analysis of ITC experiment; (b) Output from <i>NanoAnalyze</i> software using an independent model.	138
Figure 6.11 (a) Second ITC titration curve of C-pentyltetra(3-pyridyl)cavitand vs. 4-nitrobenzoic acid; (b) thermodynamic fit parameters.	139
Figure 6.12 (a) Statistical data analysis of ITC experiment; (b) Output from <i>NanoAnalyze</i> software using independent model.	139
Figure 6.13 Comparison of (a) methylene bridged (7.87Å x 7.87Å) ²⁵ and (b) ethylene bridged cavitand (9.48Å x 7.58Å) structures.	141
Figure 6.14 Crystal structure of 20 with acetonitrile molecules are shown in space filling.	142
Figure 6.15 Crystal structure of 21 showing (a) horizontal view and (b) top view with space filling model (disordered ethanol and other solvent molecules were removed for clarity).	142
Figure 6.16 IR of single crystal of 21a.	143
Figure 6.17 Crystal structure of 21a showing (a) pentameric assembly with two nitrobenzene molecules in space filling and (b) 21a colour coded for clarity (disordered 2,6-dimethyl naphthalene guest molecule is shown in yellow ball stick model).	144
Figure 6.18 Molecular structure and labelled thermal ellipsoids (50% probability level) of 21b. (a and b showing two unique molecular complexes present in crystalline lattice).	145
Figure 6.19 a) Molecular structure of 21c and (b) Extended structure of 21c showing cavitand in purple, resorcinol molecule in yellow and water molecules in red/blue.	146
Figure 6.20 Molecular capsule formed via eight OH...N hydrogen bonds; a) thermal ellipsoide plot of crystal structure and b) space filling model (solvent molecules are removed for clarity). ^{30a}	148
Figure 6.21 Molecular structure of 22a showing co-crystal formation via OH...N hydrogen bonding.	149
Figure 6.22 1D polymeric network formation in 22a via acid OH...N(bipy), OH...O(methanol), methanol OH...N(bipy). Acid cavitand 22 is shown in yellow, bipy molecules are shown in purple and methanol is shown in red.	150
Figure 6.23 Self-assembly of tetracarboxylic acid cavitand (short and extended analogue) with 2-aminopyridine. ³²	151
Figure 6.24 Molecular structure of 22b showing hydrogen bonding interaction between carboxylic acid cavitand and 2-aminopyrimidine derivative.	151

Figure 6.25 a) Hexameric capsule formed with the aid of eight water molecules. b) Dimeric capsule formed with eight <i>iso</i> -propanol molecules.	152
Figure 6.26 Extended structure of 22b showing capsule formation via OH...N/ OH...O hydrogen bonding. (a) and (b) represents different views of capsule holding the guest inside the cavity. Encapsulated guest molecule is disordered.	153
Figure 6.27 Ethylene bridged cavitand.	155
Figure 6.28 Pentameric supramolecular assembly analyzed in solution and solid-state.	155
Figure 6.29 (a) Schematic of tetracarboxylic acid cavitand 22 and (b) Representation of capsule with linkers.	156

List of Tables

Table 2.1 IR stretching frequencies (cm^{-1}) of salts and co-crystals of the ligands B1-B3.	24
Table 2.2 Hydrogen-bond Geometries for B3, B1·A11, B1·A14, B1·A16, B1·A23, B1·A24, B1·A26, B1·A27, B1·A29, B3·A7, B3·A13, B3·A14 and B3·A18.....	25
Table 2.3 Charge calculations (PM3) and outcome summary of co-crystallization experiments between pyrazines and carboxylic acids.	30
Table 2.4 Summary of IR data showing carbonyl stretches for co-crystals/salts.	31
Table 2.5 Results from IR spectroscopy arranged in order of decreasing charge on hydrogen of carboxylic acids. Empty boxes represent ‘no reaction’ and filled boxes represent a ‘reaction’	32
Table 2.6 Summary of observed synthons in crystal structures.....	35
Table 3.1 Hydrogen-bond geometries for B1·DITFB, B2·DITFB, B3·DITFB, B1·BrF4BA, B1·IF4BA, B2·BrF4BA, B2·IF4BA, B3·BrF4BA and B3·IF4BA.	47
Table 3.2 Selected IR stretches of the supramolecular complexes.	58
Table 3.3 Hydrogen and halogen bonding patterns observed in the crystal structures of co- crystals and salts.	61
Table 3.4 Summary of secondary interactions observed in crystal structures.	62
Table 4.1 CSD survey for heavy halogen atoms located <i>ortho</i> or <i>para</i> to each other on phenyl ring. All the CSDCODES represent disordered structures. The axis with the arrow indicates the disorder along that axis.	71
Table 4.2 Key geometric parameters in the relevant reported structures and in our work.	76
Table 6.1 Comparison of thermodynamic parameters for the complexation of 21 with 4- nitrobenzoic acid.	139
Table 6.2 Table summarizing crystal structure data for calixarene co-crystals.....	147
Table 6.3 Table summarizing structural data for reported cavitands crystal structures. The locations of solvents were categorized.	153
Table 6.4 Table summarizing structural data for seven cavitand crystal structures obtained. The locations of solvents were categorized.	154

Acknowledgements

A special thanks goes to my advisor, Christer Aakeröy. With his enthusiasm, motivation, and great efforts to explain things clearly and simply; he guided me to the path where chemistry became more fun to me. I truly believe that, I couldn't have gotten a better adviser than you for my PhD.

I would also like to thank my committee members, Professors Eric Maatta, Sundeep Rayat, Michal Zolkiewski and Jennifer Anthony for their input toward this dissertation as well as for being so accommodating with scheduling of the final defense.

To the members of the Aakeröy research group, both past and present, for all the good times we had during my stay at KSU. A special thanks to Kanishka for being so helpful, both inside and outside the lab.

Special thanks to Dr. John Desper for solving single crystal X-ray structures, without them, most of the results in this dissertation would not have been possible.

Thanks to the various people in the department for their assistance, especially, Tobe Eggers, Earline Dikeman, Yasmin Patel, Donna Wright, Mary Dooley and Kim Ross. A special thanks to Jim Hodgson for building/fixing glassware whenever needed. Thanks to Leila Maurmann for NMR training and for being there to help me. Special thanks to Ron Jackson for teaching new ways to fix things and for being there to chat anytime, on any topic!

To all of my friends at Kansas State who have made my time here so memorable. I would like to thank my summer cricket team members for the great time over a past four years. A special thanks to Lateef and Fahmida for the great food and the fun times over the past few years, and most importantly, to Alisha; she is truly a wonderful kid, a stress buster and fun to play with!

I would also like to thank my family for all the support throughout my life. My special thanks to my grandmother, brother and two sisters.

Lastly, and most importantly, I would like to thank my wife Smita for being there with me throughout all the ups and downs of my life. Thank you for everything!!!

Dedication

To my wife and my grandmother.

Preface

Research carried out at Kansas State University for this dissertation led to the following publications in scientific journals.

1. C. B. Aakeröy, P. D. Chopade, *Org. Lett.* **2011**, *13*, 1. Oxime decorated cavitands functionalized through solvent-assisted grinding.
2. C. B. Aakeröy, P. D. Chopade, C. Ganser, J. Desper, *Chem. Commun.* **2011**, *47*, 4688. Facile synthesis and supramolecular chemistry of hydrogen bond/halogen bond-driven multi-tasking tectons.
3. C. B. Aakeröy, A. S. Sinha, P. D. Chopade, J. Desper, *Dalton Trans.* **2011**, *40*, 12160. Halogen bonding or close packing? Examining the structural landscape in a series of Cu(II)-acac complexes.
4. C. B. Aakeröy, P. D. Chopade, N. Schultheiss, J. Desper, *Eur. J. Org. Chem.* **2011**, *33*, 6789. Versatile launch pad for facile functionalization of cavitands.
5. C. B. Aakeröy, P. D. Chopade, J. Desper, *Cryst. Growth Des.* **2011**, *11*, 5333. Avoiding “synthon crossover” in crystal engineering with halogen bonds and hydrogen bonds.
6. C. B. Aakeröy, P. D. Chopade, Wiley-VCH, Eds. Jonathan W. Steed, Philip A. Gale, in *Supramolecular Chemistry: From Molecules to Nanomaterials*, John Wiley & Sons Ltd., UK, pp 2975 – 2992, **2012**. Co-crystals: Synthesis, structure, and applications.

Chapter 1 - Introduction

1.1 Covalent vs. supramolecular chemistry?

Chemical synthesis is the science of making new molecules via covalent bonds. The synthetic chemist has gained considerable control over the covalent bond after more than 180 years of research.¹ There are endless number of tools (different reactions/conditions) that can be explored for developing multi-step synthetic routes, in which ‘intermediate products’ are isolated and purified at each step, before being subjected to further modifications in later steps. This is a major advantage in covalent synthesis that allows the modifications and route changes to take place with the same final molecular target retained. It is now possible to make natural products of previously undreamed complexity, Figure 1.1.²

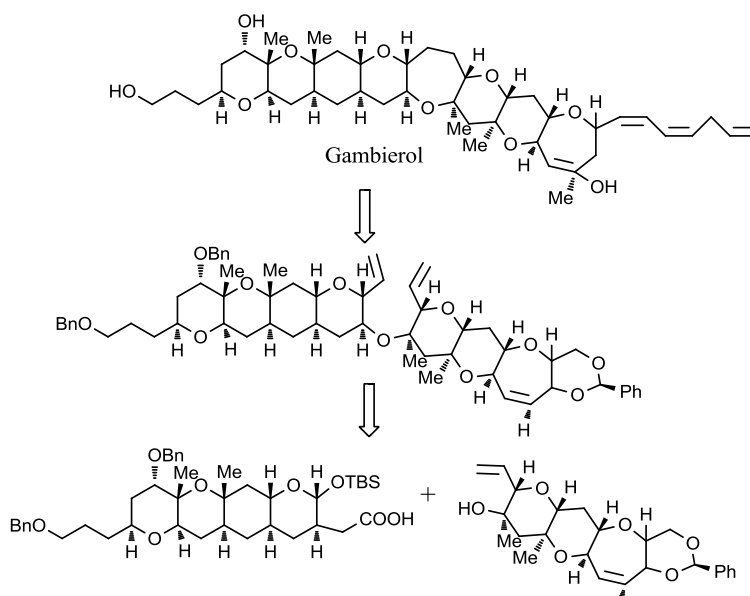


Figure 1.1 Retrosynthetic analysis of Gambierol natural product (total synthesis requires 103 steps).²

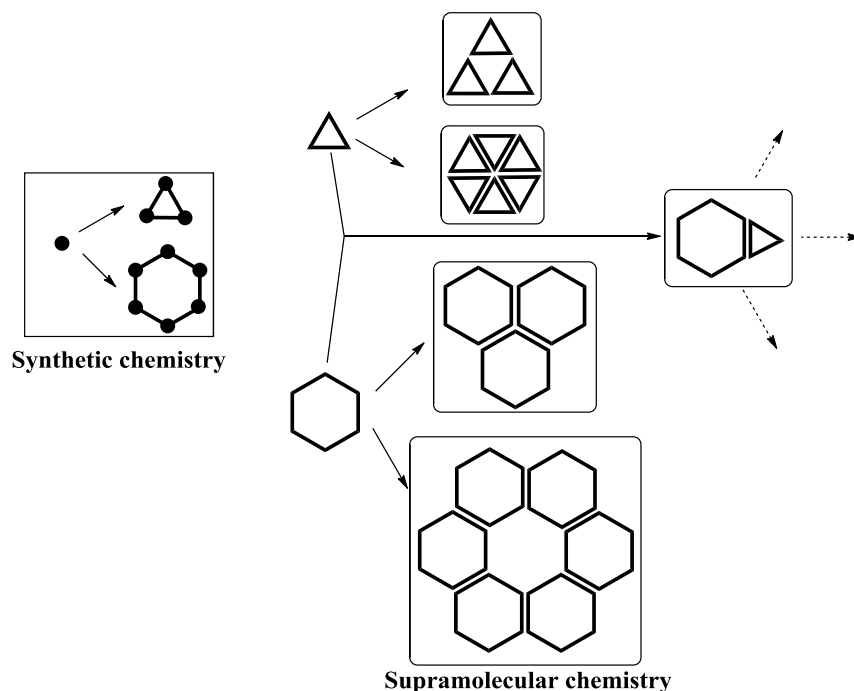


Figure 1.2 Schematic representation of synthetic (left) vs. supramolecular chemistry (right).

“Just as there is a field of *molecular chemistry* based on the covalent bond, there is a field of *supramolecular chemistry*, the chemistry of molecular assemblies and of the intermolecular bond.”³ The main focus of supramolecular chemistry is bringing together molecules without making or breaking covalent bonds to form more complex species (*supermolecules*) via non-covalent interactions (e.g. hydrogen bonds, halogen bonds, van der Waals interactions and coordination bonds). In contrast to synthetic chemists utilizing strong covalent bonds, the supramolecular chemist has to rely on readily reversible bonds, Figure 1.2.⁴ Moreover, most supramolecular syntheses are carried out as one-pot reactions with no intermediates isolated and no additional reaction optimization can be carried out, resulting in clear limitations within supramolecular synthesis, Figure 1.2. Despite these numerous challenges, supramolecular chemistry has gained a lot of insights from solid-state structures of molecular species. The subsection of supramolecular chemistry which studies non-covalent interactions in solid-state is called *crystal engineering*.

1.2 Crystal engineering

Dunitz referred to organic crystals as “supermolecule(s) *par excellence*”.⁵ The molecular recognition of molecules gives supermolecule and periodic arrangement of supermolecules gives a crystal. More than 40 years ago Schmidt coined the term *crystal engineering*.⁶ Although predicting complete molecular self-assembly in the crystalline state is not yet possible, nevertheless, great progress has been achieved in this area.

Ideally, the crystal to be designed has a specific function whether it is desired chemical reactivity,⁶ an optical,⁷ magnetic,⁸ electronic or for chemical separation.⁹ In all these examples precise arrangements of molecules must be controlled to achieve specific function. For example, Schmidt and co-workers demonstrated how crystal engineering can be used to obtain desired 2+2 photodimerization products from molecules containing olefins. The products formed were results of molecular arrangement (proximity and parallel arrangement of the double bonds) in crystal lattice, Figure 1.3.

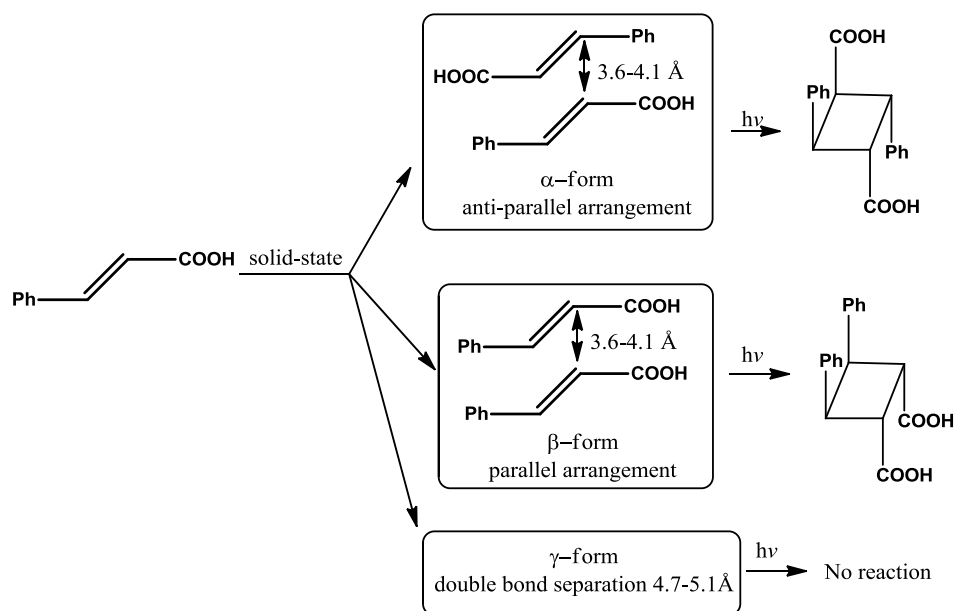


Figure 1.3 Application of crystal engineering to align molecules in desired fashion for reliable product formation.⁶

As another example, in order to obtain non-linear optical (NLO) materials, molecules must be organized in a non-centrosymmetric arrangement with appropriately aligned dipole

moments (Figure 1.4).⁷ Desiraju and co-workers showed how stilbene-based chromophores can be arranged in a non-centrosymmetric fashion to obtain NLO material.⁷

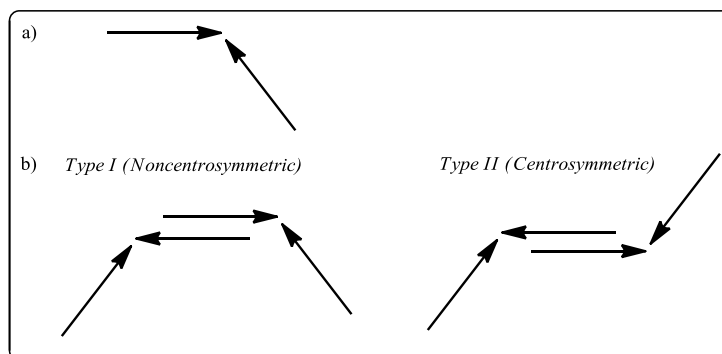


Figure 1.4 a) Primary arrangement of chromophore molecules and b) two possible orientations of the pair; type I arrangement gives NLO material and type II arrangement gives non-functional material.⁷

Furthermore, for chemical separations, the crystalline network of host-material must be able to selectively encapsulate molecules or ions.^{9,10} Atwood and co-workers used this strategy to separate C_{60} and C_{70} fullerene using calixarene based host-material, Figure 1.5. To obtain magnetic materials, arrangement of molecules must facilitate and enhance effective communication between the spins.⁸

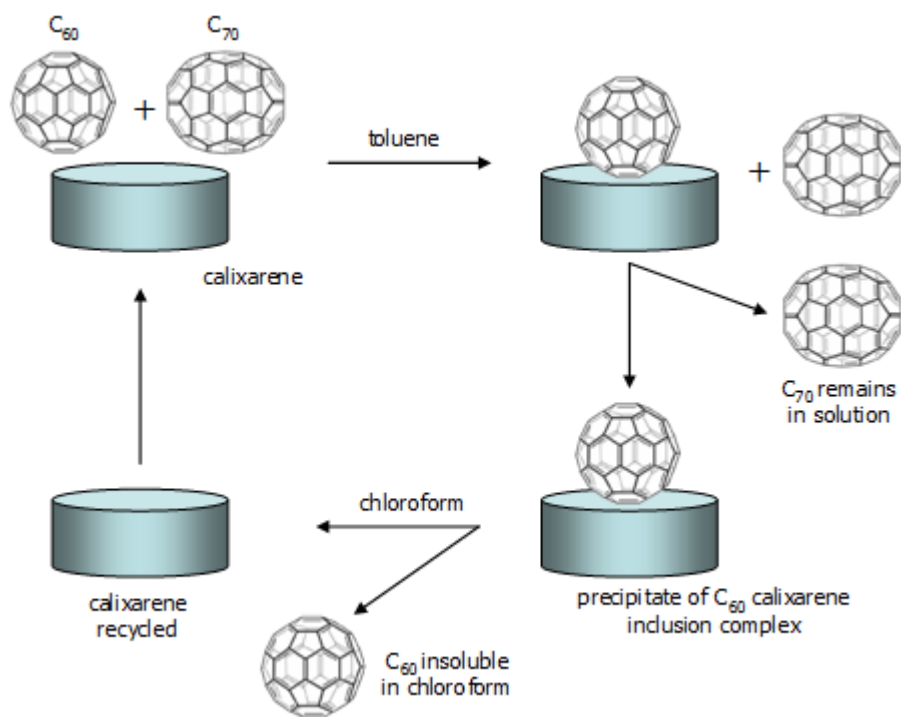


Figure 1.5 Calixarene-based purification of fullerenes from the complex mixture.¹⁰

These examples show that design of materials with specific functions is possible, as long as a great degree of *control* over molecular arrangement and connectivity is achieved. In crystal engineering, the most commonly followed approach to ‘decipher the puzzle’ of interactions in supermolecules is via designing *supramolecular reagents*¹¹ and understanding how they interact in solid-state. The intermolecular interactions covers a wide range of attractive forces, with ion-ion interactions,¹² dipole-dipole interactions,¹³ ion-dipole interactions,¹⁴ van der Waals forces,¹⁵ and π - π stacking,¹⁶ being the most important.

1.2.1 Hydrogen bonds

In the construction of supermolecules, hydrogen bonds¹⁷ have been extensively used since they are relatively strong and directional, which enables a degree of control during the self-assembly process. The hydrogen bond is present in many of Nature’s supermolecules, for example, DNA base pairs interact via hydrogen bonds, Figure 1.6.¹⁸ Mother Nature’s choice for hydrogen bonds in DNA is based on its selective and specific nature, which makes DNA one of the most predictable and programmable self-assembling material known.

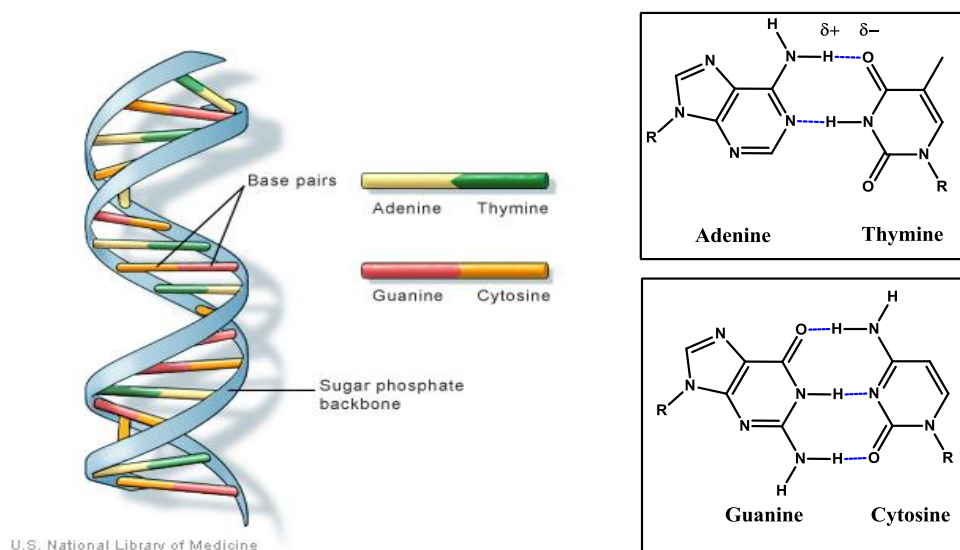
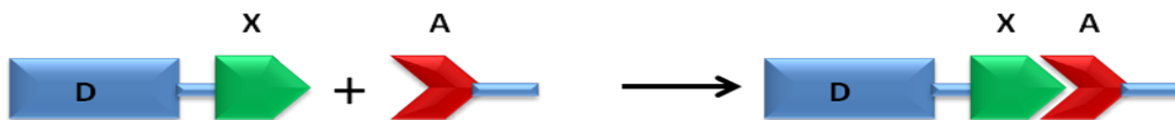


Figure 1.6 Cartoon representation of DNA helix¹⁹ (left) and hydrogen bonded base pairs (right).

1.2.2 Halogen bonds

A hydrogen bond is the attractive interaction of a hydrogen atom with an electronegative atom, such as nitrogen, oxygen that comes from another molecule or chemical group. In halogen bonding,²⁰ a halogen atom X acts as an electron acceptor from an electronegative atom; Figure 1.7. Halogen bonding is a highly directional interaction, even more so than hydrogen bonding and short interactions are more directional than long ones.^{21,22,23}



X = I, Br, Cl

A = N, O, S, Se, Cl, Br, I.

D = C, N, halogen etc.

Figure 1.7 General scheme for the formation of halogen bonds.²⁴

1.2.3 Supramolecular synthons

The patterns based on intermolecular interactions in crystal structure were termed as *supramolecular synthons* by Desiraju. Synthons can be defined as “*structural units within*

supermolecules which can be formed and/or assembled by known or conceivable operations using intermolecular interactions".²⁵ Supramolecular synthons are structural units that express the 'core features' of a crystal structure and which encapsulate the essence of crystals in terms of molecular recognition, Figure 1.8. If synthons can be predicted in a reliable manner, then it will be possible to gain control over supramolecular synthesis. Synthons can be classified as homomeric (when self complementary functional groups interact) and heteromeric (when two different functional groups interact). Some common synthons based on hydrogen-bonding and halogen-bonding interactions are shown in Figure 1.9.

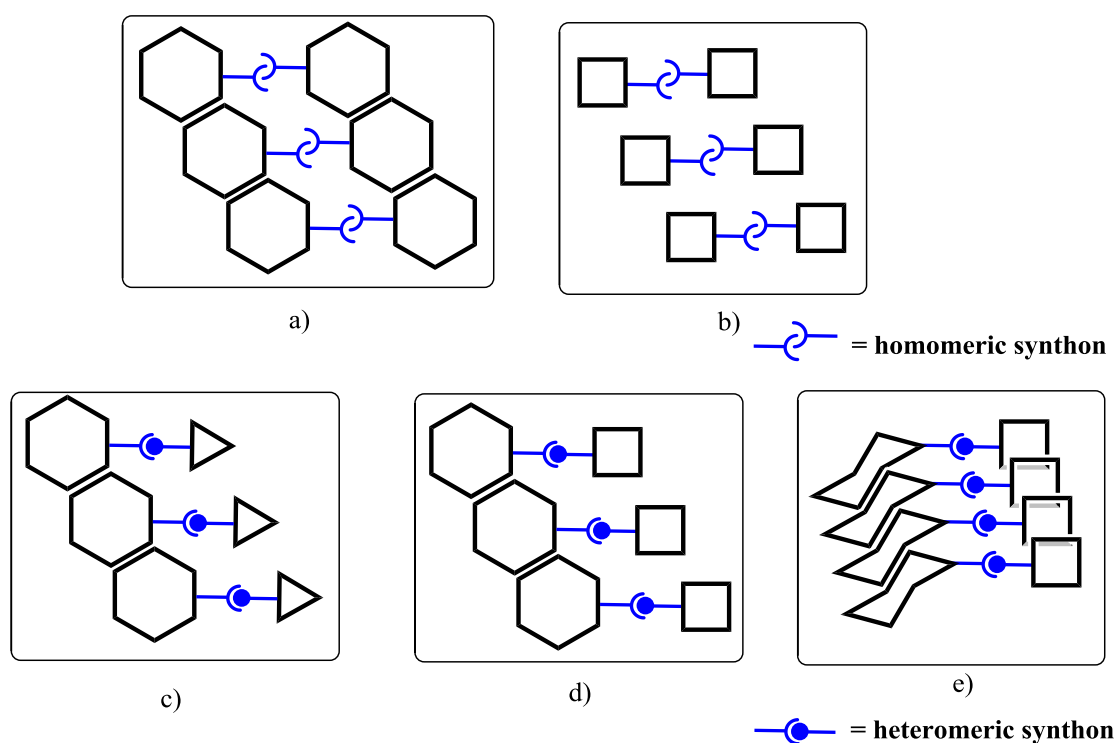


Figure 1.8 Schematic showing transferable nature of synthons; supermolecules a) and b) contains homomeric synthon, supermolecules b), c) and d) contains heteromeric synthon.

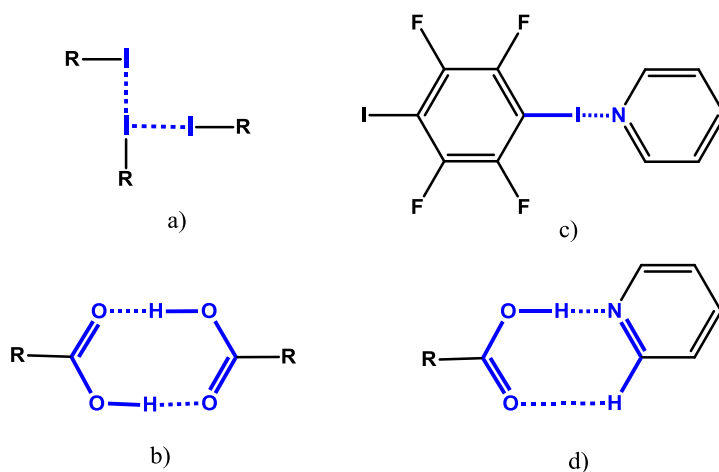


Figure 1.9 Some examples of synthons; a) Iodo...iodo,²⁶ b) acid...acid,²⁷ c) Iodo...pyridine²⁸ and d) carboxylic acid...pyridine.¹⁷

1.2.4 Co-crystallization as a tool for understanding intermolecular interactions

The use of synthons for combining different neutral molecular species within a single crystalline lattice without making or breaking covalent bonds is called co-crystallization, Figure 1.10. The overall aim of a co-crystallization reaction is to obtain a heteromeric compound, rather than a homomeric species (recrystallization), Figure 1.10.

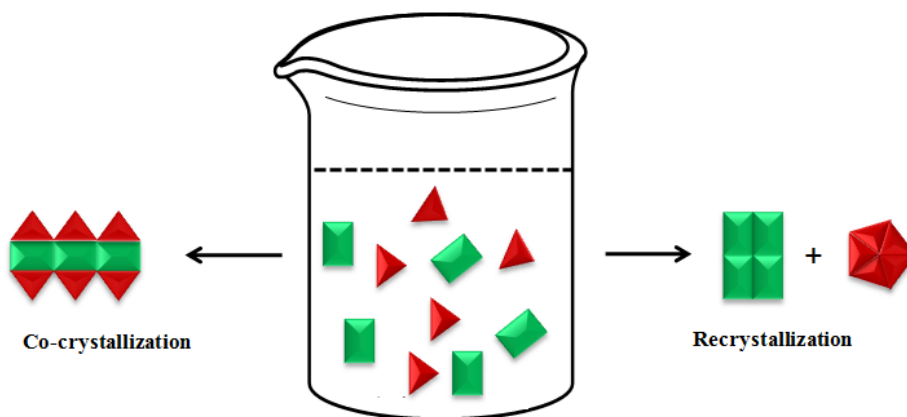


Figure 1.10 Recrystallization (right) yields homomeric solids. The co-crystallization process (left) leads to a heteromeric product.

Co-crystals have gained attention due to their ability to modulate the properties of simple organic solids, such as, solubility, thermal stability, mechanical properties (including active pharmaceutical ingredients).²⁹ The inherently selfish nature of molecules hinders co-crystal formation and they tend to stick with themselves. However, by developing new synthetic strategies we can increase the chances of obtaining a heteromeric product.

Etter developed a set of guidelines for introducing the idea of systematically looking at hydrogen-bond patterns in molecular aggregates.³⁰ An in-depth study of the structures from Cambridge Structural Database (CSD), led to a set of rules that can be followed when attempting to design and synthesize supermolecules;

- 1) All proton donors and acceptors will participate in hydrogen bonding.
- 2) A six-membered intramolecular arrangement will form in preference to intermolecular hydrogen bonds.
- 3) The best proton donor and acceptor remaining after intramolecular hydrogen-bond formation will form an intermolecular hydrogen-bond, Figure 1.11.

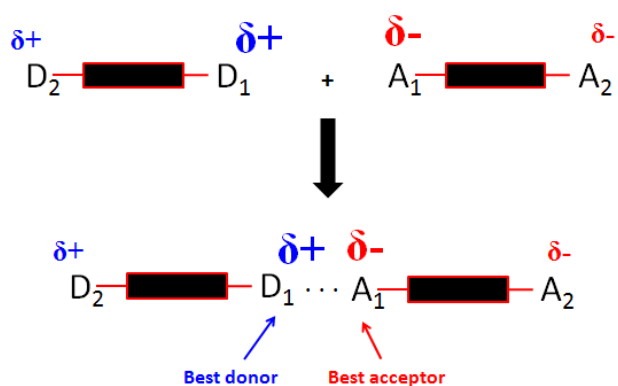


Figure 1.11 Schematic of best donor-best acceptor rule from Etter's guidelines.

Hunter has shown that hydrogen bonding mainly involves electrostatic interactions and the molecular electrostatic potential (MEP) of a given atom (donor or acceptor) which can be determined using theoretical calculations, provides a useful method for ranking different donors/acceptors.³¹ Many binary (two component) co-crystals have been synthesized,^{32,33} which agrees with Etter's rule of *the best donor hydrogen bonding to the best acceptor*, Figure 1.12.³⁴

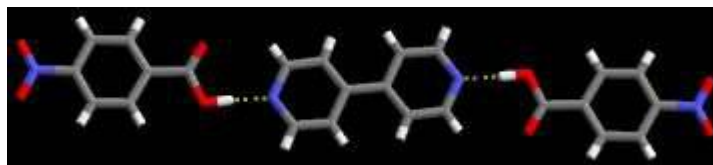


Figure 1.12 Example of supermolecule in binary 1:2 co-crystals of 4,4'-bipyridine and 4-nitrobenzoic acid.³⁴

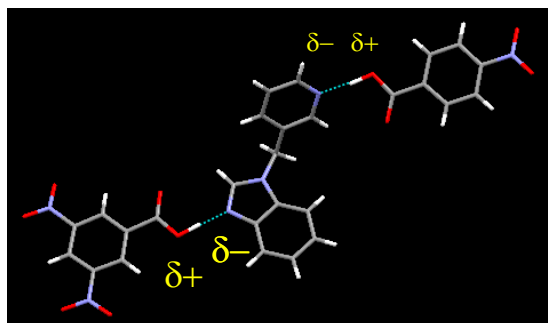


Figure 1.13 The ternary supermolecule showing the best hydrogen-bond donor binding to the best hydrogen-bond acceptor and the second-best donor binding to the second-best acceptor.³⁵

Moreover, the higher order co-crystals have been synthesized by systematically modulating the electrostatic charges on the acceptor sites via covalent modification. The probe molecules with best acceptor (highest MEP charge) and second best acceptor (second highest MEP charge) were synthesized and co-crystallized with pairs of different carboxylic acids in a 1:1:1 ratio. The outcome of these supramolecular reactions was governed by Etter's rule forming ternary co-crystal in predictable stoichiometry and connectivity, Figure 1.13.³⁵ These elegant examples clearly demonstrate how electrostatic potential charges can be translated into supramolecular reactivity and selectivity.

Above discussion provokes many questions, such as;

1. Can we achieve *synthon selectivity* in crystal engineering similar to selectivity in organic synthesis?
2. Will Etter's best donor binding to best acceptor strategy work for halogen bonding?

We will examine molecular recognition in small molecules at first and extend it into larger functional molecules to establish robust and versatile supramolecular synthetic methods. In a pursuit of finding the answers to above mentioned questions and to better understand the non-covalent interactions, the goals pursued in this thesis are as follows:

I. Control supramolecular yield via covalent modification of supramolecular reagents and to establish the binding preference of hydrogen-bond donor molecules with ditopic hydrogen-bond acceptor molecule (Chapter 2).

II. Achieve *synthon selectivity* by combining hydrogen-bonding and halogen-bonding interactions in a supramolecular system and utilizing *geometric bias* (Chapter 3).

III. Establish hierarchy in halogen-bonding interaction based on *electrostatic bias*. The library of probe molecules equipped with best halogen-bond donor and second best halogen-bond donor will be synthesized and co-crystallized with variety of halogen bond acceptors to test the hierarchy of interactions in solid-state (Chapter 4).

IV. Develop the synthetic protocols for facile functionalization of cavitand macrocycles. The versatile Suzuki-Miyaura coupling reaction and ‘solvent assisted grinding’ protocol for decorating cavitand with novel oxime functionality will be developed (Chapter 5).

V. Design and synthesize molecular capsules from cavitand functionalized with hydrogen bond donor or acceptor groups. The cavitands bearing pyridyl and carboxylic acid groups will be synthesized. Their ability to co-crystallize as well as to give hydrogen-bonded capsules will be studied (Chapter 6).

References:

- ¹ First organic molecule (urea) was reported in 1828, see; Wöhler, F. H. *Ann. Phys.Chem.* **1828**, *12*, 253.
- ² Kadota, I.; Takamura, H.; Sato, K.; Ohno, A.; Matsuda, K.; Yamamoto, Y. *J. Am. Chem. Soc.* **2003**, *125*, 46.
- ³ Lehn, J. –M. *Supramolecular Chemistry*, VCH, Weinheim, **1995**.
- ⁴ Grepioni, F.; Braga, D. (Eds.), *Making Crystals by Design-from Molecules to Molecular Materials, Methods, Techniques, Applications*, Wiley- VCH: Weinheim, Germany, **2007**.
- ⁵ a) Dunitz, J. D. *Pure Appl. Chem.* **1991**, *63*, 177. b) Dunitz, J. D. *Perspectives in Supramolecular Chemistry*; Desiraju, G. R., Ed.; Wiley: New York, **1996**; Vol. 2.
- ⁶ Schmidt, G. M. J. *Pure Appl. Chem.* **1971**, *27*, 647.
- ⁷ Muthuraman, M.; Masse, R.; Nicoud, J.-F.; Desiraju, G. R. *Chem. Mater.* **2001**, *13*, 1473.

-
- ⁸ Kahn, O. *Acc. Chem. Res.* **2000**, *33*, 1.
- ⁹ Bach, T.; Bergmann, T.; Harms, K. *Org. Lett.* **2001**, *3*, 601.
- ¹⁰ Atwood, J. L.; Koutsantonis, G. A.; Raston, C. L. *Nature* **1994**, *368*, 229.
- ¹¹ a) Aakeröy, C. B.; Desper, J.; Urbina, J. F. *Chem. Commun.* **2005**, 2820. b) Aakeröy, C. B.; Desper, J.; Scott, B. M. T. *Chem. Commun.* **2006**, 1445.
- ¹² a) Hoffart, D. J.; Tiburcio, J.; De la Torre, A.; Knight, L. K.; Loeb, S. J. *Angew. Chem. Int. Ed.* **2008**, *47*, 97. b) Immke, D.; Korn, S. J. *J. Gen. Physiol.* **2000**, *115*, 509.
- ¹³ a) Adhikari, S.; Ueren, A.; Roy, R. *J. Biol. Chem.* **2008**, *283*, 1334. b) Mu, Y.; Gao, Y. Q. *J. Chem. Phys.* **2007**, *127*, 105102. c) Persson, B. N. J.; Ryberg, R. *Phys. Rev. B* **1981**, *24*, 6954.
- ¹⁴ a) Dosi, C.; Giglio, E.; Pavel, V.; Ouagliata, C. *Acta Cryst.* **1973**, *A29*, 644. b) Bockris, J. O'M.; Reddy, K. N.; Gamboa-Aldeco, M. *Modern Electrochemistry 1*, Springer, **2000**.
- ¹⁵ Kitaigorodski, A. I. *Molecular Crystals and Molecules*, Academic press, New York, **1973**.
- ¹⁶ a) Barooah, N.; Sarma, R. J.; Baruah, J. B. *CrystEngComm* **2006**, *8*, 608. b) Motohiro, N. *CrystEngComm* **2004**, *6*, 130.
- ¹⁷ a) Aakeröy, C. B.; Salmon, D. J. *CrystEngComm* **2005**, *7*, 439. b) MacGillivray, L. *CrystEngComm* **2004**, *6*, 77. c) Lehn, J.-M. *Science* **2002**, *295*, 2400. d) Desiraju, G. R. *Acc. Chem. Res.* **2002**, *35*, 565. e) Moulton, B.; Zaworotko, M. J. *Chem. Rev.* **2001**, *101*, 1629. f) Desiraju, G. R. *Angew. Chem., Int. Ed.* **1995**, *34*, 2311. g) Wenger, M.; Bernstein, J. *Angew. Chem., Int. Ed.* **2006**, *45*, 7966. h) Childs, S. L.; Hardcastle, K. I. *CrystEngComm* **2007**, *9*, 64. i) Bosch, E. *CrystEngComm* **2007**, *9*, 191. j) Pedireddi, V. R.; Chatterjee, S.; Ranganathan, A.; Rao C. N. R. *J. Am. Chem. Soc.* **1997**, *119*, 10867.
- ¹⁸ Jeffrey, G. A.; Saenger, W. *Hydrogen Bonding in Biological Structures*, Springer-Verlag, Berlin, Heidelberg, New York, **1991**.
- ¹⁹ <http://ghr.nlm.nih.gov/handbook/basics/dna>
- ²⁰ a) Metrangolo, P.; Resnati, G. *Chem. Eur. J.*, **2001**, *7*, 2511. b) Metrangolo, P.; Neukirch, H.; Pilati, T.; Resnati, G. *Acc. Chem. Res.* **2005**, *38*, 386.
- ²¹ Legon, A. C. *Angew. Chem.* **1999**, *111*, 2850.
- ²² Legon, A. C. *Angew. Chem. Int. Ed.* **1999**, *38*, 2686.
- ²³ Legon, A. C. in *Halogen Bonding Fundamentals and Applications*, eds Metrangolo, P.; Resnati, G. Springer, Berlin, **2008**, 17-64.
- ²⁴ Metrangolo, P.; Meyer, F.; Pilati, T.; Resnati, G.; Terraneo, G. *Angew. Chem. Int. Ed.* **2008**, *47*, 6114.
- ²⁵ Desiraju, G. R. *Angew. Chem., Int. Ed.* **1995**, *34*, 2311.
- ²⁶ Reddy, C. M.; Kirchner, M. T.; Gundakaram, R. C.; Padmanabhan, K. A.; Desiraju, G. R. *Chem. Eur. J.* **2006**, *12*, 2222.
- ²⁷ a) Duchamp, D. J.; Marsh, R. E. *Acta Crystallogr.* **1969**, *B25*, 5. b) Cate, A. T. T.; Kooijman, H.; Spek, A. L.; Sijbesma, R. P.; Meijer, E. W. *J. Am. Chem. Soc.* **2004**, *126*, 3801. c) Bruno, G.; Randaccio, L. *Acta Crystallogr.* **1980**, *B36*, 1711. d) Ermer, O. *J. Am. Chem. Soc.* **1988**, *110*, 3747.

-
- ²⁸ Walsh, R. B.; Padgett, C. W.; Metrangolo, P.; Resnati, G.; Hanks, T. W.; Pennington, W. T. *Cryst. Growth Des.* **2001**, *1*, 165.
- ²⁹ Schultheiss, N.; Newman, A. *Cryst. Growth Des.* **2009**, *9*, 2950.
- ³⁰ a) Etter, M. C. *J. Phys. Chem.* **1991**, *95*, 4601. (b) Etter, M. C. *Acc. Chem. Res.* **1990**, *23*, 120.
- ³¹ Hunter, C. A. *Angew. Chem. Int. Ed.* **2004**, *43*, 5310.
- ³² Aakeröy, C. B.; Beatty, A. M.; Helfrich, B. A.; Nieuwenhuyzen, M. *Cryst. Growth Des.* **2003**, *3*, 159.
- ³³ Aakeröy, C. B.; Desper, J.; Helfrich, B. A. *CrystEngComm* **2004**, *6*, 19.
- ³⁴ Bowers, J. R.; Hopkins, G. W.; Yap, G. P. A.; Wheeler, K. A. *Cryst. Growth Des.*, **2005**, *5*, 727.
- ³⁵ Aakeröy, C. B.; Desper, J.; Urbina, J. F. *Chem. Commun.*, **2005**, 2820.

Chapter 2 - Mapping the binding preferences of 2-aminopyrazines via co-crystallizations

2.1 Introduction

Supramolecular synthesis is gathering momentum primarily due to its applications in the area of pharmaceuticals.¹ Co-crystallization is often considered a better alternative to salts in optimizing drug properties especially when salts do not have the appropriate solid state properties or cannot be formed due to the absence of ionizable sites in the API.² Pharmaceutical co-crystals can be used to address physical-property issues such as melting behavior,³ solubility,⁴ dissolution⁵ and bioavailability⁶ in pharmaceutical development without changing the chemical composition of the active pharmaceutical ingredient, API. Recently our group successfully demonstrated that, if we can achieve structural consistency, in terms of binding of API with a co-former, then it is possible to gain control over properties such as, thermal stability and solubility.⁷

Supramolecular synthesis is based on non-covalent interactions which are reversible in nature. Due to this reversibility, supramolecular chemists often come across difficulties in synthesizing desired supermolecules. However, it has been shown that if these non-covalent interactions are fine-tuned electronically and geometrically then it is possible to obtain more predictable binding.⁸ In the past few years, several efforts have been made to identify robust supramolecular synthons, and the reliability of homomeric self-complementary pair-wise hydrogen bonds, e.g. amide...amide, carboxylic acid...carboxylic acid and oxime...oxime, have been established through extensive structural⁹ and database studies (Figure 2.1a).¹⁰ Some heteromeric interactions are particularly robust, for example, carboxylic acid...pyridine,¹¹ hydroxy...pyridine,¹² and hydroxy...amine,¹³ which have allowed for the assembly of a wide range of binary cocrystals in predictable manner (Figure 2.1b). A remaining problem in supramolecular synthesis arises however, when multiple binding sites are present, yielding multiple possible outcomes (Figure 2.2).

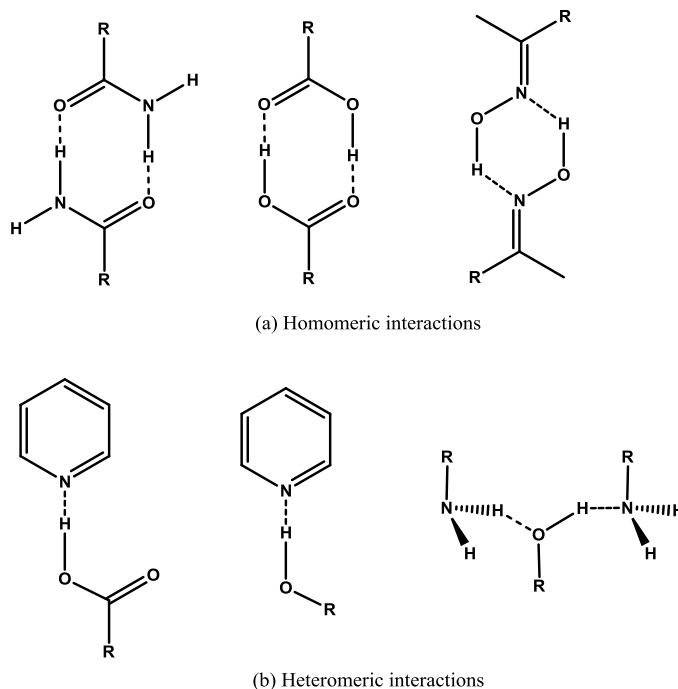


Figure 2.1 Examples of a) homomeric and b) heteromeric hydrogen-bond interactions.

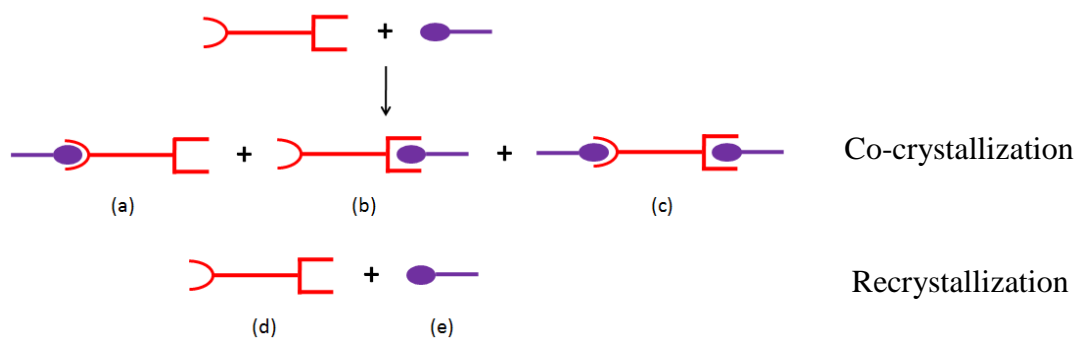


Figure 2.2 Possible outcomes when a ditopic acceptor molecule is combined with a monotopic donor molecule. Heteromeric products (a), (b) and (c); homomeric products (d) and (e).

In order to develop versatile supramolecular synthetic strategies based on hydrogen-bond (HB) driven self-assembly it is necessary to identify building blocks that display reliable binding preferences in the presence of wide range of chemical functionalities. The Cambridge Structural Database¹⁴ (CSD) plays vital role in choosing building blocks for our studies. A CSD search on a combination of carboxylic acid with 2-aminopyridine yielded 103 hits and a search based on a combination of carboxylic acid and pyridine resulted in 500 hits (Figure 2.3). The CSD structural

analysis clearly indicates that the carboxylic acid can bind to both 2-aminopyridine and pyridine based moieties.

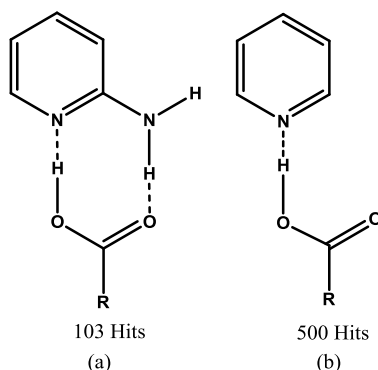


Figure 2.3 CSD structural analysis results for combination of carboxylic acid with (a) 2-aminopyridine, and (b) pyridine.

The goal of this study is to establish the binding preference of a carboxylic acid when these (Figure 2.3) two binding sites are present on same molecule. We chose 2-aminopyridine as the test system due to presence of the 2-NH₂-pyridine end and the second heterocyclic nitrogen (Figure 2.4). Furthermore, understanding the molecular recognition processes of this ditopic molecule will provide us with valuable information, which can be used to understand binding in larger and more complicated events, such as drug-protein binding.

We also wanted to investigate if we can control the heteromeric product formation over homomeric product formation (Figure 2.2). Since the electrostatic nature of hydrogen bonds is based on the Coulombic attraction between an acidic hydrogen atom and a suitable acceptor atom with partial negative charge,¹⁵ it is possible to control heteromeric product formation by modulating charges on the binding sites. Hunter^{15a} established how simple molecular electrostatic potential (MEP) surface calculations can be used to assign relative hydrogen-bond donor/acceptor strengths of chemical functionalities, and we will employ this approach to quantifying the electrostatic charge on individual atoms within molecules. We hypothesized that decreasing the charge on the hydrogen-bond acceptor would reduce the success rate of co-crystal formation. Simple covalent modifications offer (by adding electron withdrawing/electron donating group) the best opportunity for reducing/increasing the charge on each binding site. We opted for three test molecules in this study, Figure 2.4, all of which have the main two binding

sites, and where the charge on the binding sites is reduced on the nitrogen atoms through subsequent additions of one and two electron withdrawing substituents, respectively.

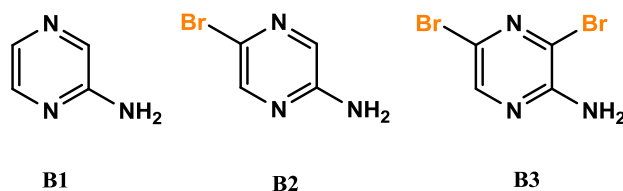


Figure 2.4 Ditopic supramolecular reagents for supramolecular synthesis.

To study binding preferences with **B1-B3**, carboxylic acids were chosen in such a way that we could cover range of aliphatic and aromatic carboxylic acids, both weak and strong, to ensure that the nature of the carboxylic acids does not affect binding preference. Based on a CSD structural analysis, we have postulated series of synthons which could result from non-covalent synthesis of **B1-B3** and carboxylic acids (Figure 2.5).

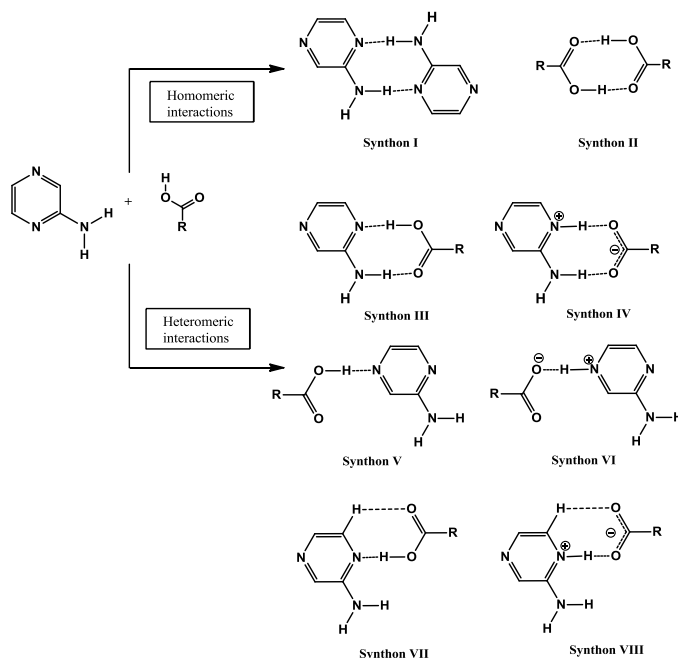


Figure 2.5 Postulated homo- and hetero synthons in supramolecular synthesis with 2-aminopyrazine derivatives and carboxylic acids.

In this chapter we will address/answer following questions:

I. Can we control the supramolecular yield by modulating charges on hydrogen-bond acceptor binding sites?

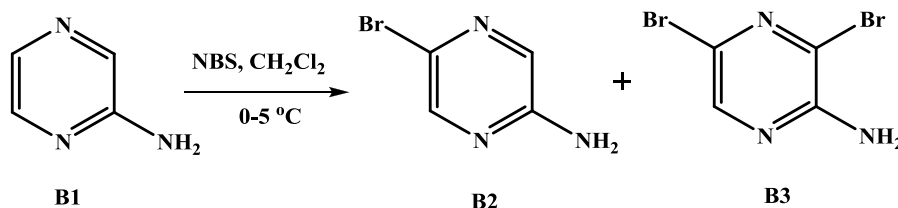
II. Is it possible to control binding preference of carboxylic acids with 2-aminopyrazine derivatives?

2.2 Experimental

2.2.1 Synthesis

All chemicals, unless otherwise noted, were purchased from Aldrich and used without further purification. *N*-bromosuccinamide was purchased from Acros chemicals. 2-aminopyrazine was purchased from Matrix scientific. Column chromatography was carried out on silica gel (150 Å pore size) from Analtech Inc. Melting points were determined on a Fisher-Johns melting point apparatus. ¹H and ¹³C NMR spectra were recorded on a Varian Unity plus 400 MHz or 200 MHz spectrometer in CDCl₃ or DMSO-d₆. Data is expressed in parts per million (ppm) downfield shift from tetramethylsilane or residual protiosolvent as an internal reference and are reported as position (in ppm), multiplicity (s = singlet, d = doublet, t = triplet, m = multiplet), coupling constant (*J* in Hz) and integration (number of protons). Infrared spectroscopy (IR) was done on a Nicolet 380 FT-IR.

2.2.2.1 Synthesis of 2-amino-5-bromopyrazine, B2 and 2-amino-3,5-dibromopyrazine, B3



A solution of *N*-bromosuccinimide (2.4 g, 13.4 mmol) in methylene chloride was added dropwise to 2-aminopyrazine (1.0 g, 10.6 mmol) dissolved in methylene chloride and cooled to 0-5 °C (using an ice bath). The reaction mixture was stirred at 0-5 °C for 2 hrs. The reaction was monitored closely by TLC and upon completion, was quenched with 10% sodium bicarbonate and 10% sodium sulfite solutions. The mixture was filtered and the precipitate washed with water. The filtrate was extracted with methylene chloride and dried over anhydrous magnesium

sulfate. The solvent was removed on a rotary evaporator and the residue was chromatographed on silica with a hexane:ethyl acetate (10:0→4:6) mixture as eluant. **B2** was isolated as a yellowish-white powder and **B3** as a white powder. The products were recrystallized from ethyl acetate:hexane (1:1). **B2** (2-amino-5-bromopyrazine), (2.70 g, 62%). M. P. 105-107 °C (Reported M. P. 105-110 °C¹⁶); ¹H NMR (δ_{H} ; 400 MHz, CDCl₃): 8.09 (s, 1H), 7.78 (s, 1H), 4.784 (br, 2H); ¹³C NMR (δ_{C} ; 400 MHz, CDCl₃):153.45, 144.11, 131.73, 126.92. IR (neat) : ν (cm⁻¹) 3397, 3280, 3167, 1626, 1566, 1530, 1458, 1405, 1376, 1209, 1101, 1009, 877, 644. **B3** (2-amino-3,5-dibromopyrazine), (0.76 g, 12%). M. P. 111-113 °C (Reported M. P. 109-110 °C¹⁷); ¹H NMR (δ_{H} ; 400 MHz, CDCl₃): 8.04 (s, 1H), 5.13 (br, 2H); ¹³C NMR (δ_{C} ; 400 MHz, CDCl₃): 151.86, 143.08, 123.91, 123.57; IR (neat) : ν (cm⁻¹) 3447, 3280, 3154, 1621, 1547, 1506, 1450, 1315, 1133, 1096, 1040, 908, 877, 696, 636.

2.2.2 Synthesis of co-crystals and salts

2-Aminopyrazine based ditopic acceptor ligands, **B1-B3** were subjected to cocrystallization reactions with thirty different carboxylic acids. We used twenty aromatic monocarboxylic acids: 4-aminobenzoic acid **A1**, 4-hydroxybenzoic acid **A2**, 3,5-dihydroxybenzoic acid **A3**, 2,4-dimethoxybenzoic acid **A4**, 3,4-dihydroxybenzoic acid **A5**, 2,3-dihydroxybenzoic acid **A6**, 2,5-dihydroxybenzoic acid **A7**, 2,3-dimethylbenzoic acid **A8**, 2,5-dimethylbenzoic acid **A9**, benzoic acid **A10**, 4-nitrobenzoic acid **A11**, 4-fluorobenzoic acid **A12**, pentafluorobenzoic acid **A13**, 3,5-dinitrobenzoic acid **A14**, 2,4-dinitrobenzoic acid **A15**, 3-nitrobenzoic acid **A16**, 2-chloro-6-fluorobenzoic acid **A17**, 2,6-difluorobenzoic acid **A18**, 3-fluorobenzoic acid **A19**, 4-cynaobenzoic acid **A20**, and ten aliphatic dicarboxylic acids: oxalic acid **A21**, malonic acid **A22**, succinic acid **A23**, glutaric acid **A24**, adipic acid **A25**, pimelic acid **A26**, suberic acid **A27**, azelic acid **A28**, sebacic acid **A29** and dodecanedioic acid **A30**.

Stoichiometric amounts of base **B1-B3** and acid, either 1:1 (monoacids, **A1-A20**) or 2 : 1 (diacids, **A21-A30**), were mixed together. ‘Solvent assisted grinding’ was performed on all 90 (30x3) combinations and IR analysis was done to determine the outcome of each reaction. Methanol was used as a solvent for the grinding experiments. If the IR data showed that the reaction occurred, then slow evaporation at room temperature was carried out using suitable solvents. Acids and bases were first dissolved separately and then mixed together in a

borosilicate vial which was left at room temperature for slow evaporation to grow single crystals for X-ray diffraction analysis (twelve single crystals were obtained using this method).

2.2.2.1 Synthesis of 2-aminopyrazine 4-nitrobenzoic acid (1:2), B1-A11

2-Aminopyrazine (0.020 g, 0.21 mmol) was dissolved in 1 mL of methanol. To this solution was added 4-nitrobenzoic acid (0.035 g, 0.21 mmol) in 3 mL of methanol. The resulting solution was warmed and allowed to stand for slow evaporation at room temperature. Colorless crystals were obtained after 5 days. M.p. 200-202 °C.

2.2.2.2 Synthesis of 2-aminopyrazinium 3,5-dinitrobenzoate, B1-A14

2-Aminopyrazine (0.020 g, 0.21 mmol) was dissolved in 1 mL of methanol. To this solution was added 3,5-dinitrobenzoic acid (0.044 g, 0.21 mmol) in 3 mL of methanol. The resulting solution was warmed and allowed to stand for slow evaporation at room temperature. Colorless crystals were obtained after 7 days. M.p. 158-160 °C.

2.2.2.3 Synthesis of 2-aminopyrazine 3-nitrobenzoic acid (1:1), B1-A16

2-Aminopyrazine (0.020 g, 0.21mmol) was dissolved in 1 mL of methanol. To this solution was added 3-nitrobenzoic acid (0.035g, 0.21 mmol) in 3 mL of methanol. The resulting solution was warmed and allowed to stand for slow evaporation at room temperature. Colorless crystals were obtained after 5 days. M.p. 134-136 °C.

2.2.2.4 Synthesis of 2-aminopyrazine succinic acid (1:1), B1-A23

2-Aminopyrazine (0.020 g, 0.21 mmol) was dissolved in 1 mL of methanol. To this solution was added succinic acid (0.006 g, 0.11 mmol) in 3 mL of methanol. The resulting solution was warmed and allowed to stand for slow evaporation at room temperature. Colorless crystals were obtained after 7 days. M.p. 140-142 °C.

2.2.2.5 Synthesis of 2-aminopyrazine glutaric acid (1:1), B1-A24

2-Aminopyrazine (0.020 g, 0.21mmol) was dissolved in 1 mL of methanol. To this solution was added glutaric acid (0.013g, 0.11 mmol) in 3 mL of methanol. The resulting solution was warmed and allowed to stand for slow evaporation at room temperature. Colorless crystals were obtained after 4 days. M.p. 126-128 °C.

2.2.2.6 Synthesis of 2-aminopyrazine pimelic acid (1:1), B1-A26

2-Aminopyrazine (0.020 g, 0.21 mmol) was dissolved in 1 mL of methanol. To this solution was added pimelic acid (0.016 g, 0.11 mmol) in 3 mL of methanol. The resulting solution was warmed and allowed to stand for slow evaporation at room temperature. Colorless crystals were obtained after 3 days. M.p. 108-110 °C.

2.2.2.7 Synthesis of 2-aminopyrazine suberic acid (1:1), B1-A27

2-Aminopyrazine (0.020 g, 0.21 mmol) was dissolved in 1 mL of methanol. To this solution was added suberic acid (0.018 g, 0.11 mmol) in 3 mL of methanol. The resulting solution was warmed and allowed to stand for slow evaporation at room temperature. Colorless crystals were obtained after 5 days. M.p. 210-212 °C.

2.2.2.8 Synthesis of 2-aminopyrazine sebacic acid (1:1), B1-A29

2-Aminopyrazine (0.020 g, 0.21 mmol) was dissolved in 1 mL of methanol. To this solution was added sebacic acid (0.021 g, 0.11 mmol) in 3 mL of methanol. The resulting solution was warmed and allowed to stand for slow evaporation at room temperature. Colorless crystals were obtained after 4 days. M.p. 124-126 °C.

2.2.2.9 Synthesis of 2-amino-3,5-dibromopyrazine 2,5-dihydroxybenzoic acid (1:1), B3-A7

2-Amino-3,5-dibromopyrazine (0.020 g, 0.08 mmol) was dissolved in 1 mL of methanol. To this solution was added 2,5-dihydroxybenzoic acid (0.012 g, 0.08 mmol) in 3 mL of methanol. The resulting solution was warmed and allowed to stand for slow evaporation at room temperature. Colorless crystals were obtained after 7 days. M.p. 180-182 °C.

2.2.2.10 Synthesis of 2-amino-3,5-dibromopyrazine pentafluorobenzoic acid (1:1), B3-A13

2-Amino-3,5-dibromopyrazine (0.020 g, 0.08 mmol) was dissolved in 1 mL of ethanol. To this solution was added pentafluorobenzoic acid (0.016 g, 0.08 mmol) in 3 mL of ethanol. The resulting solution was warmed and allowed to stand for slow evaporation at room temperature. Colorless crystals were obtained after 4 days. M.p. 98-100 °C.

2.2.2.11 Synthesis of 2-amino-3,5-dibromopyrazine 3,5-dinitrobenzoic acid (1:1), B3-A14

2-Amino-3,5-dibromopyrazine (0.020 g, 0.08 mmol) was dissolved in 1 mL of ethanol. To this solution was added 3,5-dinitrobenzoic acid (0.016 g, 0.08 mmol) in 3 mL of ethanol. The

resulting solution was warmed and allowed to stand for slow evaporation at room temperature. Colorless crystals were obtained after 7 days. M.p. 128-130 °C.

2.2.2.12 Synthesis of 2-amino-3,5-dibromopyrazine 2,6-difluorobenzoic acid (1:1), B3·A18

2-Amino-3,5-dibromopyrazine (0.020 g, 0.08 mmol) was dissolved in 1 mL of ethanol. To this solution was added 2,6-difluorobenzoic acid (0.012 g, 0.08 mmol) in 3 mL of ethanol. The resulting solution was warmed and allowed to stand for slow evaporation at room temperature. Colorless crystals were obtained after 3 days. M.p. 144-146 °C.

2.2.3 Molecular electrostatic potential charge calculations

The molecular structures of **B1-B3** were constructed using Spartan '04 (Wavefunction, Inc. Irvine, CA). All three molecules were geometry optimized using PM3, with the maxima and minima in the electrostatic potential surface (0.002 e/au isosurface) determined using a positive point charge in the vacuum as a probe. The numbers indicate the interaction energy (kJ/mol) between positive point probe and surface of molecule at that particular point. These numbers could be correlated to the electrostatic charges on the atoms with the negative number corresponding to negative charge and positive number corresponding to positive charge.

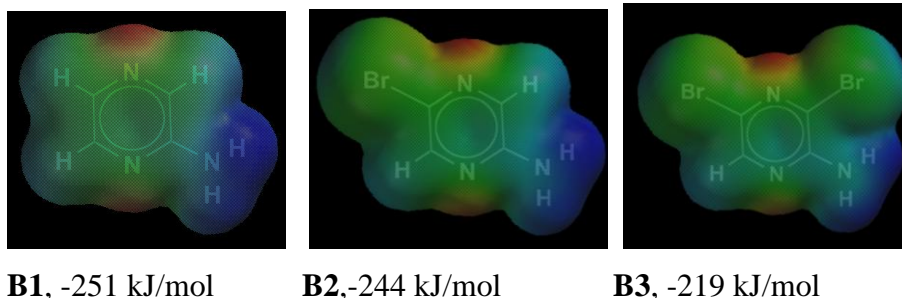


Figure 2.6 MEP surface calculations of 2-aminopyrazine and brominated analogues thereof.

Numbers reflect the charge on the N1 nitrogen atom in each molecule.

2.2.4 Single Crystal X-ray Crystallography

X-ray data were collected on a Bruker SMART APEX or a SMART 1000 diffractometer using Mo K α radiation and, where noted, were corrected for absorption using the multiscan procedure implemented by SADABS. Data were collected using SMART.

2.3 Results

2.3.1 Characterization by IR spectroscopy

The distinction between reaction (salt/co-crystal) and no reaction was made based on the presence/absence of broad stretches near 1850 and 2500 cm^{-1} which are indicative of intermolecular $\text{OH}\cdots\text{N}$ (heterocycle) hydrogen bonds, and which will only appear in salts and co-crystals, and not in physical mixtures of the two reactants. This feature is usually assigned to Fermi resonance of OH stretching and overtones of bending modes in $\text{OH}\cdots\text{N}$ complexes.¹⁸ The outcome is shown in Table 2.1. Based on IR spectroscopy we determined that base **B1**, the strongest base of the three, produced an 83% supramolecular yield followed by 40% and 20% supramolecular yields for **B2** and **B3**, respectively.

Table 2.1 IR stretching frequencies (cm⁻¹) of salts and co-crystals of the ligands **B1-B3**.

	Acid	B1	B2	B3
A1	4-Aminobenzoic acid	-	-	-
A2	4-Hydroxybenzoic acid	1898, 2521	1898, 2521	-
A3	3,5-Dihydroxybenzoic acid	1878, 2607	1878, 2607	-
A4	2,4-Dimethoxybenzoic acid	1865, 2475	1865, 2475	-
A5	3,4-Dihydroxybenzoic acid	1891, 2448	1891, 2448	-
A6	2,3-Dihydroxybenzoic acid	-	-	-
A7	2,5-Dihydroxybenzoic acid	-	1865, 2410	1818, 2481
A8	2,3-Dimethylbenzoic acid	1885, 2400	-	-
A9	2,5-Dimethylbenzoic acid	-	-	-
A10	Benzoic acid	1911, 2441	-	-
A11	4-Nitrobenzoic acid	1881, 2409	-	-
A12	4-Fluorobenzoic acid	1891, 2521	-	-
A13	Pentafluorobenzoic acid	2050, 2400	-	1879, 2407
A14	3,5-Dinitrobenzoic acid	1860, 2687	1871, 2495	1851, 2355
A15	2,4-Dinitrobenzoic acid	2018, 2381	-	-
A16	3-Nitrobenzoic acid	1898, 2428	-	1851, 2481
A17	2-Chloro-6-fluorobenzoic acid	-	-	1865, 2468
A18	2,6-Difluorobenzoic acid	2004, 2614	-	-
A19	3-Fluorobenzoic acid	1891, 2475	1851, 2521	-
A20	4-Cyanobenzoic acid	1879, 2438	1859, 2448	-
A21	Oxalic acid	2006, 2522	1911, 2349	1838, 2427
A22	Malonic acid	1854, 2455	1918, 2528	-
A23	Succinic acid	1920, 2414	-	-
A24	Glutaric acid	1854, 2400	-	-
A25	Adipic acid	1920, 2520	1859, 2545	-
A26	Pimelic acid	1877, 2495	1869, 2413	-
A27	Suberic acid	1881, 2495	-	-
A28	Azelaic acid	1861, 2483	2450, 1850	-
A29	Sebacic acid	1887, 2475	1834, 2518	-
A30	Dodecanedioic acid	1895, 2507	-	-

2.3.2 Crystal structures

A total of 13 crystal structures were obtained, out of which one crystal structure is of **B3** itself, eleven are co-crystals, and one is a salt.

A summary of the crystallographic information for the salts and co-crystals is presented in Appendix A. Hydrogen-bond geometries for **B3** and all co-crystals/salts are displayed in Table 2.2.

Table 2.2 Hydrogen-bond Geometries for **B3**, **B1·A11**, **B1·A14**, **B1·A16**, **B1·A23**, **B1·A24**, **B1·A26**, **B1·A27**, **B1·A29**, **B3·A7**, **B3·A13**, **B3·A14** and **B3·A18**.

Structure	D-H...A	d(D-H)/Å	d(H...A)/Å	d(D...A)/Å	<(DHA)/°
B3 ⁱ	N(13)-H(13A)...N(14)#1	0.830(19)	2.23(2)	3.0557(17)	174.9(18)
B1·A11 ⁱⁱ	O(17)-H(17)...N(21)	0.82	1.95	2.744(6)	163.9
	O(18)-H(18)...N(24)#1	0.82	1.89	2.704(5)	171.1
	N(22)-H(22A)...O(18)	0.92(6)	2.11(7)	3.006(10)	164(5)
	N(22)-H(22B)...O(17)#2	0.92(6)	2.28(6)	3.194(11)	175(6)
B1·A14 ⁱⁱⁱ	N(11)-H(11)...O(21)	0.97(4)	1.61(4)	2.573(4)	169(4)
	N(12)-H(12A)...O(22)	0.84(5)	1.95(5)	2.790(4)	178(4)
	N(12)-H(12B)...O(25)#1	0.92(5)	2.39(4)	3.096(4)	133(3)
	N(12)-H(12B)...O(26)#1	0.92(5)	2.29(5)	3.187(5)	166(4)
B1·A16 ^{iv}	O(11)-H(11)...N(21)	0.965(17)	1.660(17)	2.6174(14)	170.7(14)
	N(22)-H(22A)...O(12)	0.86(3)	2.12(3)	2.967(2)	167(3)
	N(22)-H(22B)...O(14)#2	0.85(3)	2.22(3)	3.027(2)	158(3)
B1·A23 ^v	O(21)-H(21)...N(14)	0.93(4)	1.72(4)	2.643(4)	168(4)
	N(12)-H(12A)...N(11)#2	0.85(5)	2.19(5)	3.036(4)	176(4)
	N(12)-H(12B)...O(22)#3	0.86(4)	2.17(5)	3.018(4)	168(4)
B1·A24 ^{vi}	N(12)-H(12A)...O(22)	0.906(19)	2.261(19)	3.1366(16)	162.3(15)
	N(12)-H(12B)...O(26)#1	0.835(19)	2.21(2)	3.0153(15)	161.5(18)
	O(21)-H(21)...N(11)	0.91(2)	1.77(2)	2.6792(13)	173.7(19)
	O(25)-H(25)...N(14)#2	0.956(19)	1.72(2)	2.6551(13)	166.7(17)
B1·A26 ^{vii}	O(21)-H(21)...N(11)	0.947(19)	1.721(19)	2.6588(11)	170.0(17)
	N(12)-H(12A)...O(22)	0.925(16)	2.140(16)	3.0459(12)	166.2(13)
	N(12)-H(12B)...O(28)#1	0.901(19)	2.10(2)	2.9616(13)	160.9(16)
	O(27)-H(27)...N(14)#2	0.98(2)	1.68(2)	2.6544(11)	170(2)
B1·A27 ^{viii}	N(12)-H(12A)...O(22)	0.84(4)	2.06(4)	2.883(3)	167(3)
	N(12)-H(12B)...O(29)#1	0.86(4)	2.13(4)	2.966(3)	164(3)
	N(15)-H(15B)...O(22)#2	0.86	2.50	3.289(16)	153.3
	N(15)-H(15A)...O(29)#3	0.86	2.13	2.962(14)	162.2

	O(21)-H(21)...N(11)	0.95(3)	1.80(3)	2.741(2)	172(3)
	O(28)-H(28)...N(14)#4	0.96(4)	1.74(4)	2.689(2)	168(3)
B1A29^{ix}	O(21)-H(21)...N(11)	0.905(17)	1.809(17)	2.6939(11)	165.2(14)
	N(12)-H(12A)...O(22)	0.85(3)	1.97(3)	2.8120(18)	177(3)
	N(12)-H(12B)...O(22)#3	0.81(3)	2.05(3)	2.7437(18)	144(3)
B3·A7^x	O(27)-H(27)...N(14)	0.80(4)	1.91(4)	2.704(3)	174(4)
	N(13)-H(13A)...O(28)	0.88	2.02	2.891(3)	167.9
	N(13)-H(13B)...O(22)#1	0.88	2.35	2.944(3)	125.4
	O(22)-H(22)...O(28)	0.78(4)	1.87(4)	2.574(3)	149(4)
	O(25)-H(25A)...O(25)#2	0.84	1.96	2.762(4)	159.5
B3·A13^{xi}	O(21)-H(21)...N(11)	0.76(2)	1.84(2)	2.5892(19)	172(3)
	N(12)-H(12A)...O(22)	0.86(2)	2.17(2)	3.0174(19)	169(2)
	N(12)-H(12B)...O(22)#1	0.82(2)	2.37(2)	3.074(2)	144(2)
B3·A14^{xii}	O(21)-H(21)...N(11)	0.73(2)	1.94(2)	2.6728(17)	176(2)
	N(12)-H(12A)...O(25)#1	0.76(2)	2.38(2)	3.031(2)	145(2)
	N(12)-H(12B)...O(23)#2	0.88(2)	2.32(2)	3.165(2)	162(2)
B3·A18^{xiii}	O(21)-H(21)...N(11)	0.81(3)	1.88(3)	2.685(2)	171(2)
	N(12)-H(12A)...O(22)	0.81(3)	2.17(3)	2.976(3)	174(2)
	N(12)-H(12B)...F(26)#1	0.82(3)	2.68(3)	3.335(2)	138(2)

Symmetry transformations used to generate equivalent atoms:

i) #1 -x+1,-y+1,-z ii) #1 -x+1,-y+1,-z+1 #2 x,-y+3/2,z+1/2 iii) #1 x-1,y,z+1 iv) #1 -x+1,-y,-z+1 #2 x,y-1,z v) #1 -x+1,-y+1,-z+1 #2 -x+1,-y,-z+1 #3 x-1,-y+1/2,z-1/2 vi) #1 -x+2,-y+1,-z+1 #2 -x+1,y-1/2,-z+1/2 vii) #1 -x+2,-y+1,-z+1 #2 -x+1,y+1/2,-z+1/2 viii) #1 -x,y+1/2,-z #2 -x+1,y-1/2,-z+1 #3 x+1,y,z+2 #4 x-1,y,z-2 ix) #1 -x+2,-y+2,-z+2 #2 -x,-y+1,-z #3 -x+2,-y+2,-z+1 x) #1 -x+1,-y+1,-z #2 -x+2,-y,-z+1 xi) #1 -x+3/2,y-1/2,-z+1/2 xii) #1 -x+2,-y,-z+1 #2 x+1,y+1,z-1 xiii) #1 -x+1,-y+2,-z+1

2.3.2.1 Crystal structure of 2-amino-3,5-dibromopyrazine, B3

The crystal structure of **B3** shows that the individual molecules form dimeric units through self-complementary symmetry related N-H...N/N...H-N (N13...N14, 3.0557(17) Å) hydrogen bonds, Figure 2.7. The anti-NH proton of amino group is structurally inactive.

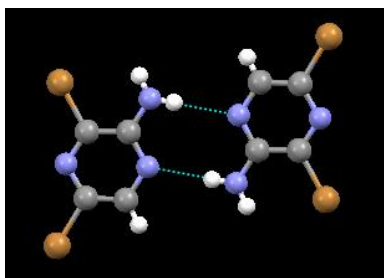


Figure 2.7 Observed homosynthon in the crystal structure of **B3**.

2.3.2.2 Crystal structures of *B1·A11* and *B1·A16*

The crystal structure determinations of **B1·A11** and **B1·A16** show 1:2 stoichiometry in each case. The hydrogen-bond interactions primarily responsible for the assembly of the co-crystal are O-H···N and C=O···H-N (Figure 2.8). Due to the disorder in **B1·A11** and **B1·A16** it was not possible to establish the secondary interaction of the anti-proton of the amino group.

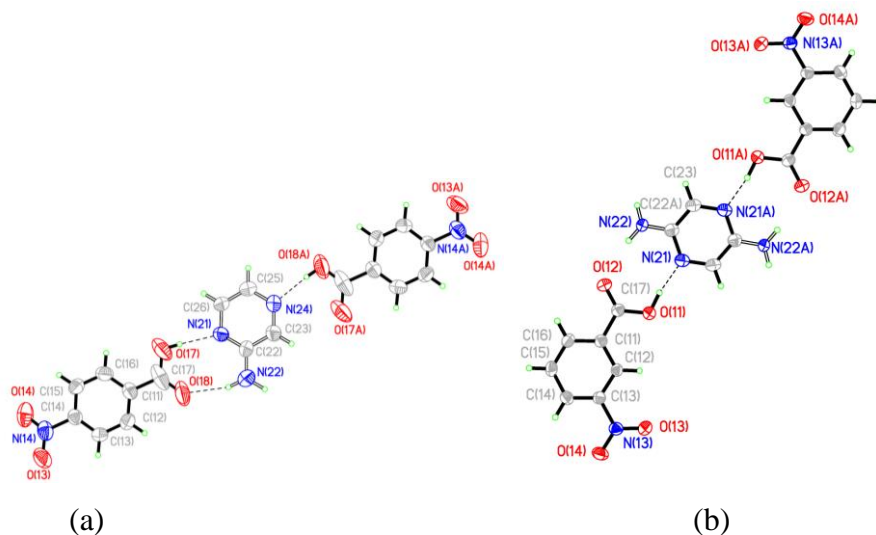


Figure 2.8 Thermal ellipsoid plots (50% probability level) of (a) **B1·A11** and (b) **B1·A16**.

2.3.2.3 Crystal structure of *2-aminopyrazinium 3,5-dinitrobenzoate*, *B1·A14*

When **B1** was combined with 3,5-dinitrobenzoic acid **A14**, the structural examination showed that a 1:1 salt was formed (Figure 2.9). The primary intermolecular interaction in this compound is the charge-assisted two-point N-H···O⁻/N-H⁺···O⁻ synthon. In addition, the anti-proton of the amino group, forms a hydrogen bond with the oxygen atom of the nitro group.

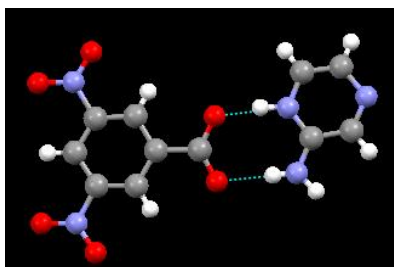


Figure 2.9 The primary synthon in the crystal structure of **B1·A14**.

2.3.2.5 Crystal structure of *2-aminopyrazine succinic acid*, *B1·A23*

The heteromeric synthon observed in co-crystal **B1·A23** is O-H···N(4). Note that the self-complementary C-H···O hydrogen bond from C-H of **B1** to the carbonyl of **A23** does not form even though the two molecules lie coplanar to one another. The C-H···O distance is 2.875 Å, which is well beyond the van der Waals distance for a hydrogen and oxygen contact, 2.72 Å (Figure 2.10). Homosynthon I (**B1** dimer) along with heterosynthon V (OH···N(4)) give rise to infinite 1D chains, moreover, these chains are extended into 2D sheets via amino anti-NH···O=C secondary interactions (Figure 2.11).

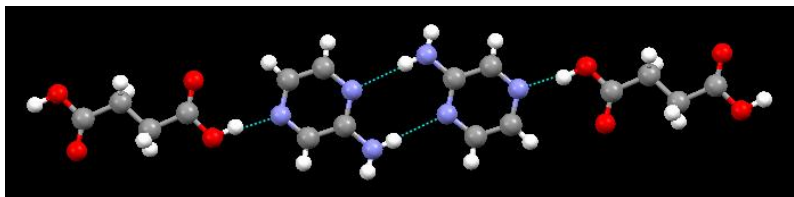


Figure 2.10 The primary hydrogen bonds in the crystal structure of **B1·A23**.

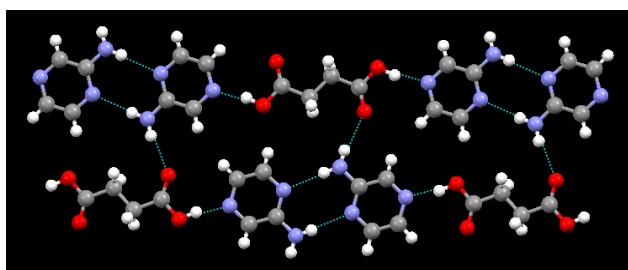


Figure 2.11 2D network formed in the co-crystal of **B1·A23**.

2.3.2.6 Crystal structures of *B1·A24*, *B1·A26*, *B1·A27* and *B1·A29*

The crystal structures of **B1·A24**, **B1·A26**, **B1·A27** and **B1·A29** all show 1:2 co-crystal formation through O-H···N/C=O···H-N synthons and the O-H···N(4) synthons (Figure 2.12). In addition, in all four structures, the anti NH proton of amino group interacts with a carbonyl oxygen atom, giving rise to a 2D extended network (Figure 2.13).

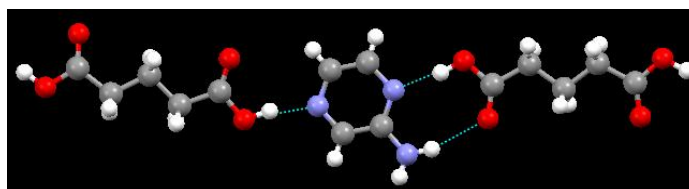


Figure 2.12 Infinite 1D chains formed in the co-crystal of **B1·A24**.

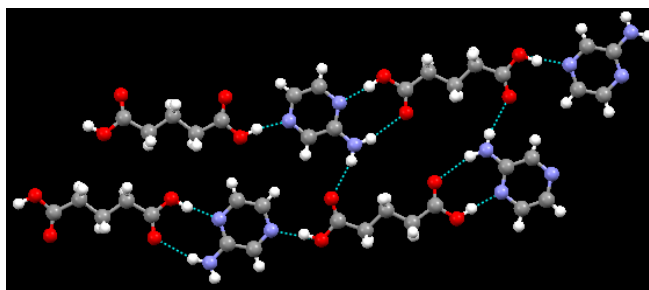


Figure 2.13 Extended 2D network formed in the co-crystal of **B1·A24**.

2.3.2.10 Crystal structures of *B3·A7*, *B3·A13* and *B3·A18*

The crystal structures of **B3·A7**, **B3·A13** and **B3·A18** show 1:1 co-crystal formation through O-H···N/C=O···H-N synthons (Figure 2.14). In the co-crystal of **B3·A13** and **B3·A18**, the anti-proton of the amino group hydrogen bond to the oxygen atom of the carbonyl group, whereas in **B3·A7** the anti-proton of the amino group is structurally inactive.

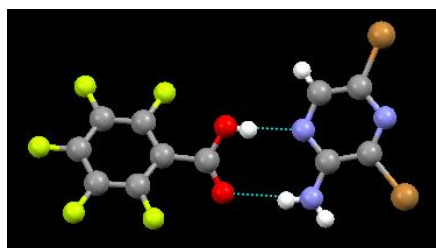


Figure 2.14 1:1 co-crystal of **B3·A13**.

2.3.2.12 Crystal structure of *2-amino-3,5-dibromopyrazine 3,5-dinitrobenzoic acid*, *B3·A14*

The crystal structure of **B3·A14** shows 1:1 co-crystal formation through the O-H···N/O···H-C heterosynthon (Figure 2.15). A secondary interaction present in **B3·A14** is the anti-proton of the amino group hydrogen bonding to the oxygen atom of the nitro group from **A14**.

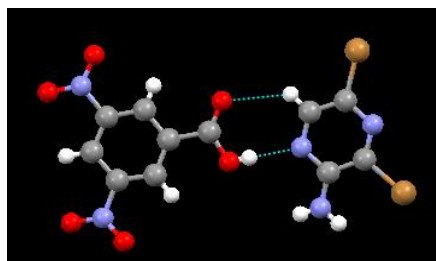


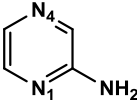
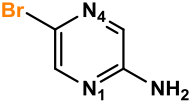
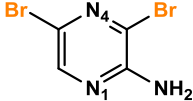
Figure 2.15 The primary hydrogen bonds in the crystal structure of **B3·A14**.

2.4 Discussion

2.4.1 Supramolecular yield based on infrared spectroscopy

Based on infrared spectroscopy, we determined that **B1**, the strongest base from the three, gave a 83% supramolecular yield followed by 40% and 20% supramolecular yield for **B2** and **B3** respectively (Table 2.3). These results can be explained in terms of the reduced electrostatic charges on both binding sites of 2-aminopyrazine derivatives due to sequential addition of electron withdrawing substituents (from **B1** to **B3**). The results are in agreement with previously reported co-crystals of substituted pyridines with carboxylic acids.^{8a}

Table 2.3 Charge calculations (PM3) and outcome summary of co-crystallization experiments between pyrazines and carboxylic acids.

	B1		B2		B3	
						
Charges kJ/mol	N(1) -251	N(4) -255	N(1) -238	N(4) -245	N(1) -222	N(4) -240
Reaction	25		12		6	
No reaction	5		18		24	
% yield	83		40		20	

Unfortunately, specific analysis regarding co-crystal or salt formation was inconclusive since all products display stretches around 2500 and 1900 cm^{-1} , regardless if the final product was a co-crystal or salt. We also attempted to track the shift of the carbonyl stretch. A typical monomeric C=O stretching band of a carboxylic acid, when on an aromatic ring, appears around 1760 cm^{-1} , while the acid dimeric C=O stretching mode absorbs at a lower frequency in the 1720-1706 cm^{-1} region. The carboxylate ion displays a strong asymmetric stretch around 1650-1550 cm^{-1} and a weaker symmetric stretch at $\sim 1400 \text{ cm}^{-1}$.¹⁹ A summary of the observed carbonyl stretches from co-crystals/salts are displayed in Table 2.4. The results do not directly correlate with what is expected based on previously reported data. It seems, within this system, that the IR data is not helpful in accurately determining whether proton-transfer occurred or not.

Table 2.4 Summary of IR data showing carbonyl stretches for co-crystals/salts.

	NAME	B1	B2	B3
		C=O	C=O	C=O
A1	4-Aminobenzoic acid	-	-	-
A2	4-Hydroxybenzoic acid	1666	1686	-
A3	3,5-Dihydroxybenzoic acid	1706	-	-
A4	2,4-Dimethoxybenzoic acid	1672	-	-
A5	3,4-Dihydroxybenzoic acid	1646	-	-
A6	2,3-Dihydroxybenzoic acid	-	-	-
A7	2,5-Dihydroxybenzoic acid	-	-	1690
A8	2,3-Dimethylbenzoic acid	1646	-	-
A9	2,5-Dimethylbenzoic acid	-	1706	-
A10	Benzoic acid	1672	-	-
A11	4-Nitrobenzoic acid	1695	-	-
A12	4-Fluorobenzoic acid	1646	-	-
A13	Pentafluorobenzoic acid	1679	-	1695
A14	3,5-Dinitrobenzoic acid	1672	1706	1619
A15	2,4-Dinitrobenzoic acid	1664	1716	-
A16	3-Nitrobenzoic acid	1699	1706	1701
A17	2-Chloro-6-fluorobenzoic acid	-	1699	1699
A18	2,6-Difluorobenzoic acid	1712	-	-
A19	3-Fluorobenzoic acid	1653	-	-
A20	4-Cyanobenzoic acid	1654	1700	-
A21	Oxalic acid	1729	1685	1697
A22	Malonic acid	1724	-	-
A23	Succinic acid	1679, 1633	1710	-
A24	Glutaric acid	1697, 1676	1703	-
A25	Adipic acid	1673, 1643	-	-
A26	Pimelic acid	1674, 1633	1717, 1694	-
A27	Suberic acid	1683, 1643	1711	-
A28	Azelaic acid	1673, 1636	-	-
A29	Sebacic acid	1685, 1650	-	-
A30	Dodecanedioic acid	1687, 1645	-	-

2.4.2 Evaluation of donor or acceptor dominance in predicting product formation

Our systematic analysis makes it clear that heteromeric product formation in this system is primarily determined by the charge on the **B1-B3** and not by the strength of the carboxylic acid (Table 2.5). We analyzed the results in the context of charges of the carboxylic acids (the charge on the acidic proton i.e. COOH), however, better correlations were found between the charges on the heterocyclic nitrogen atom and the supramolecular yield (discussed in 2.4.1). For example, a stronger acid, 2,5-dihydroxybenzoic acid **A7**, produced ‘no reaction’ with stronger bases **B1** and **B2**, whereas resulted in a ‘reaction’ with weakest base **B3**. This inconsistency of results based on carboxylic acid strengths could be due to prevailing acid-acid dimer even in presence of N-heterocyclic bases.²⁰ A stronger acid forms more stable acid-acid dimer than a weaker acid.

Table 2.5 Results from IR spectroscopy arranged in order of decreasing charge on hydrogen of carboxylic acids. Empty boxes represent ‘no reaction’ and filled boxes represent a ‘reaction’.

Acids	Label	Charge on COOH (kJ/mol)*	B1	B2	B3
Malonic acid	A22	177			
3,5-Dinitrobenzoic acid	A14	168			
Oxalic acid	A21	158			
2,3-Dihydroxybenzoic acid	A6	151			
Pentafluorobenzoic acid	A13	148			
4-Nitrobenzoic acid	A11	147			
2,5-Dihydroxybenzoic acid	A7	140			
3-Nitrobenzoic acid	A16	139			
Glutaric acid	A24	139			
Adipic acid	A25	139			
Sebacic acid	A29	138			
2,4-Dinitrobenzoic acid	A15	136			
Succinic acid	A23	136			
Suberic acid	A27	135			
Pimelic acid	A26	134			
Dodecanedioic acid	A30	133			
Azelaic acid	A28	132			
4-Fluorobenzoic acid	A12	128			
3,4-Dihydroxybenzoic acid	A5	124			
3-Fluorobenzoic acid	A19	124			
Benzoic acid	A10	118			

3,5-Dihydroxybenzoic acid	A3	116			
2,5-Dimethylbenzoic acid	A9	115			
2,6-Difluorobenzoic acid	A18	114			
4-Cyanobenzoic acid	A20	113			
2,3-Dimethylbenzoic acid	A8	112			
2-Chloro-6-fluorobenzoic acid	A17	111			
2,4-Dimethoxybenzoic acid	A4	107			
4-Hydroxybenzoic acid	A2	106			
4-Aminobenzoic acid	A1	105			

* Charges are calculated from Spartan'04 using PM3 level of theory (Unit = kJ/mol).

2.4.3 Synthon classification based on crystal structures

A collection of postulated homo- and hetero synthons resulting from reactions between **B1-B3** and carboxylic acids is shown in Figure 2.16.

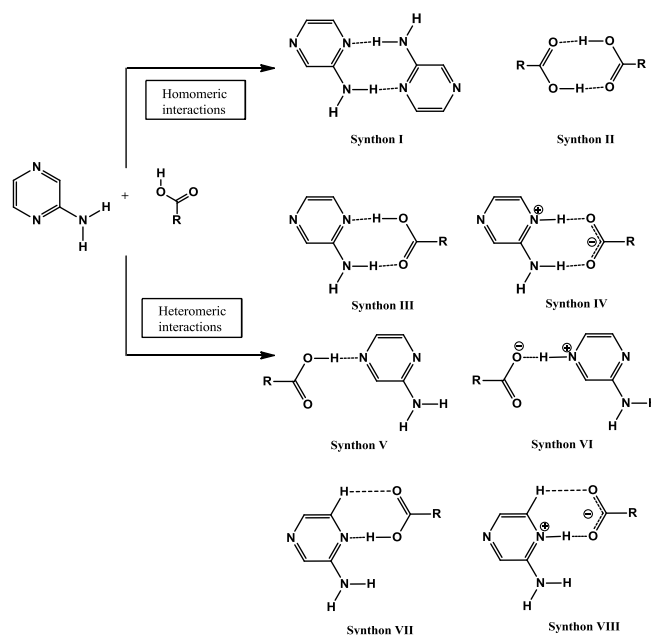


Figure 2.16 Potential homo- and hetero synthons in salts and co-crystals based on 2-aminopyrazine derivatives and carboxylic acids.

The crystal structures of all the co-crystals and salts, were classified on the basis of synthons observed. The structural analysis shows that ten out of twelve times the carboxylic acid binds to the 2-amino end of the bases (Figure 2.17). In five of these ten structure, a carboxylic acid also binds to N(4) of the base, Figure 2.17.

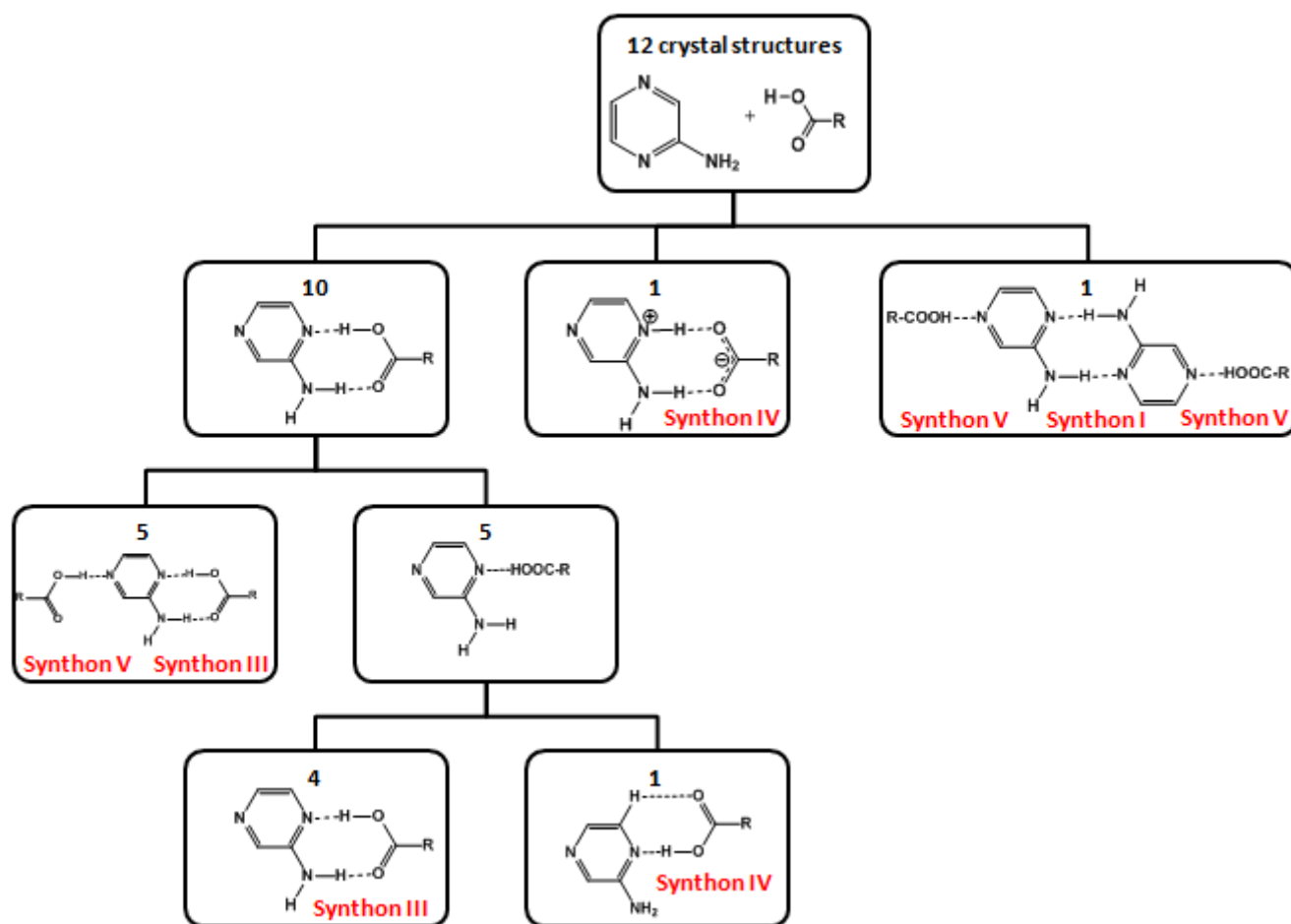


Figure 2.17 Classification of crystal structures obtained from supramolecular reactions between **B1-B3** and a variety of acids.

Table 2.6 Summary of observed synthons in crystal structures.

Crystal Structure	Synthons							
	I	II	III	IV	V	VI	VII	VIII
B1·A11			✓		✓			
B1·A16			✓		✓			
B1·A14				✓				
B1·A23	✓				✓			
B1·A24			✓		✓			
B1·A26			✓		✓			
B1·A27			✓		✓			
B1·A29			✓		✓			
B3·A7			✓					
B3·A13			✓					
B3·A14							✓	
B3·A18			✓					

In the first three structures, **B1·A11/A14/A16** of aromatic carboxylic acids and **B1**, there is no synthon selectivity due to multiple accessible binding sites for carboxylic acids (Table 2.6). Two out of three structures show carboxylic acid binding to both ends of **B1**, in the remaining case (**B1·A14**), where proton transfer from acid to **B1** takes place, it opts for the predicted 2-amino end of **B1**.

Next set of crystal structures all contained **B1** and an aliphatic dicarboxylic acid. The observed homosynthon I (**B1** dimer) in the case of **B1·A23** does persist when using longer chain aliphatic dicarboxylic acids (**B1·A26**, **B1·A26**, **B1·A27**, **B1·A29**). Also, except **B1·A23**, all four remaining co-crystals from a combination of aliphatic dicarboxylic acids and **B1**, show remarkable synthon consistency (Table 2.6). However, selective binding of carboxylic acids at expected N1 site of **B1** could not be achieved presumably due to the presence of a competitive binding site N4. Although stronger two point hydrogen-bond interaction should prevail versus single point hydrogen-bond interaction, but for synthon selectivity to occur, geometric and electrostatic factors needs to be chosen meticulously.²¹

B3, the weakest base of the three, yielded four co-crystals **B3·A7**, **B3·A13**, **B3·A14**, **B3·A18**. Three of four times, the expected heterosynthon III was observed and in one exception of **B3·A14**, it showed a rarely observed heterosynthon VII.²² Although, reaction stoichiometry was predictable (1:1) due to substantially reduced charge on binding site (N(4) site of **B3**) but synthon selectivity could not be achieved (Table 2.6).

2.4.4 Binding preference of carboxylic acids

We investigated the binding preference of carboxylic acids based on the crystal structures obtained. The structural analysis reveals that six of eight times carboxylic acid binds to both ends of **B1**. This may be rationalized by examining comparable charges on the two possible binding sites (N(1) and N(4) nitrogen atoms) thereby giving more alternatives to carboxylic acid for binding. However, in the case of heterodimeric products of **B3**, carboxylic acids opt for the N(1) site in four of four cases. This selective binding of **B3** is presumably due to reduction of charge on the N(4) of **B3** (Figure 2.18).

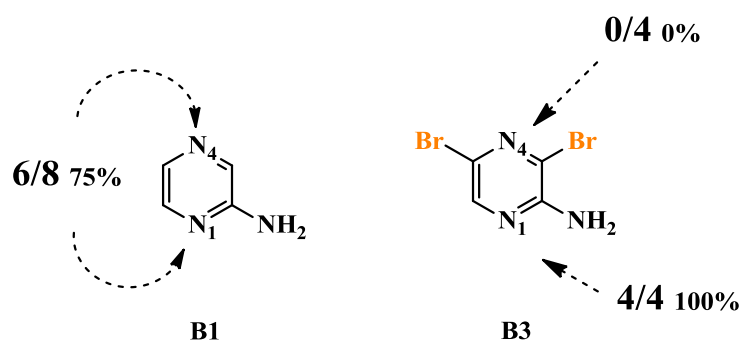


Figure 2.18 Binding preferences of carboxylic acids with **B1** and **B3**.

2.5 Conclusion

Our theoretical charge calculation and experimental results successfully demonstrate that as the charge on hydrogen-bond acceptor sites decreases the supramolecular yield decreases.

The main driving force for assembly of heteromer between **B1-B3** and carboxylic acids was found to be O-H...N/O...H-N synthon. Furthermore, we have successfully demonstrated that the binding preferences of carboxylic acids can be controlled by reducing the strength of competing binding site. However, synthon crossover (7/12 times) was observed in the structural landscape of 2-aminopyrazine derivatives and was unavoidable due to competitive binding sites present in the N-heterocyclic bases chosen.

References:

-
- ¹ (a) Vishweshwar, P.; McMahon, J. A.; Bis, J. A.; Zaworotko, M. J. *J. Pharm. Sci.* **2006**, *95*, 499; (b) Jones, W.; Motherwell, W. D. S.; Trask, A. V. *MRS Bull.* **2006**, *31*, 875; (c) Rodríguez-Hornedo, N. *Mol. Pharmaceutics* **2007**, *4*, 299; (d) Shan, N.; Zaworotko, M. J. *Drug Discov. Today*, **2008**, *13*, 440; (e) Schultheiss, N.; Newman, A. *Cryst. Growth Des.* **2009**, *9*, 2950.
- ² Miroshnyk, I.; Mirza, S.; Sandler, N. *Expert Opin. Drug Delivery* **2009**, *6*, 333.
- ³ (a) Stanton, M. K.; Bak, A. *Cryst. Growth Des.*, **2008**, *8*, 3856; (b) Braga, D.; Dichiarante, E.; Palladino, G.; Grepioni, F.; Chierotti, M. R.; Gobetto, R.; Pellegrino, L. *CrystEngComm* **2010**, *12*, 3534.
- ⁴ Good D. J.; Rodríguez-Hornedo, N. *Cryst. Growth Des.* **2009**, *9*, 2252.
- ⁵ (a) Remenar, J. F.; Morissette, S. L.; Peterson, M. L.; Moulton, B.; MacPhee, J. M.; Guzmán H. R.; Almarsson, Ö. *J. Am. Chem. Soc.*, **2003**, *125*, 8456; (b) Aitipamula, S.; Chow P. S.; Tan, R. B. H. *CrystEngComm*, **2009**, *11*, 1823.
- ⁶ (a) McNamara, D. P.; Childs, S. L.; Giordano, J.; Iarriccio, A.; Cassidy, J.; Shet, M. S.; Mannion, R.; O'Donnel, E.; Park, A. *Pharm. Res.* **2006**, *23*, 1888; (b) Hickey, M. B.; Peterson, M. L.; Scoppettuolo, L. A.; Morrisette, S. L.; Vetter, A.; Guzmán, H.; Remenar, J. F.; Zhang, Z.; Tawa, M. D.; Haley, S.; Zaworotko, M. J.; Almarsson, Ö. *Eur. J. Pharm. Biopharm.* **2007**, *67*, 112.
- ⁷ Aakeröy, C. B.; Forbes, S.; Desper, J. *J. Am. Chem. Soc.* **2009**, *131*, 17048.
- ⁸ (a) Aakeröy, C. B.; Rajbanshi, A.; Desper, J. *CrystEngComm*. **2010**, *12*, 4231; (b) Aakeröy, C. B.; Beatty, A. M.; Helfrich, B. A. *J. Am. Chem. Soc.* **2002**, *124*, 14425.
- ⁹ (a) Leiserowitz, L. *Acta Crystallogr.* **1976**, *B32*, 775; (b) Leiserowitz, L.; Tuval, M. *Acta. Crystallogr.*, **1978**, *B34*, 1230; (c) Dunitz, J. D. *Pure Appl. Chem.* **1991**, *63*, 177.
- ¹⁰ Allen, F. H.; Motherwell, W.D.S.; Raithby, P.R.; Shields, G.P.; Taylor, R. *New J. Chem.* **1999**, *1*, 25.
- ¹¹ (a) Kane, J. J.; Liao, R.-F.; Lauher, J.W.; Fowler, F.W. *J. Am. Chem. Soc.* **1995**, *117*, 12003; (b) Sharma, C.V.K.; Zaworotko, M. J. *Chem. Commun.* **1996**, 2655 (c) Grunert, M.; Howie, R.A.; Kaeding, A.; Imrie, C.T. *J. Mater. Chem.* **1997**, *7*, 211; (d) Pedireddi, V.R.; Chatterjee, S.; Ranganathan, A. *Tetrahedron* **1998**, *54*, 9457, (e) Amai, M.; Endo, T.; Nagase, H.; Ueda, H.; Nakagaki, M. *Acta Crystallogr.* **1998**, *C54*, 1367; (f) Palmore, G.T.R.; Luo, T.-J.M.; McBride-Wieser, M.T.; Picciotto, E.A.; Reynoso-Paz, C.M. *Chem. Mater.* **1999**, *11*, 3315; (g) Aakeröy, C.B.; Beatty, A.M.; Tremayne, M.; Rowe, D. *Cryst. Growth Des.* **2001**, *1*, 377 (h) Vishweshwar, P.; Nangia, A.; Lynch, V.M. *J. Org. Chem.* **2002**, *67*, 556.
- ¹² (a) Huang, K.-S.; Britton, D.; Etter, M.C.; Byrn, S.R. *J. Mater. Chem.* **1997**, *7*, 713; (b) MacGillivray, L. R.; Reid, J.L.; Ripmeester, J. A. *J. Am. Chem. Soc.* **2000**, *122*, 7817.
- ¹³ Ermer, O.; Eling, A. *J. Chem. Soc., Perkin Trans. 2* **1994**, 925.
- ¹⁴ CSD search carried out on ConQuest Version 1.13.
- ¹⁵ (a) Hunter, C. A. *Angew. Chem. Int. Ed.* **2004**, *43*, 5310. (b) Henry, M.; Hosseini, M. W. *New J. Chem.* **2004**, *28*, 897.
- ¹⁶ Ellingson R. C., Henry R. L., *J. Am. Chem. Soc.* **1949**, *71*, 2798.
- ¹⁷ Paudler W. W., Jovanovic M. V., *J. Org. Chem.* **1983**, *48*, 1064.
- ¹⁸ Castaneda, J. P.; Denisov, G. S.; Kucherov, S. Y.; Schreiber, V. M.; Shurukhina, A. *J. Mol. Struct.* **2003**, *660*, 25.

¹⁹ Silverstein, R. M.; Bassler, G. C.; Morrill, T. C. *Spectroscopic Identification of Organic Compounds*, John Wiley and Sons: New York, 1991.

²⁰ (a) Wash, P. L. ; Maverick, E.; Chiefari, J.; Lightner, D. A. *J. Am. Chem. Soc.*, **1997**, *119*, 3802; (b) Aakeroy, C. B.; Beatty, A. M.; Lorimer, K. R. *Dalton*, **2000**, *21*, 3869.

²¹ (a) Aakeröy, C. B.; Desper, J.; Helfrich, B. A.; Metrangolo, P.; Pilati, T.; Resnati, G.; Stevenazzi, A. *Chem. Commun.*, **2007**, 4236; (b) Aakeröy, C. B.; Schultheiss, N.; Rajbanshi, A.; Desper, J.; Moore, C. *Cryst. Growth Des.*, **2009**, *9*, 432.

²² CSD search shows no hits on this type of synthon in the presence of 2-aminopyridine based heterocycles.

Chapter 3 - Avoiding 'synthon crossover' in synthetic strategies based on halogen bonds and hydrogen bonds

3.1 Introduction

Hydrogen bonds remain the most commonly utilized tools in the assembly of co-crystals due to their relatively high strength and directionality,^{1,2} and many successful studies have been reported where overall assembly of binary and ternary co-crystals is guided by a synthetic scheme based on hydrogen bonds of varying strengths in a predictable manner.³ However, for designing co-crystals of higher complexity, a strategy that relies solely on hydrogen bonds could soon fail because of unavoidable interference between the intended hydrogen-bond donors/acceptors which could lead to 'synthon crossover'. Supramolecular strategies, that can accommodate two or more different non-interfering interactions may alleviate this problem. A suitable accompaniment to a hydrogen-bond based strategy may be provided by halogen bonds, which are typically formed between activated iodine- or bromine atoms (the halogen-bond donor) and an appropriate halogen-bond acceptor (electron-pair donor) such as an *N*-heterocycle.⁴ Although halogen bonding is similar to hydrogen bonding in some regards,^{5a} a halogen-bond will mostly involve single-point synthons,⁵ whereas hydrogen-bonded synthons are often multi-point interactions, Figure 3.1. In this chapter, we will be focus on the design and synthesis of supramolecular architectures formed through combinations of both hydrogen and halogen bonds in a systematic manner.

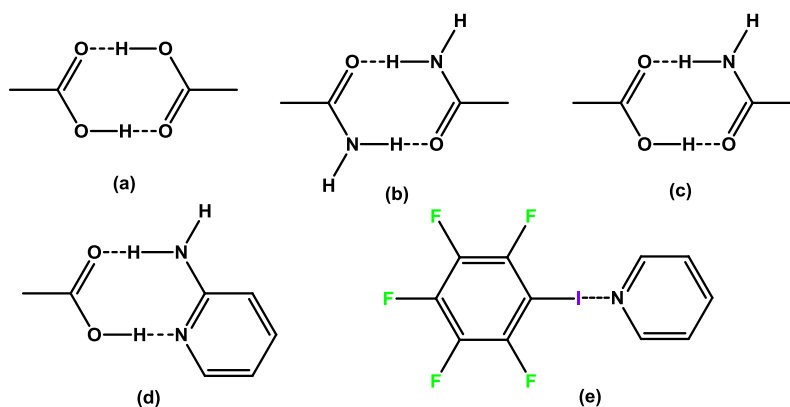


Figure 3.1 Examples of commonly occurring supramolecular synthons, a) acid-acid b) amide-amide c) acid-amide d) acid-aminopyridine and e) single-point iodo-N(py).

In the past, it has been shown that supermolecules can be constructed via combinations of hydrogen bonds and halogen bonds.⁶ A notable example of non-covalent synthesis uses *iso*-nicotinamide and 1,4-diodotetrafluorobenzene (DITFB) building blocks (Figure 3.2).^{6a} The supramolecular assembly is held together by amide...amide hydrogen-bonded homomeric motifs and N...I halogen bonds, giving rise to 1D chains. Moreover, these 1D chains are extended into 2D ribbons by the *anti*-proton of the amino group hydrogen bonding to a neighboring carbonyl oxygen atom.

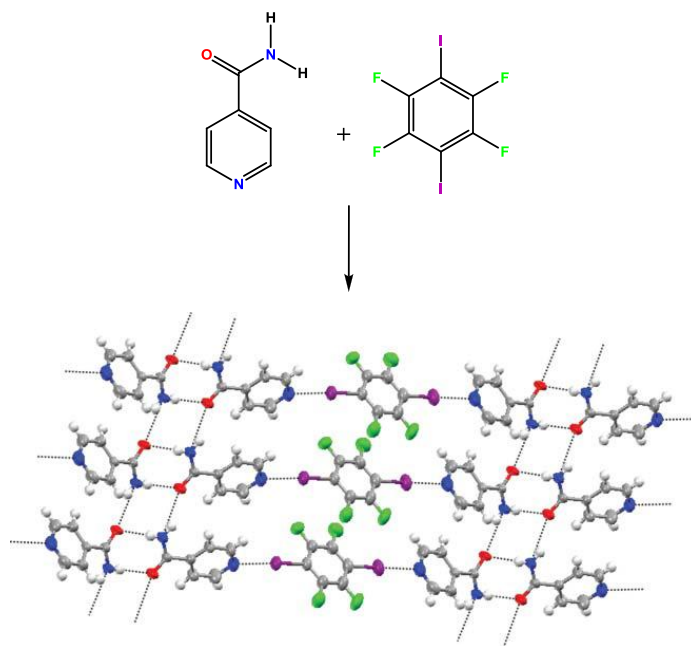


Figure 3.2 Supramolecular assembly from *iso*-nicotinamide and **DITFB**.^{6a}

In Chapter 2, it was shown that carboxylic acids preferentially bind to the amino end of 2-aminopyrazine derivative (10/12 cases). However, in some cases (7/12), the carboxylic acid also binds to the N4 nitrogen atom site (Figure 3.3), causing ‘synthon crossover’.

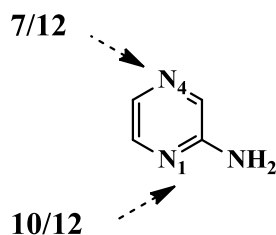


Figure 3.3 Results obtained by combining 2-aminopyrazine derivatives with carboxylic acids. Numbers indicate carboxylic acid binding preference.

Against this background, we decided to use a strategy based on hydrogen bonds and halogen bonds to avoid ‘synthon crossover’. We thought of replacing a carboxylic acid from 2-aminopyrazine system studied in Chapter 2, with 1,4-diiodotetrafluorobenzene (**DITFB**) as the halogen-bond donor due to its proven ability to form halogen bonding with N-heterocyclic acceptors (Figure 3.4a).⁷ In the absence of a strong and complementary two-point hydrogen bond donor/acceptor moiety such as a carboxylic acid, the amino-pyrazine site is perfectly capable of forming a self-complementary homo synthon, Figure 3.4b. A CSD search on 2-aminopyrazine and its derivatives uncovered several examples of HB homosynthon formation between 2-aminopyrazine molecules.⁸ In addition, this homodimer is frequently accompanied by an *anti* NH(amino)⋯N4(pyrazine) secondary interaction (Figure 3.4c). Consequently, a potential N⋯I halogen bond, Figure 3.4a, would have to compete successfully with the N-H⋯N hydrogen bond if co-crystal formation is to take place (Figure 3.6a). It should be noted that, in the previous study of *iso*-nicotinamide·**DITFB** system an *anti*-NH(amino) proton was not available for competition with a N⋯I halogen bond.^{6a}

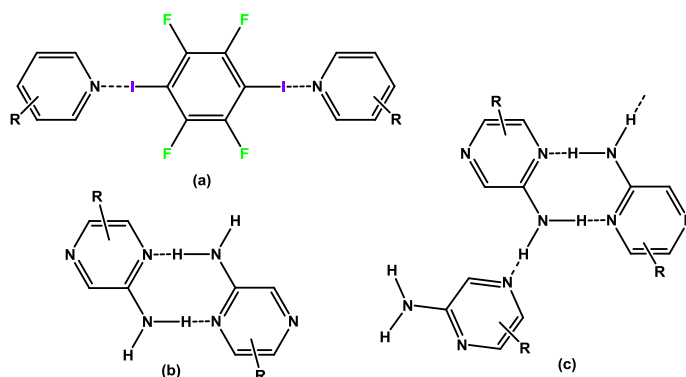


Figure 3.4 Observed synthons in the CSD database search for (a) co-crystals of substituted pyridines and 1,4-diiodotetrafluorobenzene, (b) substituted 2-aminopyrazine by itself and (c) its extended network.

We also wanted to investigate, how a combination of hydrogen-bond donor and halogen-bond donor functionalities on a probe molecule, binds to a 2-aminopyrazine backbone. The intriguing question is; will the hydrogen-bond donor bind to both the ends of 2-aminopyrazine in the presence of strong halogen-bond donor? We therefore needed to combine a hydrogen-bond donor (carboxylic acid) and halogen bond donor (iodo or bromo) functionality on a same backbone. Based on the structural data obtained in Chapter 2, we hypothesized that a carboxylic acid should bind to amino end of 2-aminopyrazine and the halogen bond donor should opt for remaining N4 nitrogen atom (Figure 3.6b). Moreover, the strength of the halogen bond donor can be increased by adding electron withdrawing group (fluorination), which can lead to an increase in the electron-acceptor capabilities of the iodine or bromine atoms. Given the requirements described above, it seemed logical to select 2,3,5,6-tetrafluoro-4-iodobenzoic acid (**IF4BA**) and 2,3,5,6-tetrafluoro-4-bromobenzoic acid (**BrF4BA**) as our donor-containing tectons.

However, the reported preparation of **IF4BA** and **BrF4BA** required a laborious five-step procedure,⁹ and we therefore developed a new one-step strategy to synthesize **IF4BA** and **BrF4BA** starting from commercially available 1,4-dihalo-2,3,5,6-tetrafluorobenzene (iodo **IF4BA**, bromo **BrF4BA**) via a single lithium-halogen exchange followed by addition of CO₂.¹⁰

We also wanted to examine the role of the electrostatic charge at the intended halogen-bond acceptor site (N4 on 2-aminopyrazine) and hydrogen-bond acceptor site (amino end of 2-aminopyrazine). Based on reported literature,¹¹ we postulated that if we could reduce the charge on the hydrogen-bond acceptor sites then it will be possible to control salt vs. co-crystal formation while maintaining the expected supramolecular assembly, which is of great interest in the pharmaceutical industry.¹² We therefore attached one, and two electron-withdrawing bromo substituents, respectively to the 2-aminopyrazine backbone (Figure 3.5) in order to reduce the charge on the acceptor sites. If proton transfer was to take place, it was expected to happen with the most basic of the acceptor molecules, **B1**.

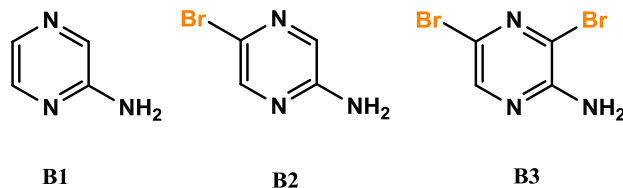


Figure 3.5 Ditopic supramolecular reagents for supramolecular synthesis.

Since **DITFB**, **XF4BA** and **B1-B3** have binding sites present in a co-linear manner, the resulting supramolecular assembly should result in infinite 1-D chains *via* a combination of hydrogen-bond and halogen-bonds, Figure 3.6.

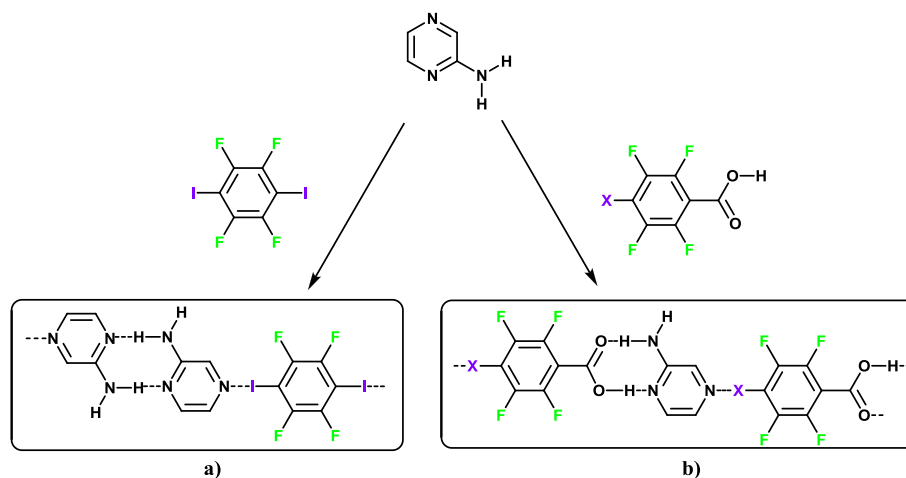


Figure 3.6 1D networks formed by postulated hydrogen and halogen bonds (X = I, Br).

In order to study the hierarchical approach to supramolecular synthesis through hydrogen and halogen bonding, supramolecular reactions were carried out between 2-aminopyrazine based compounds (**B1-B3**) and a powerful halogen-bond donor (**DITFB**), ditopic hydrogen-bond/halogen-bond donors (**IF4BA** and **BrF4BA**). In this chapter we will attempt to answer the following questions:

I) Can we synthesize co-crystals of 2-aminopyrazine and its derivatives using halogen bonds?

II) Will an N...I halogen bond prevail in the face of a potential N-H...N hydrogen bond?

III) Can the strength of the halogen bond be modulated as a function of charge on the halogen-bond acceptor?

IV) Can we avoid 'synthon crossover' using suitable combinations of hydrogen-bonds and halogen-bonds?

V) Can we control salt vs. co-crystal formation by modulating the electrostatic charge on the hydrogen-bond acceptor sites?

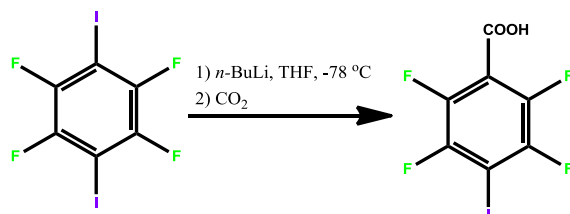
VI) Is it possible to achieve structural consistency?

3.2 Experimental

3.2.1 Synthesis of ligands

All chemicals, unless otherwise noted, were purchased from Aldrich and used without further purification. 2-amino-5-bromopyrazine, **B2** and 2-amino-3,5-dibromopyrazine, **B3** were synthesized using procedure reported in Chapter 2. Melting points were determined on a Fisher-Johns melting point apparatus. ^1H and ^{13}C NMR spectra were recorded on a Varian Unity plus 400 MHz or 200 MHz spectrometer in CDCl_3 or $\text{D}_6\text{-DMSO}$. Data is expressed in parts per million (ppm) downfield shift from tetramethylsilane or residual protiosolvent as internal reference and are reported as position (in ppm), multiplicity (s = singlet, d = doublet, t = triplet, m = multiplet), coupling constant (J in Hz) and integration (number of protons). Infrared spectroscopy (IR) was done on a Nicolet 380 FT-IR.

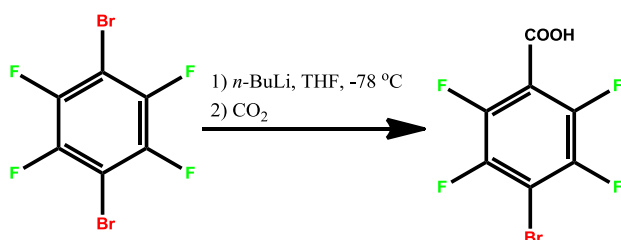
3.2.1.1 Synthesis of 2,3,5,6-tetrafluoro-4-iodobenzoic acid, IF4BA



To oven dried one-necked round-bottomed flask with stir bar was added 1,4-diiodo-2,3,5,6-tetrafluorobenzene (1g, 2.5 mmol) under a stream of Ar and the flask was sealed with rubber septum. To this flask was added dry, freshly distilled THF (70ml) via canula. This solution was cooled to $-78\text{ }^\circ\text{C}$ by immersing into dry ice –acetone bath for 5-7 mins. To this solution was then slowly added *n*-butyllithium (1.6 M solutions in hexanes, 1.65 ml, 2.6 mmol).

After 20 minutes, carbon dioxide gas was purged into reaction mixture for 15 mins followed by addition of excess solid dry ice. The reaction mixture was slowly warmed to 0 °C and quenched with 2M HCl carefully. The solvent was removed on a rotary evaporator and the product was extracted in methylene chloride. The organic phase was washed with saturated sodium thiosulfate solution, brine solution and dried using anhydrous magnesium sulfate. The solvent was removed on a rotary evaporator to yield the crude product which was triturated with cold hexane and filtered off to yield pure **IF4BA** (0.414g, 52% yield). Dec. 140 °C (Lit. dec. 140 °C) and all other characterization data matches with previously reported data.¹³

3.2.1.2 Synthesis of 2,3,5,6-tetrafluoro-4-bromobenzoic acid, BrF4BA



To oven dried one-necked round-bottomed flask with stir bar added 1,4-dibromo-2,3,5,6-tetrafluorobenzene (1g, 3.2 mmol) under a stream of Ar and flask was sealed with rubber septum. To this flask was added dry, freshly distilled THF (70ml) via canula. This solution was cooled to -78 °C by immersing into dry ice–acetone bath for 5-7 mins. To this solution was then slowly added *n*-butyllithium (1.6 M solutions in hexanes, 2.06 ml, 3.3 mmol). After 20 minutes, carbon dioxide gas was purged into reaction mixture for 15 mins followed by addition of excess solid dry ice to reaction mixture. The reaction mixture was slowly warmed to 0 °C and quenched with 2M HCl carefully. The solvent was removed on a rotary evaporator and the product was extracted in methylene chloride. The organic phase was washed with saturated sodium thiosulfate solution, brine solution and dried using anhydrous magnesium sulfate. The solvent was removed on a rotary evaporator to yield pure **BrF4BA** (0.764g, 86% yield). M.p. 128-130 °C (Lit. M.p. 128-130 °C) and all other characterization data matches with previously reported data.¹³

3.2.1.3 Synthesis of 2-aminopyrazine 1,4-diiodotetrafluorobenzene (2:1), B1-DITFB

2-Aminopyrazine (20 mg, 0.02 mmol) and **DITFB** (40 mg, 0.01 mmol) were placed in a 2 dram borosilicate vial and dissolved in 2 mL of chloroform. After four days of slow evaporation, colorless needle-shaped crystals were obtained. M. p. 132-134 °C.

3.2.1.4 Synthesis of 2-amino-5-bromopyrazine 1,4-diiodotetrafluorobenzene (2:1), B2-DITFB

2-Amino-5-bromopyrazine (20 mg, 0.01 mmol) and **DITFB** (23 mg, 0.005 mmol) were placed in a 2 dram borosilicate vial and dissolved in 2 mL of methanol. After three days of slow evaporation, colorless plate-shaped crystals were obtained. M. p. 114-116 °C.

3.2.1.5 Synthesis of 2-amino-3,5-dibromopyrazine 1,4-diiodotetrafluorobenzene (2:1), B3-DITFB

2-amino-3,5-dibromopyrazine (20 mg, 0.08 mmol) and **DITFB** (15 mg, 0.04 mmol) were placed in a clear 2 dram borosilicate vial and dissolved in 2 mL of methanol. After five days of slow evaporation, clear plate-shaped crystals were obtained. M. p. 104-106 °C.

3.2.1.6 Synthesis of 2-aminopyrazinium 2,3,5,6-tetrafluoro-4-iodobenzoate, B1-IF4BA

2-aminopyrazine (10 mg, 0.10 mmol) and 2,3,5,6-tetrafluoro-4-iodobenzoic acid (33 mg, 0.10 mmol) were placed in a 2 dram borosilicate vial and dissolved in 2 mL of methanol. After four days of slow evaporation, colorless plate-shaped crystals were obtained. M. p. 184-186 °C.

3.2.1.7 Synthesis of 2-aminopyrazinium 2,3,5,6-tetrafluoro-4-bromobenzoate, B1-BrF4BA

2-aminopyrazine (10 mg, 0.10 mmol) and 2,3,5,6-tetrafluoro-4-bromobenzoic acid (27 mg, 0.10 mmol) were placed in a clear 2 dram borosilicate vial and dissolved in 2 mL of ethanol: water (9:1) mixture. After seven days of slow evaporation, plate-shaped crystals were obtained. Dec. 135 °C.

3.2.1.8 Synthesis of 2-amino-5-bromopyrazine 2,3,5,6-tetrafluoro-4-iodobenzoic acid (1:1), B2-IF4BA

2-amino-5-bromopyrazine (10 mg, 0.05 mmol) and 2,3,5,6-tetrafluoro-4-iodobenzoic acid (18 mg, 0.05 mmol) were placed in a clear 2 dram borosilicate vial and dissolved in 2 mL of dichloromethane: ethyl acetate: hexane (1:1:1) mixture. After five days of slow evaporation, plate-shaped crystals were obtained. Dec. 150 °C.

3.2.1.9 Synthesis of 2-amino-5-bromopyrazine 2,3,5,6-tetrafluoro-4-bromobenzoic acid (1:1), B2·BrF4BA

2-amino-5-bromopyrazine (10 mg, 0.05 mmol) and 2,3,5,6-tetrafluoro-4-bromobenzoic acid (14 mg, 0.05 mmol) were placed in a 2 dram borosilicate vial and dissolved in 2 mL of ethanol: water (9:1) mixture. After five days of slow evaporation, colorless plate-shaped crystals were obtained. M. p. 120-124 °C.

3.2.1.10 Synthesis of 2-amino-3,5-dibromopyrazine 2,3,5,6-tetrafluoro-4-iodobenzoic acid (1:1), B3·IF4BA

2-amino-3,5-dibromopyrazine (10 mg, 0.03 mmol) and 2,3,5,6-tetrafluoro-4-iodobenzoic acid (12 mg, 0.03 mmol) were placed in a clear 2 dram borosilicate vial and dissolved in 4 mL of ethanol: water (9:1) mixture. After four days of slow evaporation, colorless plate-shaped crystals were obtained. M. p. 139-141 °C.

3.2.1.11 Synthesis of 2-amino-3,5-dibromopyrazine 2,3,5,6-tetrafluoro-4-bromobenzoic acid (1:1), B3·BrF4BA

2-amino-3,5-dibromopyrazine (10 mg, 0.03 mmol) and 2,3,5,6-tetrafluoro-4-bromobenzoic acid (8 mg, 0.03 mmol) were placed in a clear 2 dram borosilicate vial and dissolved in 4 mL of ethanol: water (1:1) mixture. After ten days of slow evaporation, colorless plate-shaped crystals were obtained. M. p. 106-107 °C.

3.3 Results

Hydrogen-bond geometries for **B1·DITFB**, **B2·DITFB**, **B3·DITFB**, **B1·BrF4BA**, **B1·IF4BA**, **B2·BrF4BA**, **B2·IF4BA**, **B3·BrF4BA** and **B3·IF4BA** are reported in Table 3.1

Table 3.1 Hydrogen-bond geometries for **B1·DITFB**, **B2·DITFB**, **B3·DITFB**, **B1·BrF4BA**, **B1·IF4BA**, **B2·BrF4BA**, **B2·IF4BA**, **B3·BrF4BA** and **B3·IF4BA**.

Structure	D-H···A	d(D-H)/Å	d(H···A)/Å	d(D···A)/Å	<(DHA)/°
B1·DITFB ⁱ	N(22)-H(22A)...N(21)#2	0.88	2.13	3.006(4)	176.9
B2·DITFB ⁱⁱ	N(22)-H(22A)...N(21)#2	0.85(4)	2.24(4)	3.086(3)	175(4)

B3•DITFB ⁱⁱⁱ	N(23)-H(23A)...N(24)#2	0.94(3)	2.11(3)	3.051(3)	176(3)
B1•BrF4BA ^{iv}	N211-H211...O111	0.91(2)	1.77(2)	2.6800(19)	177(2)
	N212-H212...O112	0.90(3)	1.75(3)	2.636(2)	168(3)
	N221-H22A1...O121	0.91(3)	1.81(3)	2.710(2)	171(3)
	N222-H22A2...O122	0.84(3)	1.93(3)	2.754(2)	169(3)
	N221-H22B1...O122#1	0.89(3)	1.94(3)	2.779(2)	158(2)
	N222-H22B2...O111#2	0.94(3)	2.01(3)	2.893(2)	154(2)
B1•IF4BA ^v	N211-H211...O111	0.91(2)	1.77(2)	2.6800(19)	177(2)
	N212-H212...O112	0.90(3)	1.75(3)	2.636(2)	168(3)
	N221-H22A1...O121	0.91(3)	1.81(3)	2.710(2)	171(3)
	N222-H22A2...O122	0.84(3)	1.93(3)	2.754(2)	169(3)
	N221-H22B1...O122#1	0.89(3)	1.94(3)	2.779(2)	158(2)
	N222-H22B2...O111#2	0.94(3)	2.01(3)	2.893(2)	154(2)
B2•BrF4BA ^{vi}	N(12)-H(12A)...O(22)	0.83(3)	2.30(3)	3.084(3)	158(3)
	N(12)-H(12B)...O(22)#1	0.79(3)	2.22(3)	2.904(2)	144(3)
	O(21)-H(21)...N(11)	0.77(3)	1.87(3)	2.635(2)	168(3)
B2•IF4BA ^{vii}	N(15)-H(15A)...O(21)	0.88	3.2	3.758(3)	123.3
	N(15)-H(15B)...O(22)#1	0.88	2.24	2.973(4)	140.4
	O(21)-H(21)...N(14)	0.84	1.83	2.666(3)	170
B3•BrF4BA ^{viii}	O(21)-H(21)...N(11)	0.86(3)	1.78(3)	2.630(2)	169(3)
	N(12)-H(12A)...O(22)	0.86(3)	2.17(3)	3.005(2)	166(3)
	N(12)-H(12B)...O(22)#1	0.85(3)	2.48(3)	3.196(2)	142(2)
B3•BrF4BA ^{ix}	O211-H211...N111	0.84	1.8	2.629(17)	170
	O212-H212...N112	0.84	1.81	2.639(17)	170.2
	O213-H213...N113	0.84	1.81	2.637(17)	169.8
	N121-H12A1...O221	0.88	2.15	2.995(17)	162.2
	N122-H12A2...O222	0.88	2.07	2.929(18)	166.4
	N123-H12A3...O223	0.88	2.1	2.966(17)	168.1

Symmetry transformations used to generate equivalent atoms:

i) #1 -x+1,-y+1,-z+1 #2 -x+2,-y,-z+2 ii) #1 -x,-y+1,-z #2 -x+1,-y+1,-z+1 iii) #1 -x,-y+1,-z #2 -x+3,-y,-z+1 iv) #1 -x+1,-y+1,-z+1 #2 x,y-1,z v) #1 -x+1,-y,-z #2 -x,-y+1,-z+1 vi) #1 -x+1,-y+1,-z+1 vii) #1 -x+1,-y+1,-z+1 viii) #1 -x+1,y+1/2,-z+1/2 ix) #1 x-1,y,z

3.3.1 Molecular Electrostatic Potential Calculations

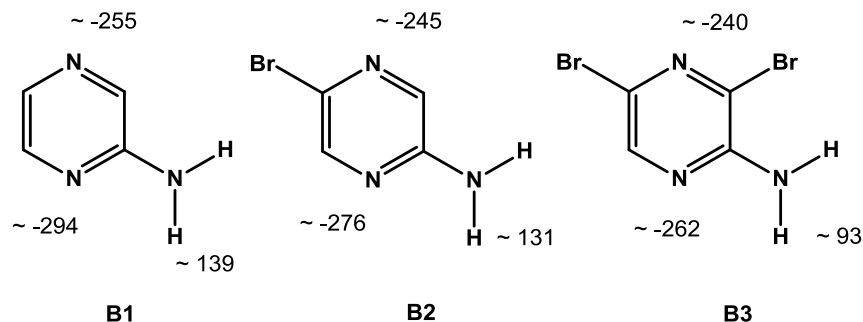


Figure 3.7 MEP surface calculations of 2-aminopyrazine, **B1**; 2-amino-5-bromopyrazine, **B2** and 2-amino-3,5-dibromopyrazine, **B3**. Numbers reflect the MEPs on atoms in kJ/mol.

Molecular electrostatic potential calculations for **B1-B3** were performed using Spartan '04 (Wavefunction, Inc., Irvine, CA). All three molecules were optimized using PM3, with the maxima and minima in the electrostatic potential surface (0.002 e au^{-1} isosurface) determined using a positive point charge in the vacuum as a probe.

3.3.2 Crystal structures

3.3.2.1 Crystal structure of 2-aminopyrazine 1,4-diiodotetrafluorobenzene, **B1**·DITFB

The crystal structure of **B1**·DITFB shows halogen bond is formed between the halogen bond donor and the 2-aminopyrazine, $\text{N}(24)\cdots\text{I}(1)$ 2.822(3) Å, Figure 3.8. The heteromer is further extended into an infinite 1-D chain through the two symmetry related $\text{NH}\cdots\text{N}$ hydrogen bonds, $\text{N}(21)\cdots\text{N}(22)$ 3.006(4) Å, Figure 3.9.

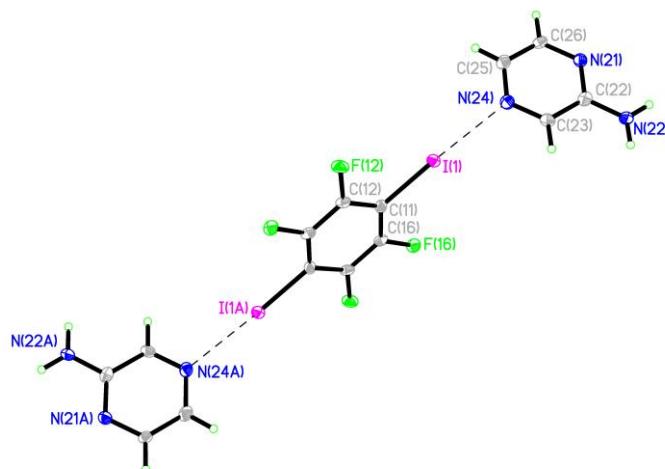


Figure 3.8 Thermal ellipsoid plot (50% probability level) and the labeling scheme of the supermolecule **B1·DITFB**.

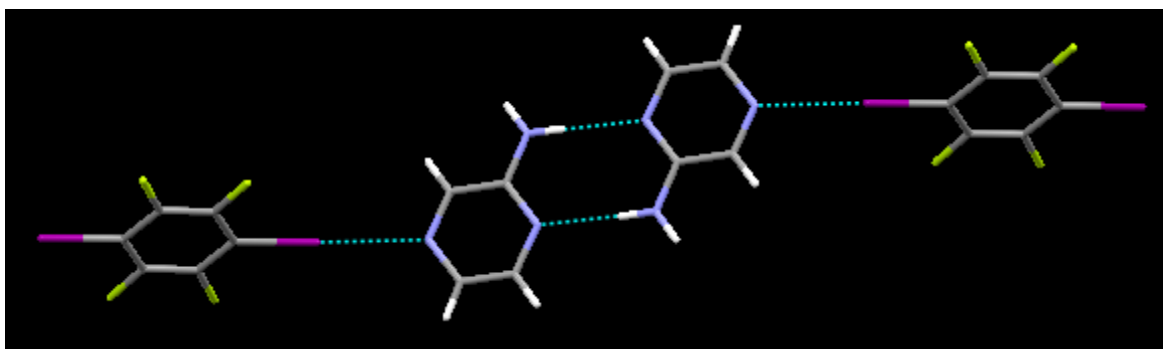


Figure 3.9 Infinite 1-D chains produced through a combination of hydrogen- and halogen bonds in the crystal structure of **B1·DITFB**.

3.3.2.2 Crystal structure of 2-amino-5-bromopyrazine 1,4-diiodotetrafluorobenzene (2:1), *B2·DITFB*

The crystal structure of **B2·DITFB** shows halogen bond is formed between the halogen bond donor and the 2-amino-5-bromopyrazine, $I(1) \cdots N(24)$ 3.025(2) Å, Figure 3.10. The heteromer is further extended into an infinite 1-D chain through the two symmetry related $NH \cdots N$ hydrogen bonds, $N(21) \cdots N(22)$ Å, 3.086(3) Å, Figure 3.11.

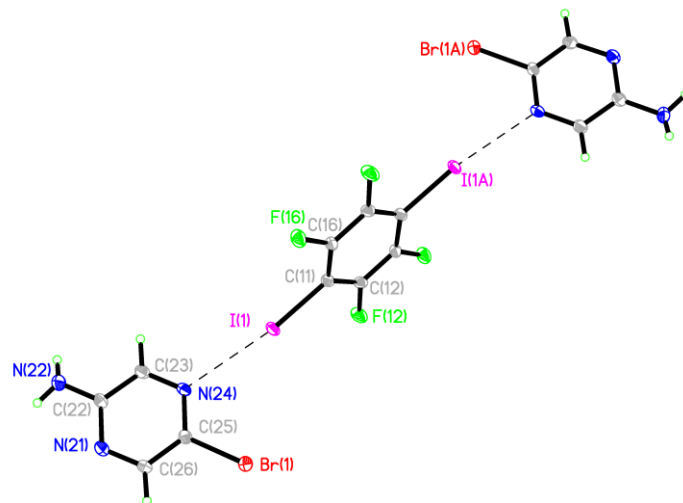


Figure 3.10 Thermal ellipsoid plot (50% probability level) and the labeling scheme of the supermolecule **B2·DITFB**.

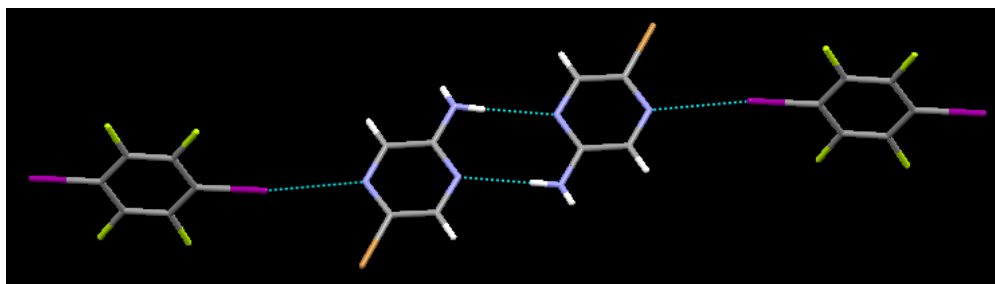


Figure 3.11 1-D motif in the crystal structure of **B2·DITFB** constructed from HB homosynthon and near-linear N...I halogen bonds (the latter is responsible for the primary assembly of the co-crystal).

3.3.2.3 Crystal structure of 2-amino-3,5-dibromopyrazine 1,4-diiodotetrafluorobenzene (2:1), **B3·DITFB**

The crystal structure of **B3·DITFB** shows halogen bond is formed between the halogen bond donor and the 2-amino-5-bromopyrazine, I(1)···N(24) 3.0459(18) Å, Figure 3.12. The heteromer is further extended into an infinite 1-D chain through the two symmetry related NH···N hydrogen bonds, N(13)···N(14), 3.051(3) Å, Figure 3.13.

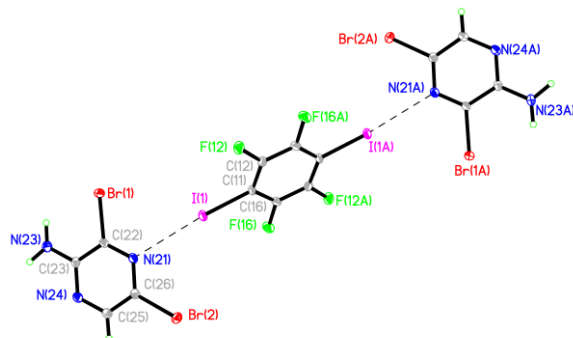


Figure 3.12 Thermal ellipsoid plot (50% probability level) and the labeling scheme of the supermolecule **B3·DITFB**.

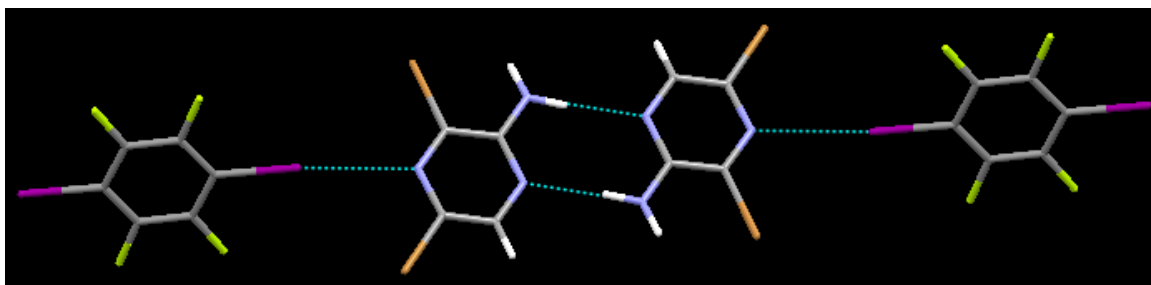


Figure 3.13 Part of an infinite chain in the structure of **B3·DITFB** produced through hydrogen bonds and halogen bonds.

3.3.2.4 Crystal structure of 2-aminopyrazinium 2,3,5,6-tetrafluoro-4-iodobenzoate, **B1·IF4BA**

When **B1** was combined with **IF4BA**, the structural examination showed that a 1:1 salt was formed (Figure 3.14). The primary intermolecular interaction in this compound is the charge-assisted two-point $\text{N-H}\cdots\text{O}^-/\text{N-H}^+\cdots\text{O}^-$ synthon. The heteromer is further extended into 1D chains via $\text{N}\cdots\text{I}$ halogen bond, $\text{N}(24)\cdots\text{I}(1)$, Figure 3.15.

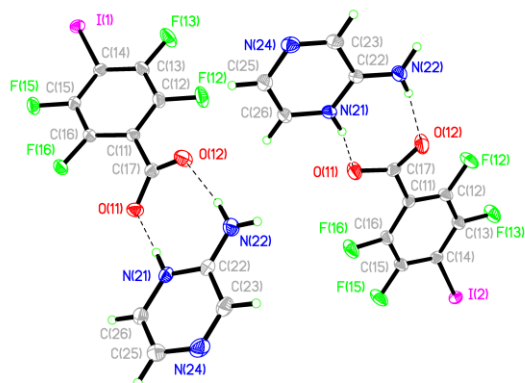


Figure 3.14 Thermal ellipsoid plot (50% probability level) and the labeling scheme of the supermolecule **B1·IF4BA**.

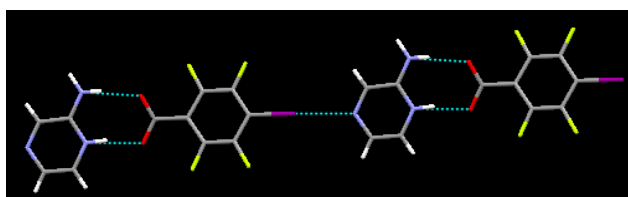


Figure 3.15 The 1:1 salt of **B1·IF4BA**. 1-D chain produced through combination of hydrogen and halogen bond.

3.3.2.5 Crystal structure of 2-aminopyrazinium 2,3,5,6-tetrafluoro-4-bromobenzoate, **B1·BrF4BA**

When **B1** was combined with **BrF4BA**, the structural examination showed that a 1:1 salt was formed (Figure 3.16). The primary intermolecular interaction in this compound is the charge-assisted two-point $\text{N-H}\cdots\text{O}^-/\text{N-H}^+\cdots\text{O}^-$ synthon. The heteromer is further extended into 1D chains via $\text{N}\cdots\text{Br}$ halogen bond, $\text{N}(24)\cdots\text{Br}(1)$, Figure 3.17.

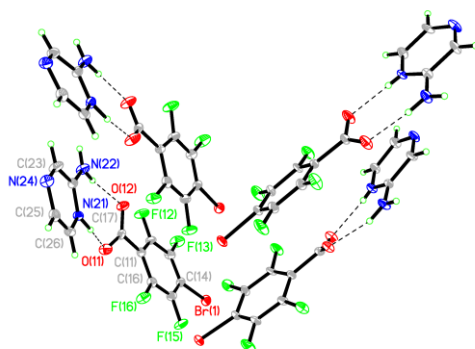


Figure 3.16 Thermal ellipsoid plot (50% probability level) and the labeling scheme of the supermolecule **B1·BrF4BA**.

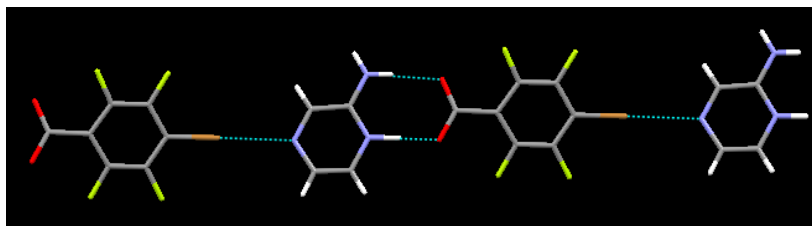


Figure 3.17 The 1:1 salt of **B1·BrF4BA**. 1-D chain produced through combination of hydrogen and halogen bond.

3.3.2.6 Crystal structure of 2-amino-5-bromopyrazine 2,3,5,6-tetrafluoro-4-iodobenzoic acid (1:1), **B2·IF4BA**

The crystal structure determination of **B2·IF4BA** confirmed 1:1 co-crystal was formed via primary O-H···N/N-H···O hydrogen-bond synthon (Figure 3.18), which is further extended into infinite 1D chain through N···I halogen bond, Figure 3.19.

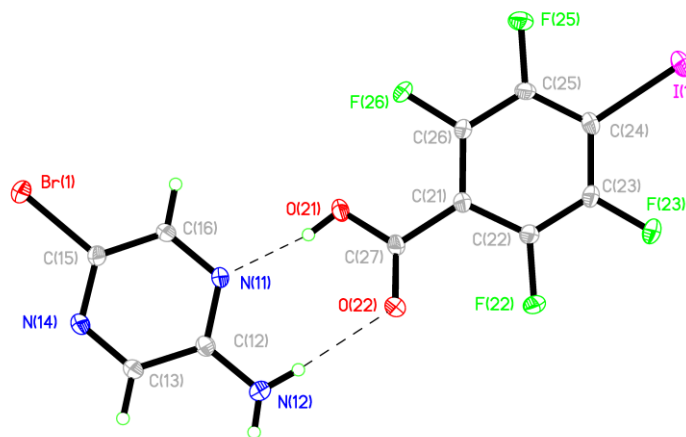


Figure 3.18 Thermal ellipsoid plot (50% probability level) and the labeling scheme of the supermolecule **B2·IF4BA**.

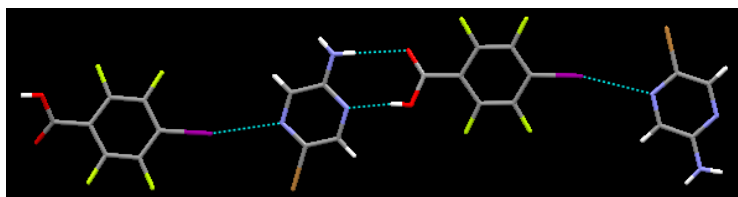


Figure 3.19 1-D motif formed in crystal structure of **B2·IF4BA**. Binary co-crystal formed through hydrogen bond and N···I halogen bond.

3.3.2.7 Synthesis of 2-amino-5-bromopyrazine 2,3,5,6-tetrafluoro-4-bromobenzoic acid (1:1), *B2·BrF4BA*

The crystal structure determination of **B2·BrF4BA** confirmed 1:1 co-crystal was formed via primary O-H···N/N-H···O hydrogen-bond synthon (Figure 3.20), which is further extended into infinite 1D chain through N···Br halogen bond, Figure 3.21.

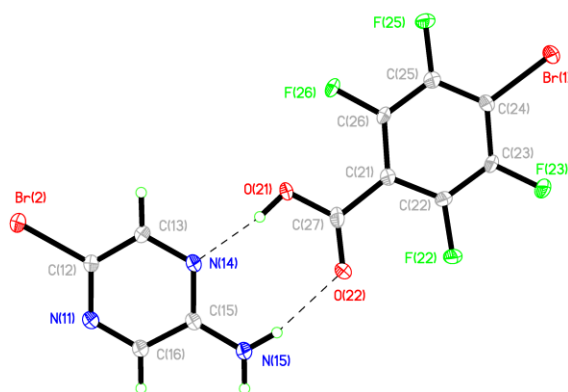


Figure 3.20 Thermal ellipsoid plot (50% probability level) and the labeling scheme of the supermolecule **B2·BrF4BA**.

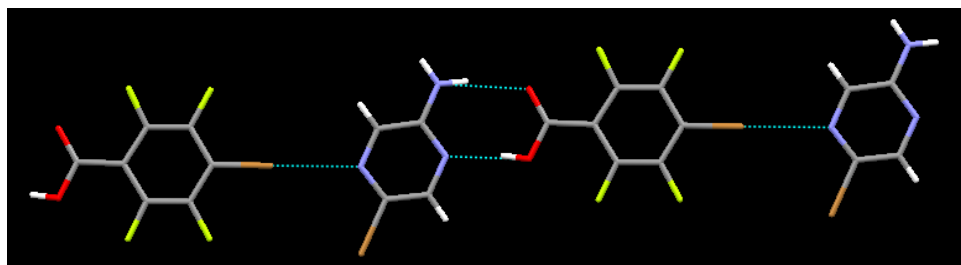


Figure 3.21 1-D motif formed in crystal structure of **B2·BrF4BA**. Binary co-crystal formed through hydrogen bond and N···Br halogen bond.

3.3.2.8 Crystal structure of 2-amino-3,5-dibromopyrazine 2,3,5,6-tetrafluoro-4-iodobenzoic acid (1:1), *B3·IF4BA*

The crystal structure determination of **B3·IF4BA** confirmed 1:1 co-crystal was formed via primary O-H···N/N-H···O hydrogen-bond synthon (Figure 3.22), which is further extended into infinite 1D chain through N···I halogen bond, Figure 3.23.

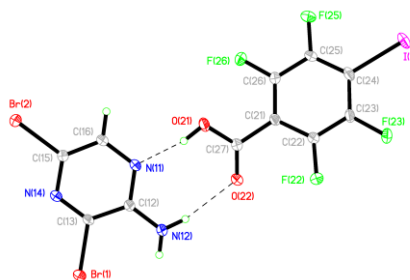


Figure 3.22 Thermal ellipsoid plot (50% probability level) and the labeling scheme of the supermolecule **B3·IF4BA**.

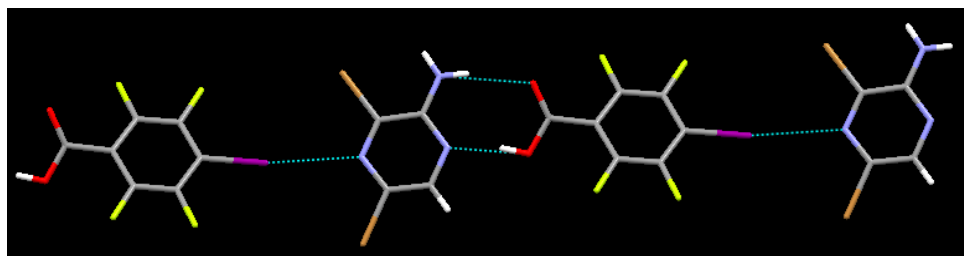


Figure 3.23 1-D motif formed in crystal structure of **B3·IF4BA**. Binary co-crystal formed through hydrogen bond and N···Br halogen bond.

3.3.2.9 Crystal structure of 2-amino-3,5-dibromopyrazine 2,3,5,6-tetrafluoro-4-bromobenzoic acid (1:1), **B3·BrF4BA**

The crystal structure determination of **B3·BrF4BA** confirmed 1:1 co-crystal was formed via primary O-H···N/N-H···O hydrogen-bond synthon (Figure 3.22), which is further extended into infinite 1D chain through N···Br halogen bond, Figure 3.23.

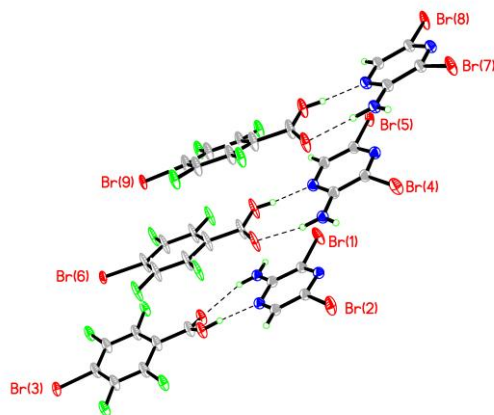


Figure 3.24 Thermal ellipsoid plot (50% probability level) and the labeling scheme of the supermolecule **B3·BrF4BA**.

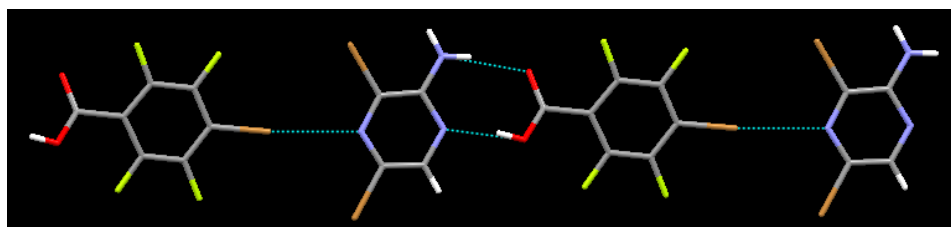


Figure 3.25 1-D motif formed in crystal structure of **B3·BrF4BA**. Binary co-crystal formed through hydrogen bond and $N \cdots Br$ halogen bond.

3.4 Discussion

3.4.1 Characterization of co-crystals or salts through IR spectroscopy

Because of the vibrational frequency and strength changes in a non-covalent interaction, FT-IR spectroscopy is a common useful tool to detect the formation of intermolecular interactions between halogen-bond donor and acceptor. Therefore, the results of the co-crystallization reactions, between **DITFB** with **B1-B3**, were first screened using IR spectroscopy, paying particular attention to the shifts in the C-I band for confirmation of halogen bonding. According to reported literature, in a “free” **DITFB**, the C-I stretch is observed around 938 cm^{-1} , however upon complexation (with a N-heterocycle) the C-I stretch shifts to lower wavenumbers by $5\text{-}10 \text{ cm}^{-1}$.¹⁴ However, we observed shifts in the range of -4 to $+4 \text{ cm}^{-1}$ (Table 3.2), this could be attributed to weaker halogen bonding interaction due to presence of weaker

bases in the current study compared to the ones studied in the literature (e.g. Pyridines, N-oxides, etc).

Table 3.2 Selected IR stretches of the supramolecular complexes.

Compounds	Free C-X stretch ¹ (cm ⁻¹)	Complexed C-X stretch (cm ⁻¹)	O-H...N (cm ⁻¹)
B1·DITFB	938	937	-
B2·DITFB		934	-
B3·DITFB		940	-
B1·IF4BA	978	977	1952, 2688
B1·BrF4BA	983	982	2024, 2707
B2·IF4BA	978	977	1887, 2406
B2·BrF4BA	983	983	1891, 2435
B3·IF4BA	978	978	1878, 2461
B3·BrF4BA	983	986	1862, 2369

¹ In corresponding to halogen bond donor (X = I or Br).

For the next set of supramolecular reactions between **IF4BA**, **BrF4BA** and **B1-B3**, product formation was confirmed by presence of broad O-H...N hydrogen bonding stretches in 1800 and 2500 cm⁻¹ region (Table 3.2). Furthermore, attempts were made at detecting whether or not an actual N...I or N...Br halogen bond had formed through changes in the C-X (X = I or Br) stretch in the IR spectrum (Table 3.2). We assigned the bands at 978 cm⁻¹ and 983cm⁻¹ band to the C-I and C-Br stretches of “free” halogenated benzoic acids **IF4BA** and **BrF4BA**, however upon complexation, we observed minimal (1 cm⁻¹) to no shift. This may be explained based on attempting to track band shifts between relatively weak interactions, which would produce very small changes in the IR spectra.

3.4.2 Establishing balance between hydrogen bonding and halogen bonding

Systematic co-crystallization reactions of **DITFB** with **B1-B3** shows the self-complementary homosynthon, N-H...N of 2-aminopyrazine was robust, and appeared intact in each of the three structures. Despite possibilities for ‘synthon crossover’ each primary interaction showed high fidelity, as the amino anti proton was unable to compete with I...N(pyrazine) interaction (Figure 3.26).

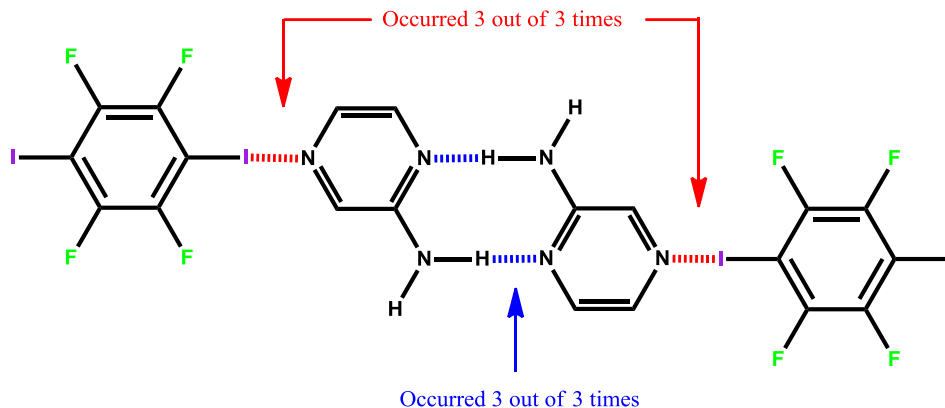


Figure 3.26 Interactions observed in crystal structures between **DITFB** and **B1-B3**.

As expected for attractive intermolecular interactions, the $N\cdots I$ distances in all three structures are shorter than the sum of the van der Waals radii of the participating atoms. Furthermore, the $N\cdots I$ distance increases as the charge on the acceptor site N4 decreases; **B1·DITFB** 2.822(3) Å; **B2·DITFB** 3.025(2) Å and **B3·DITFB** 3.046(2) Å. Despite the lower charge at the binding site N4, the $I\cdots N$ interaction prevailed against the potentially competing $N\cdots H-N(\text{amine})$ hydrogen bond. A space filling representation also indicates that the observed lengthening of the $I\cdots N$ bond is unlikely to be due to steric congestion and can therefore be ascribed to electrostatics (Figure 3.28). These findings are also in agreement with previous suggestions that halogen bonding involves some degree of electron donation from the halogen-bond acceptor (N4 in this case) to the anti-bonding bonding orbital (σ^*) of C-I.¹⁴ The C-I bond is longer, 2.095(3) Å in **B1·DITFB** (which contains the shorter $I\cdots N$ distance), than in the other two structures (**B2·DITFB** and **B3·DITFB**), 2.085(3) and 2.088(2) Å, respectively (Table 3.3).

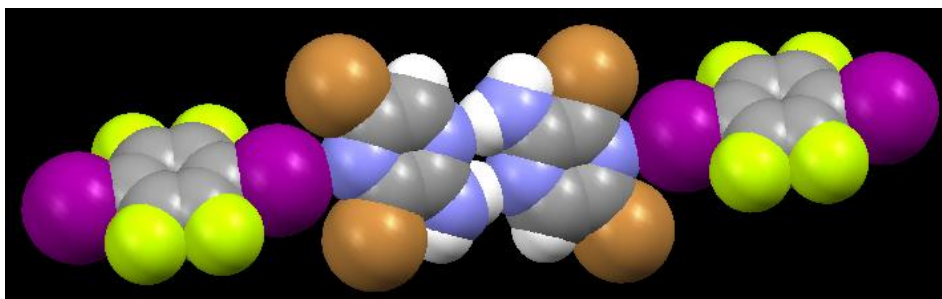


Figure 3.27 Space filling representation of a portion of the crystal structure of **B3·DITFB**.

In Chapter 2, we investigated the binding preference of the carboxylic acids and the synthon crossover was unavoidable, causing carboxylic acids binding to both ends of 2-aminopyrazine derivatives in six out of twelve cases. However, in the previous study we observed a remarkable preference of carboxylic acids (ten out of twelve times), binding to the 2-amino end of **B1-B3**. Since the two cyclic nitrogen atoms in pyrazine have comparable electrostatic charges, the carboxylic acid is far more likely to bind to the end that also contains an auxiliary amino group, capable of complementing and strengthening the O-H...N contact with a N-H(amino)...O=C(carbonyl) interaction. Supramolecular reactions between the strongest base of this study, **B1** and **IF4BA** or **BrF4BA** resulted in proton transfer from carboxylic acid to base. The remaining four reactions of weaker bases **B2** and **B3** with carboxylic acids resulted in 1:1 co-crystal formation with no proton transfer. This control over proton transfer is caused by reduction in electrostatic charge on N1 nitrogen of 2-aminopyrazine derivatives, due to addition of electron withdrawing bromine group. As predicted in 6/6 structures the carboxylic acid binds to the 2-amino end of **B1-B3** (Figure 3.28). This leaves the N4 nitrogen atom free to act as an acceptor for either an activated iodine or bromine atom. This latter interaction is, in all six cases, able to organize either ion-pairs (**B1**·**IF4BA** and **B1**·**BrF4BA**) or neutral supermolecules into infinite chains (Figure 3.28). The geometry of the resulting assembly is pre-determined due to the relative position (co-linear) of the two synthons with respect to each other. The presence of additional bromine atoms on **B2** and **B3** does not pose a supramolecular problem as the bromine/iodine atoms on **B1**·**IF4BA** and **B1**·**BrF4BA** (activated by fluorination of the ring) are significantly better halogen-bond donors and will therefore bind far more strongly to the remaining N4 atom in aminopyrazine. Moreover, proton transfer occurred only when strongest base **B1** was combined with **IF4BA** and **BrF4BA**. In the remaining four co-crystals of **B2** and **B3**, the acid proton was found to be intact due to reduced charge on N1 nitrogen atom.

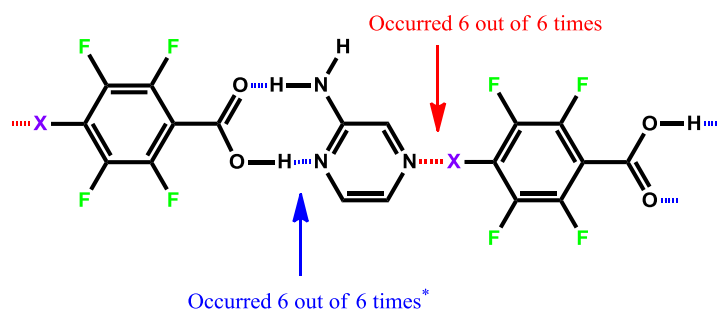


Figure 3.28 Summary of observed synthons in the crystal structures. (X = I/Br, * Including two cases where proton transfer occurred from carboxylic acid to the base **B1**)

Table 3.3 Hydrogen and halogen bonding patterns observed in the crystal structures of co-crystals and salts.

Structure	Type of hydrogen bond	Hydrogen bond distance (Å)	Type of halogen bond	Halogen bond distance (Å)	1D chains	
B1·DITFB	N-H...N	3.006(4)	I...N	2.822(3)	✓	
B2·DITFB	N-H...N	3.086(3)	I...N	3.025(2)	✓	
B3·DITFB	N-H...N	3.051(3)	I...N	3.0459(18)	✓	
B1·IF4BA	N-H...O ⁻	2.710(2)	I...N	2.9014(16)	✓	
		2.754(2)				2.8622(17)
	N-H ⁺ ...O ⁻	2.6800(19)				
		2.636(2)				
B1·BrF4BA	N-H...O ⁻	2.812(3)	Br...N	2.934(2)	✓	
		2.787(3)				
		2.795(3)				
		2.797(3)				
	N-H ⁺ ...O	2.616(3)				
		2.617(3)				
		2.653(3)				
		2.623(3)				
B2·IF4BA	N-H...O	3.084(3)	I...N	3.0057(19)	✓	
	O-H...N	2.635(2)				
B2·BrF4BA	N-H...O	2.973(4)	Br...N	2.896(3)	✓	
	O-H...N	2.666(3)				
B3·IF4BA	N-H...O	3.005(2)	I...N	3.1325(15)	✓	
	O-H...N	2.630(2)				
B3·BrF4BA	N-H...O O-H...N	2.966(17)	Br...N	3.000(13)	✓	
		2.929(18)				
		2.995(17)				
		2.6379(17)				
		2.639(17)				
		2.629(17)				

3.4.3 Secondary hydrogen bonding motifs

In addition to the primary hydrogen bonding and halogen bonding motifs found in the crystal structures, there are interactions which further stabilize these assemblies. In the co-crystals of **DITFB** with **B1-B3**, since homomeric N-H...N interaction originally present in the pyrazine derivatives is replaced by heteromeric I...N halogen bond, the anti N-H proton opts for different acceptors (Table 3.4). The anti proton (of the amino group) did not establish any structural patterns and it is therefore unlikely that it plays any significant structure-directing role in co-crystals of **DITFB**. However, in five of the six structures of **IF4BA** and **BrF4BA** (**B3·BrF4BA** is the exception) the anti-proton of the amino group is engaged in a hydrogen bond to either a carboxylate oxygen atom or the C=O moiety of a neutral acid (Table 3.4). This anti amino proton hydrogen-bonding interaction connects 1D chains into 2D networks.

Table 3.4 Summary of secondary interactions observed in crystal structures.

Structure	Anti N-H close contact
B1·DITFB	C-I...H(-N)
B2·DITFB	inactive
B3·DITFB	C-F...H(-N)
B1·IF4BA	N-H...O(of COOH)
B1·BrF4BA	N-H...O(of COOH)
B2·IF4BA	N-H...O(of COOH)
B2·BrF4BA	N-H...O(of COOH)
B3·IF4BA	N-H...O(of COOH)
B3·BrF4BA	inactive

3.5 Conclusions

In the co-crystals of **DITFB** with **B1-B3**, the self-complementary homosynthon, N-H...N of 2-aminopyrazine appeared in all three structures. Despite possibilities for ‘synthon crossover’

each primary interaction showed high fidelity, as the amino anti proton was unable to compete with the I...N(pyrazine) interaction.

Moreover, by carefully selecting hydrogen-bond and halogen-bond donor/acceptor moieties (**IF4BA**, **BrF4BA** and **B1-B3**) with appropriate complementarity and intermolecular preference, it is possible to combine both non-covalent interactions in such a way that no structural crossover or interference takes place (observed in Chapter 2). The role of charge in controlling the presence/absence of proton transfer was also highlighted as the acceptor molecule with the highest negative charge was capable of abstracting a proton from both **IF4BA** and **BrF4BA**, leading to two salts. No sign of proton transfer was observed in the other structures.

In addition, it is important to note that in order to meet specific and well-defined supramolecular challenges it is often necessary to employ custom-designed molecules with the appropriate functionalities; this led us to develop a facile one step synthetic path to 2,3,5,6-tetrafluoro-4-iodobenzoic acid and 2,3,5,6-tetrafluoro-4-bromobenzoic acid. These molecules combine two powerful halogen bond, and halogen bond donors, respectively, and may therefore find uses in a broad range of future crystal engineering efforts especially since they promote and facilitate supramolecular selectivity due to their built-in geometric differences.

This study has demonstrated the effective use of different intermolecular interaction in the synthesis of supramolecular architectures can be facilitated by ensuring that geometric complementarity minimizes possible ‘synthon crossover’ during the assembly process.

References:

- ¹ (a) Etter, M. C. *J. Phys. Chem.* **1991**, *95*, 4601. (b) Etter, M. C. *Acc. Chem. Res.* **1990**, *23*, 120. (c) Steiner, T. *Angew. Chem., Int. Ed.* **2002**, *41*, 48. (d) Thalladi, V. R.; Goud, B. S.; Hoy, V. J.; Allen, F. H.; Howard, J. A. K.; Desiraju, G. R. *Chem. Commun.* **1996**, 401.
- ² (a) Aakeröy, C. B.; Salmon, D. J. *CrystEngComm* **2005**, *7*, 439. (b) MacGillivray, L. *CrystEngComm* **2004**, *6*, 77. (c) Lehn, J.-M. *Science* **2002**, *295*, 2400. (d) Desiraju, G. R. *Acc. Chem. Res.* **2002**, *35*, 565. (e) Moulton, B.; Zaworotko, M. J. *Chem. Rev.* **2001**, *101*, 1629. (f) Wenger, M.; Bernstein, J. *Angew. Chem., Int. Ed.* **2006**, *45*, 7966. (g) Childs, S. L.; Hardcastle, K. I. *CrystEngComm* **2007**, *9*, 64. (h) Bosch, E. *CrystEngComm* **2007**, *9*, 191. (j) Pedireddi, V. R.; Chatterjee, S.; Ranganathan, A.; Rao, C. N. R. *J. Am. Chem. Soc.*, **1997**, *119*, 10867.
- ³ (a) Aakeröy, C. B.; Beatty, A. M.; Helfrich, B. A. *J. Am. Chem. Soc.* **2002**, *124*, 14425; (b) Aakeröy, C. B.; Beatty, A. M.; Helfrich, B. A. *Angew. Chem., Int. Ed.* **2001**, *40*, 3240.

⁴ *Halogen Bonding: Fundamentals and Applications*; Metrangolo, P.; Resnati, G. Eds.; Structure and Bonding; Springer: Berlin, **2008**; Vol. 126.

⁵ (a) Metrangolo, P.; Neukirch, H.; Pilati, T.; Resnati, G. *Acc. Chem. Res.* **2005**, *38*, 386. (b) Metrangolo, P.; Pilati, T.; Resnati, G.; Stevenazzi, A. *Chem. Commun.* **2004**, 1492. (c) De Santis, A.; Forni, A.; Liantonio, R.; Metrangolo, P.; Pilati, T.; Resnati, G. *Chem. Eur. J.* **2003**, *9*, 3974. (d) Cincić, D.; Friscić, T.; Jones, W. *J. Am. Chem. Soc.* **2008**, *130*, 7524. (e) Cincić, D.; Friscić, T.; Jones, W. *Chem. Eur. J.* **2008**, *14*, 747. (f) Shirman, T.; Freeman, D.; Posner, Y. D.; Feldman, I.; Fachetti, A.; van der Boom, M. E. *J. Am. Chem. Soc.*; **2008**, *130*, 8162. (g) Nguyen, H. L.; Horton, P. N.; Hursthouse, M. B.; Legon, A. C.; Bruce, D. W. *J. Am. Chem. Soc.* **2004**, *126*, 1617. (h) Triguero, S.; Llusar, R.; Polo, V.; Fourmigué, M. *Cryst. Growth Des.* **2008**, *8*, 2241. (i) Meyer, E. A.; Castellano, R. K.; Diederich, F. *Angew. Chem. Int. Ed.* **2003**, *42*, 1210. (j) Espallargas, G. M.; Brammer, L.; Sherwood, P. *Angew. Chem. Int. Ed.* **2006**, *45*, 435.

⁶ (a) Aakeröy, C. B.; Desper, J.; Helfrich, B. A.; Metrangolo, P.; Pilati, T.; Resnati, G.; Stevenazzi, A. *Chem. Commun.* **2007**, 4236. (b) Aakeröy, C. B.; Schultheiss, N.; Rajbanshi, A.; Desper, J.; Moore, C. *Cryst. Growth Des.* **2009**, *9*, 432.

⁷ A CSD analysis shows that there are currently about 37 co-crystals containing halogen bonds between **DITFB** and pyridine derivatives.

⁸ CSD search carried out on ConQuest Version 1.12 (Updated till February 2010). CSD codes for the 2-aminopyrazine based compounds showing homosynthon are; AMCPYZ, AMPYRZ, AMXPYZ. Allen, F. A., *Acta Crystallogr. Sect. B: Struct. Sci.* **2002**, *58*, 380.

⁹ J. Leroy, B. Schollhorn, J.-L. Syssa-Magale, K. Boubekeur, P. Palvadeau, *J. Fluorine Chem.* **2004**, *125*, 1379; F. C. Krebs, T. Jensen, *J. Fluorine Chem.* **2003**, *120*, 77; M. J. Robson, J. Williams, European Patent 0 196 156 B1, 1986.

¹⁰ Aakeröy, C. B.; Chopade, P. D.; Ganser, C.; Desper, J. *Chem. Commun.* **2011**, *47*, 4688.

¹¹ Aakeröy, C. B.; Rajbanshi, A.; Li, J.; Desper, J. *CrystEngComm* **2010**, *12*, 4231.

¹² (a) Aakeröy, C. B.; Fasulo, M. E.; Desper, J. *Mol. Pharm.* **2007**, *4*, 317; (b) Aakeröy, C. B.; Forbes, S.; Desper, J. *J. Am. Chem. Soc.* **2009**, *131*, 17048.

¹³ C. B. Aakeröy, N. C. Schultheiss, A. Rajbanshi, J. Desper, C. Moore, *Cryst. Growth Des.* **2009**, *9*, 432.

¹⁴ (a) Ananthavel, S. P.; Manoharan, M. *Chem. Phys.* **2001**, *269*, 49. (b) Lu, Y.-X.; Zou, J.-W.; Wang, Y.-H.; Jiang, Y.-J.; Yu, Q.-S. *J. Phys. Chem. A* **2007**, *111*, 10781.

Chapter 4 - Hierarchical halogen bonding

4.1 Introduction

In the past, we have demonstrated how co-crystallizations of ditopic hydrogen-bond acceptors with ditopic hydrogen-bond donors allows for ranking the binding strengths of different intermolecular contacts.¹ The stronger hydrogen-bond donor binds to the best hydrogen-bond acceptor whereas the weaker hydrogen-bond donor binds to the second-best acceptor site, Figure 4.1.² This observation is in agreement with work by Hunter who has demonstrated how calculated molecular electrostatic potential (MEP) surfaces can be employed for ranking the relative hydrogen-bond donor/acceptor strengths across a wide range of chemical functional groups.³ The observed hierarchical hydrogen bonding can be explained using simple electrostatic description of the hydrogen bond.

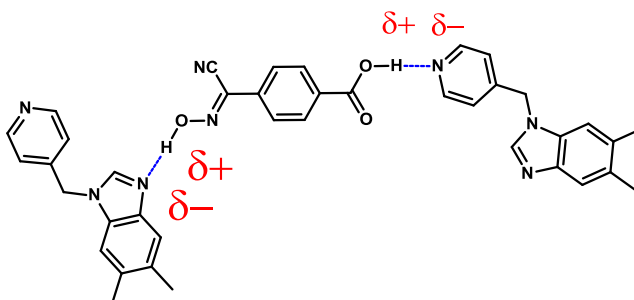


Figure 4.1 The best hydrogen-bond donor (oxime group), binds to the best acceptor, while the second-best donor (carboxylic acid) interacts with the second-best acceptor.¹

Halogen bonding (XB) has features that parallel those of hydrogen bonds in terms of strength and directionality.⁴ Resnati, and co-workers have demonstrated that XB plays a vital role in crystal engineering⁵ and has been employed in a wide range of applications, including liquid crystals,⁶ conducting and magnetic materials,⁷ alkali metal halide receptor,⁸ anion receptor,⁹ porous material design.¹⁰

Although much progress has been made, our understanding of XB remains limited in important fundamental respects. In particular, how different halogen-bond donors compete with each other for acceptors is still not clear. The goal of this chapter is to develop effective supramolecular synthetic strategies around a hierarchy of halogen bonds. We hypothesize that,

halogen bonding is primarily electrostatic in nature and electrostatic charges on halogen-bond donors and acceptors should therefore govern the outcome of the supramolecular reaction (best donor to best acceptor, second best donor to second-best acceptor, etc). To test this hypothesis we will need ditopic halogen-bond donor moieties appended with two different halogen-bond donor groups that can be ranked according to relative halogen-bonding ability. Experimental data from the solid, liquid, and gas phases confirm the theoretical predictions that the strength of the halogen-bond donor increases in the order $F < Cl < Br < I$ (Figure 4.2).¹¹

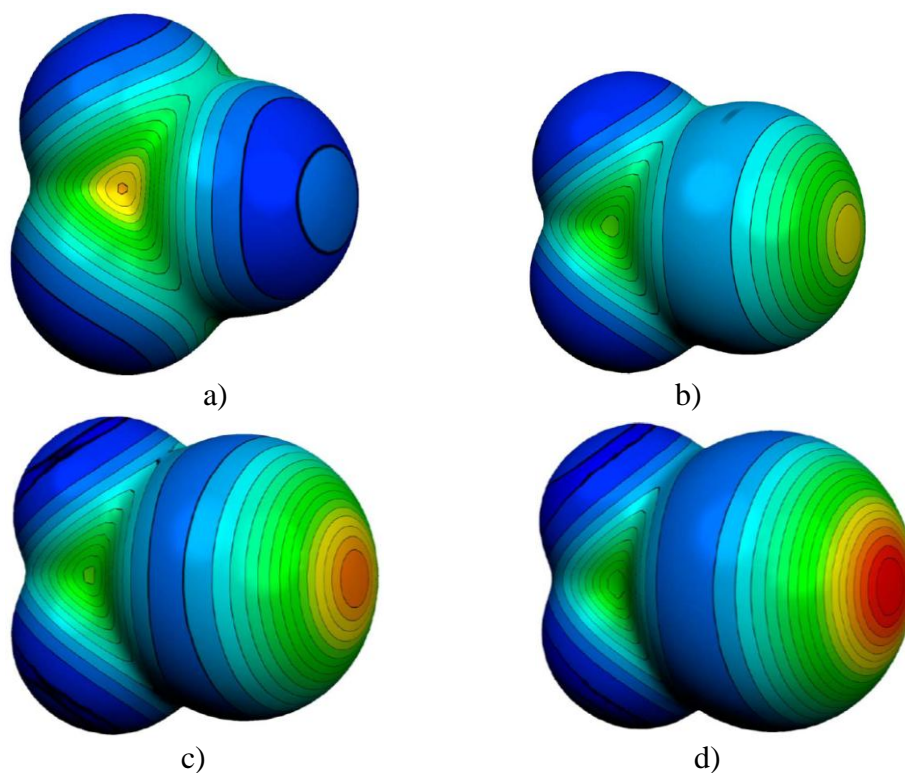


Figure 4.2 Schematic showing molecular electrostatic potential (MEP) of a) CF_4 , b) CF_3Cl , c) CF_3Br , d) CF_3I .^{11a} (Red indicates positive MEP and blue indicating negative MEP)

Moreover, the strength of the halogen-bond donor increases as the electron-withdrawing ability of the moiety, bound to a given halogen atom increases, the order of $C(sp)-X > C(sp^2)-X > C(sp^3)-X$ is generally followed.¹² Another way to control the strength of halogen-bond donors is by changing the number of electron withdrawing groups (e.g. most commonly used are fluorine atoms) on the aryl ring directly connected to the halogen atom.

To test our hypothesis, we will co-crystallize molecules equipped with two different halogen-bond donors with a variety of halogen-bond acceptors, Figure 4.3.

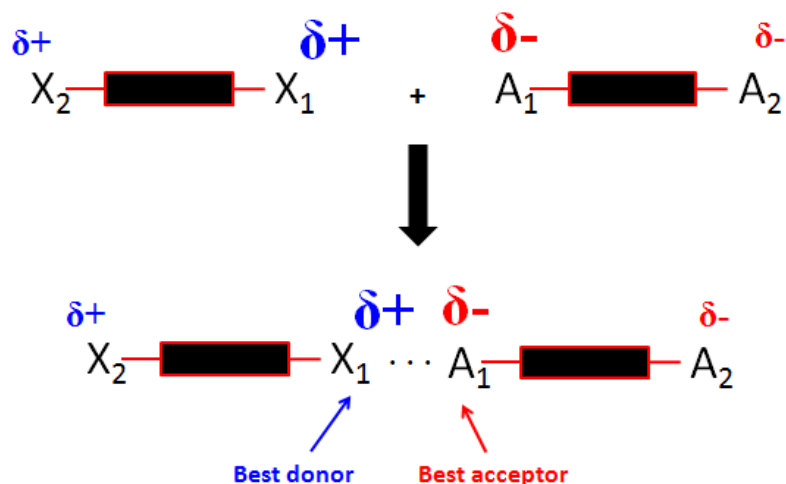


Figure 4.3 Co-crystallization reaction of ditopic halogen-bond donor with a ditopic halogen-bond acceptor.

Some of the most commonly used halogen-bond donors in crystal engineering are 1,4-diiodo-2,3,5,6-tetrafluorobenzene (**DITFB**)¹³ and 1,4-dibromo-2,3,5,6-tetrafluorobenzene (**DBTFB**).¹⁴ Therefore it seemed reasonable to combine these two powerful XB donors (iodo and bromo) to obtain the ditopic halogen-bond donor, which is 1-bromo-4-iodo-2,3,5,6-tetrafluorobenzene having iodo as the best halogen-bond donor and bromo, the second best halogen-bond donor, combined with a fluorinated aromatic ring to enhance the donor ability (Figure 4.4).

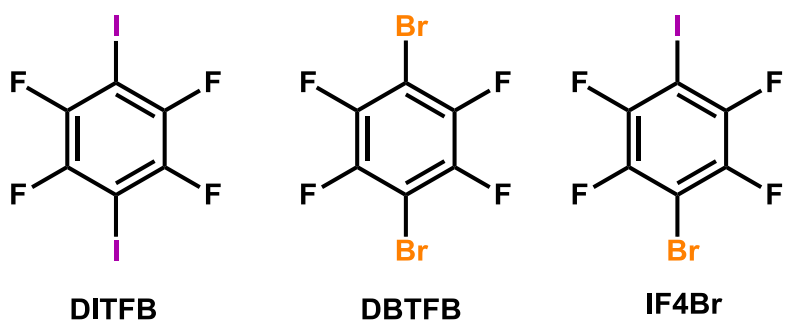


Figure 4.4 Scheme representing existing powerful halogen-bond donor molecules **DITFB**, **DBTFB** and target ditopic halogen-bond donor molecule **IF4Br**.

Our library of halogen-bond donors will also contain an extended analogue of **IF4Br**, **IF8Br**, Figure 4.5. We will co-crystallize ditopic halogen-bond donor molecules with variety of halogen-bond acceptor molecules.

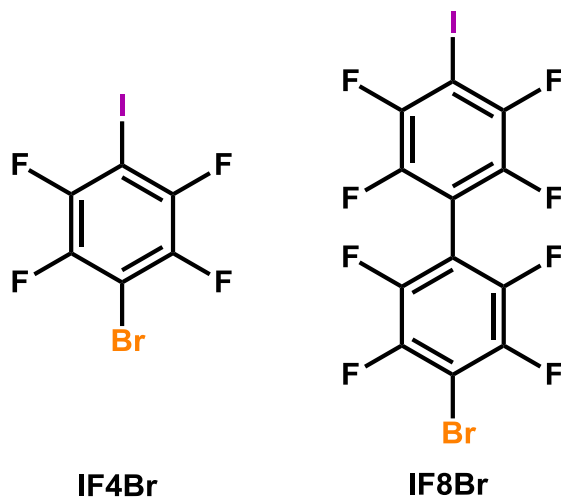


Figure 4.5 Target ditopic halogen bond donor molecules.

4.1.1 Goals

In this chapter we will focus on achieving the following goals:

- I. Design and synthesize a library of molecules equipped with two different halogen-bond donors.
- II. Co-crystallize ditopic halogen-bond donor molecules with a variety of halogen-bond acceptor molecules.
- III. Establish if a hierarchy of halogen-bond interactions can be based on electrostatics.

4.2 Result and discussion

4.2.3 Halogen bonded co-crystals

We based our synthesis of **IF4Br**, on a synthetic scheme developed in Chapter 3 for preparing **BrF4BA**, Figure 4.6.¹⁵ Since selective single metal-halogen exchange could be achieved with 1,4-dibromotetrafluorobenzene, we added iodine as an electrophile to obtain **IF4Br** in good yields (Figure 4.6). A similar synthetic protocol on 4,4'-dibromooctafluorobiphenyl yielded **IF8Br**.

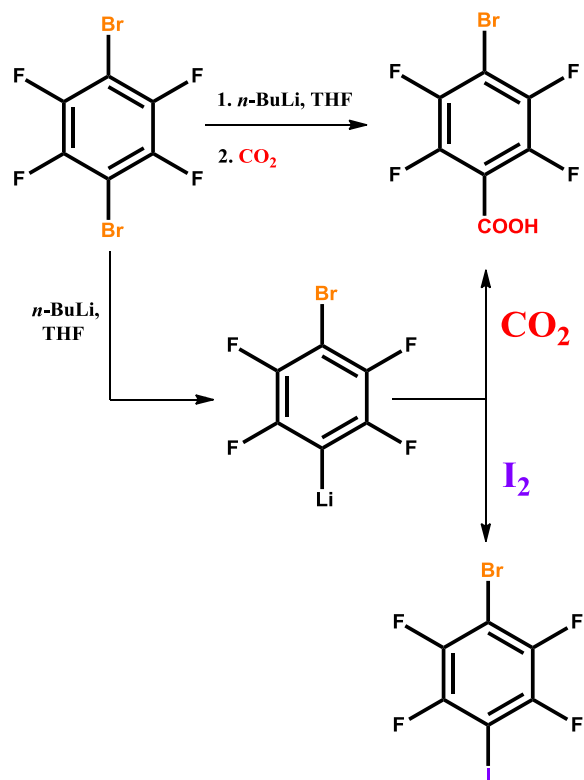


Figure 4.6 Synthetic scheme for **IF4Br**.

To quantify electrostatic charges on different XB donors, we opted for well established computational methods. It has been shown that the molecular electrostatic potential of a hydrogen atom can be correlated with its hydrogen-bond donor ability,¹⁶ which is also supported by several experimental studies.² Although many different charge calculation theories are used to predict halogen-bonding ability.^{6b,17} We selected low cost PM3 semi-empirical methods which offer reliable trends. The molecular electrostatic potential (MEP) charge calculations were performed on **IF4Br** and **IF8Br** using PM3 level of theory, Figure 4.7. The calculations confirm that iodine has a higher electrostatic positive charge than bromine.

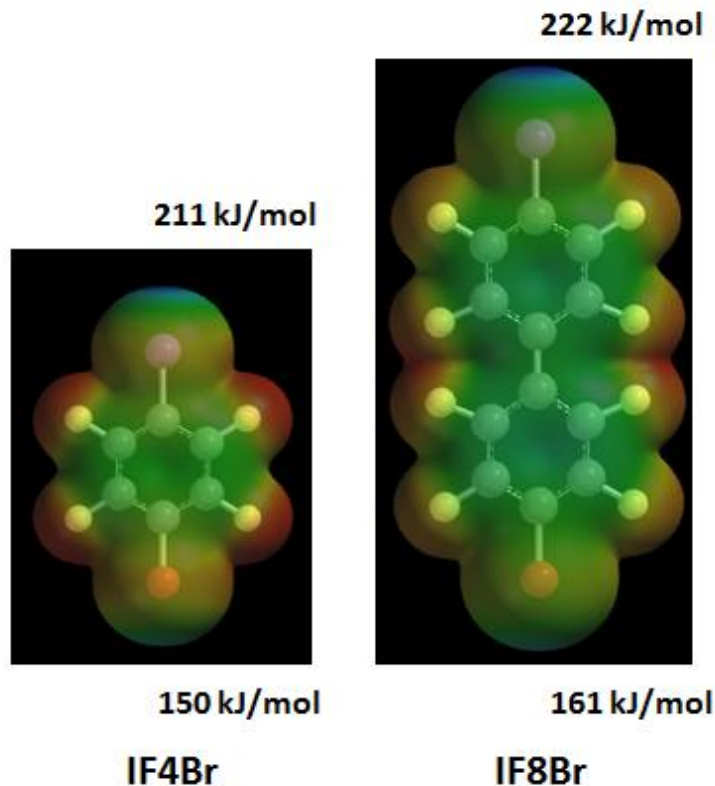


Figure 4.7 Molecular electrostatic potential charges on activated ditopic halogen bond donor sites based on PM3 semi-empirical calculation.

To test our hypothesis that halogen bonding is driven by electrostatics, we co-crystallized **IF4Br** and **IF8Br** with a ditopic symmetric halogen-bond acceptor, tetramethylpyrazine due to its proven hydrogen-bond acceptor ability (15 hydrogen-bonded co-crystals reported in the CSD). Moreover, halogen-bonded co-crystals of tetramethylpyrazine with **DITFB**¹⁸ and **I₂**¹⁹ are reported. In both, 1D chains are formed via N···I halogen bonds. However, N···Br halogen-bond based co-crystals of tetramethylpyrazine are not reported in the literature.

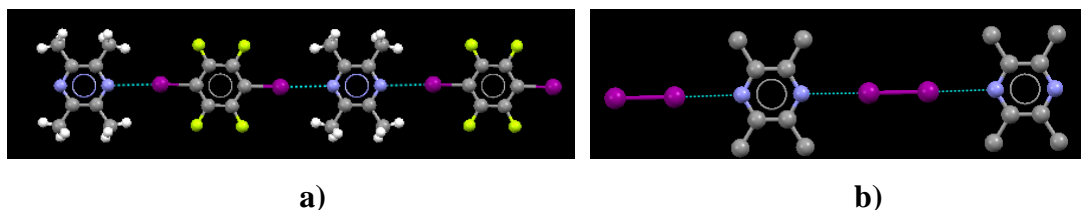


Figure 4.8 Halogen bonded co-crystals of tetramethylpyrazine with a) **DITFB**²⁰ and b) **I₂**.^{18,19,21}

We obtained a co-crystal from the reaction of **IF4Br** with tetramethylpyrazine **A** (Figure 4.9), formed via N \cdots I/Br halogen bonding giving rise to 1D chain formation. However, **IF4Br·**A** shows disordered halogen atoms at the *para* position. The occupancy factors for iodine/bromine are 0.50/0.50. Due to this positional disorder it is not possible to establish the hierarchy of supramolecular interactions.**

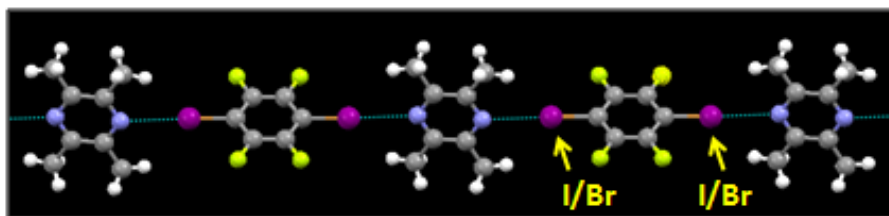
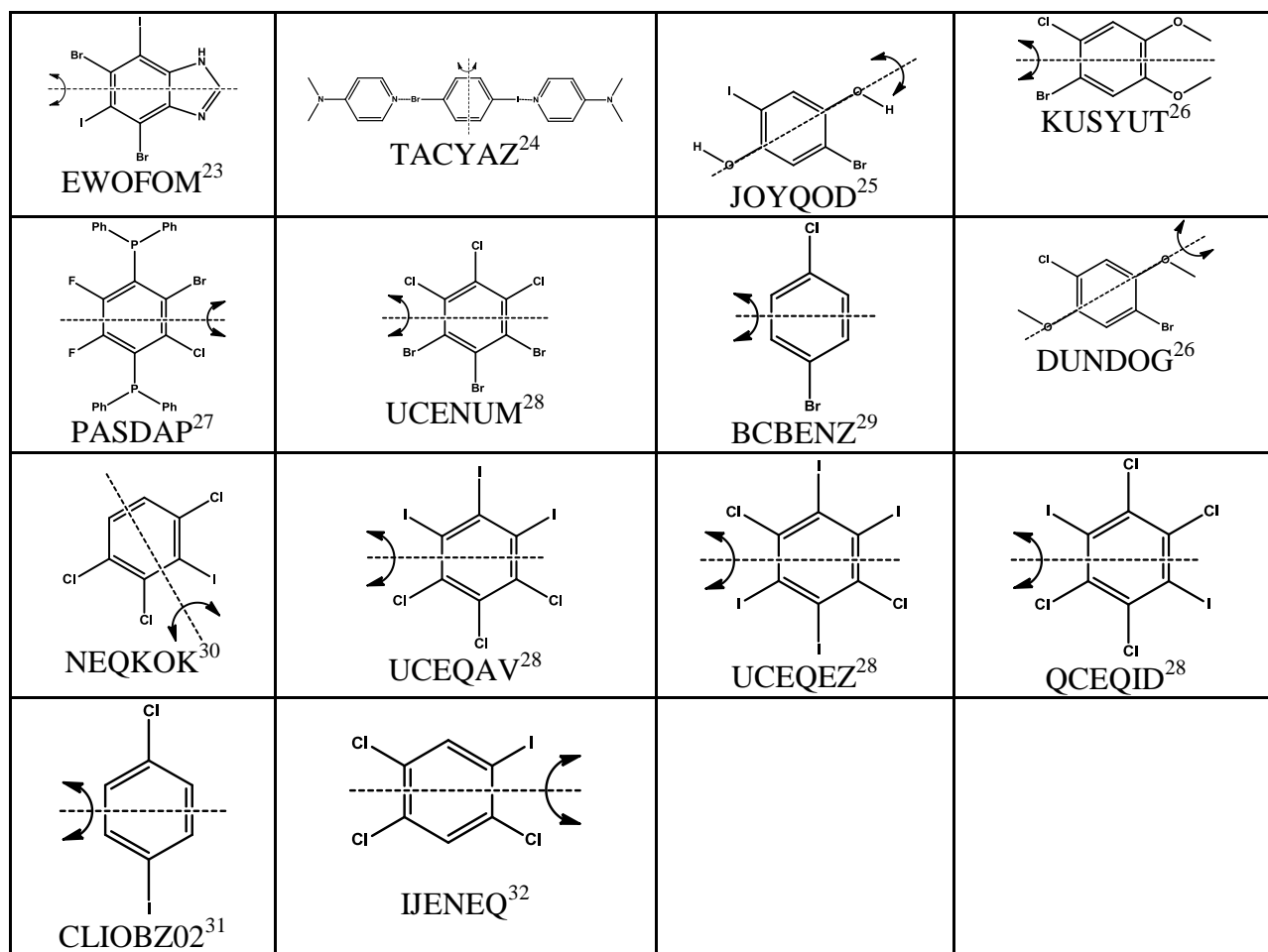


Figure 4.9 1D network formed in **IF4Br**·**A**. Structure shows disordered **IF4Br** halogen bonded to tetramethylpyrazine.

The positional disorder is a commonly occurring problem for atoms of similar sizes. The disorder between fluorine and hydrogen atoms has been studied in depth by Guru Row and co-workers.²² Their study shows that of all reported structure containing fluorine at *ortho* or *meta* to hydrogen atom around 18% are disordered. Chlorine atoms also exhibit positional disorder with nitro groups [CSD REFCODE: JOCMYI, RAZZOI and XIKKOS] and methyl groups [IHATIU, LATWIN and NULVOG]. Bromine atoms apart from exhibiting positional disorder with methyl and nitro groups, also show positional disorder with the methoxy group [EBOBEC].

In the context, we analyzed crystal structures of *ortho* and *para* phenyl substituted pairs of heavy halogen atoms in CSD. The search was performed on phenyl substituted halogens located *ortho* or *para* to each other. In all symmetric molecules (seventeen structures) disorder is found between iodo-bromo, iodo-chloro and bromo-chloro atoms, except two structures (CSD codes- UCENOG01 and UCEPAU), Table 4.1. Moreover, *para* iodo/bromo positional disorder is observed in co-crystal of N,N-dimethylpyridin-4-amine with 1-bromo-4-iodobenzene, which is akin to observation in our work.

Table 4.1 CSD survey for heavy halogen atoms located *ortho* or *para* to each other on phenyl ring. All the CSDCODES represent disordered structures. The axis with the arrow indicates the disorder along that axis.



The CSD survey shows that disorder is a commonly occurring issue which prevents the analysis of intermolecular interactions.. The crystal structure of **IF8Br·A** shows 1D chain formed via N···I/Br halogen bonds and, again iodine/bromine occupancy is 0.50/0.50 (Figure 4.10).

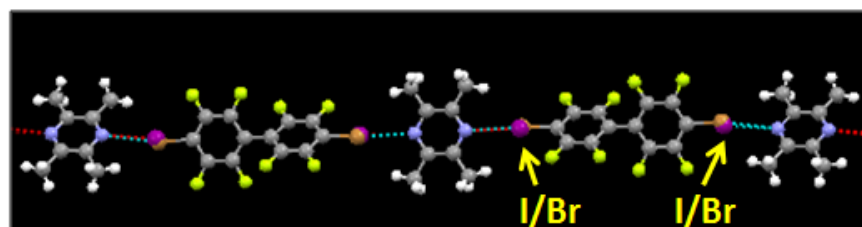


Figure 4.10 1D network formed in IF8Br·A. Structure shows I/Br disorder.

Another widely studied hydrogen-bond acceptor functionality is the *N*-oxide. In fact, the electrostatic charge on pyridine-*N*-oxide is a higher than on a pyridyl nitrogen because of its anionic character.³³ This is also supported by molecular electrostatic surface potential charges at the electronegative atoms (N -282 kJ/mol, and O⁻ -422 kJ/mol).

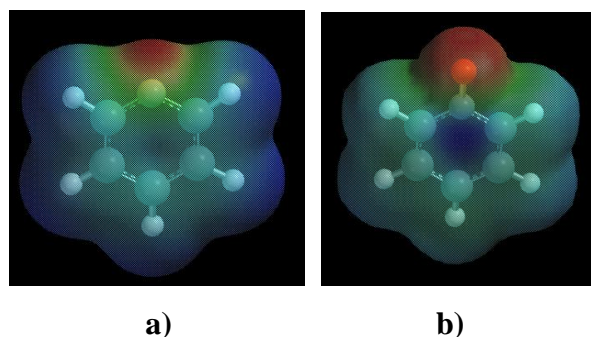


Figure 4.11 MEP surfaces of a) pyridine and b) pyridine-*N*-oxide.

Co-crystals of *N*-oxides with carboxylic acids, phenols,³⁴ amides^{34b} are prevalent. Moreover, a halogen-bonded co-crystal of *N*-oxide with **DITFB** has been reported by Resnati and co-workers (Figure 4.12).³⁵ The co-crystal is formed via O \cdots I halogen bonds.

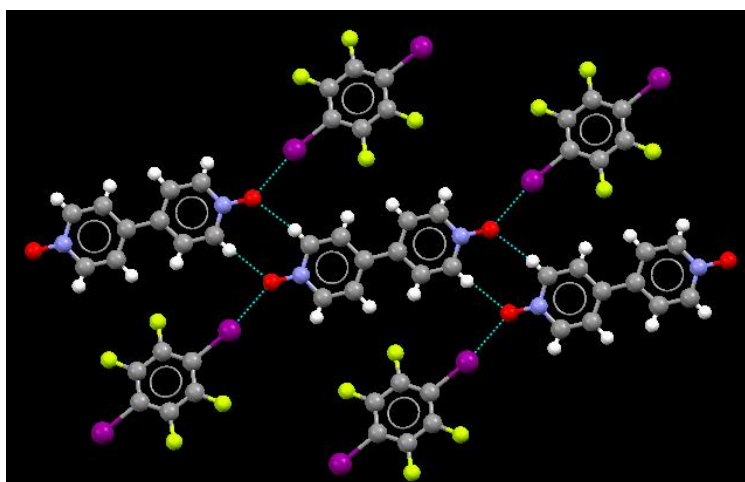


Figure 4.12 Co-crystal of **DITFB** with 4,4'-bipyridine *N,N'*-dioxide (CSD code – OCOMUO).

In order to overcome the problem with disorder, we hypothesized that if we were to add asymmetry to the halogen-bond acceptor (tetramethylpyrazine) we might avoid positional disorder. We therefore made tetramethylpyrazine mono-*N*-oxide **B** and 4,4'-bipyridine mono-*N*-oxide **C** producing two acceptor sites of different strengths, Figure 4.13. The electrostatic

charges on O are -306 kJ/mol and -307 kJ/mol for **B** and **C** respectively, which are higher than the corresponding charges on the nitrogen atoms -260 kJ/mol and -279 kJ/mol, respectively.

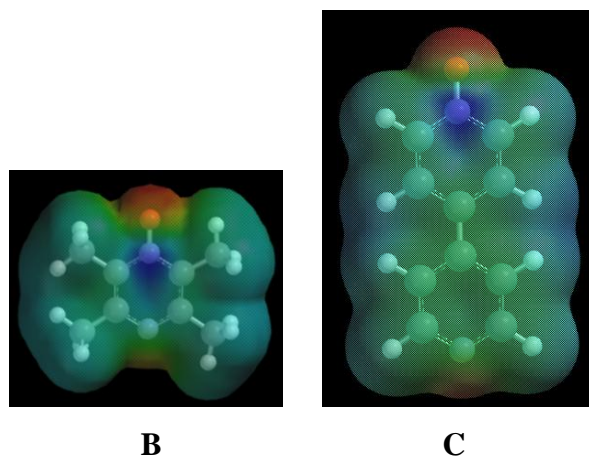
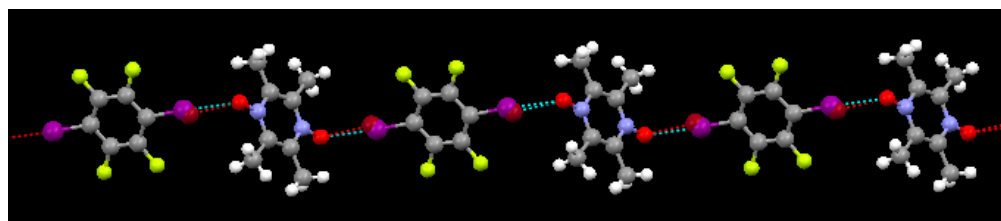
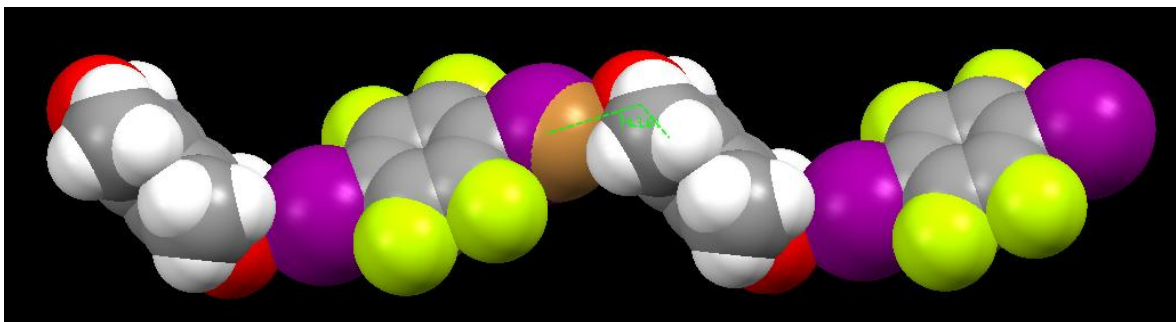


Figure 4.13 MEP surfaces of a) tetramethylpyrazine mono-*N*-oxide, **B** and b) 4,4'-bipyridine mono *N*-oxide, **C**.

If the disorder is absent in the co-crystals of **B** and **C** with ditopic halogen-bond donor molecules and if our proposed hypothesis is true, then the iodine atom should halogen bond to the oxygen atoms of *N*-oxides (best acceptor) and the bromine atom should halogen bond to the nitrogen atom (second best acceptor), Figure 4.3. However, the crystal structure of **IF4Br·B** shows, once again, I/Br disorder (50:50). Moreover, the N-O and O groups of **B** are disordered (50:50). Similar disorder was observed in co-crystals based on N-H/S (imino/thio) and N-H/O (imino/oxo) acceptor groups.³⁶



a)



b)

Figure 4.14 1D network formed in **IF4Br·B**. Structure shows disordered **IF4Br** and **B**. a) Ball and stick model and b) Space filling model.

When **B** and **IF8Br** were combined, the crystal structure shows that, I/Br positional disorder (50:50) is present, Figure 4.15. In the next attempt, we combined **IF4Br** with 4,4'-bipyridine mono *N*-oxide **C**, and still disorder persists, Figure 4.16.

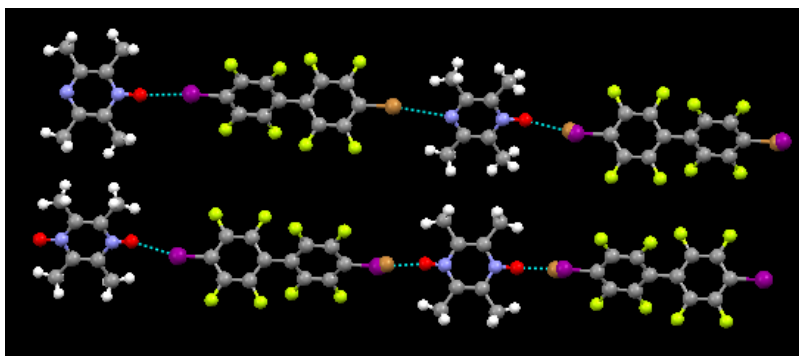


Figure 4.15 1D halogen bonded network formed in **IF8Br·B**. Structure shows disordered **IF8Br** and **B**.

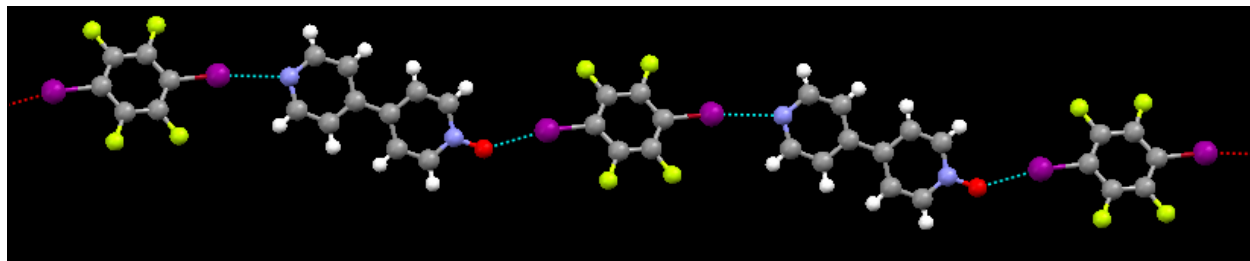


Figure 4.16 1D halogen bonded network formed in **IF4Br·C**. Structure shows disordered **IF4Br**.

The asymmetry of the acceptors was not enough to resolve the problem of positional disorder. Therefore, we made a ‘bent’ shaped acceptor equipped with two different acceptors. The acceptor containing benzimidazole and pyridine bridged by methylene bridge (to impart the bent shape)³⁷ could be suitable due to the presence of a benzimidazole (-326 kJ/mol) and pyridine (-267 kJ/mol). However, the co-crystallization product of **D** with **IF8Br** shows, once again, positional disorder in **IF8Br**, Figure 4.17.

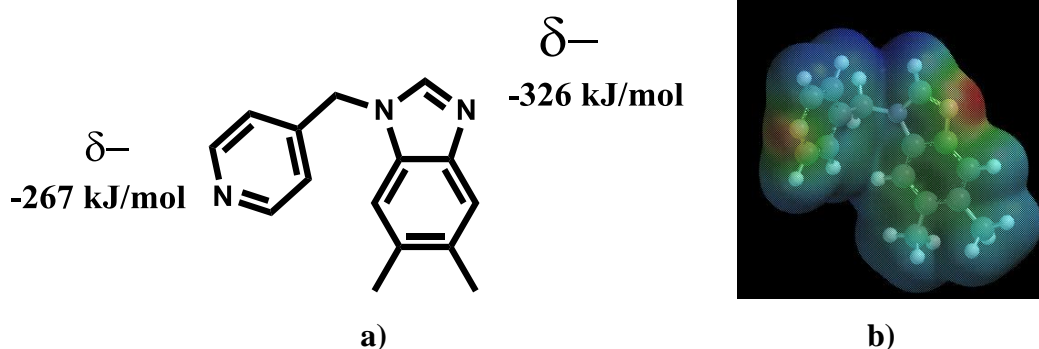


Figure 4.17 Schematic of ditopic asymmetric halogen bond acceptor a) molecular structure of **D** with MEP charges and b) its MEP surface.

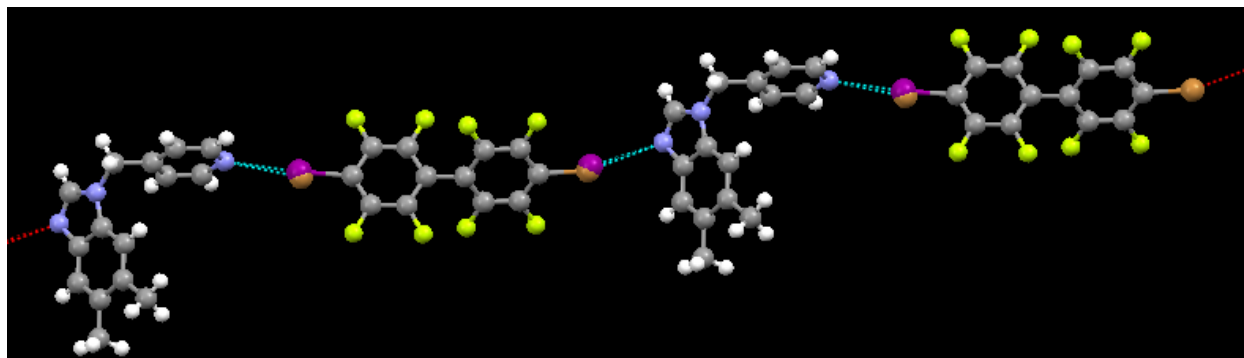


Figure 4.18 Halogen bonded network formed in **IF8Br·D** via C-X_{I/Br}...N interaction.

We analyzed the halogen-bond geometries for six structures and compared with the literature values, Table 4.2. The N...X_{I/Br}-C angle is linear and the N-O...X_{I/Br} angle is close to 120° (the angle at which the lone pairs of the oxygen atom are located).

Table 4.2 Key geometric parameters in the relevant reported structures and in our work.

	Distance (Å)	Angle (°)
	$N_{\text{aromatic}} \cdots X_{\text{I/Br}} - C_{\text{aromatic}}$	
Reported	2.97	170.82
Current study	2.97	170.52
	$N_{\text{aromatic}} - O \cdots X_{\text{I/Br}}$	
Reported	2.91	131.66
Current Study	2.61	136.17

Next, we decided to use single-point acceptor molecules (e.g. substituted pyridines). According to molecular electrostatic potential surface calculations, an iodine atom should be the best XB donor site (compared to bromine atom), thus bind preferentially to only available acceptor site. Our choice of XB acceptor is based on proven halogen-bond forming ability of 4-(*N*-alkylamino)pyridines with halogen-bond donors of varying strengths.³⁸ We chose 4-(*N*-pyrrolidinyl)pyridine **E** and 4-(*N,N*-dimethylamino)pyridine **F** as XB acceptor molecules. We obtained two crystal structures, Figure 4.19, and in both of them, 1:1 co-crystals are formed. The disorder **IF8Br·E** is I/Br 85:15/15:85. However, **IF8Br·F** co-crystal shows I/Br 81:19 disorder, with the iodine atom halogen bonding to the pyridyl nitrogen and the bromine atom is structurally inactive. Although disorder is present, the majority (81%) of the co-crystal fits with a best donor-best acceptor hypothesis.



Figure 4.19 1:1 co-crystal formed by combination of **IF8Br** with a) 4-(*N*-pyrrolidinyl)pyridine **E** and b) 4-(*N,N*-dimethylamino)pyridine **F** (Disorder is removed for clarity).

Overall, our proposed strategy for adding asymmetry to the XB acceptor molecules was ineffective in solving disorder problem. Therefore, we decided to add asymmetry to the XB donor molecules. We opted for a molecule with two different activated halogen bond donors (fluorinated phenyl ring bearing iodo or bromo) bridged via an ester linkage. We synthesized

four novel halogen-bond donor molecules **I**, **II**, **III** and **IV**, bearing at least two halogen atoms of varying electrostatic charges, Figure 4.20. **I-IV** were synthesized from the corresponding carboxylic acid and phenols using DCC (*N,N'*-dicyclohexylcarbodiimide). However, we were unable to obtain single crystals from co-crystallization reactions of **I-IV** with variety of halogen bond acceptors as, in all cases, oils were obtained.

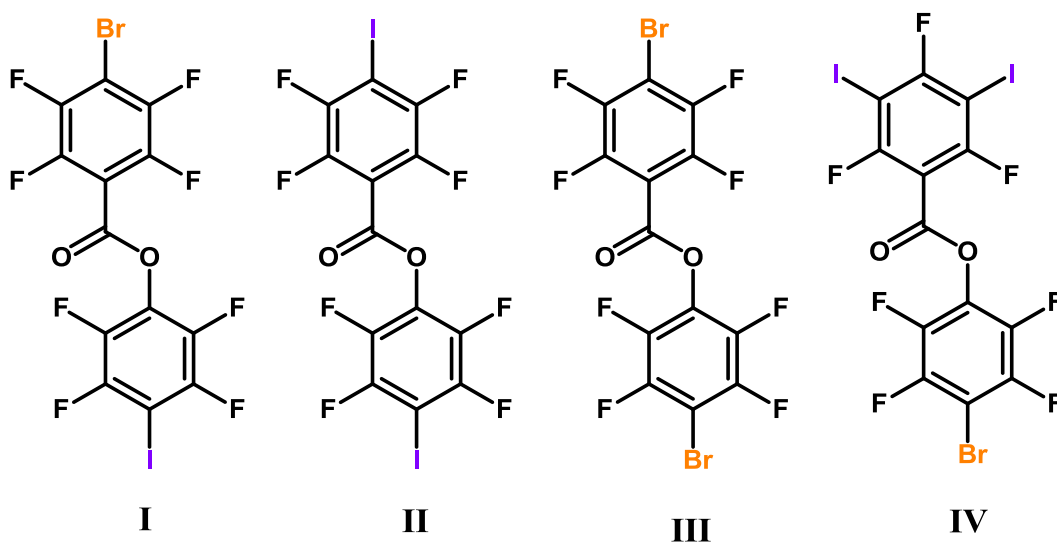


Figure 4.20 An ester bridged halogen-bond donor molecule library.

The problem of crystal growth is a commonly occurring issue, and sometimes it may take years until the exact experimental conditions for crystallizations are found. We anticipated that if hydrogen-bond donor and acceptor groups are added to the XB donor molecule, then the hydrogen-bond interaction might help in crystal growth. Therefore we synthesized XB donor molecules with an amide linker **V** using an acid chloride and amine coupling reaction, Figure 4.21. Amides are known to form amide \cdots amide self-complementary hydrogen bonds³⁹ and this will also ensure that we have no interference from the N-H donor competing with XB donors for the acceptor site.

The crystal structure of **V** shows that C=O \cdots H-N hydrogen bonds forms ladder with no disorder in I and Br atoms. The strategy of adding asymmetry works in resolving positional disorder. However, we were unable to obtain single crystals from co-crystallization reactions of **V** with XB acceptors. Therefore we synthesized another amide based XB donor **VI**, with both halogen atoms (I and Br) activated, which should help in forming halogen bonds.

We coupled 4-bromotetrafluoroaniline with 4-iodotetrafluorocarboxylic acid chloride to obtain **VI**. Since the NH group is directly connected to phenyl ring bearing bromo donor, it should lower the charge (due to electron donating NH lone pair) and the presence of C=O on the phenyl ring of the iodo donor will enhance the electrostatic charge on the iodine atom. The PM3 calculations on **VI** confirms the desired trend with the charge on the iodine atom being highest (232 kJ/mol) and on bromine atom (148 kJ/mol) being the lowest, Figure 4.21.

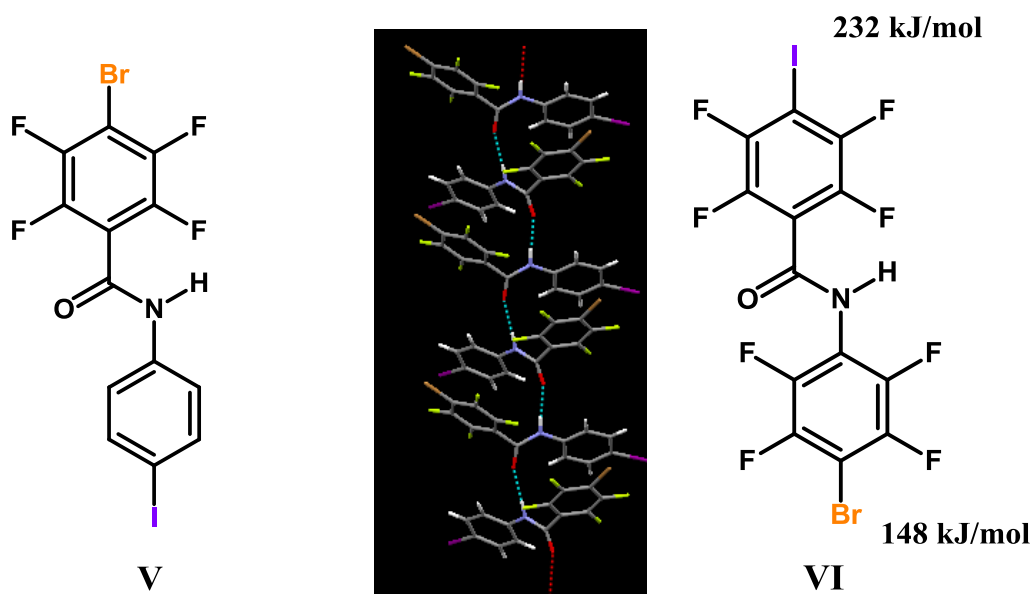


Figure 4.21 The molecular structure of **V** (left), ladder formation via C=O \cdots H-N interactions in the crystal structure of **V** (center) and **VI** with MEP charges on iodo and bromo XB donor (right).

The first crystal structure from a combination of **VI** and 1,2-*bis*(4-pyridyl)ethylene⁴⁰ **bipyethylene** shows no disorder for I and Br atoms but the desired C=O \cdots H-N interaction, Figure 4.22. Both bromo and iodo XB donors are halogen bonded to nitrogen atoms of **bipyethylene**, the N-X \cdots N distance and angle for X = I are 2.73 Å and 177.63°, which is shorter distance and closer angle to 180° compared to that for X = Br (2.75 Å and 178.66°). Although the differences in distances and angles are small, they do follow the trend observed in the literature.⁴¹

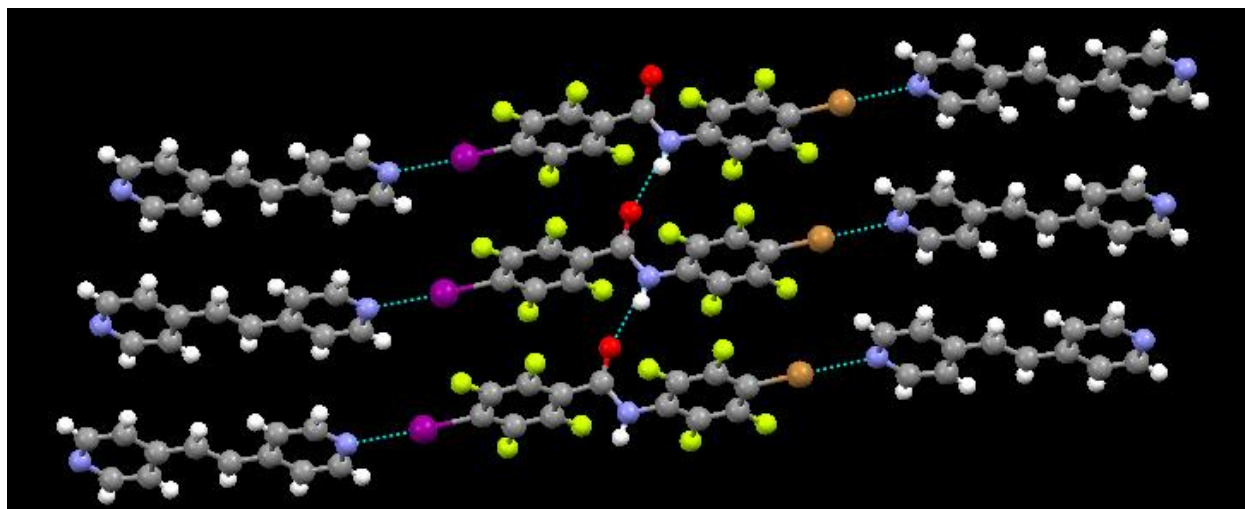


Figure 4.22 2D sheet generated in the crystal structure of **VI**·**bipyethylene** via combination of $N\cdots I$, $N\cdots Br$ and $C=O\cdots H-N$ interactions.

In our next attempt we combined **VI** with 1,2-*bis*(4-pyridyl)ethane⁴² **bipyethane**. The crystal structure of **VI**·**bipyethane** shows that I/Br disorder is absent, Figure 4.23 and the desired $I\cdots N(\text{pyridyl})$ halogen bond is formed. However, the amide ladder ($C=O\cdots H-N$) is disrupted and $N-H\cdots N$ (pyridyl from **bipyethane**) interaction is observed.⁴³ Another salient feature of this structure is that the activated bromine atoms are not taking part in a self-assembly (although a carbonyl oxygen atom was available⁴⁴). The preferential $I\cdots N$ interaction over $Br\cdots XB$ acceptor unambiguously proves our hypothesis that halogen bonding is governed by electrostatic charges on the halogen bond donors.

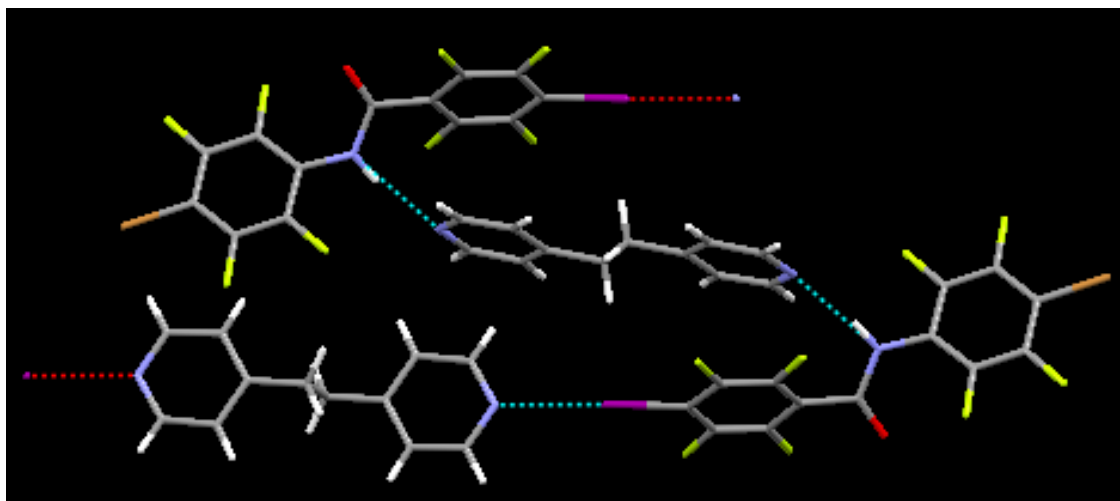


Figure 4.23 Zig-zag network formed via a combination of I···N and N-H···N interactions in the structure of **IF8Br·bipyethane**.

The last co-crystal we obtained was from a combination of **VI** and 4,4'-bipyridine (**bipy**). The crystal structure of **VI·bipy** shows that 2:1 co-crystal is formed via the expected N···I halogen bond giving rise to 1D chains. The chains are connected via amide C=O···H-N interactions to form 2D sheets similar to **VI·bipyethylene** structure. Moreover, bromine atoms once again do not participate in the self assembly instead, Br···Br type I contacts are present.⁴⁵ Once again, our hypothesis of best donor (iodo) halogen bonding to best acceptor (py). Moreover, in the absence of second best acceptor, the second best donor (bromo) does not take part in halogen bonding.

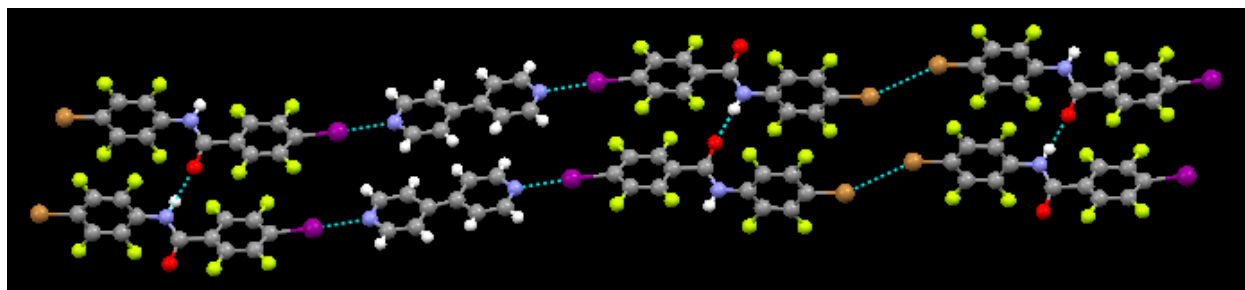


Figure 4.24 2D sheets in the crystal structure of **VI·bipy** via a combination of N···I, N···Br and C=O···H-N interactions.

Our results support our idea that hierarchical halogen bonds are based on the electrostatic potential charges of the donors.

4.3 Conclusions

Figure 4.25 summarizes pathway followed in this chapter to solve problem of disorder and establish hierarchical halogen bonding. The steps are as follows:

1. Co-crystallized symmetric halogen-bond donors (**IF4Br** and **IF8Br**) with symmetric halogen-bond acceptor. The co-crystals show I/Br disorder.
2. Co-crystallized symmetric halogen-bond donors (**IF4Br** and **IF8Br**) with asymmetric halogen-bond acceptor. The co-crystals again show I/Br disorder.

3. Co-crystallized symmetric halogen-bond donor (**IF8Br**) with a ‘bent’ asymmetric halogen-bond acceptor. The I/Br disorder persists.

4. Co-crystallized symmetric halogen-bond donor (**IF8Br**) with single point halogen-bond acceptor. The I/Br disorder is reduced to ca.15%. One co-crystal shows hierarchical halogen bonding.

5. Introduced asymmetry to the halogen-bond donor. The co-crystallizations of the asymmetric halogen-bond donor with bipyridyl based moieties show no I/Br disorder and hierarchical halogen-bonding interaction.

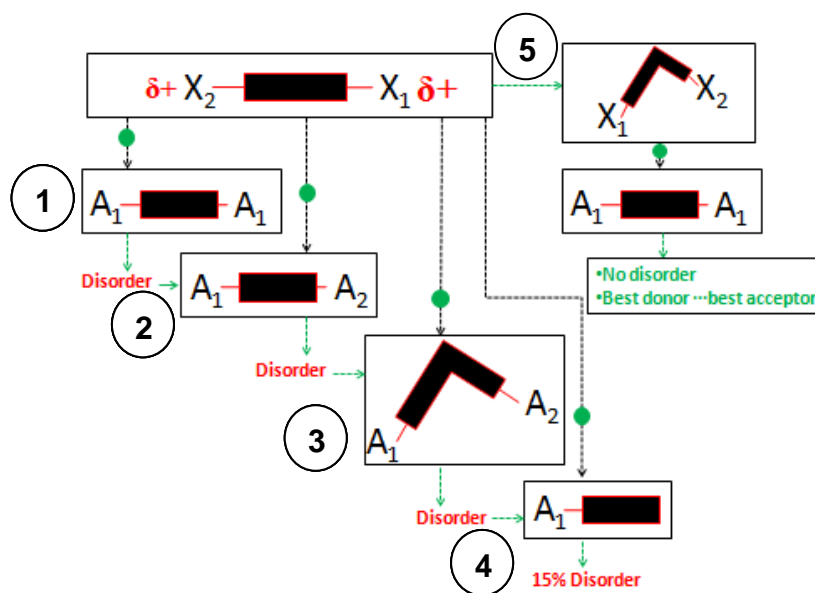


Figure 4.25 Flow chart summarizing outline of the chapter. Numbers indicate path direction. Green circles represent co-crystallization reaction.

In this chapter following goals are achieved:

I. Designed and synthesized a library of eight molecules equipped with at least two different halogen bond donors.

II. Positional disorder problem of I/Br atoms is solved by introducing asymmetry in halogen bond donor molecules.

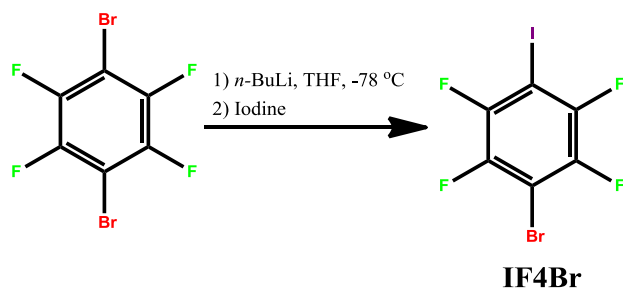
III. Successfully established a hierarchy in halogen-bond interaction based on electrostatics.

4.4 Experimental

4.4.1 Synthesis of halogen bond donors

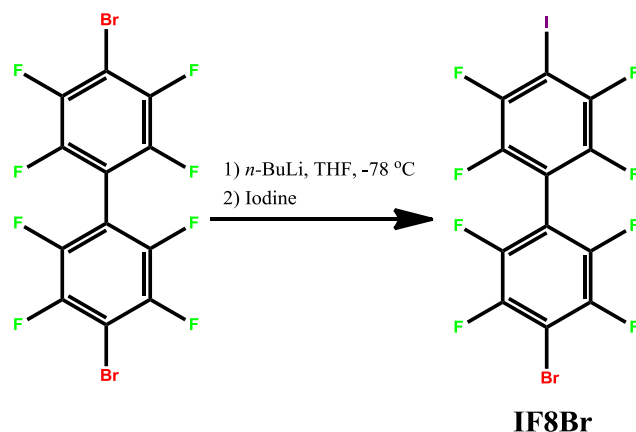
^1H NMR spectra were recorded on a Varian Unity plus 400 MHz spectrometer in CDCl_3 or *d*-DMSO. Data is expressed in parts per million (ppm) downfield shift from tetramethylsilane or residual protiosolvent as internal reference and are reported as position (in ppm), multiplicity (s = singlet, d = doublet, t = triplet, m = multiplet), coupling constant (*J* in Hz) and integration (number of protons). Melting points were recorded on a Fisher-Johns melting point apparatus and are uncorrected. Infrared spectroscopy (IR) was done on a Nicolet 380 FT-IR. All chemicals were purchased from Aldrich and Fisher and used without further purification, unless otherwise noted.

4.4.1.1 Synthesis of 1-bromo-2,3,5,6-tetrafluoro-4-iodobenzene, IF4Br



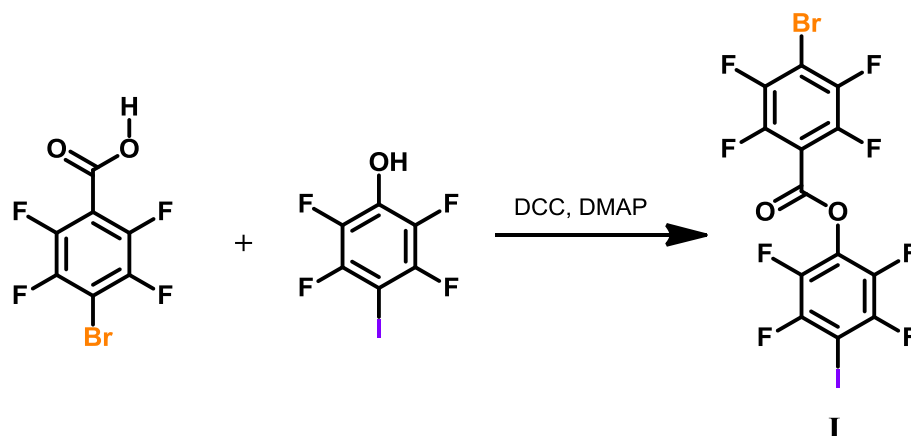
To an oven dried flask was added 1,4-dibromo-2,3,5,6-tetrafluorobenzene (1g, 3.2 mmol) under a stream of Ar and sealed the flask with rubber septum. To this flask was added dry, freshly distilled THF (70mL) via canula. This solution was cooled to $-78\text{ }^\circ\text{C}$ by immersing into dry ice-acetone bath for 5-7 mins. To this solution was then slowly added *n*-butyllithium (1.6 M solutions in hexanes, 2.06 mL, 3.3 mmol). After 20 minutes, iodine (2.06g, 8 mmol) was added and the reaction mixture was slowly warmed to room temperature and saturated sodium thiosulfate solution was added to obtain a clear solution. The product was extracted with methylene chloride (3x100 mL). The organic phase was dried using anhydrous magnesium sulfate. The solvent was removed on a rotary evaporator to yield pure **IF4Br** (0.95g, 82% yield). M.p. $87\text{-}89\text{ }^\circ\text{C}$. ^{19}F NMR (δ_{H} ; 400 MHz, CDCl_3): $-118.74 - -118.94$ (m, 2F), $-131.06 - -131.47$ (m, 2F). IR: 2919, 2361, 1667, 1469, 1440, 1356, 1224, 976, 948, 771, 757, 572.

4.4.1.2 Synthesis of 4-bromo-2,2',3,3',5,5',6,6'-octafluoro-4'-iodo-1,1'-biphenyl, IF8Br



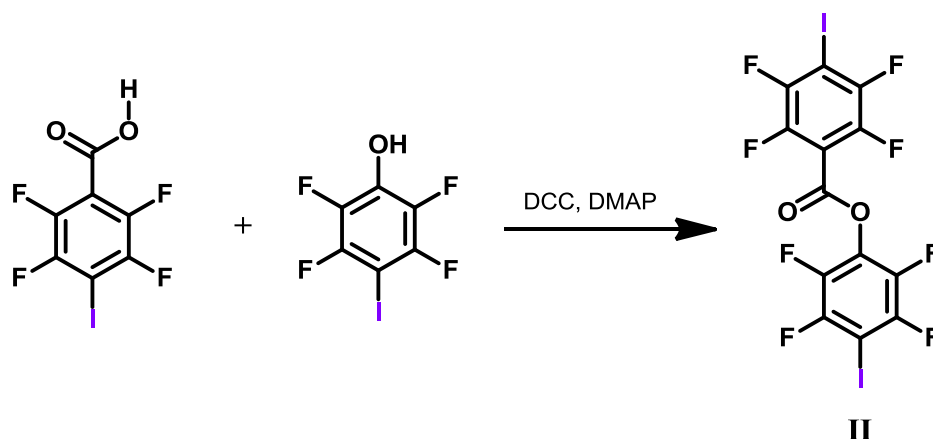
To an oven dried flask was added 4,4'-dibromo-2,2',3,3',5,5',6,6'-octafluoro-1,1'-biphenyl (1g, 2.2 mmol) under stream of Ar and the flask was sealed with rubber septum. To this flask was added dry, freshly distilled THF (40mL) via canula. This solution was cooled to $-78\text{ }^{\circ}\text{C}$ by immersing into dry ice –acetone bath for 5-7 mins. To this solution was then slowly added *n*-butyllithium (1.6 M solutions in hexanes, 1.4 mL, 2.26 mmol). After 20 minutes, iodine (0.57 g, 2.2 mmol) was added into a reaction mixture. The reaction mixture was slowly warmed to room temperature and saturated sodium thiosulfate solution was added to obtain a clear solution. The product was extracted with methylene chloride (3x100 mL). The organic phase was dried using anhydrous magnesium sulfate. The solvent was removed on rotary evaporator to yield pure **IF8Br** (1.02g, 93 % yield). M.p. 104-108 $^{\circ}\text{C}$. ^{19}F NMR (δ_{H} ; 400 MHz, CDCl_3): $-119.78 - -120.10$ (m, 2F), $-132.60 - -132.93$ (m, 2F), $-137.30 - -137.64$ (M, 2F), $-137.70 - -137.98$ (m, 2F). IR: 2940. 2856, 1631, 1465, 1366, 1221, 1221, 1109, 975, 954, 861, 716, 582..

4.4.1.3 Synthesis of 4-bromo-2,3,5,6-tetrafluorophenyl 2,3,5,6-tetrafluoro-4-iodobenzoate, I



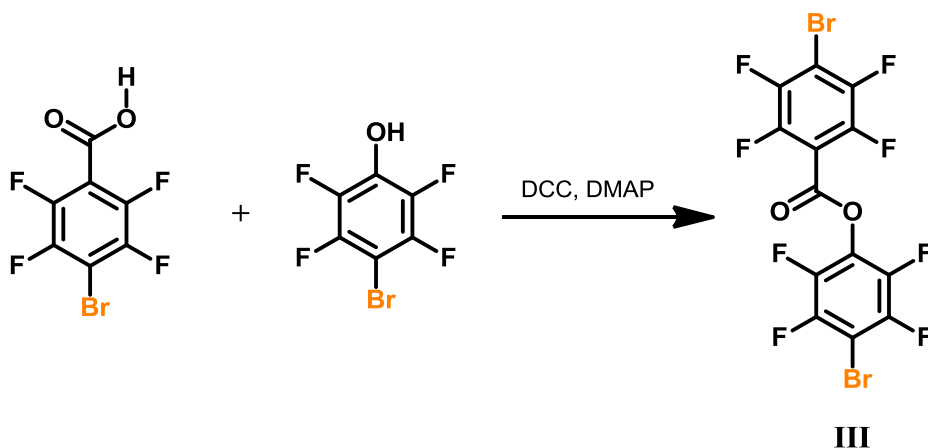
To an oven dried 50 mL flask was added 4-bromotetrafluorobenzoic acid (1.07g, 3.9 mmol), 4-iodotetrafluorophenol (1.14g, 3.9mmol) and 20 mL dry methylene chloride under a nitrogen atmosphere. To this solution DCC (0.89g, 4.32 mmol) and DMAP (0.04g, 34.4 mmol) were added. The reaction mixture was allowed to stir at room temperature for 48 hours. The white precipitate was filtered off and was washed with aqueous acetic acid (5%, 100 mL). The organic layer was separated; the solvent removed by rotary evaporation and a yellow solid was collected. The crude product was purified by column chromatography (100 g silica, hexane → hexane: ethyl acetate 100:1) to give pure **I** (0.80g, 40%). M. p. 58-60 °C. ^{19}F NMR (δ_{H} ; 400 MHz, CDCl_3): -118.96 - -119.53 (m, 2F), -130.29 - -130.75 (m, 2F), -135.05 - -135.50 (m, 2F), -150.03 - -150.46 (m, 2F). IR: 1775, 1634, 1473, 1401, 1299, 1266, 1133, 1067, 984, 970, 854, 807.

4.4.1.4 Synthesis of 2,3,5,6-tetrafluoro-4-iodophenyl 2,3,5,6-tetrafluoro-4-iodobenzoate, II



To an oven dried 50 mL flask was added 4-iodotetrafluorobenzoic acid (0.2g, 0.46 mmol), 4-iodotetrafluorophenol (0.14g, 0.46mmol) and 10 mL dry methylene chloride under nitrogen atmosphere. To this solution DCC (0.11g, 0.5 mmol) and DMAP (0.005g, 0.04 mmol) were added. The reaction mixture was allowed to stir at room temperature for 48 hours. The white precipitate was filtered off and washed with aqueous acetic acid (5%, 100 mL). The organic layer was separated; the solvent removed by rotary evaporation and a yellow solid was collected. The crude product was purified by column chromatography (100 g silica, hexane → hexane: ethyl acetate 97:3) to give pure **II** (0.12g, 42%). M. p. 80-82 °C. ¹⁹F NMR (δ_H; 400 MHz, CDCl₃): -117.48 - -117.78 (m, 2F), -119.16 - -119.41 (m, 2F), -135.01 - -135.23 (m, 2F), -150.09 - -150.35 (m, 2F). IR: 1771, 1623, 1467, 1291, 1263, 1142, 1134, 970, 806, 771.

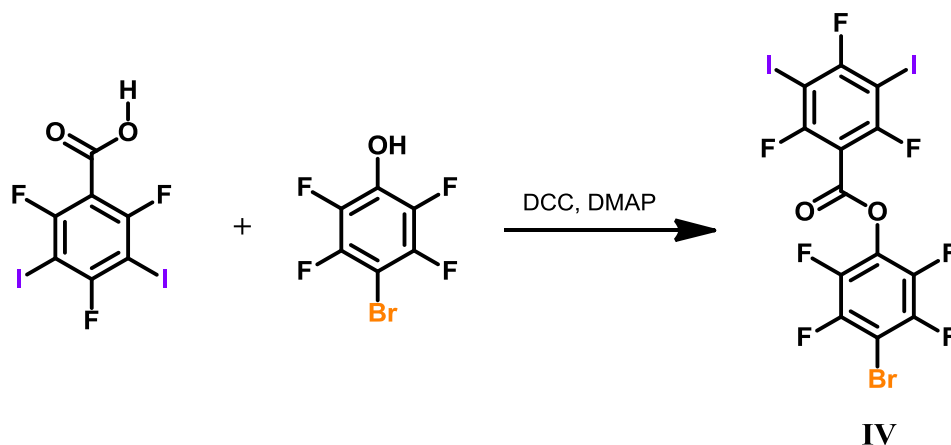
4.4.1.5 Synthesis of 4-bromo-2,3,5,6-tetrafluorophenyl 4-bromo-2,3,5,6-tetrafluorobenzoate, **III**



To an oven dried 50 mL round bottom flask was added 4-bromotetrafluorobenzoic acid (0.5g, 1.8mmol), 4-bromotetrafluorophenol (0.45g, 1.8mmol) and 10 mL dry methylene chloride under nitrogen atmosphere. To above solution DCC (0.42g, 2 mmol) and DMAP (0.02g, 0.16 mmol) were added. The reaction mixture was allowed to stir at room temperature for 48 hours. The white precipitate was filtered off and the filtrate was washed with aqueous acetic acid (5%, 100 mL). The organic layer was separated; the solvent removed by rotary evaporation and a yellow solid was collected. The crude product was purified by column chromatography (100 g silica, hexane → hexane: ethyl acetate 95:5) to give pure **III** (0.43g, 46%). M. p. 81-83 °C. ¹⁹F NMR (δ_H; 400 MHz, CDCl₃): -130.17 - -130.72 (m, 2F), -132.21 - -132.52 (m, 2F), -135.07 -

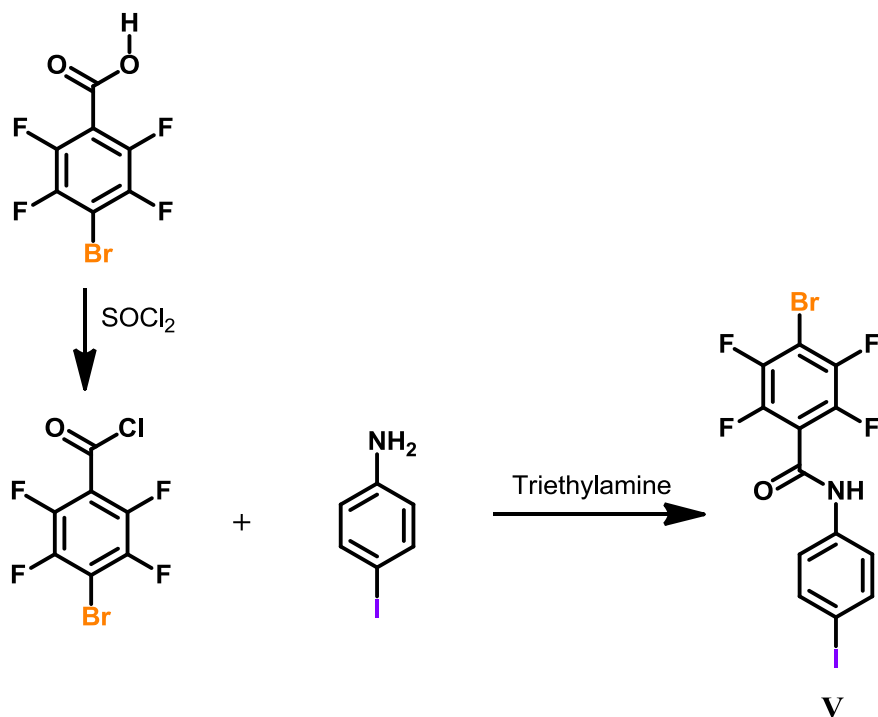
-135.38 (m, 2F), -150.48 - -151.02 (m, 2F). IR:1758, 1633, 1477, 1402, 1305, 1156, 1138, 1065, 977, 938, 833, 782.

4.4.1.6 Synthesis of 4-bromo-2,3,5,6-tetrafluorophenyl 2,4,6-trifluoro-3,5-diiodobenzoate, **IV**



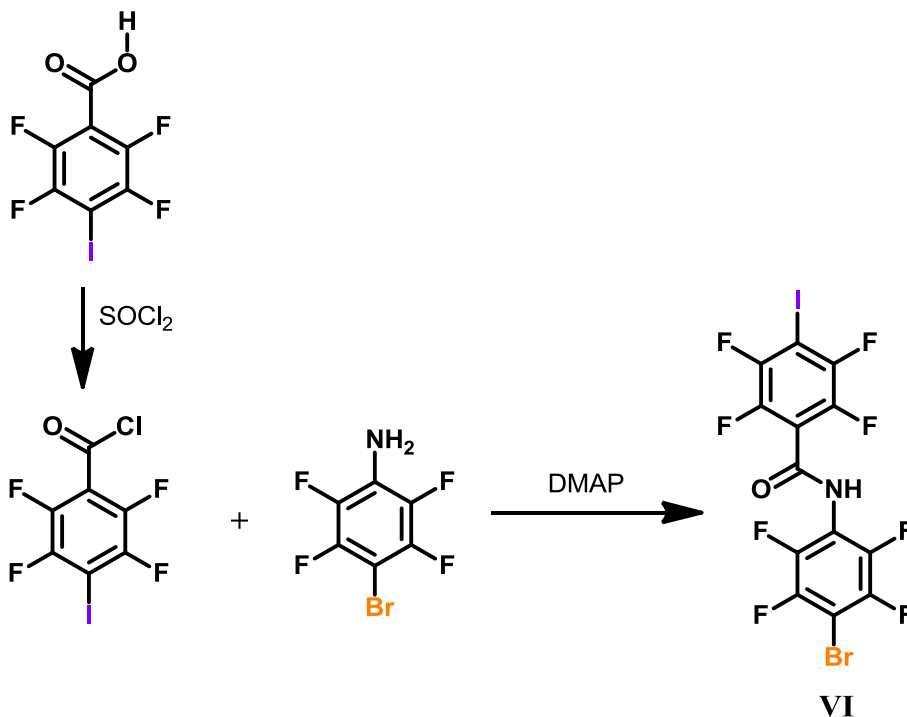
To an oven dried 50 mL flask was added 2,4,6-trifluoro-3,5-diiodobenzoic acid (1g, 2.31mmol), 4-bromotetrafluorophenol (0.57g, 2.31mmol) and 10 mL dry methylene chloride under nitrogen atmosphere. To this solution DCC (0.53g, 2.54mmol) and DMAP (0.012g, 0.1 mmol) were added. The reaction mixture was allowed to stir at room temperature for 48 hours. The white precipitate was filtered off and the filtrate was washed with aqueous acetic acid (5%, 100 mL). The organic layer was separated; the solvent removed by rotary evaporation and a yellow solid was collected. The crude product was purified by column chromatography (100 g silica, hexane → hexane: ethyl acetate 97:3) to give pure **IV** (0.46g, 30%). M. p. 125-127 °C. ¹⁹F NMR (δ_H; 400 MHz, CDCl₃): -59.73 - -59.92 (m, 1F), -84.26 - -84.49 (m, 2F), -132.39 - -133.34 (m, 2F), -140.61 - -141.10 (m, 2F). IR:1764, 1594, 1489, 1210, 1101, 1064, 977, 835, 665.

4.4.1.7 Synthesis of 4-bromo-2,3,5,6-tetrafluoro-N-(4-iodophenyl)benzamide, V



To an oven dried 50 mL round bottom flask was added 4-bromotetrafluorobenzoic acid (0.5g, 1.8 mmol) and 10 mL dichloromethane under nitrogen atmosphere. An excess of oxalyl chloride (1.50 mL) and catalytic amount of DMF were added via syringe to the reaction flask. The reaction mixture was stirred until all the acid had gone into solution (typically 1-2 h), and the methylene chloride and excess oxalyl chloride were removed under reduced pressure. The acid chloride was used without further purification. To another oven dried 100 mL round bottom flask 4-iodoaniline (0.40g, 1.82mmol) and triethylamine (0.254 mL, 1.82 mmol) were added under nitrogen atmosphere. To this flask was added acid chloride (dissolved in 5 mL methylene chloride) via syringe in lots over 10 minutes. The reaction mixture was stirred at room temperature for 5 hours. The white precipitate was filtered off and washed with methylene chloride to yield white solid of **V** (0.64g, 98%). M. p. > 250 °C. ^1H NMR (δ_{H} ; 400 MHz, D_6 -DMSO): 11.11 (s, 1H), 7.74 (d, $J = 8\text{Hz}$, 2H), 7.51 (d, $J = 8\text{Hz}$, 2H). ^{19}F NMR (δ_{H} ; 400 MHz, D_6 -DMSO): -132.78 - -133.34 (m, 2F), -140.61 - -141.10(m, 2F). IR: 3247, 3179, 3108, 3059, 1669, 1637, 1597, 1584, 1537, 1473, 1391, 1323, 1247, 1004, 974, 817, 788, 729.

4.4.1.8 Synthesis of *N*-(4-bromo-2,3,5,6-tetrafluorophenyl)-2,3,5,6-tetrafluoro-4-iodobenzamide, VI



To an oven dried 50 mL flask was added 4-iodotetrafluorobenzoic acid (0.5g, 1.6 mmol) under nitrogen atmosphere. An excess of thionyl chloride (2 mL) was added via syringe to the reaction flask. The reaction mixture was refluxed at 90 °C for 20 hours, and excess thionyl chloride was removed under reduced pressure. The acid chloride was used without further purification. To another oven dried 100 mL flask was added 4-bromotetrafluoroaniline (0.763g, 3.12 mmol), DMAP (0.190g, 1.76 mmol) and dry methylene chloride under nitrogen atmosphere. The reaction mixture was stirred at room temperature for 48 hours. The white precipitate was filtered, to yield white solid of **VI** (0.55g, 65%). Dec. 225 °C. ^{19}F NMR (δ_{H} ; 400 MHz, D_6 -DMSO): -120.82 - -121.02 (m, 2F), -134.40 - -134.93 (m, 2F), -140.47 - -141.00(m, 2F), -143.54 - -144.07. IR: 3213, 1686, 1632, 1540, 1474, 1313, 1219, 979, 966, 863, 830, 786, 775, 693.

4.4.2 Synthesis of Co-crystals

4.4.2.1 Synthesis of 1-bromo-2,3,5,6-tetrafluoro-4-iodobenzene tetramethylpyrazine (1:1), IF4Br·A

1-Bromo-2,3,5,6-tetrafluoro-4-iodobenzene (10 mg, 0.02 mmol) and tetramethylpyrazine (1.9mg, 0.01 mmol) were placed in a 2 dram borosilicate vial and dissolved in 2 mL of methanol After two days of slow evaporation, plate-shaped colorless crystals were obtained. M. p. 104-106 °C.

4.4.2.2 Synthesis of 4-bromo-2,2',3,3',5,5',6,6'-octafluoro-4'-iodo-1,1'-biphenyl tetramethylpyrazine (1:1), IF8Br·A

4-Bromo-2,2',3,3',5,5',6,6'-octafluoro-4'-iodo-1,1'-biphenyl (10 mg, 0.01 mmol) and tetramethylpyrazine (0.68 mg, 0.005 mmol) were placed in a 2 dram borosilicate vial and dissolved in 2 mL of methanol After three days of slow evaporation, plate-shaped colorless crystals were obtained. M. p. 144-146 °C.

4.4.2.3 Synthesis of 1-bromo-2,3,5,6-tetrafluoro-4-iodobenzene tetramethylpyrazine mono-N-oxide (1:1), IF4Br·B

1-Bromo-2,3,5,6-tetrafluoro-4-iodobenzene (10 mg, 0.02 mmol) and tetramethylpyrazine mono-N-oxide (3.04 mg, 0.02 mmol) were placed in a 2 dram borosilicate vial and dissolved in 2 mL of methylene chloride After one day of slow evaporation, plate-shaped crystals were obtained. M. p. 106-108 °C.

4.4.2.4 Synthesis of 4-bromo-2,2',3,3',5,5',6,6'-octafluoro-4'-iodo-1,1'-biphenyl tetramethylpyrazine mono-N-oxide (1:1), IF8Br·B

4-Bromo-2,2',3,3',5,5',6,6'-octafluoro-4'-iodo-1,1'-biphenyl (10 mg, 0.01 mmol) and tetramethylpyrazine mono-N-oxide (1.52 mg, 0.01 mmol) were placed in a 2 dram borosilicate vial and dissolved in 2 mL of methylene chloride After two days of slow evaporation, plate-shaped colorless crystals were obtained. M. p. 140-142 °C.

4.4.2.5 Synthesis of 1-bromo-2,3,5,6-tetrafluoro-4-iodobenzene 4,4'-bipyridine mono N-oxide (1:1), IF4Br·C

1-Bromo-2,3,5,6-tetrafluoro-4-iodobenzene (10 mg, 0.02 mmol) and 4,4'-bipyridine mono N-oxide (3.44 mg, 0.02 mmol) were placed in a 2 dram borosilicate vial and dissolved in 2 mL of methylene chloride After five days of slow evaporation, plate-shaped crystals were obtained. M. p. 107-109 °C.

4.4.2.6 Synthesis of 4-bromo-2,2',3,3',5,5',6,6'-octafluoro-4'-iodo-1,1'-biphenyl 5,6-dimethyl-1-(pyridin-4-ylmethyl)-1H-benzo[d]imidazole (1:1), IF8Br·D

4-Bromo-2,2',3,3',5,5',6,6'-octafluoro-4'-iodo-1,1'-biphenyl (10 mg, 0.01 mmol) and 6-dimethyl-1-(pyridin-4-ylmethyl)-1H-benzo[d]imidazole (2.37 mg, 0.01 mmol) were placed in a 2 dram borosilicate vial and dissolved in 2 mL of ethanol:nitromethane (1:1) After five days of slow evaporation, block-shaped colorless crystals were obtained. M. p. 185-187 °C.

4.4.2.7 Synthesis of 4-bromo-2,2',3,3',5,5',6,6'-octafluoro-4'-iodo-1,1'-biphenyl 4-(N-pyrrolidinyl)pyridine (1:1), IF8Br·E

4-Bromo-2,2',3,3',5,5',6,6'-octafluoro-4'-iodo-1,1'-biphenyl (10 mg, 0.01 mmol) and 4-(N-pyrrolidinyl)pyridine (1.48 mg, 0.01 mmol) were placed in a 2 dram borosilicate vial and dissolved in 2 mL of methanol After three days of slow evaporation, plate-shaped crystals were obtained. M. p. 144-146 °C.

4.4.2.8 Synthesis of 4-bromo-2,2',3,3',5,5',6,6'-octafluoro-4'-iodo-1,1'-biphenyl 4-(N,N-dimethylamino)pyridine (1:1), IF8Br·F

4-Bromo-2,2',3,3',5,5',6,6'-octafluoro-4'-iodo-1,1'-biphenyl (10 mg, 0.01 mmol) and 4-(N,N-dimethylamino)pyridine (1.22 mg, 0.01 mmol) were placed in a 2 dram borosilicate vial and dissolved in 2 mL of methanol After three days of slow evaporation, plate-shaped colorless crystals were obtained. M. p. 95-97 °C.

4.4.2.9 Synthesis of N-(4-bromo-2,3,5,6-tetrafluorophenyl)-2,3,5,6-tetrafluoro-4-iodobenzamide 1,2-bis(4-pyridyl)ethylene (1:1), VI·G

N-(4-bromo-2,3,5,6-tetrafluorophenyl)-2,3,5,6-tetrafluoro-4-iodobenzamide (10 mg, 18.3 μmol) and 1,2-bis(4-pyridyl)ethylene (1.33 mg, 73.2 μmol) were placed in a clear 2 dram

borosilicate vial and dissolved in 2 mL of ethyl acetate:nitromethane (1:1). After six days of slow evaporation, plate-shaped colorless crystals were obtained. M. p. 215-217 °C.

4.4.2.10 Synthesis of N-(4-bromo-2,3,5,6-tetrafluorophenyl)-2,3,5,6-tetrafluoro-4-iodobenzamide 1,2-bis(4-pyridyl)ethane (1:1), VI·H

N-(4-bromo-2,3,5,6-tetrafluorophenyl)-2,3,5,6-tetrafluoro-4-iodobenzamide (10 mg, 18.3 μmol) and 1,2-bis(4-pyridyl)ethane (1.34 mg, 73.2 μmol) were placed in a clear 2 dram borosilicate vial and dissolved in 2 mL of ethyl acetate:nitromethane (1:1). After five days of slow evaporation, plate-shaped colorless crystals were obtained. M. p. 205-207 °C.

4.4.2.11 Synthesis of N-(4-bromo-2,3,5,6-tetrafluorophenyl)-2,3,5,6-tetrafluoro-4-iodobenzamide 4,4'-bipyridine (1:1), VI·bipy

N-(4-bromo-2,3,5,6-tetrafluorophenyl)-2,3,5,6-tetrafluoro-4-iodobenzamide (10 mg, 18.3 μmol) and 4,4'-bipyridine (1.14 mg, 73.2 μmol) were placed in a clear 2 dram borosilicate vial and dissolved in 2 mL of ethyl acetate:nitromethane (1:1). After six days of slow evaporation, plate-shaped colorless crystals were obtained. M. p. 175-177 °C.

References:

- ¹ Aakeröy, C. B.; Desper, J.; Smith, M. M. *Chem. Commun.* **2007**, 3936.
- ² a) Etter, M. C. *J. Phys. Chem.* **1991**, *95*, 4601. b) Etter, M. C. *Acc. Chem. Res.* **1990**, *23* 120.
- ³ Hunter, C. A. *Angew. Chem. Int. Ed.* **2004**, *43*, 5310.
- ⁴ a) Metrangolo, P.; Resnati, G. *Chem. Eur. J.* **2001**, *7*, 2511. b) Metrangolo, P.; Neukirch, H.; Pilati, T.; Resnati, G. *Acc. Chem. Res.* **2005**, *38*, 386.
- ⁵ a) Hassel, O. *Science* **1970**, *170*, 497. b) Metrangolo, P.; Meyer, F.; Pilati, T.; Resnati, G.; Terraneo, G. *Angew. Chem., Int. Ed.* **2008**, *47*, 6114.
- ⁶ Nguyen, H. L.; Horton, P. N.; Hursthouse, M. B.; Legon, A. C.; Bruce, D. W. *J. Am. Chem. Soc.* **2004**, *126*, 16.
- ⁷ a) Fourmigué, M.; Batail, P. *Chem. Rev.* **2004**, *104*, 5379. b) Fourmigué, M. *Struct. Bonding* **2008**, *126*, 181. c) Metrangolo, P.; Pilati, T.; Biella, S.; Terraneo, G.; Resnati, G. *CrystEngComm* **2009**, *11*, 1187.
- ⁸ Mele, A.; Metrangolo, P.; Neukirch, H.; Pilati, T.; Resnati, G. *J. Am. Chem. Soc.* **2005**, *127*, 14972.
- ⁹ a) Chudzinski, M. G.; McClary, A. C.; Taylor, M. S. *J. Am. Chem. Soc.*, **2011**, *133*, 10559. b) Sarwar, M. G.; Dragisic, B.; Sagoo, S.; Taylor, M. S. *Angew. Chemie.* **2010**, *122*, 1718.

-
- ¹⁰ Raatikainen, K.; Rissanen, K. *Chem. Sci.* **2012**, Advance article, DOI: 10.1039/c0xx00000x.
- ¹¹ a) Legon, A. C. *Angew. Chem., Int. Ed.* **1999**, *38*, 2686. b) Sarwar, M. G., Dragisic, B., Salsberg, L. J., Gouliaras, C., and Taylor, M. S. *J. Am. Chem. Soc.* **2010**, *132*, 1646, c) Desiraju, G. R.; Harlow, R. L. *J. Am. Chem. Soc.* **1989**, *111*, 6757.
- ¹² a) Sun, A.; Goroff, N. S.; Lauher, J. W. *Science* **2006**, *312*, 1030. b) Zou, J-W.; Jiang, Y-J.; Guo, M.; Hu, G.-X.; Zhang, B.; Liu, H.-C.; Yu, Q.-S. *Chem. Eur. J.* **2005**, *11*, 740. c) Gao, K.; Goroff, N. S.; *J. Am. Chem. Soc.* **2000**, *122*, 9320. d) Borgen, B.; Hassel, O.; Romming, C. *Acta Chem. Scand.* **1962**, *16*, 2469.
- ¹³ A CSD analysis shows that there are currently about 62 co-crystals containing halogen bonds between **DITFB** and pyridine derivatives. CSD search carried out on ConQuest Version 1.13 (Updated till November 2011).
- ¹⁴ A CSD analysis shows that there are currently about 13 co-crystals containing halogen bonds between **DITFB** and pyridine derivatives. CSD search carried out on ConQuest Version 1.13 (Updated till November 2011).
- ¹⁵ Aakeröy, C. B.; Chopade, P. D.; Ganser, C.; Desper, J.; *Chem. Commun.*, **2011**, *47*, 4688.
- ¹⁶ a) Auffinger, P.; Hays, F. A.; Westhof, E.; Ho, P. S. *Proc. Natl. Acad. Sci. U.S.A.* **2004**, *101*, 16789. b) Clark, T.; Hennemann, M.; Murray, J. S.; Politzer, P. *J. Mol. Model.* **2007**, *13*, 291. c) Zordan, F.; Brammer, L.; Sherwood, P. *J. Am. Chem. Soc.* **2005**, *127*, 5979.
- ¹⁷ Sarwar, M. G.; Dragisic, B.; Salsberg, L. J.; Gouliaras, C.; Taylor, M. S. *J. Am. Chem. Soc.*, **2010**, *132*, 1646.
- ¹⁸ Syssa-Magale, J.-L.; Boubekour, K.; Palvadeau, P.; Meerschaut, A.; Schollhorn, B. *CrystEngComm*, **2005**, *7*, 302.
- ¹⁹ Bailey, R. D., Buchanan, M. L.; Pennington, W. T. *Acta Crystallogr., Sect. C: Cryst. Struct. Commun.*, **1992**, *48*, 2259.
- ²⁰ CSD code JAQMAQ.
- ²¹ CSD code VUDOU.
- ²² Nayak, S. K.; Kishore Reddy, M.; Chopra, D.; Guru Row, T. N. *CrystEngComm* **2012**, *14*, 200.
- ²³ Latosinska, J. N.; Latosinska, M.; Seliger, J.; Zagar, V.; Maurin, J. K.; Orzeszko, A.; Kazimierzuk, Z. *J. Phys. Chem. A* **2010**, *114*, 563.
- ²⁴ Roper, L. C.; Prasang, C.; Whitwood, A. C.; Bruce, D. W. *CrystEngComm* **2010**, *12*, 3382.
- ²⁵ Hoger, S.; Bonrad, K.; Schafer, G.; Enkelmann, V. *Z. Naturforsch., B: Chem. Sci.* **1998**, *53*, 960.
- ²⁶ Song, Y.; Parkin, S.; Lehmler, H.-J. *Acta Crystallogr., Sect. E: Struct. Rep. Online* **2010**, *66*, o813.
- ²⁷ Kongprakaiwoot, N.; Bultman, M. S.; Luck, R. L.; Urnezisus, E. *Inorg. Chim. Acta* **2005**, *358*, 3423.
- ²⁸ Reddy, C. M.; Kirchner, M. T.; Gundakaram, R. C.; Padmanabhan, K. A.; Desiraju, G. R. *Chem. Eur. J.* **2006**, *12*, 2222.
- ²⁹ Klug, A. *Nature* **1947**, *160*, 570.
- ³⁰ Shaikh, N. S.; Swenson, D. C.; Lehmler, Hans-J. *Acta Crystallogr., Sect. E: Struct. Rep. Online* **2006**, *62*, o4672.
- ³¹ Meriles, C. A.; de Almeida Santos, R. H.; do Prado Gambardella, M.T.; Ellena, J.; Mascarenhas, Y. P.; Brunetti, A. H. *J. Mol. Struct.* **1999**, *513*, 245.
- ³² Kania-Korwel, I.; Lehmler, H. -J.; Robertson, L. W.; Parkin, S. *Acta Crystallogr., Sect. E: Struct. Rep. Online* **2003**, *59*, o1048.
- ³³ Reddy, L.S.; Babu, J.N.; Nangia, A. *Chem. Commun.* **2006**, 1369.

-
- ³⁴ a) Bowers, J. R.; Hopkins, G. W.; Yap, G. P. A.; Wheeler, K. A. *Cryst.Growth Des.* **2005**, *5*, 727. b) Arora, K. K.; Talwelkar, M. S.; Pedireddi, V. *New J. Chem.* **2009**, *33*, 57. c) Zeng, Q.; Wu, D.; Liu, C.; Ma, H.; Lu, J.; Xu, S.; Li, Y.; Wang, C.; Bai, C. *Cryst.Growth Des.* **2005**, *5*, 1041. d) Lou, B; Huang, Y. *Acta Crystallogr., Sect.C:Cryst. Struct. Commun.* **2007**, *63*, o246. e) Zeng, Q.; Wu, D.; Ma, H.; Shu, C.; Li, Y.; Wang, C. *CrystEngComm* **2006**, *8*, 189.
- ³⁵ Messina, M. T.; Metrangolo, P.; Panzeri, W.; Pilati, T.; Resnati, G. *Tetrahedron*, **2001** *57*, 8543.
- ³⁶ For examples of disorder in 1,4-thiomorpholine and 1,4-thioxane see; a) Cincic, D.; Friscic, T.; Jones, W. *J. Am. Chem. Soc.* **2008**, *130*, 7524. b) Cincic, D.; Friscic, T.; Jones, W. *Chem. Eur. J.* **2008**, *14*, 747.
- ³⁷ Aakeröy, C. B.; Desper, J.; Urbina, J. F. *Chem. Commun.* **2005**, 2820.
- ³⁸ Präsang, C.; Whitwood, A. C.; Bruce, D. W. *Cryst. Growth Des.* **2009**, *9*, 5319.
- ³⁹ a) Aakeröy, C. B.; Scott, B. M. T.; Desper, J. *New J. Chem.* **2007**, *31*, 2044. b) Lauher, J. W., Fowler, F. W.; Goroff, N. S. *Acc. Chem. Res.* **2008**, *41*, 1215. c) Aakeröy, C. B.; Forbes, S.; Desper, J. *J. Am. Chem. Soc.* **2009**, *131*, 17048.
- ⁴⁰ The halogen bonded co-crystals of **bipyethylene** with **DITFB** and **DBTFB** are reported (CSD codes - QIHCAL and IKUHUR respectively). The C-I...N distance in QIHCAL is 2.811 Å and angle is 179.29. The C-Br...N distance in IKUHUR is 2.814 Å and angle is 179.11.
- ⁴¹ CSD survey for C-I...N short contact shows average distance of 2.90 Å and angle of 171.95° as compared to C-Br...N (3.12 Å distance and 167.79° angle).
- ⁴² The halogen bonded co-crystals of **bipyethane** with **DITFB** and **DBTFB** are reported (CSD codes - MEKWOO and QIHDAM respectively). The C-I...N distance in MEKWOO is 2.811 Å and angle is 175.84. The C-Br...N distance in QIHDAM is 3.025 Å and angle is 172.26.
- ⁴³ There are 58 examples where an amide N-H donor preferentially binds to a pyridine nitrogen atom over an oxygen atom of a carbonyl group.
- ⁴⁴ For halogen bonded co-crystals based on C=O as acceptor, see; Syssa-Magalé, J. L.; Boubekeur, K.; Palvadeau, P.; Meerschaut, A.; Schollhorn, B. *CrystEngComm* **2005**, *7*, 302.
- ⁴⁵ a) Desiraju, G. R., Parthasarathy, R. *J. Am. Chem. Soc.* **1989**, *III*, 8725. b) Price, S. L.; Stone, A. L.; Lucas, J.; Rowland, R. S.; Thornley, A. E. *J. Am. Chem. Soc.* **1994**, *116*, 4910. c) Pedireddi, V. R.; Reddy, D. S.; Goud, B. S.; Craig, D. C.; Rae, A. D.; Desiraju, G. R.; *J. Chem. Soc. Perkin Trans. 2* **1994**, 2353. d) Navon, O.; Bernstein, J.; Khodorkovsky, V. *Angew. Chem.* **1997**, *109*, 640.

Chapter 5 - Facile functionalization of cavitands

5.1 Introduction

Cavitands are bowl shaped macromolecules which are capable of encapsulating cations, anions, solvents and guest molecules.¹ One of the most important applications of such molecules is in the design and assembly of discrete molecular capsules that can subsequently be used, for example, for catalysis,² molecular sensing,³ stabilization of reactive intermediates,⁴ and recently as photosensitizers and as a protection against undesired photochemical reactions.⁵ All these properties are a function of the assembled state and unique to the defined space, volume, and chemical characteristics of the internal volume of the capsule. The ability to decorate the rim of a cavitand with a variety of functional groups in any geometric configuration therefore continues to be the focus of intensive research,⁶ since the presence of appropriate molecular recognition groups on these molecular container compounds can produce a range of capsules of different shapes and sizes. The presence of self-complementary functional groups (in the context of intermolecular interactions) can result in the formation of homomeric capsules,⁷ whereas if complementary entities are located on two different host, heteromeric capsule can be assembled.^{8,9} In addition, two different cavitands can be brought together into a capsule using a linker with appropriate molecular recognition sites (Figure 5.1).¹⁰

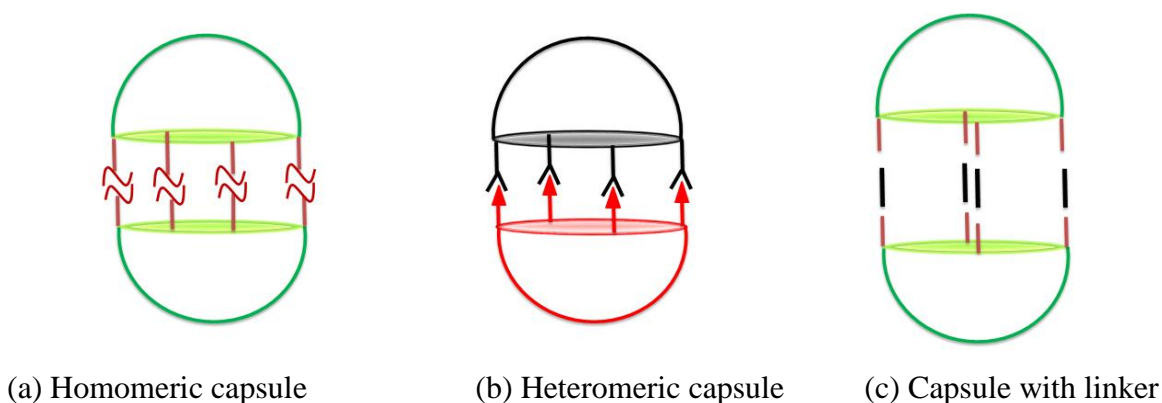


Figure 5.1 Schematic representation of molecular capsule formation.

Resorcin[4]arene-based cavitands are versatile molecules due the large variation of covalent modifications that can be achieved in three general positions, without altering the overall structural integrity of the cavity-bearing framework, Figure 5.2. Covalent modifications

to the ‘feet’ for improving solubility have been reported.¹¹ However, most modifications occur at the ‘upper-rim’ or ‘bridges’ producing a variety of functionalized products.¹² Our efforts will mainly focus on covalent modifications to the upper-rim of resorcin[4]arene-based cavitands, while the methylene bridges (-CH₂-) and pentyl feet will not be altered, Figure 5.2.

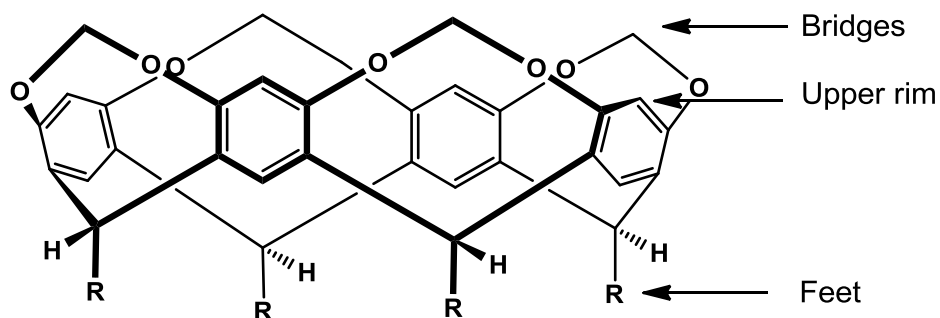


Figure 5.2 Resorcin[4]arene cavitand scaffold with labeled possible adaptable locations.

To date, methylene bridged resorcinarene based cavitands have been decorated with hydrogen-bonding functionalities such as pyridyl,¹³ carboxylic acid,¹⁰ hydroxyl group,⁹ to facilitate the reversible non-covalent synthesis of molecular capsules. However, only a small number of potentially suitable hydrogen-bonding moieties have been employed in this context, primarily due to major synthetic challenges, such as; multi-step synthesis, purification issues, fewer developed synthetic protocols. As a result, the potential of cavitands as a foundation for functional molecular capsules has yet to be fully realized.

In this chapter, we will focus on developing synthetic strategies for versatile and facile functionalization of the upper rim of cavitands.

5.1.1 Choice of reaction - Suzuki-Miyaura coupling

Carbon-carbon bond formation, utilizing a palladium catalyst, is a well-known and versatile synthetic process in organic chemistry.¹⁴ More specifically, the Suzuki-Miyaura reaction, where a palladium species catalyzes the coupling of organic halides or triflates with organoboronic acids or esters, is arguably one of the most useful and important of such reactions.¹⁵ There are several reasons for its diversity and wide-acceptance: (1) it is tolerable to a large variety of electron-donating or withdrawing functional groups; (2) it utilizes mild reaction conditions (i.e. 25-70 °C), low catalyst loading, and dried solvents are not necessary); (3) many

boronic acids/esters are stable over long periods of time.¹⁶ Furthermore, the palladium-catalyzed Suzuki-Miyaura reaction is highly efficient and, consequently, has been employed extensively in the synthesis of, e.g., natural products,¹⁷ potential drug candidates,¹⁸ and a range of functional materials.¹⁹

Within the last few years, the Suzuki-Miyaura reaction, has also been utilized in the synthesis of functionalized resorcinarene-based cavitand receptor molecules.²⁰ In every report, except one, a tetrahalogenated (I or Br) cavitand was cross-coupled with a substituted (e.g., pyridyl, benzonitrile, or methoxyphenyl) aryl boronic acid or ester. In the one exception, a tetraboronic acid cavitand was synthesized a cross-coupled with 3-bromopyridine, albeit in very low yields (*ca.* 20 %).^{20m}

The limited range of functional groups that have been successfully appended to cavitands, can be attributed in part to the fact that a relatively small number of suitable inexpensive boronic acids and esters are commercially available for cross-coupling. Moreover, arylboronic acids are often synthesized by low-temperature transmetalation reactions and can be difficult to isolate. In addition, effective coupling of tetrahalogenated cavitands to aryl boronic acid or esters demands optimization of reaction conditions (e.g., change of base, catalyst or ligand etc.) depending on the type of aryl boronic acid or ester used.²⁰ Sometimes coupling reactions with tetrahalogenated cavitands yields multisubstituted and multi-‘protio’-cavitands as byproducts causing tedious chromatographic separations and very low yields.²¹

Against this background, we sought to design a more stable (compared to its boronic acid counterpart) a tetraboronic ester cavitand for facile functionalization of cavitand ‘upper rim’(Figure 5.3).²²

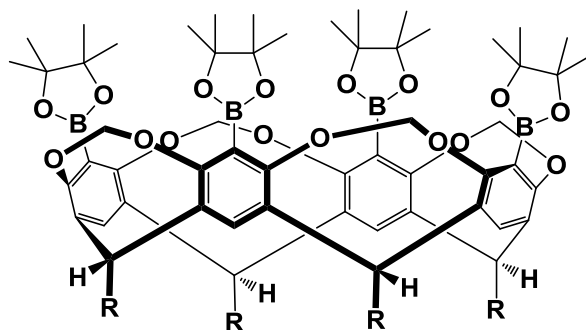


Figure 5.3 Tetraboronic pinacolyl ester cavitand precursor for a Suzuki-Miyaura reaction.

5.1.2 Oxime decorated cavitands

Only a small number of potentially suitable hydrogen-bonding moieties have been attached to the ‘upper rim’ of the cavitand, primarily due to synthetic challenges, and as a result, the potential of cavitands as a foundation for functional molecular capsules has yet to be fully realized. Oximes are highly effective and versatile hydrogen-bonding groups capable of forming self-complementary hydrogen-bonded dimers and chains²³ and they can also form strong and directional intermolecular interactions with a wide range of other hydrogen-bond acceptors, Figure 5.4.²⁴ Oximes typically exhibit pK_a values in a range between that of carboxylic acids and amides and, consequently, are less pH sensitive than carboxylic acids. They are therefore unlikely to undergo ‘proton transfer’ to many N-heterocycle acceptors thereby avoiding the formation of organic salts which could lead to unwanted solubilities, unpredictable chemical compositions and unexpected intermolecular interactions.^{24,25}

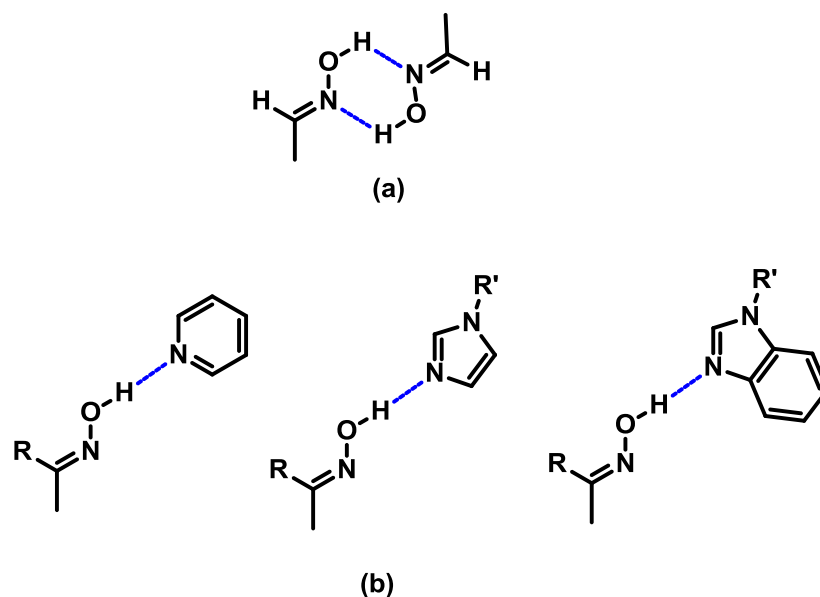


Figure 5.4 Schematic of possible homomeric and heteromeric interactions of oximes.

Moreover, oximes offer the possibility of greater tunability by facile variation of the substituent R (Figure 5.5), which is not present in carboxylic acids or primary amides. Choice of this substituent also permits the solubility of the oxime to be modified, enabling supramolecular synthesis in a wider range of solvent systems.

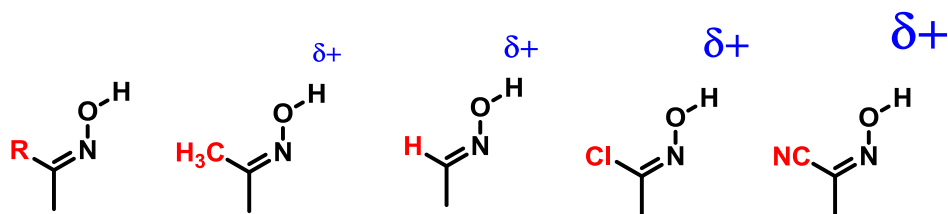


Figure 5.5 Schematic showing tunable nature of oxime group.

Despite the above mentioned advantages of oximes as reliable supramolecular synthetic vectors, there have been no reports of oxime functionalized cavitands to date. Our efforts will focus on facile synthesis of a variety of oxime decorated cavitands with significantly different depth and interior volume (Figure 5.6).

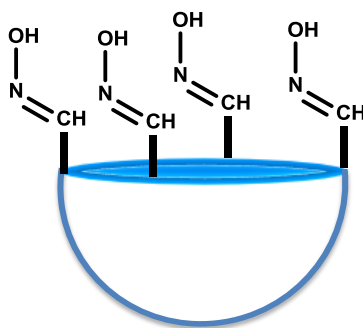


Figure 5.6 Cartoon representation of oxime decorated cavitand.

5.1.3 Goals

In this chapter we will focus on achieving the following goals:

I. To develop a versatile Suzuki-Miyaura cross-coupling reaction protocol of tetraboronic ester cavitand with an (Figure 5.7):

- arene bearing electron donating group.
- arene bearing electron withdrawing group
- aromatic heterocycle.
- arene bearing iodo and bromo groups (to demonstrate chemoselectivity).

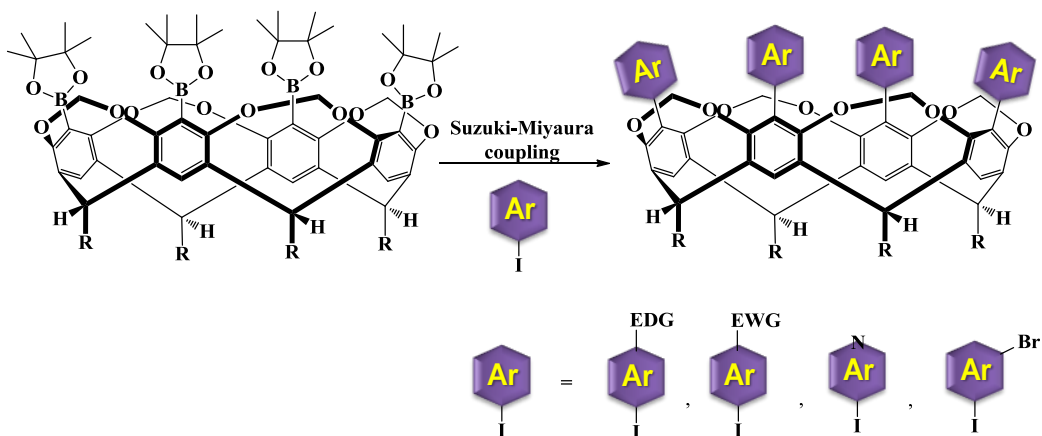


Figure 5.7 Schematic showing proposed Suzuki-Miyaura coupling protocol with target arenes.

II. To design and develop oxime functionalized cavitands using ‘solvent assisted grinding’. We will focus on synthesizing oxime cavitand derivatives with:

- an oxime group directly attached to ‘upper rim’ of cavitand.
- a deeper cavity.
- a deeper and more flexible cavity.

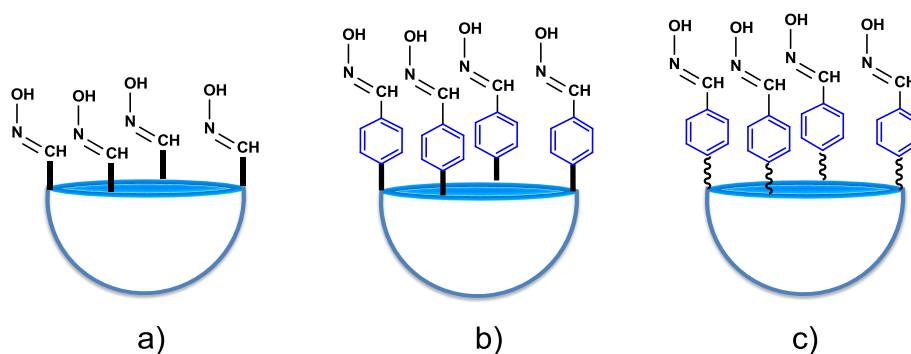


Figure 5.8 Schematic representation of; a) shallow, b) deeper and c) deep and more flexible oxime cavitands.

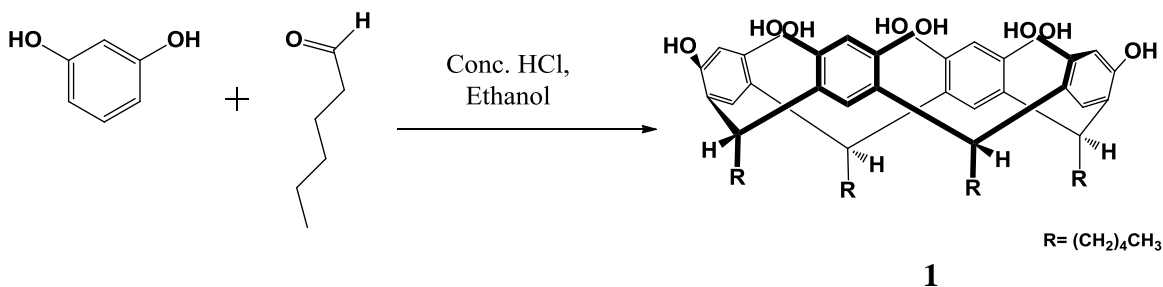
5.2 Experimental

5.2.1 Synthesis

^1H NMR spectra were recorded on a Varian Unity plus 400 MHz spectrometer in CDCl_3 or d -DMSO. Data is expressed in parts per million (ppm) downfield shift from tetramethylsilane or residual protiosolvent as internal reference and are reported as position (in ppm), multiplicity (s = singlet, d = doublet, t = triplet, m = multiplet), coupling constant (J in Hz) and integration

(number of protons). ^{13}C NMR spectra were recorded on a Varian Unity plus 400 MHz spectrometer in CDCl_3 or *d*-DMSO with complete proton decoupling. Data is expressed in parts per million (ppm) shift relative to CDCl_3 (77.00 ppm) or *d*-DMSO (39.51 ppm) and are reported as position (δ). Melting points were recorded on Fisher-Johns melting point apparatus and are uncorrected. Electrospray Ionization spectra were acquired on a LCT Premier (Waters Corp., Milford MA) time of flight mass spectrometer. The instrument was operated at 10,000 resolution (W mode) with a dynamic range enhancement that attenuates large intensity signals. The cone voltage was 60eV. Spectra were acquired at 16666 Hz pusher frequency covering the mass range 100 to 1200 u and accumulating data for 2 seconds per cycle. Mass correction for exact mass determinations was made automatically with the lock mass feature in the MassLynx data system. A reference compound in an auxiliary sprayer is sampled every third cycle by toggling a “shutter” between the analysis and reference needles. The reference mass is used for a linear mass correction of the analytical cycles. Samples are presented in acetonitrile as a 100ul loop injection using an auto injector (LC PAL, CTC Analytics AG, Zwingen, Switzerland). Infrared spectroscopy (IR) was done on a Nicolet 380 FT-IR. 4-formylphenylboronic acid and 3-formylphenylboronic acid were purchased from Matrix Scientific. All the other chemicals were purchased from Aldrich and Fisher and used without further purification, unless otherwise noted.

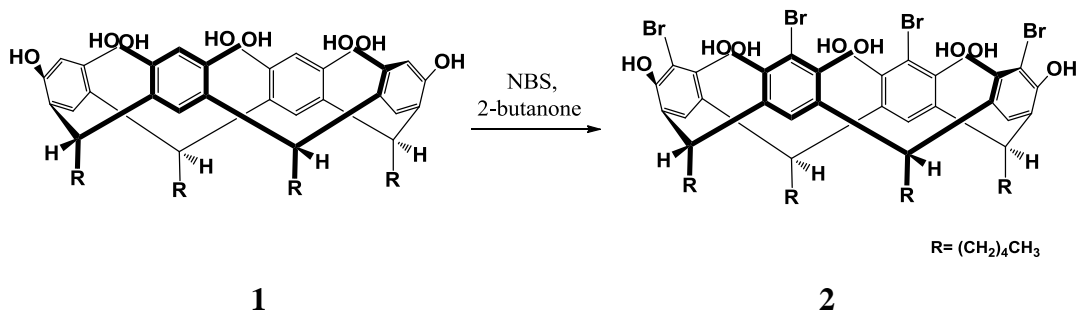
5.2.1.1 Synthesis of *C*-pentylcalix[4]resorcinarene, **1**²⁶



To a solution of resorcinol (100.0 g, 0.9 mol) in ethanol (900 mL) was added hexanal (91.0 g, 0.9 mol). The mixture was cooled to 0 °C under a dinitrogen atmosphere. Then conc. HCl (145 mL) was added dropwise over 15 minutes. A condenser was attached and the mixture heated to 70 °C for 16 hours. The reaction mixture was allowed to cool to room temperature, and then diluted with 1L water. A dark brownish precipitate formed which was filtered using a fritted Buchner funnel and washed with hot water until neutral pH and air dried. The product was dried

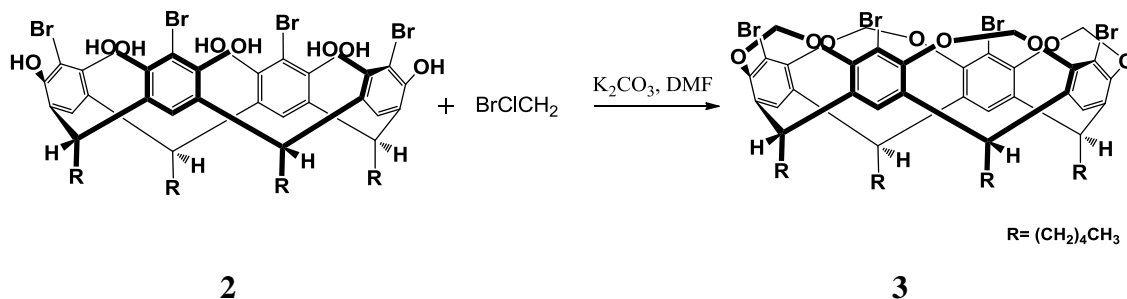
in oven at 100 °C for removal of excess water or solvents to yield **1**, (167 g, 95 %). M.p. > 280 °C. ¹H NMR (δ_H; 400 MHz, D₆-DMSO): 8.87 (s, 8H), 7.15 (s, 4H), 6.15 (s, 4H), 4.21 (t, J = 7.6Hz, 4H), 2.03 (m, 8H), 1.16-1.25 (m, 24H), 0.83 (t, J = 6.4Hz, 12 H); ¹³C NMR (δ_C; 400 MHz, CDCl₃): 151.66, 124.89, 123.07, 102.35, 31.50, 27.48, 22.26, 13.98.

5.2.1.2 Synthesis of *C*-pentyltetrabromocalix[4]resorcinarene, **2**²⁷



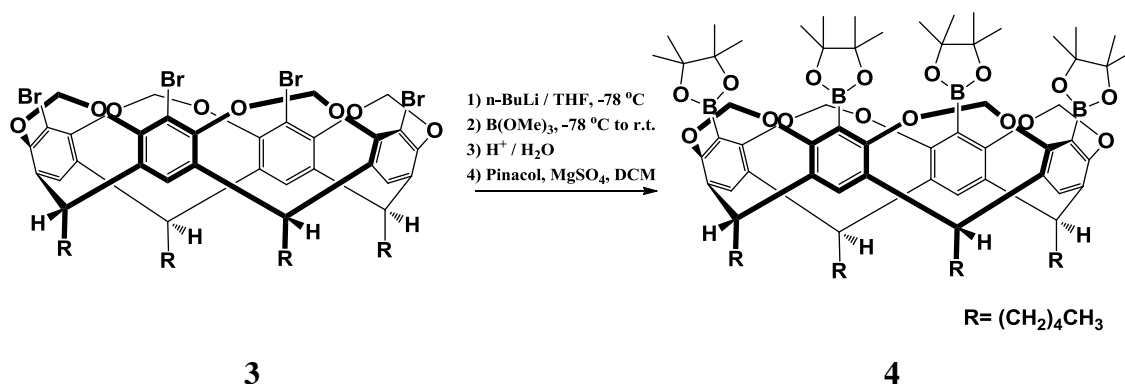
C-pentylcalix[4]resorcinarene **1** (50.0 g, 0.065 mol) was added to the flask containing -butanone (375 mL) at 0 °C. *N*-bromosuccinamide (69 g, 0.39 mol) was added slowly to a round bottom flask over a period of 1 hour. The reaction flask was covered with aluminum foil and a condenser was attached. The reaction mixture was stirred at room temperature for 16 hours under dinitrogen atmosphere. The precipitate from the reaction was filtered and washed with cold 2-butanone (3 x 50 mL) then cold acetone (3 x 100 mL). Product **2** was air dried followed by drying in the oven overnight (at 100 °C) producing a white solid, (58 g, 82 %). M.p. >280 °C; ¹H NMR (δ_H; 400 MHz, D₆-DMSO) 9.09 (s, 8H), 7.35 (s, 4H), 4.38 (t, J = 7.6Hz, 4H), 2.15 – 2.17 (m, 8H), 1.18 – 1.32 (m, 24H), 0.84 (t, J = 7Hz, 12H); ¹³C NMR (δ_H; 400 MHz, D₆-DMSO): 148.60, 125.48, 123.64, 101.29, 35.46, 33.48, 31.35, 27.38, 22.25, 13.94.

5.2.1.3 Synthesis of *C*-pentyltetrabromocavitand, **3**²⁸



To a stirred solution of C-pentyltetrabromoresorcin[4]arene **2** (30.00 g, 27.80 mmol) in DMF (500 mL) was added K_2CO_3 (50.00 g, 510.0 mmol) and CH_2BrCl (54.15 g, 418.51 mmol). The solution was heated at 65 °C for 24 h. An additional amount of CH_2BrCl (7.50 g, 58.01 mmol) was then added, and the reaction mixture was stirred at 65 °C for a further 24 h. After cooling to room temperature, the mixture was poured into an aqueous HCl solution (2%, 600 mL). The solid, which contained mainly **3**, was filtered off. The aqueous layer was extracted with Et_2O (3 x 500 mL) and the combined organic layers were dried over $MgSO_4$. After filtration, the solvent was removed on rotary evaporator. Both fractions of solid **3** were then purified by column chromatography (SiO_2 , Hexane \rightarrow 1:1 Hexane : Dichloromethane). Product **3** was isolated as a white solid, (26.50 g, 85 %). M.p. >280 °C; 1H NMR (δ_H ; 400 MHz, $CDCl_3$): 7.04 (s, 4H), 5.97 (d, $J = 7.2$ Hz, 4H), 4.85 (t, $J = 8.2$ Hz, 4H), 4.39 (d, $J = 7.2$ Hz, 4H), 2.18 – 2.24 (m, 8H), 1.32 – 1.43 (m, 24H), 0.87 – 0.94 (m, 12H); ^{13}C NMR (δ_C ; 400 MHz, $CDCl_3$): 152.03, 139.26, 119.01, 113.50, 98.45, 37.66, 31.84, 29.80, 27.39, 22.60, 14.03.

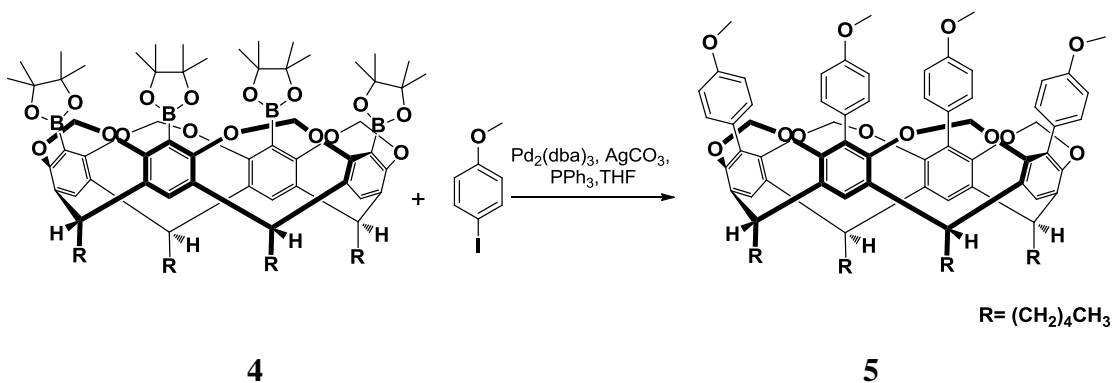
5.2.1.4 Synthesis of C-pentyltetraboronic acid dipinacolyl ester Cavitand, **4**



C-pentyltetrabromocavitand **3** (1.00g, 0.883 mmol) was dissolved in dry tetrahydrofuran (10 mL), and then the solution was evaporated and dried at 100 °C (0.1 mmHg) for 2 h under an argon atmosphere. This procedure was repeated twice. The resulting cavitand was dissolved in dry tetrahydrofuran (70 mL) and cooled to -78 °C (dry ice/acetone bath), under a dinitrogen atmosphere. To this solution, n-butyllithium (1.6 M in hexanes, 2.54 mL, 4.06 mmol) was added dropwise over 10 minutes and stirred for an additional 0.5h. Trimethoxyborane (0.60 mL, 5.3 mmol) was added dropwise over 10 minutes and the resulting solution was stirred at -78 °C for 0.5 h, at which time the dry ice/acetone bath was removed and the reaction mixture was allowed

to reach room temperature. Upon reaching room temperature, the reaction mixture was quenched with a 1M hydrochloric acid solution (100 mL) and stirred for 0.5 h. The mixture was extracted with dichloromethane (3x100 mL), the organic portions collected and dried over magnesium sulfate. The solvent was removed *via* rotary evaporator and the resulting residue dissolved in dichloromethane (100 mL). Excess pinacol (750 mg, 6.30 mmol) and magnesium sulfate (2.25 g) were added to the mixture, which was stirred for 12 h and then filtered and brought to dryness *via* a rotary evaporator. The residue was dissolved in dichloromethane and added to a beaker of acetone to induce precipitation of product and solid was filtered resulting in pure product **4** (570 mg, 50 %). Product can be recrystallized from dichloromethane:ethyl acetate:hexane (1:1:1). M. p. >280 °C; ¹H NMR (δ_H; 400 MHz, CDCl₃): 7.10 (s, 4H), 5.59 (d, J = 6.8 Hz, 4H), 4.75 (t, J = 7.2 Hz, 4H), 4.54 (d, J = 7.6 Hz, 4H), 2.17-2.15 (m, 8H), 1.40-1.29 (m, 72H), 0.90-0.88 (m, 12H); ¹³C NMR (δ_C; 200 MHz, CDCl₃): 157.72, 137.77, 122.37, 99.42, 83.53, 36.11, 31.91, 30.89, 29.88, 27.54, 24.70, 22.65, 14.02; IR : 2977, 2931, 1705, 1592, 1442, 1358, 1316, 1145, 978, 851, 582; MALDI-TOF / TOF-MS *m/z* 1343.75 ([**4** + (Na)]⁺); Anal. Calcd. for C₇₆H₁₀₈O₁₆B₄: C, 69.09; H, 8.18. Found: C, 69.24 ; H, 8.44.

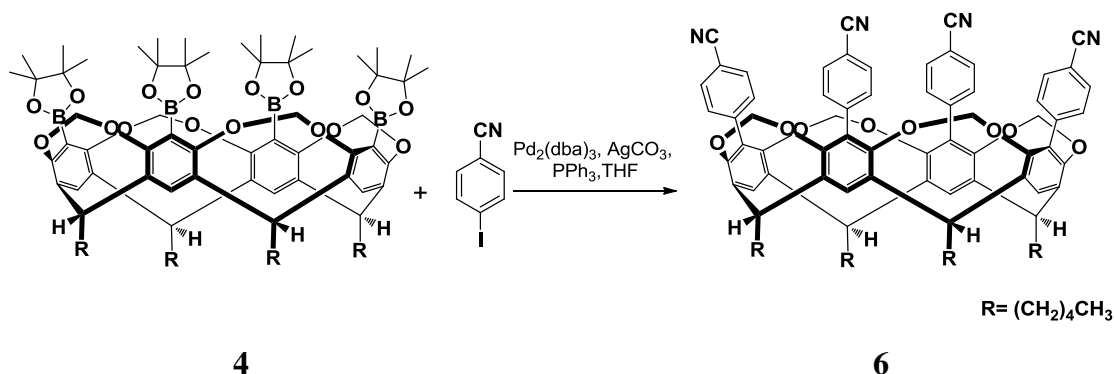
5.4.1.5 Synthesis of *C*-pentyltetra(4-methoxyphenyl)cavitand, **5**



An oven-dried round-bottom flask was placed under an argon atmosphere and charged with *C*-pentyltetraboronic acid dipinacolyl ester **4** (100 mg; 75.7 μmol), 4-iodoanisole (80 mg, 378 μmol, 5 mol equiv), silver carbonate (608 μmol, 8.0 mol equiv), *tris*(dibenzylideneacetone) dipalladium(0) (36 μmol, 0.12 mol equiv), and triphenylphosphine (151 μmol, 2 mol equiv). The flask was evacuated and refilled with nitrogen three times, and then dry tetrahydrofuran (5 mL) was added. The reaction mixture was stirred at room temperature in the dark condition for 72 h then filtered through a short plug of celite, washed three times with chloroform and the solvent

was evaporated to afford the crude product. The crude product was purified by column chromatography (100 g silica, hexane → 8:2 hexane : ethyl acetate) to give **5** (73 mg, 78%). M.p. > 280 °C. ¹H NMR (δ_H; 400 MHz, CDCl₃): 7.32 (s, 4H), 6.76 (d, J = 8Hz, 8H), 6.59 (d, J = 8Hz, 8H), 5.03 (d, J = 4Hz, 4H), 4.88 (t, 8 Hz, 4H), 4.10 (d, J = 4Hz, 4H), 3.00 (br s, 8H), 2.40 – 2.33 (m, 8H), 1.50 – 1.38 (m, 24H), 0.97 (t, J = 8Hz, 12 H); ¹³C NMR (δ_C; 400 MHz, CDCl₃): 158.26, 152.84, 138.46, 130.90, 129.73, 125.84, 119.48, 113.15, 99.88, 75.03, 37.12, 32.03, 27.63, 24.81, 22.71, 14.17. IR: 3403, 2927, 1611, 1514, 1447, 1244, 1156, 1110, 1018, 973, 949, 827, 805, 673. ESI-TOF-MS *m/z* 1241.6 ([M+H]⁺) and 1258.6 ([M+NH₄]⁺).

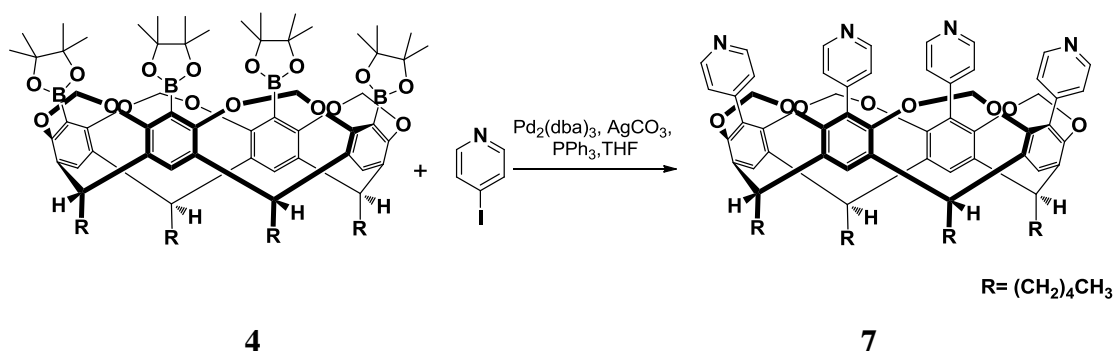
5.4.1.6 Synthesis of *C*-pentyltetra(4-cyanophenyl)cavitand, **6**



An oven-dried round-bottom flask was placed under an argon atmosphere and charged with *C*-pentyltetraboronic acid, dipinacolyl ester **4** (100 mg; 75.7 μmol), 4-iodobenzonitrile (86 mg, 378 μmol, 5 mol equiv), silver carbonate (608 μmol, 8.0 mol equiv), *tris*(dibenzylideneacetone)dipalladium(0) (36 μmol, 0.12 mol equiv), and triphenylphosphine (151 μmol, 2 mol equiv). The flask was evacuated and refilled with nitrogen three times, and then dry tetrahydrofuran (5 mL) was added. The reaction mixture was stirred at room temperature in the dark condition for 72 h then filtered through a short plug of celite, washed three times with chloroform and the solvent was evaporated to afford the crude product. The crude product was purified by column chromatography (100 g silica, hexane → 8:2 chloroform : ethyl acetate) to give **6** (69 mg, 75%). m. p. > 280 °C. ¹H NMR (δ_H; 400 MHz, CDCl₃): 7.64 (d, 8 Hz 8H), 7.38 (s, 4H), 7.17 (d, J = 8Hz, 8H), 5.25 (d, 8Hz, 4H), 4.83 (t, 8 Hz, 4H), 4.20 (d, 4Hz, 4H), 2.40 – 2.33 (m, 8H), 1.50 – 1.38 (m, 24H), 0.97 (t, J = 8Hz, 12 H); ¹³C NMR (δ_C; 400 MHz, CDCl₃): 152.25, 138.59, 131.70, 130.80, 127.69, 120.86, 118.52, 111.27, 100.43, 37.06, 31.98,

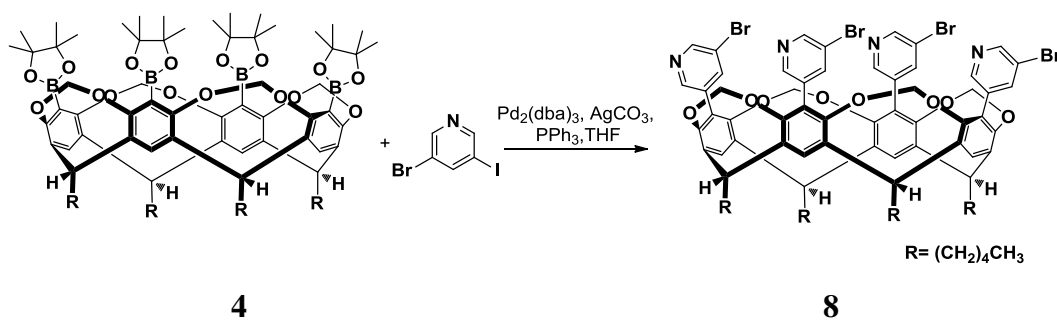
27.59, 22.67, 14.12. IR: 2925, 2226, 1608, 1447, 1157, 1082, 971, 839, 805, 740, 692. ESI-TOF-MS m/z 1265.5 ($[M+CH_2O_2-H]^+$).

5.2.1.7 Synthesis of *C*-pentyltetra(3-pyridyl)cavitand, **7**



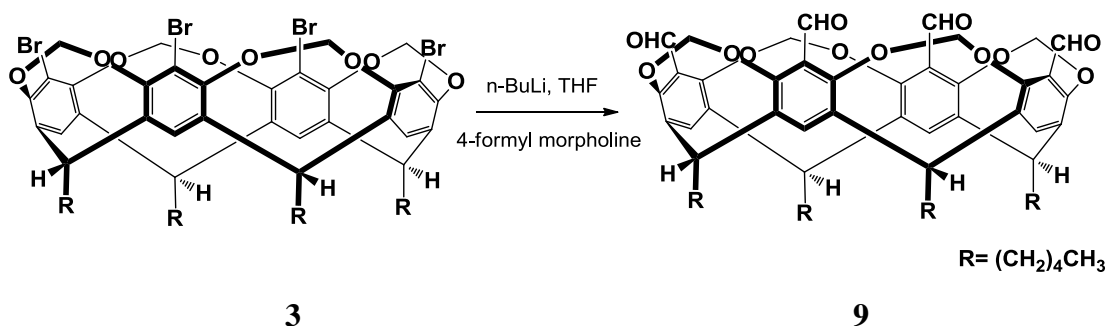
An oven-dried round-bottom flask was placed under a argon atmosphere and charged with *C*-pentyltetraboronic acid, dipinacolyl ester **4** (100 mg; 75.7 μ mol), 4-iodopyridine (77 mg, 378 μ mol, 5 mol equiv), silver carbonate (608 μ mol, 8.0 mol equiv), *tris*(dibenzylideneacetone)dipalladium(0) (36 μ mol, 0.12 mol equiv), and triphenylphosphine (151 μ mol, 2 mol equiv). The flask was evacuated and refilled with nitrogen three times then dry tetrahydrofuran (5 mL) was added. The reaction mixture was stirred at room temperature in the dark condition for 72 h then filtered through a short plug of celite, washed three times with chloroform and the solvent was evaporated to afford the crude product. The crude product was purified by column chromatography (100 g silica, hexane \rightarrow hexane: ethyl acetate \rightarrow 1:1 ethyl acetate : Ethanol : 3% triethyl amine) to give **7** (63 mg, 74%). M. p. $> 280^\circ C$. 1H NMR (δ_H ; 400 MHz, $CDCl_3$): 8.59 (d, $J = 6.0$ Hz, 8H), 7.37 (s, 4H), 6.98 (d, 6 Hz, 8H), 5.29 (d, 6 Hz, 4H), 4.84 (t, 8 Hz, 4H), 4.23 (d, 8.0 Hz, 4H), 2.34 (m, 8H), 1.46 (m, 24H), 0.96 (t, 7Hz, 12 H); ^{13}C NMR (δ_C ; 400 MHz, $CDCl_3$): 152.17, 149.46, 142.02, 138.00, 126.83, 124.91, 120.85, 100.39, 43.23, 37.01, 31.99, 30.24, 27.58, 22.68, 14.14. IR: 2929, 2859, 1583, 1450, 1408, 1160, 1084, 975, 716. ESI-TOF-MS m/z 1125.5 ($[M+H]^+$).

5.4.1.8 Synthesis of *C*-pentyltetra(3-bromopyridyl)cavitand, **8**



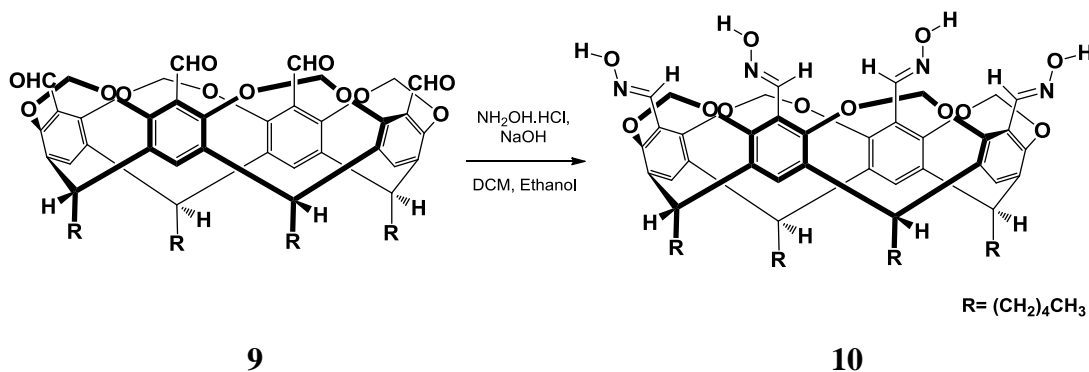
An oven-dried round-bottom flask was placed under an argon atmosphere and charged with *C*-pentyltetraboronic acid, dipinacolyl ester **4** (100 mg; 75.7 μmol), 3-bromo-5-iodopyridine (116 mg, 378 μmol , 5 mol equiv), silver carbonate (608 μmol , 8.0 mol equiv), *tris*(dibenzylideneacetone)dipalladium(0) (36 μmol , 0.12 mol equiv), and triphenylphosphine (151 μmol , 2 mol equiv). The flask was evacuated and refilled with nitrogen three times then dry tetrahydrofuran (5 mL) was added. The reaction mixture was stirred at room temperature in the dark condition for 72 h then filtered through a short plug of celite, washed three times with chloroform and the solvent was evaporated to afford the crude product. The crude product was purified by column chromatography (100 g silica, hexane \rightarrow hexane: ethyl acetate \rightarrow 8:2 ethyl acetate : ethanol) to give **8** (84 mg, 77%). m. p. $> 280^\circ\text{C}$. ^1H NMR (δ_{H} ; 400 MHz, CDCl_3): 8.59 (d, $J = 2.0$ Hz, 4H), 8.14 (s, 4H), 7.62 (t, 2 Hz, 4H), 7.37 (s, 4H), 5.38 (d, 8 Hz, 4H), 4.83 (t, 8 Hz, 4H), 4.21 (d, 4.0 Hz, 4H), 2.34 (m, 8H), 1.46 (m, 24H), 0.96 (t, 6Hz, 12 H); ^{13}C NMR (δ_{C} ; 400 MHz, CDCl_3): 152.53, 149.59, 147.88, 140.28, 138.56, 130.93, 124.48, 121.05, 37.03, 31.97, 30.21, 27.57, 22.67, 14.12. IR: 2921, 2850, 1583, 1459, 1400, 1299, 1259, 1177, 1080, 1013, 970, 732. ESI-TOF-MS m/z 1441.3 ($[\text{M}+\text{H}]^+$).

5.2.1.9 Synthesis of *C*-pentyltetraaldehydecavitand, **9**²⁹



Dry THF (10.0 mL) was transferred to a dry round bottom flask containing C-pentyltetrabromocavitand **3** (2.00 g, 1.77 mmol) and a football shaped stir-bar. The resulting solution was evaporated to dryness and heated to 80°C for one hour under vacuum. The vacuum was replaced with nitrogen and the procedure was repeated two more times. Dry THF (100 mL) was added to the dried tetrabromo cavitand. The reaction vessel was chilled to -78° C with a dry ice temperature bath and n-butyllithium (6.64 mL of 1.60 M in hexanes, 6 equiv) was added. After 30 minutes of stirring, 4-formyl morpholine (3.00 ml, 30.0 mmol) was added to the reaction vessel at -78° C. After stirring overnight, the reaction mixture was cooled to 0 °C and 2 M of HCl was added dropwise to the reaction vessel and allowed to stir for an additional 30 minutes. The solvent was removed using a rotary evaporator. A yellowish solid was filtered off and triturated with water. This crude product was submitted to column chromatography, hexane → hexane: dichloromethane → 96:4 dichloromethane: ethyl acetate, to yield white solid **9** (1.19 g, 70 %). M. p. > 280°C. ¹H NMR (δ_H; 400 MHz, CDCl₃): 10.26 (s, 4H), 7.29 (s, 4H), 5.91 (d, 4 Hz, 4H), 4.91 (t, 8 Hz, 4H), 4.47 (d, 4 Hz, 4H), 2.29-2.21 (m, 8H), 1.45-1.32 (m, 24H), 0.96 (t, 8Hz, 12 H); ¹³C NMR (δ_C; 400 MHz, CDCl₃): 139.15, 124.78, 124.28, 100.12, 35.89, 29.50, 27.43, 22.68, 14.09.

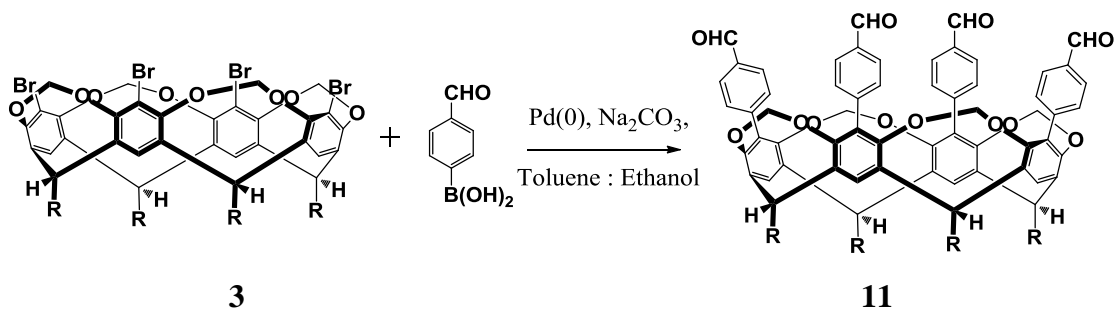
5.2.1.10 Synthesis of C-pentyltetraaldoximecavitand, **10**



Tetraaldehyde cavitand **10** (0.20 g, 0.21 mmol), hydroxylamine hydrochloride (0.09 g, 1.29 mmol), and sodium hydroxide (0.05 g, 1.29 mmol) were added in ceramic mortar and pestle, to this mixture 4-5 drops of dichloromethane and ethanol were added and grounded at room temperature for 5 minutes. The reaction mixture was then washed with water to remove inorganic salts and the residue dried in air. The product is further vacuum dried at 80 °C to get pure **10** in quantitative yield. M.p. >270°C dec. ¹H NMR (δ_H; 400 MHz, *d*-DMSO): 11.34 (br s,

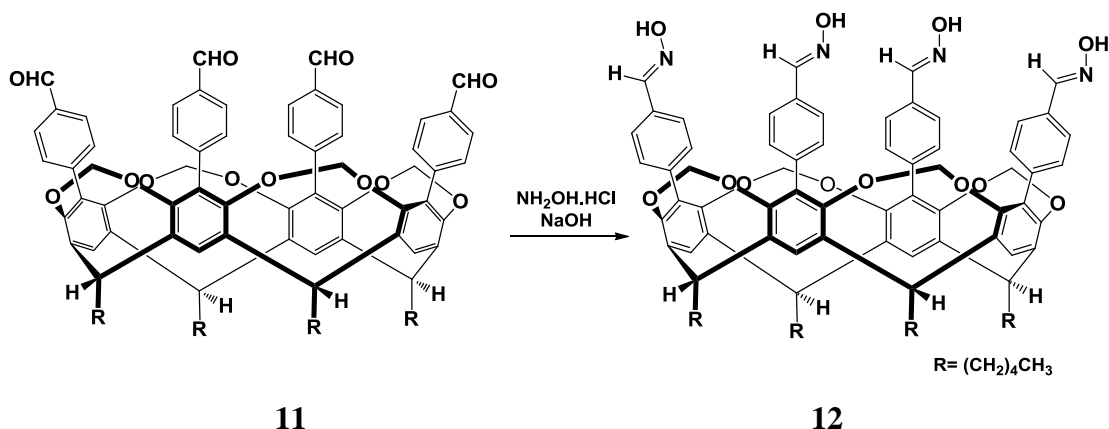
4H), 7.95 (s, 4H), 7.62 (s, 4H), 5.69 (d, J = 8Hz, 4H), 4.70 (t, 8 Hz, 4H), 4.31 (d, J = 8Hz, 4H), 2.41-2.35 (m, 8H), 1.41-1.29 (m, 24H), 0.88 (t, J = 8Hz, 12 H); ^{13}C NMR (δ_{H} ; 400 MHz, *d*-DMSO): 151.86, 142.27, 138.44, 122.40, 120.30, 99.24, 36.55, 31.36, 28.92, 27.27, 22.21, 13.84. IR: 3323, 2928, 2863, 1582, 1445, 1297, 1236, 1149, 1080, 1016, 932. ESI-TOF-MS m/z 989.4 ($[\text{M}+\text{H}]^+$).

5.2.1.11 Synthesis of *C*-pentyltetra(4-phenylformyl)cavitand, **11**



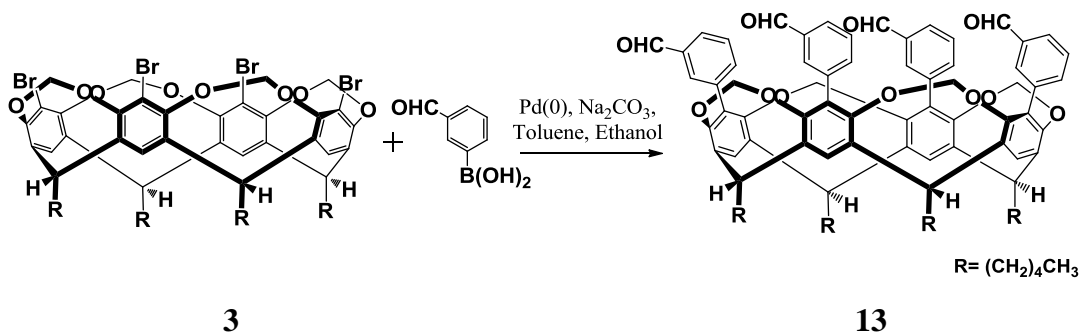
A mixture of tetrabromocavitand **3** (2.0 g, 1.76 mmol) and *tetrakis*triphenylphosphine palladium (0) (420 mg, 0.362 mmol) were added to a round-bottom flask under a stream of dinitrogen. Toluene (40 mL), ethanol (30 mL), and aqueous sodium bicarbonate (2.00 g) were all purged with dinitrogen, then added to the round bottom flask along with 4-formylphenyl boronic acid (2.64 g, 17.6 mmol). The reaction mixture was refluxed for 72 hours under a dinitrogen atmosphere. Upon completion, the reaction was cooled to room temperature and diluted with water (200 mL). The aqueous phase was extracted with chloroform (3 x 100 mL) the combined organic phases were washed with saturated brine (3 x 100 mL), and dried over anhydrous magnesium sulfate. The solvent was removed on a rotary evaporator and the residue purified by column chromatography (SiO_2) using a hexanes/ethyl acetate (6:4) mixture as the eluant. The product was further purified by reprecipitation (chloroform:hexanes). The product **11** was isolated as a white powder, (2gm, 95%). M.p. >270 °C; ^1H NMR (δ_{H} ; 400 MHz, CDCl_3): 10.00 (s, 4H), 7.85 (d, J = 8.4Hz, 8H), 7.38 (s, 4H), 7.20 (d, J = 8.4Hz, 8H), 5.16 (d, J = 6.8Hz, 4H), 4.86 (t, J = 8Hz, 4H), 4.23 (d, 6.8 Hz, 4H), 2.39 – 2.34 (m, 8H), 1.50 – 1.38 (m, 24H), 0.95 (t, J = 7Hz, 12 H); ^{13}C NMR (δ_{H} ; 200 MHz, CDCl_3): 191.75, 152.29, 140.40, 138.49, 135.09, 130.58, 128.30, 128.00, 120.58, 100.42, 37.02, 31.99, 30.26, 27.60, 22.68, 14.13. IR : 2928, 1701, 1606, 1449, 1209, 1168, 1082, 1018, 972, 828, 752, 729. ESI-TOF-MS m/z 1255.5 ($[\text{M}+\text{Na}]^+$).

5.2.1.12 Synthesis of *C*-pentyltetra(4-phenylaldoxime)cavitand, **12**



C-pentyltetra(4-phenylformyl)cavitand **11** (0.20 g, 0.16 mmol), hydroxylamine hydrochloride (0.07 g, 0.9 mmol) and sodium hydroxide (0.04 g, 0.9 mmol) were added in ceramic mortar and pestle, to this mixture 4-5 drops of dichloromethane and ethanol were added and grounded at room temperature for 5 minutes. The reaction mixture was then washed with water to remove inorganic salts and the residue dried in air. The product is further vacuum dried at 80 °C to get pure **12** in quantitative yield. M.p. >270°C. ¹H NMR (δ_{H} ; 400 MHz, d-DMSO): 11.27 (br s, 4H), 8.10 (s, 4H), 7.82 (s, 4H), 7.53 (d, $J = 8\text{Hz}$, 8H), 7.10 (d, $J = 8\text{Hz}$, 8H), 5.21 (d, $J = 8\text{Hz}$, 4H), 4.68 (t, 8 Hz, 4H), 4.32 (d, $J = 8\text{Hz}$, 4H), 1.45-1.34 (m, 24H), 0.90 (t, $J = 8\text{Hz}$, 12 H); ¹³C NMR (δ_{H} ; 400 MHz, d-DMSO): 151.79, 147.71, 138.20, 134.15, 131.69, 130.37, 128.50, 125.87, 121.84, 99.78, 33.16, 31.43, 30.63, 29.54, 27.37, 22.22, 13.92. IR : 3448, 2932, 1685, 1465, 1448, 1250, 1158, 1084, 970, 848. ESI-TOF-MS m/z 1293.6 ([$\text{M}+\text{H}$]⁺).

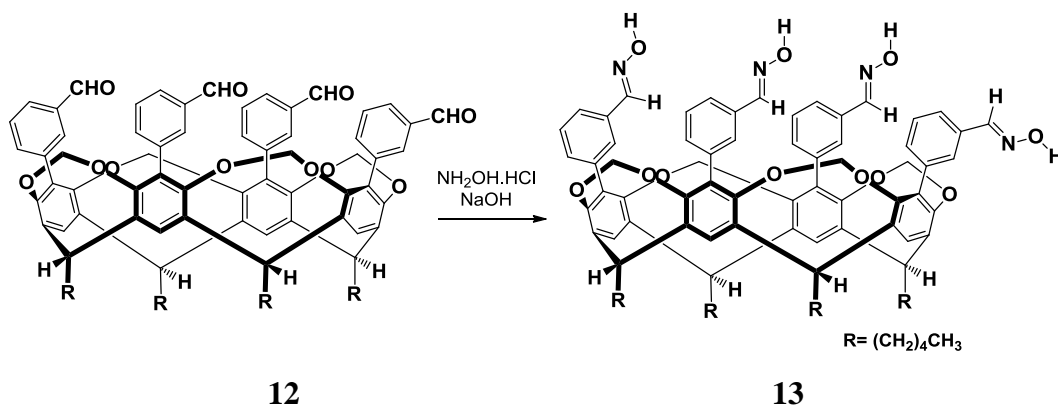
5.2.1.13 Synthesis of *C*-pentyltetra(3-phenylformyl)cavitand, **13**



A mixture of tetrabromocavitand **3** (2.0 g, 1.76 mmol) and *tetrakis*triphenylphosphine palladium (0) (420 mg, 0.362 mmol) were added to a round bottom flask under a stream of dinitrogen. Toluene (40 mL), ethanol (30 mL), and aqueous sodium bicarbonate (2.00 g) were all

purged with dinitrogen, then added to the round-bottom flask along with 3-formylphenyl boronic acid (2.64 g, 17.6 mmol). The reaction mixture was refluxed for 72 hours under a dinitrogen atmosphere. Upon completion the reaction was cooled to room temperature and diluted with water (200 mL). The aqueous phase was extracted with chloroform (3 x 100 mL) the combined organic phases were washed with saturated brine (3 x 100 mL), dried over anhydrous magnesium sulfate. The solvent was removed on a rotary evaporator. Cavitant **13** is purified by column chromatography (SiO₂) using a hexanes/ethyl acetate (65:35) mixture as the eluant. The product was further purified by reprecipitation (chloroform:hexanes). The product **13** was isolated as a white powder, (40%). M.p. 184-186°C. ¹H NMR (δ_H; 400 MHz, CDCl₃): 10.00 (s, 4H), 7.78 (d, J = 7.6Hz, 4H), 7.54 (s, 4H), 7.51 (t, J = 7.6Hz, 8H), 7.38 (overlapping s+d, 4H, 4H), 5.16 (d, J = 7.2Hz, 4H), 4.85 (t, 8 Hz, 4H), 2.40 – 2.34 (m, 8H), 1.50 – 1.38 (m, 24H), 0.96 (t, J = 8Hz, 12 H); ¹³C NMR (δ_H; 400 MHz, CDCl₃): 192.36, 152.72, 138.60, 136.30, 135.18, 130.58, 129.96, 128.47, 120.59, 100.63, 37.29, 33.25, 31.18, 30.49, 27.87, 22.93, 14.38. IR: 2929, 1698, 1465, 1243, 1153, 1084, 973, 791, 700, 650. ESI-TOF-MS *m/z* 1250.5 ([M+NH₄]⁺).

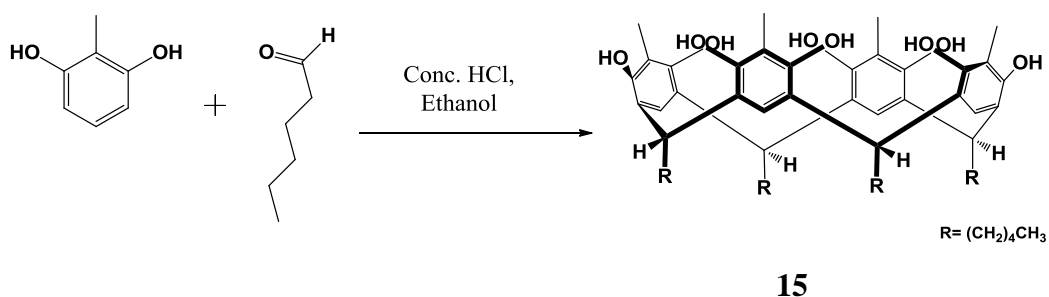
5.2.1.14 Synthesis of C-pentyltetra(3-phenylaldoxime)cavitant, **14**



C-pentyltetra(3-phenylformyl)cavitant **13** (0.20 g, 0.16 mmol), hydroxylamine hydrochloride (0.07 g, 0.9 mmol) and sodium hydroxide (0.04 g, 0.9 mmol) were added in ceramic mortar and pestle, to this mixture 4-5 drops of dichloromethane and ethanol were added and grounded at room temperature for 5 minutes. The reaction mixture was then washed with water to remove inorganic salts and the residue dried in air. The product is further vacuum dried at 80 °C to get pure **14** in quantitative yield. M.p. 193-195°C. ¹H NMR (δ_H; 400 MHz, *d*-DMSO): 11.29 (br s, 4H), 8.08 (s, 4H), 7.83 (s, 4H), 7.52 (d, J = 8Hz, 4H), 7.36 (t, J = 8Hz, 4H),

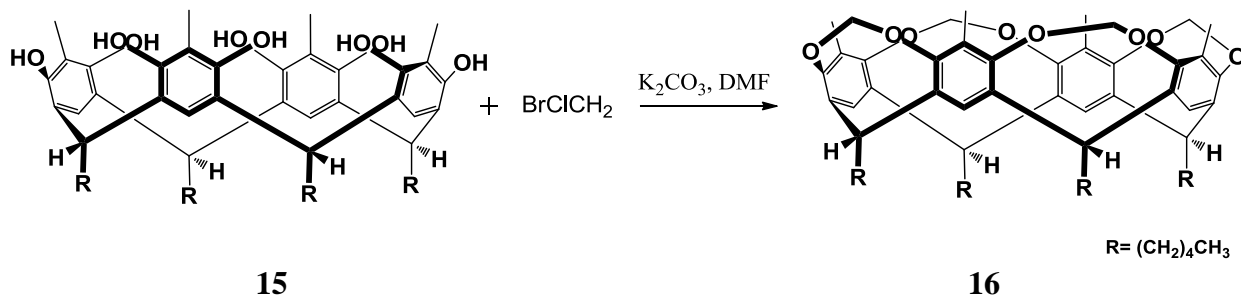
7.10 (d, $J = 8\text{Hz}$, 8H), 5.18 (d, $J = 8\text{Hz}$, 4H), 4.69 (t, 8 Hz, 4H), 4.33 (d, $J = 8\text{Hz}$, 4H), 1.46-1.34 (m, 24H), 0.91 (t, $J = 8\text{Hz}$, 12 H); ^{13}C NMR (δ_{H} ; 400 MHz, $d\text{-DMSO}$): 151.82, 147.97, 138.22, 133.73, 132.60, 130.45, 128.54, 128.35, 124.69, 121.73, 99.68, 37.13, 31.43, 29.51, 27.35, 22.21, 13.90. IR : 3378, 2927, 1465, 1279, 1154, 1082, 976, 793, 683. ESI-TOF-MS m/z 1293.6 ($[\text{M}+\text{H}]^+$).

5.2.1.15 Synthesis of *C*-pentyltetramethylresorcin[4]arene, 15³⁰



To a solution of 2-methylresorcinol (10.0 g, 0.08 mol) in ethanol (90 mL) was added hexanal (8.1 g, 0.081 mol). The solution was cooled to 0 °C under a dinitrogen atmosphere. Then conc. HCl (14.5 mL) was added dropwise over 15 minutes. A condenser was attached and the mixture heated to 70 °C for 12 hours. The reaction mixture was allowed to cool to room temperature, and then diluted with water. A dark brownish precipitate formed which was filtered using a fritted Buchner funnel and washed with hot water until neutral pH and air dried. The product dried in oven at 100 °C for removal on excess water or solvents to yield, (13.8 g, 90 %). M.p. >280 °C; ^1H NMR (δ_{H} ; 400 MHz, $\text{D}_6\text{-DMSO}$): 8.65 (s, 8H), 7.25 (s, 4H), 4.20 (t, $J = 7.6\text{Hz}$, 4H), 2.22 (m, 8H), 1.95 (s, 12H), 1.16-1.25 (m, 24H), 0.85 (t, $J = 6.4\text{Hz}$, 12 H); ^{13}C NMR (δ_{C} ; 400 MHz, CDCl_3): 148.98, 124.78, 111.58, 31.48, 27.68, 22.32, 13.98, 10.03.

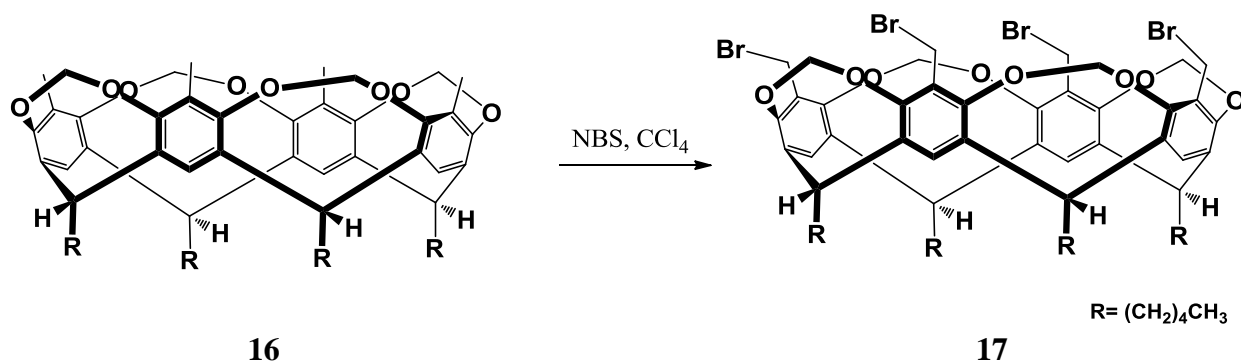
5.2.1.16 Synthesis of *C*-pentyltetramethylcavitand, 16³⁰



To a stirred solution of C-pentyltetramethylresorcin[4]arene **15** (5.00 g, 6.5 mmol) in DMF (300 mL) was added K_2CO_3 (18.46 g, 133.0 mmol) and CH_2BrCl (10.09 mL, 5.23 g, 78.00 mmol). The solution was heated at 70 °C for 24 h. The reaction mixture was poured into cold ice

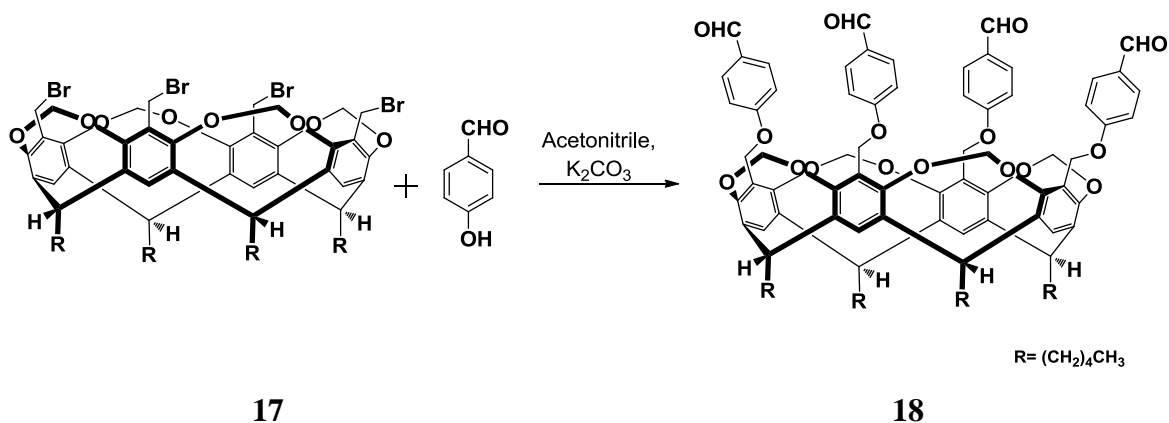
water and the brown solid was collected by suction filtration. The crude product was dissolved in dichloromethane and dried using $MgSO_4$. The product was flushed through a SiO_2 column using dichloromethane to yield a brown solid **16** (2.65 g, 48%). M.p. >280 °C; 1H NMR (δ_H ; 400 MHz, $CDCl_3$): 6.98 (s, 4H), 5.88 (d, $J = 4Hz$, 4H), 4.76 (t, $J = 8Hz$, 4H), 4.26 d, $J = 4Hz$, 4H), 2.20 (m, 8H), 1.95 (s, 12H), 1.16-1.25 (m, 24H), 0.90 (t, $J = 6.4Hz$, 12 H); ^{13}C NMR (δ_C ; 400 MHz, $CDCl_3$): 153.21, 137.93, 123.57, 117.53, 98.48, 36.99, 32.08, 30.08, 27.65, 22.68, 14.09, 10.31.

5.2.1.17 Synthesis of C-pentyltetra(bromomethyl)cavitand, 17³⁰



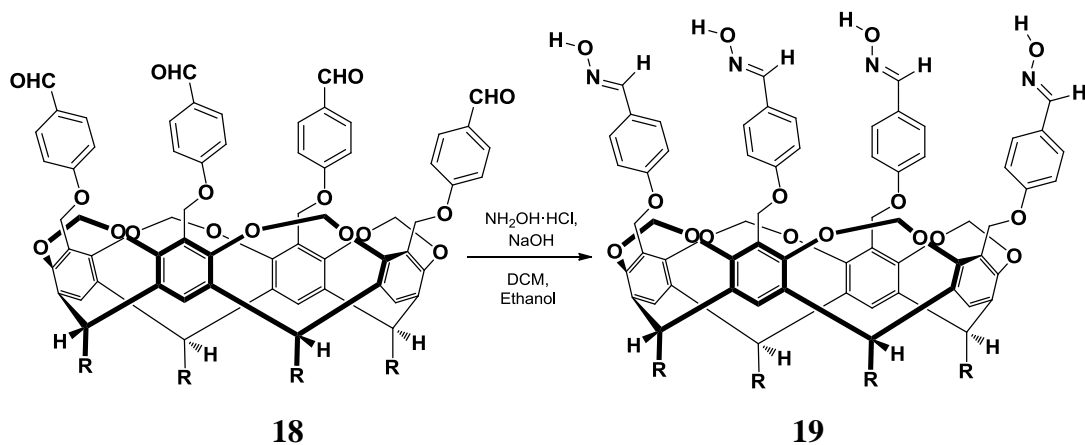
Dry C-pentyltetramethylcavitand, **16** (2.65 g, 3.05 mmol) and AIBN (119 mg, catalytic amount) dissolved in 170 mL degassed CCl_4 . Then NBS (2.71 g, 15.2 mmol) was added and the reaction mixture was reflux overnight. The reaction was monitored by TLC (*Note* – In some cases for completion of the reaction it is necessary to add excess NBS and AIBN). After completion the solid precipitate (succinimide) was filtered off and CCl_4 was evaporated to yield white product **17** (2.20 g, 61%). M.p. >280 °C; 1H NMR (δ_H ; 400 MHz, $CDCl_3$): 7.31 (s, 4H), 6.02 (d, $J = 4Hz$, 4H), 4.77 (t, $J = 8Hz$, 4H), 4.56 d, $J = 4Hz$, 4H), 4.41(s, 8H), 2.20 (m, 8H), 1.30-1.43 (m, 24H), 0.90 (t, $J = 8Hz$, 12 H); ^{13}C NMR (δ_C ; 400 MHz, $CDCl_3$): 153.49, 138.02, 124.46, 120.91, 99.08, 36.84, 31.94, 27.51, 22.62, 14.02.

5.2.1.18 Synthesis of *C*-pentyltetra(4-formylmethoxyphenyl)cavitand, **18**³¹



A mixture of dry *C*-pentyltetra(bromomethyl)cavitand, **17** (0.2 g, 0.16 mmol), anhydrous K_2CO_3 (6.35g, 4.59 mmol) and *p*-hydroxybenzaldehyde (0.08 g, 0.67 mmol) in 15 mL of dry acetonitrile was refluxed for 12 hours. The solvent was removed using rotary evaporator and residue was mixed with dichloromethane (50 mL) and washed with 2N HCl (3 x 50 mL). The organic layer was separated, dried using MgSO_4 , concentrated on rotary evaporator to yield white solid **18** (0.18 g, 80%). M.p. >280 °C; ^1H NMR (δ_{H} ; 400 MHz, CDCl_3): 9.98 (s, 4H), 7.82(d, $J = 4$ Hz, 4H), 7.31 (s, 4H), 7.01 (d, $J = 4$ Hz, 4H), 5.75(d, $J = 4$ Hz, 4H), 5.00 (s, 8H), 4.86 (t, $J = 8$ Hz, 4H), 4.61 (d, $J = 4$ Hz, 4H), 2.29 (m, 8H), 1.30-1.43 (m, 24H), 0.93 (t, $J = 8$ Hz, 12 H); ^{13}C NMR (δ_{C} ; 400 MHz, CDCl_3): 190.64, 163.40, 154.31, 138.18, 132.31, 132.06, 130.23, 121.88, 121.52, 114.61, 99.97, 60.93, 36.91, 31.96, 27.54, 22.68, 14.14.

5.2.1.19 Synthesis of *C*-pentyltetra(4-aldoximemethoxyphenyl)cavitand, **19**



C-pentyltetra(4-formylmethoxyphenyl)cavitand, **18** (0.23 g, 0.16 mmol), hydroxylamine hydrochloride (0.07 g, 0.9 mmol) and sodium hydroxide (0.04 g, 0.9 mmol) were added in ceramic mortar and pestle, to this mixture 4-5 drops of dichloromethane and ethanol were added and grounded at room temperature for 5 minutes. The reaction mixture was then washed with water to remove inorganic salts and the residue dried in air. The product is further vacuum dried at 80 °C to get pure **19** in quantitative yield. M.p. >300°C. ¹H NMR (δ_H; 400 MHz, *d*-DMSO): 10.87 (br s, 4H), 8.04 (s, 4H), 7.75 (s, 4H), 7.48 (d, J = 8Hz, 8H), 6.94 (d, J = 8Hz, 8H), 5.795 (d, J = 4Hz, 4H), 4.84 (s, 8 Hz, 8H), 4.71 (t, J = 8Hz, 4H), 4.48 (d, J = 8Hz, 4H), 2.43(shoulder to *d*-DMSO peak br m, 12H) 1.50-1.24 (m, 24H), 0.89 (t, J = 8Hz, 12 H); ¹³C NMR (δ_C; 400 MHz, *d*-DMSO): 159.19, 153.48, 147.44, 137.95, 127.75, 125.91, 122.66, 114.76, 60.52, 36.83, 31.35, 29.20, 27.31, 22.18, 13.84. IR : 3463, 2923, 1608, 1514, 1458, 1301, 1251, 1172, 1090, 970, 877, 847, 828. ESI-TOF-MS *m/z* 1413.6 ([M+H]⁺).

5.3 Results and discussion

5.3.1 Versatile Suzuki-Miyaura coupling protocol for cavitand functionalization

The starting point for cavitand scaffold synthesis was the condensation of resorcinol with hexanal to obtain the calix[4]resorcinarene. Choice of aldehyde (i.e. hexanal) in this reaction is based on the required ‘pentyl feet’ on the cavitand products for their desired solubility in organic solvents. The upper rim was then brominated with N-bromosuccinimide, as adding the bromo group on upper rim opens many options of functionalization in the later stages. Rigidity was imparted to the structure by bridging the hydroxyl groups using bromochloromethane (as a bridging agent for methylene bridged cavitands) to obtain a tetrabromocavitand **3**. Although a synthetic methodology is well developed for the synthesis of **3**, scale-up of the reactions required special glassware design and optimization of reaction conditions to get higher yields with maximum purity as mentioned in Section 5.2.

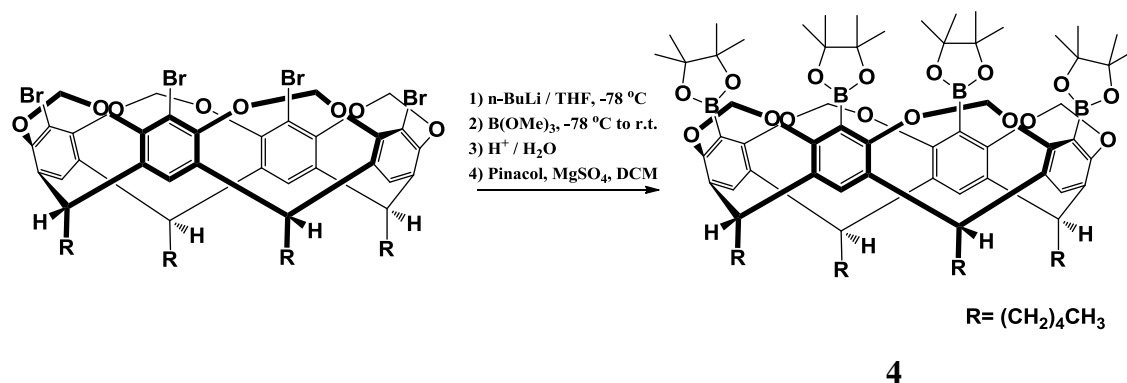


Figure 5.9 Synthesis of tetraboronic pinacolyl ester cavitand **4**.

The synthesis of **4** was achieved in 50 % yield, following a modified procedure.³² It should be noted that in the reported case, the goal was to only convert two of the four bromine atoms into the pinacolyl boronate derivative. In our case, the C-pentyltetrabromo cavitand, **3** (carefully dried using Sherburn's procedure³³) was allowed to react with 4.6 equiv of *n*-butyllithium at $-78\text{ }^{\circ}\text{C}$ for 0.5 h resulting in a fourfold lithium-halogen exchange. To this, 6 equiv of dry trimethoxyborane was added and the reaction was allowed to reach room temperature after 0.5 h. The mixture was acidified with hydrochloric acid, producing the tetraboronic acid cavitand, which was then converted to the desired tetraboronic pinacolyl ester cavitand **4**, by addition of excess pinacol and magnesium sulfate (Figure 5.9). Purification was carried out by dissolving the reaction mixture in dichloromethane and adding excess acetone, resulting in the formation of a white precipitate.

In order to successfully couple **4** to different representative haloarenes we had to identify the optimum reaction conditions for versatile and facile tetrafunctionalization on the 'upper rim' of the cavitand. Our choice of suitable haloarenes was based on two criteria -

- 1) The haloarenes should represent different classes of functional groups to establish the versatility of this system.
- 2) The end product, the resulting tetrafunctionalized cavitand, should have obvious applications and utility in host-guest chemistry.

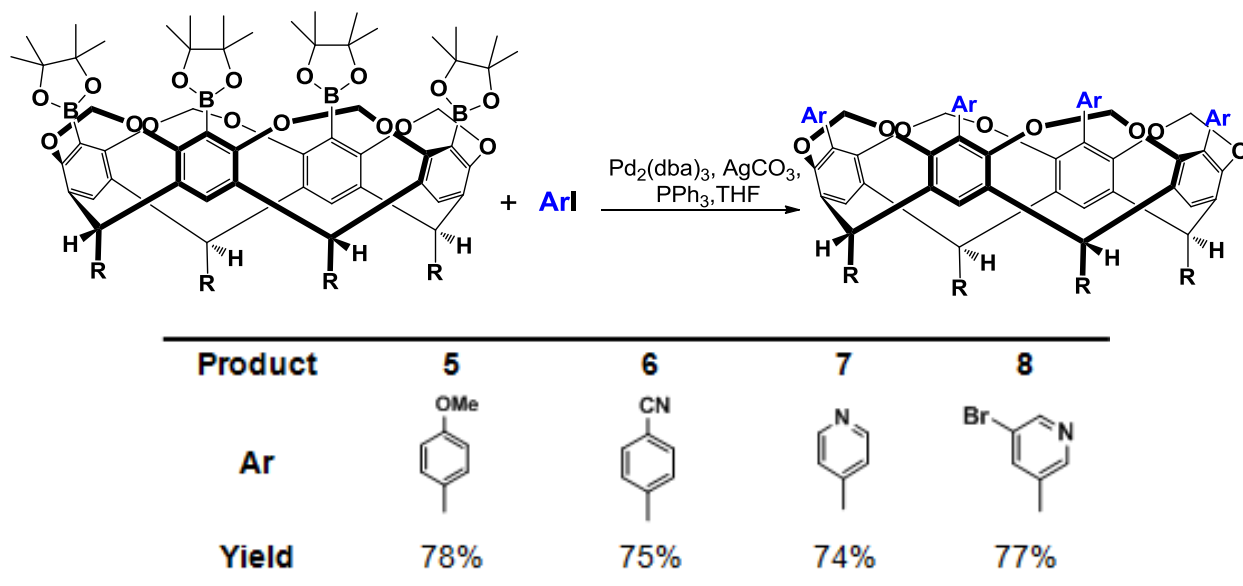


Figure 5.10 Synthetic route for Suzuki-Miyaura cross coupling reaction of cavitand **4**.

We chose 4-iodoanisole as a representative of arenes bearing an electron-donating group. The targeted product, tetra-4-methoxyphenyl cavitand is an important precursor for the construction of heteromeric capsules.³⁴ Consequently, **4** was allowed to react at room temperature with 4-iodoanisole (5 equiv), Pd₂(dba)₃ as a catalyst, Ag₂CO₃ as a base, PPh₃ as a ligand in THF (18 M) to give tetra-4-methoxyphenyl cavitand³⁵ (Figure 5.10, **5**).³⁶

Our next goal was to couple **4** to an iodoarene bearing an electron-withdrawing group. We chose 4-iodobenzonitrile as a haloarene because the target product, the tetra-4-cyanophenyl cavitand **6**, can be employed in the construction of a variety of homo- and hetero- cavitand metal cages.³⁷ Using the coupling protocol outlined for the synthesis of **5**, we were successful in tetracoupling 4-iodobenzonitrile to the precursor **4** (Figure 5.10, **6**).

Cavitands bearing heterocyclic moieties on the ‘upper rim’ are of great interest in the assembly of non-covalent capsules,¹⁰ as multi-dentate ligands for coordination complexes^{18d} as well as in systematic co-crystal studies.³⁸ We therefore treated **4** with 4-iodopyridine, yielding the desired tetrapyrindyl cavitand **7** (Figure 5.10).

Finally, we wanted to determine if this platform could display ‘chemoselective coupling’ to arenes bearing both iodo and bromo halogen atoms. We chose 3-bromo-5-iodopyridine, as a representative substrate because the desired tetrafunctionalized product will have active nitrogen atoms capable of forming coordination cages with metals and can be used to assemble non-

covalent capsules (bulky bromo group at 3-position should aid pyridyl nitrogens to orient upward, facilitating capsule formation). Using our coupling protocol with **4** and 3-bromo-5-iodopyridine, we achieved complete selective cross-coupling with iodine and no reaction was observed with the bromo functional group, yielding, the desired tetra-(3-bromopyridyl)-cavitand **8** (Figure 5.10).

5.3.2 Oxime decorated cavitands via ‘solvent assisted grinding’

Despite numerous advantages of oximes as reliable supramolecular functional group, there have been no reports of oxime functionalized cavitands to date.

Over the last two decades, a major problem in the field of organic synthetic chemistry has been a lack of more environmentally friendly processes using safer reagents, generating fewer side products, and requiring less use of organic solvents.³⁹ In response to such concerns, the use of ‘dry grinding’ or ‘solvent assisted grinding’ for synthesis of new materials has gained considerable attention and importance in recent literature.⁴⁰ Our efforts on appending oxime groups on the ‘upper rim’ of cavitands were focused on the use of ‘solvent assisted grinding’. It is worth mentioning that so far no examples of cavitand functionalization by use of ‘solvent assisted grinding’ have been reported. These cavitands have the potential to provide homomeric and heteromeric nanosized molecular capsules held together by hydrogen bonding and they also have the capability to form extended capsules with linker molecules, for example; 4,4'-bipyridine, pyrazine (Figure 5.11). In addition, oximes can also act as ligands for transition-metal ions⁴¹ and it is therefore possible to envision metal ions as the glue for bringing together extended cavitand-based architectures.

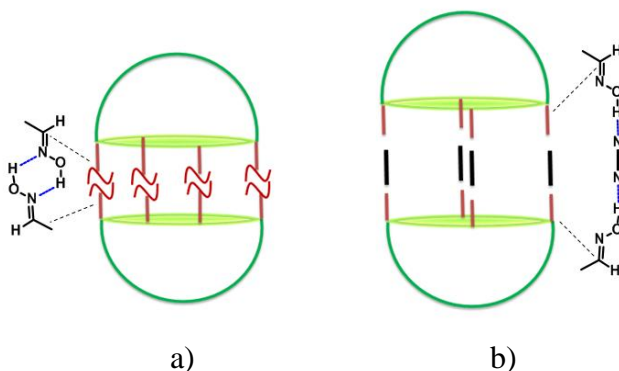


Figure 5.11 Possible homomeric and heteromeric capsule formation using oximes.

The interior of each host can also be altered by controlling the exact location of the supramolecular functional group on the cavitand. Herein, we have employed stepwise and modular approaches for the synthesis of four new tetra-oxime functionalized cavitands.

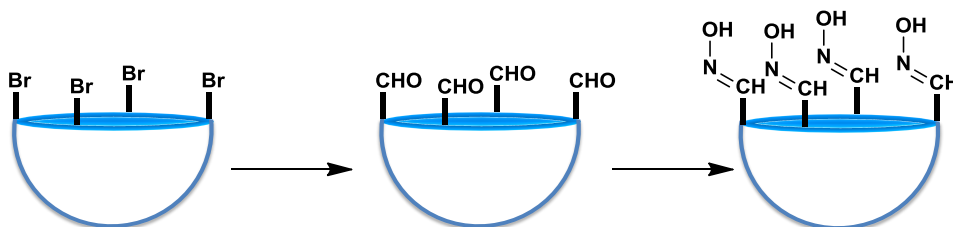


Figure 5.12 Cartoon representation for oxime cavitand synthetic scheme.

We based our strategy for decorating cavitands with oxime groups by appending aldehyde functionalities onto the cavitand backbone followed by transformations to the desired aldoxime. Our starting points for obtaining the desired precursors were tetrabromocavitand **3**⁴² and tetrabromomethylcavitand **17**,²⁹ which were synthesized from their respective resorcinol derivatives in three steps and two steps respectively as per reported literature procedures. To synthesize these aldoxime bearing cavitands we lithiated (*n*BuLi, THF) tetrabromocavitand **3**, Figure 5.13, followed by addition of *n*-formylmorpholine as the electrophile, which yielded tetraaldehyde cavitand **9** (60%).⁴³ When we tried to convert aldehyde **9** to oxime **10** using solution based synthesis it took 72 hrs for all aldehydes to react and substantial byproduct formation was unavoidable. In contrast, treatment of tetraaldehyde cavitand **9** with 6 eq. of hydroxylamine hydrochloride in presence of a strong base, NaOH with a few drops of dichloromethane and methanol and grinding for 5 mins yielded tetraaldoxime cavitand **10** (Figure 5.13) without any byproduct formation. ‘Solvent assisted grinding’ have advantages as,

- 1) it saves reaction time as compared to conventional minimum solution-based synthesis,
- 2) saves solvent for the reaction,
- 3) no substantial byproducts were formed thereby avoiding tedious purification procedures.

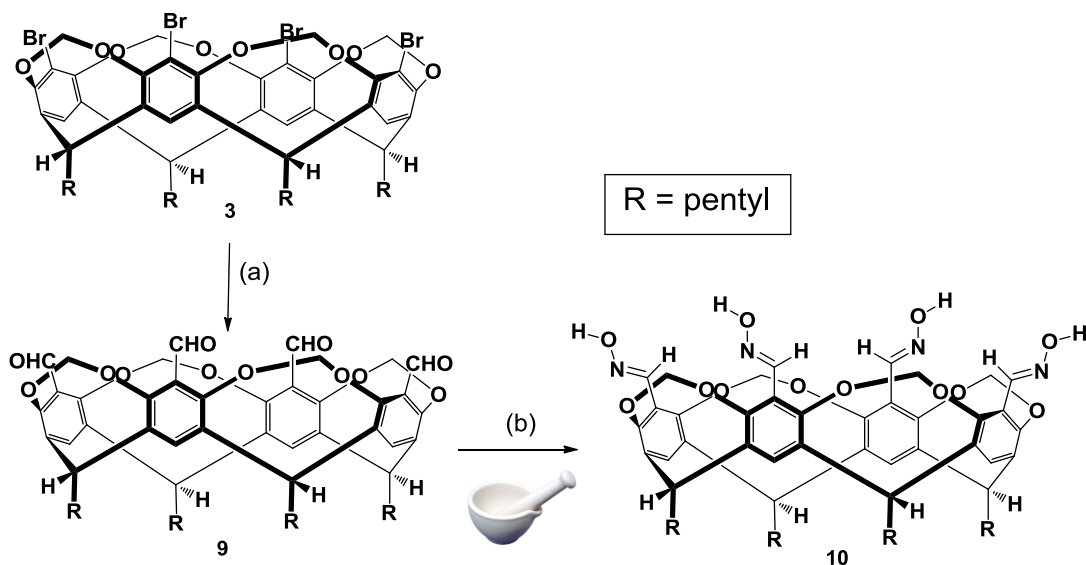


Figure 5.13 Synthetic scheme for tetraaldoxime cavitand **10**. (a) (1) *n*-BuLi, THF, -78 °C; (2) *n*-formylmorpholine, -78 °C to rt; (b) NH₂OH·HCl, NaOH, DCM, Ethanol, rt.

To synthesize the deeper cavitands **12** and **14** with aldoxime group at 4 and 3-position respectively, we made use of Suzuki-Miyaura crosscoupling reactions to access the necessary parent aldehydes.⁴⁴ Coupling tetrabromocavitand **3** with 4-formylphenylboronic acid yielded cavitand **11** in 95% yield after column chromatography. When **3** was coupled with 3-formylphenylboronic acid it gave **13** in 40% yield on purification (mono-protio species was formed as byproduct). The ‘solvent assisted grinding’ protocol on cavitands **11** and **13** yielded aldoxime cavitands **12** and **14** respectively with no side reactions (Figure 5.14).

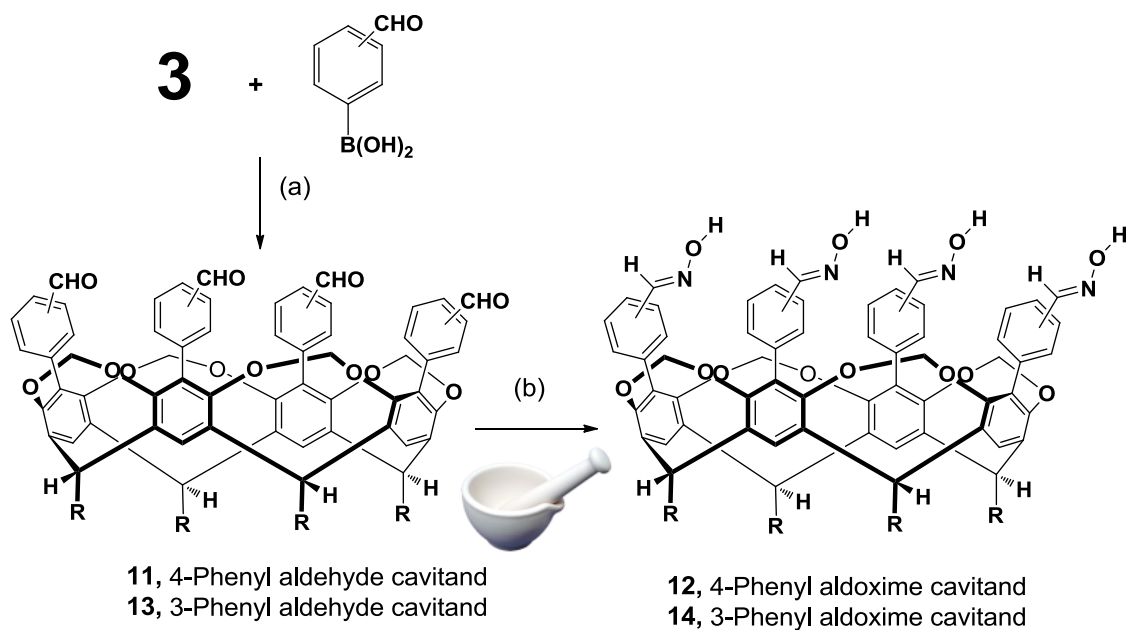


Figure 5.14 Synthetic scheme for tetraphenyl aldoxime cavitand **12** and **14** (R = pentyl). (a) Toluene/Ethanol/ Water, Pd(PPh₃)₄, Na₂CO₃, Reflux, 72hrs; (b) NH₂OH·HCl, NaOH, DCM, Ethanol, rt.

To obtain somewhat deeper cavity with the potential for a more flexible interior space, we combined a tetrabromomethyl cavitand **17** precursor and 4-hydroxy benzaldehyde. Substitution reaction of **17** with 4-hydroxy benzaldehyde with K₂CO₃ as a base yielded tetraaldehyde cavitand³¹ **18** which upon treatment with hydroxylamine hydrochloride in basic condition afforded the flexible tetraaldoxime cavitand **19**.

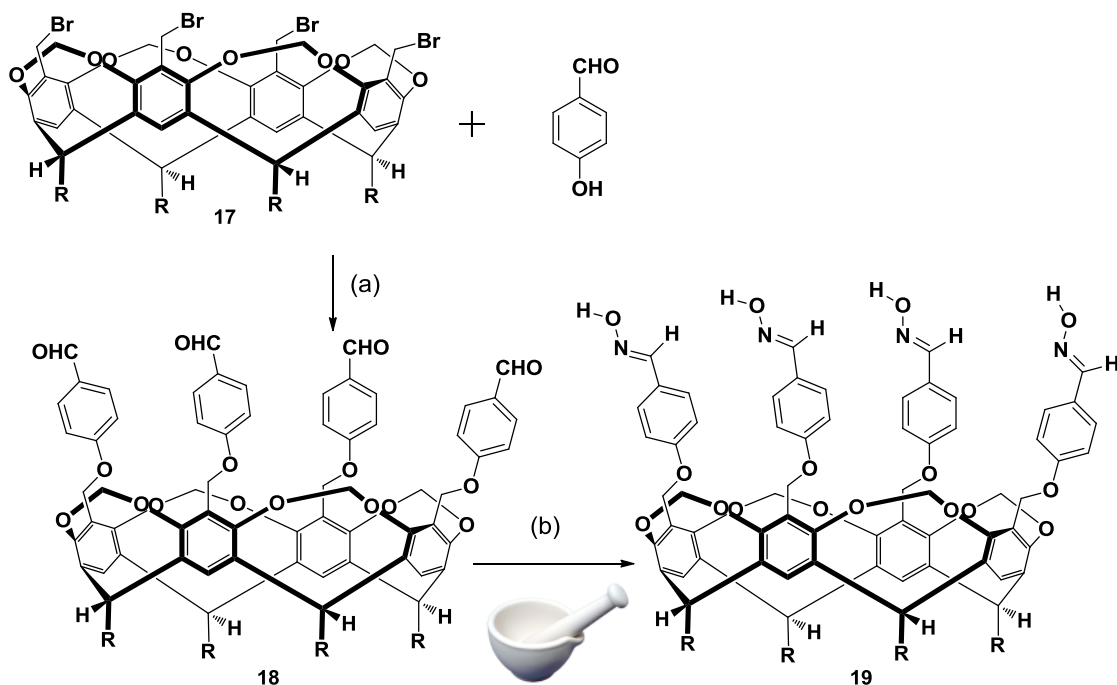


Figure 5.15 Synthesis of deep tetra aldoxime cavitanol **19** (R = pentyl) . (a) K_2CO_3 , Acetonitrile (b) $NH_2OH \cdot HCl$, NaOH, DCM, Ethanol, rt.

5.4 Conclusions

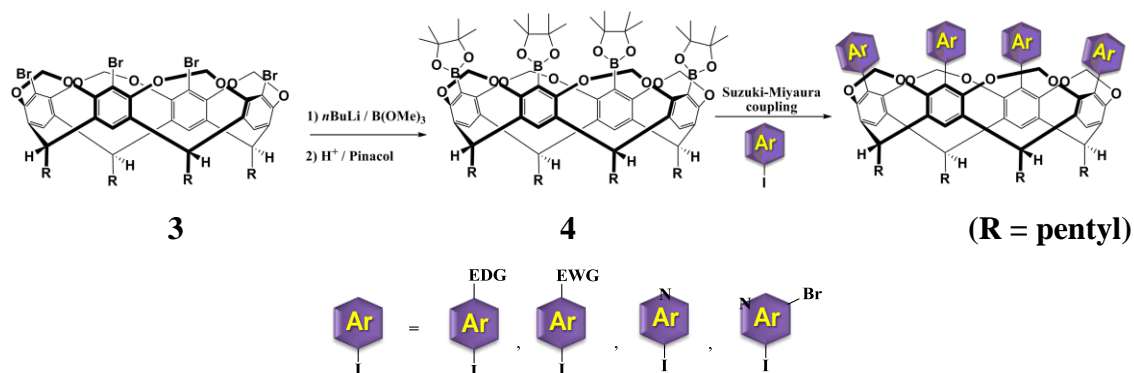


Figure 5.16 Schematic of developed versatile Suzuki-Miyaura coupling protocol.

We have described the design, synthesis, and characterization of a tetraboronic pinacolyl ester cavitanol that can be prepared in good yields, Figure 5.16. High yielding Suzuki-Miyaura coupling reactions of **4** to iodoarenes covering a range of functional groups (electron withdrawing group, electron donating group and a heterocycle) shows the robustness and versatility of this tetraboronic ester cavitanol, making it a ‘launch pad’ for the synthesis of many

new cavitands in a facile manner, Figure 5.16. The presented coupling protocol of **4** has many advantages compared to conventional routes, such as no byproduct formation, no need of tedious chromatographic separation, and highly improved economical efficiency due to the need of fewer equivalents of inexpensive iodoarenes compared to their expensive boronic acid/ester counterparts (which also need to be used in 8-10 fold excess).

It is also notable that so far no examples of cavitand cross coupling with successful chemoselectivity have been reported, but our work opens new avenues for designing and synthesizing macrocycles (Figure 5.16). The depth and electronic nature of the interior of the cavitand can be readily altered through suitable choice of haloarenes, and new molecular capsules can also be envisioned in a straightforward manner.

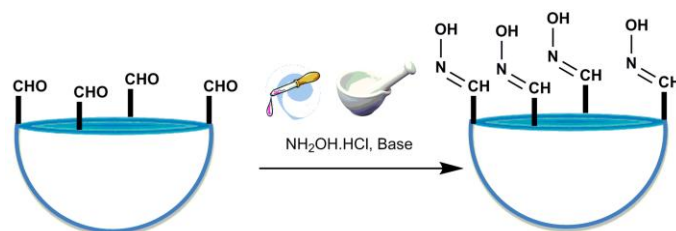


Figure 5.17 Tetraaldehyde to tetraaldoxime cavitand synthesis via ‘solvent assisted grinding’.

We have also successfully demonstrated cavitand functionalization from tetraaldehyde to tetraoximes using ‘solvent assisted grinding’, irrespective of the position of the aldehyde, Figure 5.17.

We have synthesized four new cavitands, each bearing four aldoxime groups, having shallow, deep, and deeper, and more flexible cavity (Figure 5.18).

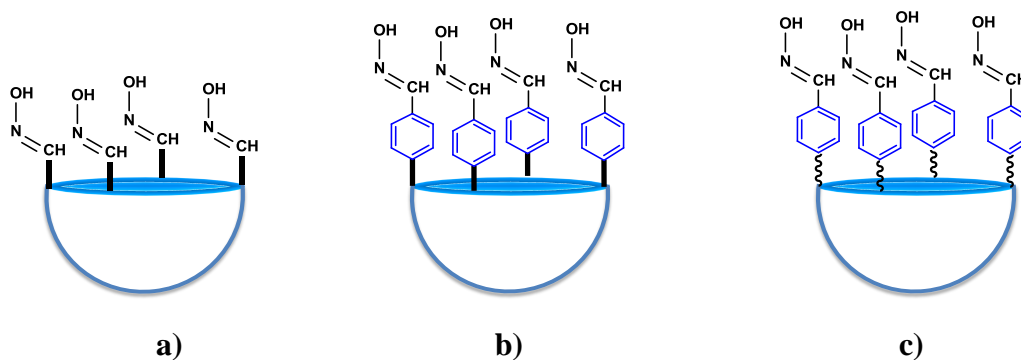


Figure 5.18 Schematic representation of; a) shallow, b) deeper and c) deeper and flexible oxime cavitands.

The presence of aldoxime functionalities with their well-established and reliable supramolecular capabilities on a cavitand scaffold opens up previously unexplored options for constructing homomeric, and heteromeric capsules as well as metal-ion assembled architectures that may have unique structural features and function.

References

- ¹ Cram, D. J.; Karbach S.; Kim, H.; Knobler, C.; Maverick, E.; Ericson, J.; Helgeson, R.; *J. Am. Chem. Soc.* **1988**, *110*, 2229.
- ² Hooley, R.; Rebek, J., Jr. *Org. Biomol. Chem.* **2007**, *5*, 3631.
- ³ (a) Zampolli, S.; Betti, P.; Elmi, I.; Dalcanale, E. *Chem. Commun.* **2007**, 2790. (b) Pirondini, L.; Dalcanale, E. *Chem. Soc. Rev.* **2007**, *36*, 695. (c) Pinalli R., Suman M., Dalcanale E., *Eur. J. Org. Chem.* **2004**, 451.
- ⁴ Iwasawa, T.; Hooley, R.; Rebek J., Jr. *Science* **2007**, *317*, 493.
- ⁵ Nishimura, N.; Kobayashi, K.; *J. Org. Chem.* **2010**, *75*, 6079.
- ⁶ (a) Srinivasan, K.; Gibb, B. *Org. Lett.* **2007**, *9*, 745. (b) Irwin, J. L.; Sherburn, M. S. *J. Org. Chem.* **2000**, *65*, 602. (c) Irwin, J. L.; Sherburn, M. S. *J. Org. Chem.* **2000**, *65*, 5846. (d) Irwin, J.; Sherburn M. *Org. Lett.* **2001**, *3*, 225. (e) Dalcanale, J.; *Angew. Chem. Int. Ed. Engl.* **1997**, *36*, 613.
- ⁷ Rebek J., Jr. *Acc. Chem. Res.* **2009**, *42*, 1660.
- ⁸ Kobayashi, K.; Ishii, K.; Sakamoto, S.; Shirasaka, T.; Yamaguchi, K. *J. Am. Chem. Soc.* **2003**, *125*, 10615.
- ⁹ Kitagawa, H.; Koboria, Y.; Yamanaka, M.; Yozab, K.; Kobayashi, K. *Proc. Natl. Acad. Sci. USA* **2009**, *106*, 10444.
- ¹⁰ (a) Kobayashi, K.; Shirasaka, T.; Yamaguchi, K.; Sakamoto, S.; Hornac, E.; Furukawa, N. *Chem. Commun.* **2000**, 41. (b) Yamanaka, M.; Ishii, K.; Yamada, Y.; Kobayashi, K. *J. Org. Chem.* **2006**, *71*, 8800.
- ¹¹ (a) Tunstad, L. M.; Tucker, J. A.; Dalcanale, E.; Weiser, J.; Bryant, J. A.; Sherman, J. C.; Helgeson, R. C.; Knobler, C. B.; Cram, D. J. *J. Org. Chem.* **1989**, *54*, 1305. (b) Mezo, A. R.; Sherman, J. C. *J. Org. Chem.* **1998**, *63*, 6824.
- ¹² For examples see; (a) Högberg, A. C. S. *J. Am. Chem. Soc.* **1980**, *102*, 6046. (b) Högberg, A. C. S. *J. Org. Chem.* **1980**, *45*, 4498. (c) Moran, J. R.; Karbach, S.; Cram, D. J. *J. Am. Chem. Soc.* **1982**, *104*, 5826. (d) Cram, D. J.; Stewart, K. D.; Goldberg, I.; Trueblood, K. N. *J. Am. Chem. Soc.* **1985**, *107*, 2574. (e) Barrett, E. S.; Irwin, J. L.; Turner, P.; Sherburn, M. S. *J. Org. Chem.* **2001**, *66*, 8227.
- ¹³ Aakeröy; C. B.; Schultheiss, N.; Desper, J. *Org. Lett.*, **2006**, *8*, 2607.
- ¹⁴ (a) Tsuji, J. In *Palladium Reagents and Catalysts, New Perspectives for the 21st Century*; John Wiley and Sons: 2004. (b) Tsuji, J. In *Transition Metal Reagents and Catalysts: Innovations in Organic Synthesis*; John Wiley and Sons: 2002. (c) Li, J. J.; Gribble, G. W. In *Palladium in Heterocyclic Chemistry, A Guide for the Synthetic Chemist*; Pergamon: 2000. (d) Fiaud, J. C., Malleron, J.-L., Legros, J. Y. In *Handbook of Palladium-Catalyzed Organic*

-
- Reactions; Academic Press: 1997. (e) Suzuki, A. In *Metal-Catalyzed Cross-Coupling Reactions*; Diederich, F.; Stang, P. J., Eds.; Wiley-VCH: Weinheim, Germany, 1998; Chapter 2.
- ¹⁵ (a) Corbet, J.-P.; Mignani, G. *Chem Rev.* **2006**, *106*, 2651. (b) Felpin, F.-X.; Ayad, T.; Mitra, S. *Eur. J. Org. Chem.* **2006**, 2679. (c) Lin, L.; Liebscher, J. *Chem. Rev.* **2007**, *1*, 133.
- ¹⁶ Felpin, F.-X.; Ayad, T.; Mitra, S. *Eur. J. Org. Chem.* **2006**, 2679.
- ¹⁷ (a) Garg, N. K.; Sarpong, R.; Stoltz, B. *J. Am. Chem. Soc.* **2002**, *124*, 13179. (b) Yang, C.-G.; Liu, G.; Jiang, B. *J. Org. Chem.* **2002**, *67*, 9392. (c) Yoo, D. J.; Jeon, Y. H.; Kim, D. W.; Han, G. S.; Shim, S. *Bull. Korean Chem. Soc.* **1995**, *16*, 1212. (d) Jones, K.; Keenan, M.; Hibert, F. *Synlett*, **1996**, 509. (e) Boger, D. L.; Miyazaki, S. H.; Kim, S. H.; Wu, J. H.; Castle, S. L.; Loiseleur, O.; Jin, Q. *J. Am. Chem. Soc.* **1999**, *121*, 10004.
- ¹⁸ (a) Chen, C.-Y.; Dagneau, P.; Grabowski, E. J. J.; Oballa, R.; O'Shea, P.; Prasit, P.; Robichaud, J.; Tillyer, R.; Wang, X. *J. Org. Chem.* **2003**, *68*, 2633. (b) Urawa, Y.; Naka, H.; Miyazawa, M.; Souda, S.; Ogura, K. *J. Organomet. Chem.* **2002**, *653*, 269. (c) Smith, G. B.; Dezeny, G. C.; Hughes, D. L.; King, A. O.; Verhoeven, T. R. *J. Org. Chem.* **1994**, *59*, 8151.
- ¹⁹ (a) Bo, Z.; Schafer, A.; Franke, P.; Schluter, A. D. *Org. Lett.* **2000**, *11*, 1645. (b) Hadizad, T.; Zhang, J.; Wang, Z. Y.; Gorjanc, T. C.; Py, C. *Org. Lett.* **2005**, *7*, 795. (c) Jiang, Y.; Wang, J.-Y.; Ma, Y.; Cui, Y.-X.; Zhou, Q.-F.; Pei, J. *Org. Lett.* **2006**, *8*, 4287.
- ²⁰ (a) Aakeröy, C. B.; Schultheiss, N.; Desper, J. *Org. Lett.* **2006**, *8*, 2607. (b) Aakeröy, C. B.; Chopade P. D. *Org. Lett.*, **2011**, *13*, 1 (c) Yamanaka, M.; Ishii, K.; Yamada, Y.; Kobayashi, K. *J. Org. Chem.* **2006**, *71*, 8800. (d) Kobayashi, K.; Yamada, Y.; Yamanaka, M.; Sei, Y.; Yamaguchi, K. *J. Am. Chem. Soc.* **2004**, *126*, 13896. (e) Haino, T.; Kobayashi, M.; Chikaraishi, M.; Fukazawa, Y. *Chem. Commun.* **2005**, 2321. (f) von dem Bussche-Hünnefeld C.; Helgeson R. C.; Bühring D.; Knobler C. B.; Cram D. J. *Croat. Chem. Acta* **1996**, *68*, 447. (g) Ma S.; Rudkevich D. M.; Rebek, Jr. J. *J. Am. Chem. Soc.* **1998**, *120*, 4977. (h) Sinclair D. J.; Sherburn M. S.; *J. Org. Chem.* **2005**, *70*, 3730. (i) Jude H.; Sinclair D. J.; Das N.; Sherburn M. S.; Stang P. J. *J. Org. Chem.* **2006**, *71*, 4155. (j) Hass O.; Schierholt A.; Jordan M.; Lützen A. *Synthesis* **2006**, *3*, 519. (k) Ihm C.; Paek K. *Tetrahedron Lett.* **2007**, *48*, 3263. (l) Sebo L.; Diederich F.; Gramlich V. *Helv. Chim. Acta* **2000**, *83*, 93. For tetraboronic acid cavitated coupling see, (m) Kobayashi, K.; Ishii, K.; Sakamoto, S.; Shirasaka, T.; Yamaguchi, K. *J. Am. Chem. Soc.* **2003**, *125*, 10615.
- ²¹ Aakeröy, C. B.; Chopade, P. D.; Rajbanshi, A.; Schultheiss, N., unpublished results.
- ²² (a) Spencer J.; Baltus C. B.; Patel H.; Press N. J., Callear S. K., Male L.; Coles S. J. *ACS Comb. Sci.* **2011**, *13*, 24. (b) Hall, D. G. *Boronic Acids-Preparation, Applications in Organic Synthesis and Medicine*; Hall, D. G., Ed.; Wiley-VCH: Weinheim, Germany, **2005**, pp 1–99.
- ²³ (a) Bruton, E. A.; Brammer, L.; Pigge, C.; Aakeröy, C. B.; Leinen, D. *New J. Chem.*, **2003**, *27*, 1084. (b) Maurin, J. K. *Acta Cryst.* **1998**, *B54*, 866.
- ²⁴ Aakeröy, C. B.; Salmon, D. J.; Smith, M. M.; Desper, J. *Cryst. Growth Des.* **2006**, *6*, 1033.
- ²⁵ Aakeröy, C. B.; Fasulo, M. E.; Desper, J. *Mol. Pharmaceutics*, **2007**, *4*, 317.
- ²⁶ Aoyama, Y.; Tanaka, Y.; Sugahara, S. *J. Am. Chem. Soc.* **1989**, *111*, 2167.
- ²⁷ Bryant, J. A.; Blanda, M. T.; Vincenti, M.; Cram, D. J. *J. Am. Chem. Soc.* **1991**, *113*, 2167.

-
- ²⁸ Modified procedure from - El Moll, H.; Semeril, D.; Matt, D.; Youinou, M.-T.; Toupet, L. *Org. Biomol. Chem.* **2009**, *7*, 495.
- ²⁹ Quan, M.; Cram, D. *J. Am. Chem. Soc.*, **1991**, *113*, 2754.
- ³⁰ Boerrigter, H.; Verboom, W.; Reinhoudt, D. N. *J. Org. Chem.* **1997**, *62*, 7148.
- ³¹ Kazakova, E.; Prosvirkin, A. V.; Yanilkin, V. V.; Froehlich, R.; Habicher, W. D. *J. Inclusion. Phenom.* **2003**, *47*, 149.
- ³² Jude, H.; Sinclair, D. J.; Das, N.; Sherburn, M. S.; Stang, P. J. *J. Org. Chem.* **2006**, *71*, 4155.
- ³³ Barrett, E. S.; Irwin, J. L.; Turner, P.; Sherburn, M. S. *J. Org. Chem.* **2001**, *66*, 8227.
- ³⁴ (a) Kobayashi, K., Kitagawa, R., Yamada, Y., Yamanaka, M., Suematsu, T., Sei, Y. and Yamaguchi, K. *J. Org. Chem.* **2007**, *72*, 3242. (b) Kitagawa, H., Kobori, Y., Yamanaka, M., Yoza, K., and Kobayashi, K. *Proc. Natl. Acad. Sci. U.S.A.* **2009**, *106*, 10444.
- ³⁵ From crude product ¹H NMR and low-res mass spectroscopy only tetrafunctionalized cavitand as a product was observed.
- ³⁶ Modified from reported coupling reaction which was done on mono-boronic ester cavitand with different iodoarenes, Nguyen T. V., Sinclair D. V., Willis A. C., Sherburn M. S. *Chem. Eur. J.* **2009**, *15*, 5892.
- ³⁷(a) Pirondini L.; Bertolini F.; Cantadori B.; Ugozzoli F.; Massera C.; Dalcanale E. *Proc. Natl. Acad. Sci. USA* **2002**, *99*, 4911. (b) Cuminetti N.; Ebbing M. H. K.; Prados P.; Mendoza J.; Dalcanale E. *Tetrahedron Lett.* **2001**, *42*, 527.
- ³⁸ (a) Aakeröy C. B.; Schultheiss N.; Desper J. *CrystEngComm*, **2007**, *9*, 211. (b) Aakeröy C. B.; Schultheiss N.; Desper J. *CrystEngComm*, **2006**, *8*, 502.
- ³⁹ (a) Anastas, P. T.; Warner, J. C. *Green Chemistry: Theory and Practice*; Oxford University Press: Oxford, UK, 1998. (b) Tundo, P.; Perosa, A.; Zecchini, F. *Methods and Reagents for Green Chemistry*; John Wiley & Sons: Hoboken, NJ, 2007.
- ⁴⁰ Frišić, T. *J. Mater. Chem.*, 2010, **20**, 7599.
- ⁴¹ (a) Peng, W.-J.; Gamble, A. S.; Templeton, J. L.; Brookhart, M. *Inorg. Chem.* **1990**, *29*, 463. (b) Sharutin, V. V.; Sharutina, O. V.; Rokhmanenko, S. I.; Troinina, T. G.; Krivolapov, D. V.; Gubaidullin, A. T.; Litvinov, I. A. *Russ. J. Gen. Chem.* **2000**, *70*, 1990.
- ⁴² (a) Aoyama, Y.; Tanaka, Y.; Sugahara, S. *J. Am. Chem. Soc.* **1989**, *111*, 2167. (b) Bryant, J. A.; Blanda, M. T.; Vincenti, M.; Cram, D. J. *J. Am. Chem. Soc.* **1991**, *113*, 2167.
- ⁴³ Quan, M.; Cram, D. *J. Am. Chem. Soc.*, **1991**, *113*, 2754.
- ⁴⁴ (a) Miyaura, N.; Yanagi, T.; Suzuki, A. *Synth. Commun.* **1981**, *11*, 513. (b) Suzuki, A. *J. Organomet. Chem.* **1999**, *576*, 147 and references therein.

Chapter 6 - From cavitand co-crystals to molecular capsules

6.1 Introduction

6.1.1 Ethylene bridged cavitands

Cram defined the term ‘cavitand’ in 1982 as a molecule with an inner cavity large enough to accommodate guest molecules or ions.¹ Ever since the invention of cavitands, they have been extensively used in designing molecular capsules having specific function. Molecular capsules based on dynamic covalent bonds,² metal-coordination bonds,³ ionic interactions,⁴ hydrogen bonds,⁵ and solvophobic interactions⁶ have been employed in catalysis,⁷ molecular sensing,⁸ stabilization of reactive intermediates,⁹ and recently as a masking agent against undesired photochemical reactions.¹⁰ Most of the above mentioned reports are based on self-assembled capsules encapsulating guest molecules within methylene/phenyl bridged C_{4v} symmetric cavitands. However, to encapsulate asymmetric guest molecules there is need for asymmetric molecular capsules. To design asymmetric capsules, asymmetric cavitands are needed. Reduction of the symmetry in cavitand scaffolds has been achieved by introduction of multifunctional groups on the ‘upper rim’ of the cavitand.¹¹ Nevertheless, this approach is synthetically challenging and requires multi-step approach to introduce different functional groups; moreover, the shape of the cavity remains unaltered thereby lacking shape selectivity of guests.

We based our approach to design a C_{2v} symmetric cavitand on the introduction of ethylene bridges in the cavitand scaffold, Figure 6.1.¹² This approach will directly alter the shape and size of the cavitand framework in the early stages of synthesis thereby avoiding the synthetic challenges for imparting asymmetry in the later stages of cavitand ‘upper rim’ functionalization, Figure 6.2.

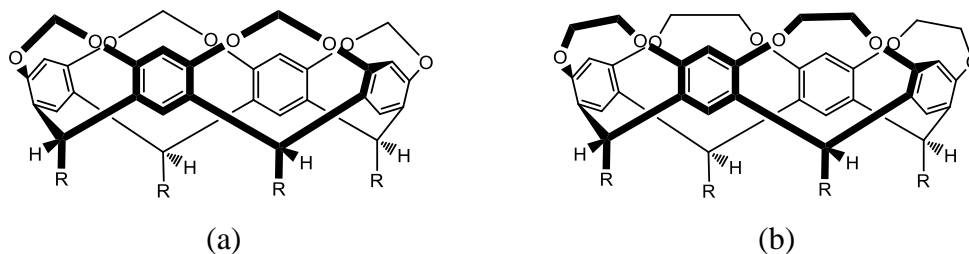
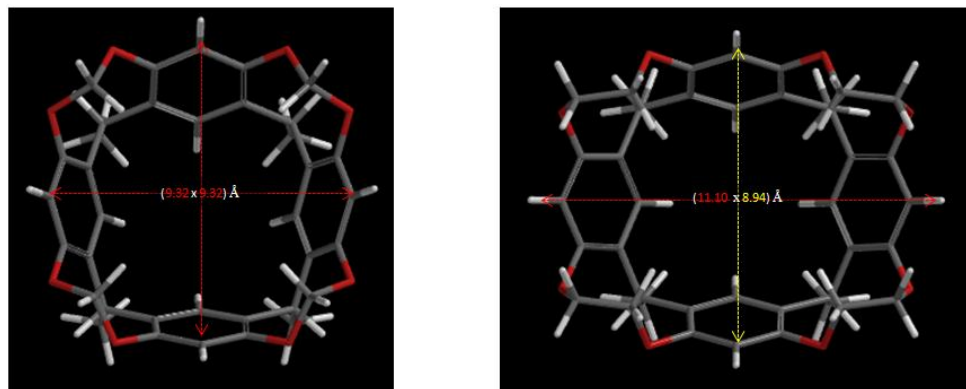


Figure 6.1 Schematic showing (a) methylene bridged cavitand and (b) ethylene bridged cavitand.



(a)

(b)

Figure 6.2 Energy minimized structures of (a) methylene bridged cavitand and (b) ethylene bridged cavitand showing top view with interior cavity dimensions.¹³

6.1.2 Isothermal titration calorimetry

Designing large supramolecular structures from multicomponent systems with predictable connectivity and stoichiometry is a challenging goal in supramolecular chemistry. The best characterization method to study intermolecular interactions in the solid state is X-ray crystal structure determination; however, growing single crystals of X-ray diffraction quality is a challenging task. Also, the strengths of intermolecular interactions cannot be directly quantified from the crystal structure.

However, isothermal titration calorimetry (ITC) is a thermodynamic technique commonly used for measuring biomolecular interactions.¹⁴ ITC can also be used to study the intermolecular interactions between two molecular entities in solution. The amount of heat lost/gained during the process is a measure of strength of interaction between these species. A single experiment ITC can determine:

1. enthalpy change (ΔH),
2. entropy change (ΔS),
3. Gibbs free energy changes (ΔG) of the system,
4. binding constants (K_a) and

5. binding stoichiometry (N).

In this chapter, we will utilize ITC experiments as a way to determine the solution stoichiometry of the supramolecular complex and how this solution stoichiometry correlates in the solid-state. Also, the thermodynamic parameters (ΔH , ΔS , K_a and ΔG) will provide more insights towards strength of intermolecular interaction.

6.1.3 Pyridyl and carboxylic acid functionalized cavitands

Based upon extensive results from continued efforts in design and synthesis of co-crystals, it is apparent that pyridine, a widely used hydrogen-bond acceptor, can form intermolecular interactions to drive the formation of binary co-crystals, Figure 6.3.¹⁵ The reliable and robust heterosynthons involving carboxylic acids (-COOH) or alcohols (-OH) with pyridine are extensively studied in literature.^{16,17} Therefore, we based our efforts on preparing capsules using pyridyl functionalized cavitand as a tetradentate hydrogen-bond acceptors and carboxylic acid and phenols as hydrogen-bond donors.

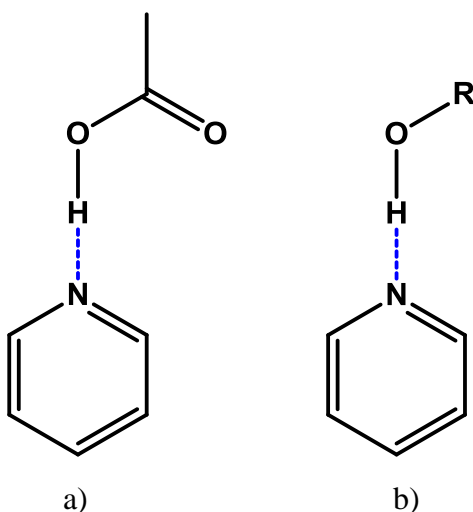


Figure 6.3 Schematic of commonly occurring a) pyridine-carboxylic acid and b) pyridine-hydroxy synthons.

Also, we will functionalize the cavitand ‘upper rim’ with carboxylic acid functionalities which can be used in molecular capsule formation using N-heterocyclic linker molecules such as; bipyridine or 2-aminopyrimidine derivatives (Figure 6.4).

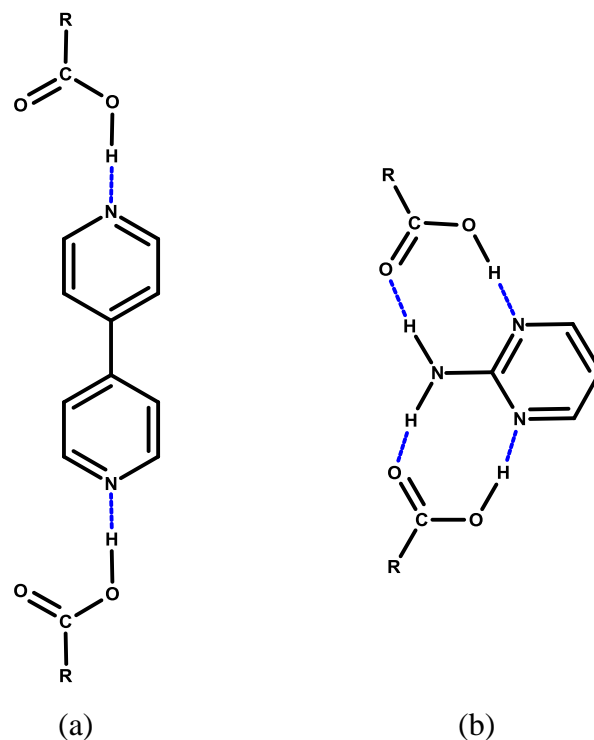


Figure 6.4 Schematic showing carboxylic acid hydrogen-bond with, (a) 4,4'-bipyridine and (b) 2-aminopyrimidine.

6.1.4 Goals

Overall goals of this chapter are as follows –

To incorporate ethylene bridge in cavitand scaffold to expand cavity size and to impart asymmetry, Figure 6.5.

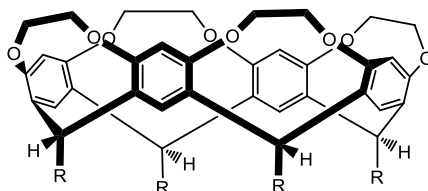


Figure 6.5 Ethylene bridged cavitand.

To synthesize pyridyl functionalized cavitand and study supramolecular complex formation with carboxylic acids in solution (using ITC) and solid-state, Figure 6.6.

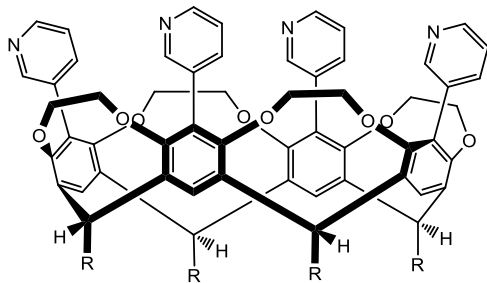


Figure 6.6 Target tetrapyrrolyl cavitand.

To synthesize a tetracarboxylic acid cavitand (Figure 6.7) and construct molecular capsules using linker molecules.

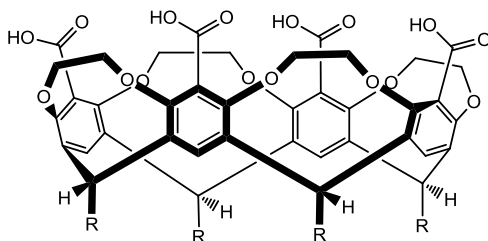


Figure 6.7 Target tetracarboxylic acid cavitand.

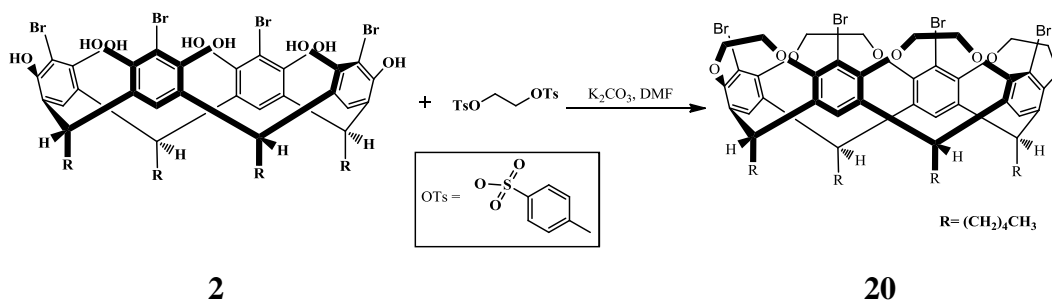
6.2 Experimental

6.2.1 Synthesis

^1H NMR spectra were recorded on a Varian Unity plus 400 MHz spectrometer in CDCl_3 or d -DMSO. Data is expressed in parts per million (ppm) downfield shift from tetramethylsilane or residual protiosolvent as internal reference and are reported as position (in ppm), multiplicity (s = singlet, d = doublet, t = triplet, m = multiplet), coupling constant (J in Hz) and integration (number of protons). ^{13}C NMR spectra were recorded on a Varian Unity plus 400 MHz spectrometer in CDCl_3 or d -DMSO with complete proton decoupling. Data is expressed in parts per million (ppm) shift relative to CDCl_3 (77.00 ppm) or d -DMSO (39.51 ppm) and are reported as position (δ). Melting points were recorded on a Fisher-Johns melting point apparatus and are uncorrected. Electrospray Ionization spectra were acquired on a LCT Premier (Waters Corp., Milford MA) time of flight mass spectrometer. The instrument was operated at 10,000 resolution (W mode) with a dynamic range enhancement that attenuates large intensity signals. The cone voltage was 60eV. Spectra were acquired at 16666 Hz pusher frequency covering the

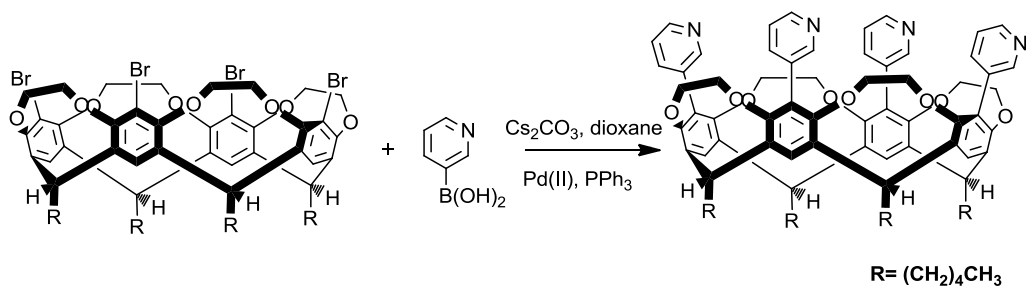
mass range 100 to 1200 u and accumulating data for 2 seconds per cycle. Mass correction for exact mass determinations was made automatically with the lock mass feature in the MassLynx data system. A reference compound in an auxiliary sprayer is sampled every third cycle by toggling a “shutter” between the analysis and reference needles. The reference mass is used for a linear mass correction of the analytical cycles. Samples are presented in acetonitrile as a 100ul loop injection using an auto injector (LC PAL, CTC Analytics AG, Zwingen, Switzerland). Infrared spectroscopy (IR) was done on a Nicolet 380 FT-IR. All the other chemicals were purchased from Aldrich and Fisher and used without further purification, unless otherwise noted.

6.2.1.1 Synthesis of *C*-pentyltetrabromocavitand, **20**¹⁸



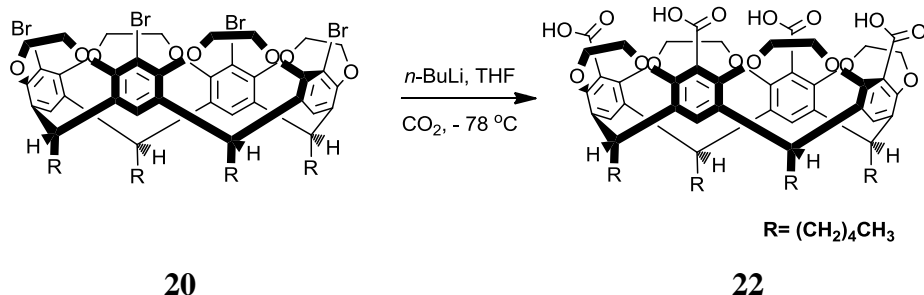
To a stirred solution of 18 g (16.6 mmol) of **2** and 50 g (135 mmol) of TsOCH₂CH₂OTs in 60 mL of DMSO was added 45 g (0.33 mol) of K₂CO₃. The mixture was stirred for 24 h at 25 °C and 4 days at 60 °C. The suspension was poured into 3 L of H₂O, filtered, and dried, and the residue was chromatographed on silica gel with hexane:ethyl acetate (85:15) as the mobile phase to give 7.23 g (46%) of **20**: mp >300 °C; ¹H NMR (δ_H; 400 MHz, CDCl₃): 7.25 (s, 4H), 5.27, J = 8 Hz, 4H), 0.87 (t, J = 7.0 Hz, 12H, CH₃), 1.21–1.35 (m, 24H, (CH₂)₃), 2.05 (m, 8H, CHCH₂), 3.60–3.80 (m, 8H, inner OCH₂CH₂O), 4.26–4.48 (m, 8H, outer OCH₂CH₂O), 5.28 (t, J = 8.1 Hz, 4H, CH methine), 7.31 (s, 4H, ArH); M.p. >280 °C; ¹H NMR (δ_H; 400 MHz, CDCl₃): 7.04 (s, 4H), 5.97 (d, J = 7.2Hz, 4H), 4.85 (t, J = 8.2Hz, 4H), 4.26–4.48 (m, 8H), 3.60–3.80 (m, 8H), 2.01–2.10 (m, 8H), 1.21–1.36 (m, 24H), 0.87 (t, J = 8Hz, 12H); ¹³C NMR (δ_C; 400 MHz, CDCl₃): 151.45, 136.97, 122.99, 113.20, 70.47, 34.99, 34.50, 31.80, 27.37, 22.55, 14.04. IR (neat) : 2926, 1455, 1445, 1301, 1090, 1060, 1040, 792, 681, 623.

6.2.1.2 Synthesis of *C*-pentyltetra(3-pyridyl)cavitand, **21**¹⁹



To a 250 mL round-bottom flask, water (4 mL), pyridyl-3-boronic acid (1.76 g, 14 mmol), and PPh_3 (0.83 g, 32 mmol) in dioxane (75 mL) were added to a mixture of **20** (1.90 g, 16 mmol), $[\text{PdCl}_2(\text{PPh}_3)_2]$ (278 mg, 50 mol %), and Cs_2CO_3 (7.81 g, 23 mmol) in dioxane (90 mL). After stirring for 5 h at 110 °C in the dark, the reaction mixture was filtered on a celite pad and washed three times with chloroform, and the solvent was evaporated to afford the crude product. The crude product was purified by column chromatography (500 g silica, hexane → hexane: ethyl acetate → 8:2 ethyl acetate : ethanol : 3% triethyl amine) to give **21** (0.65 g, 35%). M. p. > 280 °C. ^1H NMR (δ_{H} ; 400 MHz, CDCl_3): 8.57 (d, $J = 4.0$ Hz, 4H), 8.37 (s, 4H), 7.63 (s, 4H), 7.56 (d, $J = 4$ Hz, 4H), 7.34 (d, $J = 4$ Hz, 4H), 5.27 (t, $J = 8$ Hz, 4H), 3.82-3.89 (m, 8H), 3.37-3.44 (m, 8H), 2.27-2.19 (m, 12H), 1.43- 1.29 (m, 24H), 0.91 (t, $J = 8$ Hz, 12H); ^{13}C NMR (δ_{C} ; 400 MHz, CDCl_3): 151.86, 149.72, 148.76, 137.45, 136.21, 131.05, 127.60, 124.72, 123.09, 72.17, 34.66, 33.91, 31.84, 27.55, 22.63, 14.08. IR: 2924, 1567, 1480, 1269, 1089, 1061, 1042, 872, 809.

6.2.1.3 Synthesis of C-pentyltetracarboxylic acid cavitand, **22**²⁰



C-pentyltetrabromocavitand **3** (0.9 g, 0.75 mmol) was dissolved in dry tetrahydrofuran (10 mL), and then the solution was evaporated and dried at 100 °C (0.1 mmHg) for 2 h under an argon atmosphere. This procedure was repeated twice. The resulting cavitand was dissolved in dry tetrahydrofuran (100 mL) and cooled to -78 °C (dry ice/acetone bath), under a dinitrogen

atmosphere. To this solution, n-butyllithium (1.6 M in hexanes, 5.24 mL, 7.5 mmol) was added dropwise over 10 minutes and stirred for an additional 0.5h. Carbon dioxide generated from dry ice (Note – To generate carbon dioxide gas, take dry ice in one neck round-bottom flask sealed using rubber septum and transfer carbon dioxide to the reaction flask via canula.) and was purged in the reaction mixture for 20 minutes at $-78\text{ }^{\circ}\text{C}$. Attach a CO_2 balloon, which was exchanged to a fresh CO_2 balloon two or three times until absorption of CO_2 gas into the reaction solution ceased at $-78\text{ }^{\circ}\text{C}$. The reaction mixture was warmed to room temperature under CO_2 atmosphere overnight. A NaOH (1 M) aqueous solution (100 mL) was added to the reaction mixture at room temperature. After evaporation of THF, the aqueous layer was washed with Et_2O (200 mL \times 3) and then acidified with concentrated HCl at $0\text{ }^{\circ}\text{C}$. The resulting precipitate in aqueous layer was extracted with Et_2O (300 mL \times 2). The organic layer was washed with water (100 mL) and brine (100 mL) and dried over anhydrous MgSO_4 . After evaporation of solvent, the residue was taken up in hexane (200 mL) and then filtered off. Product can be recrystallized from ethanol:dichloromethane (1:1). M. p. $> 300\text{ }^{\circ}\text{C}$; ^1H NMR (δ_{H} ; 400 MHz, d_6 -DMSO): 7.91 (s, 4H), 5.07 (t, $J = 8\text{ Hz}$, 4H), 4.25-4.20 (m, 8H), 3.65-3.58 (m, 8H), 2.26-2.20 (m, 12H), 1.35- 1.26 (m, 24H), 0.83 (t, $J = 4\text{ Hz}$, 12H); ^{13}C NMR (δ_{C} ; 400 MHz, d_6 -DMSO) : 210.33, 167.07, 149.68, 135.81, 125.77, 72.81, 56.08, 33.13, 31.30, 27.35, 22.25, 13.93. IR : 3530, 2925, 1690, 1578, 1442, 1273, 1239, 1087, 1054, 1027, 859, 625.

6.2.2 Isothermal Titration Calorimetry (ITC) studies

6.2.2.1 ITC experiments

Dry chloroform, from Fisher scientific, was used as a solvent for the ITC experiments to minimize any inconsistency resulting from presence of water. Dry and analytically pure samples of tetra(3-pyridyl)cavitand **21** and 4-nitrobenzoic acid were used for titrations. All ITC measurements were performed on Nano ITC instrument.²¹

In a typical experiment, the sample cell of the calorimeter was rinsed five times with methanol, followed by five times with chloroform. A similar procedure was repeated on the reference cell. Finally, reference cell was filled with chloroform and the sample cell was filled with 0.188 mM 4-nitrobenzoic acid. A 12 mM solution of tetra(3-pyridyl)cavitand **21** in chloroform was taken in a 250 μL syringe and equilibrated at $25\text{ }^{\circ}\text{C}$ for 1 hour. After thermal equilibrium was attained, 8 μL aliquots of 4-nitrobenzoic acid (0.188mM) were injected into the

sample cell; 30 such injections were made with a time delay of 400 s between each addition. The enthalpy change after each addition was measured. The titration was repeated twice.

Data analysis and data fit procedures were performed using the software *NanoAnalyze*. The signals from the experiment are plotted in $\mu\text{cal}/\text{sec}$ as a function of time, interpreting the power needed to maintain the reference and sample cell at the same temperature. The number of pulses corresponds to the heat released/absorbed with injection of the ligand. These can be integrated to obtain the total heat change per injection.

6.2.2.2 ITC data for titration of tetra(3-pyridyl)cavitand 21 into 4-nitrobenzoic acid

The ITC study consists of titration, injection of tetra(3-pyridyl)cavitand **21** into the chloroform solution of the 4-nitrobenzoic acid in the sample cell. The reading from the first injection is typically rejected because the sample solution in the needle is in contact with the chloroform in the cell and unavoidable diffusion prior to the start of the titration could lead to partial dilution of the sample. The second injection of the ligand results in the binding of most of the injected ligand, and hence maximum heat is generated in the process as seen by the exothermic nature of the curve. With the subsequent injections of **21**, the fewer and fewer of the acid molecules are available for binding with the injected ligand and hence amount of heat liberated is reduced. In due course, with repeated injection of **21**, no more acid molecules are available for binding and no further heat release is observed.

The heat resulting from each individual injection is then integrated with respect to time and plotted against molar ratio of the two components. These values are fitted using the independent model from the software *NanoAnalyze* to get output in terms of enthalpy change (ΔH), entropy (ΔS), association constant (K_a), and stoichiometry (N). The free energy change (ΔG) can be calculated, from the equation; $\Delta G = \Delta H - T\Delta S$.

6.2.3 Crystallizations

6.2.3.1 C-pentyltetrabromocavitand, 20; C-pentyltetra(3-pyridyl)cavitand, 21

Crystals suitable for single-crystal X-ray diffraction, of **20** were grown by slow evaporation of an acetonitrile solution at room temperature over three days. Crystals suitable for

single-crystal X-ray crystallography, of **21** were grown by placing a vial containing an ethanolic solution of **21** in container filled with hexane at room temperature over four days.

6.2.3.2 C-pentyltetra(3-pyridyl)cavitand : 4-nitrobenzoic acid (1:4); 21a

C-pentyltetra(3-pyridyl)cavitand **21** (10 mg, 0.009 mmol) and 4-nitrobenzoic acid (6.0 mg, 0.04 mmol) were placed in a vial containing nitrobenzene (2 mL) and heated until a clear homogeneous solution was obtained. After several days, prism-shaped colorless crystals were obtained. Dec. 230 °C; IR (neat) ν 2436 and 1940 cm^{-1} (O-H \cdots N, br), 1708 cm^{-1} (C=O).

6.2.3.3 C-pentyltetra(3-pyridyl)cavitand : 3,5-dinitrobenzoic acid (1:2); 21b

C-pentyltetra(3-pyridyl)cavitand **21** (10 mg, 0.009 mmol) and 3,5-dinitrobenzoic acid (7.6 mg, 0.04 mmol) were placed in a vial containing nitromethane (2 mL) and heated until a clear homogeneous solution was obtained. After three days, yellow needle-shaped crystals were obtained. Dec. 240 °C; IR (neat) ν 2403 and 1932 cm^{-1} (O-H \cdots N, br), 1730 cm^{-1} (C=O).

6.2.3.4 C-pentyltetra(3-pyridyl)cavitand : resorcinol (1:1); 21c

C-pentyltetra(3-pyridyl)cavitand **21** (10 mg, 0.009 mmol) and resorcinol (1.8 mg, 0.02 mmol) were placed in a vial containing acetonitrile: ethyl acetate (2:1 mL) and heated until a clear homogeneous solution was obtained. After four days, transparent plate-shaped crystals were obtained. M.p. > 250 °C; IR (neat) – 3256 cm^{-1} (OH, br), 2921 cm^{-1} , 1455 cm^{-1} . (Note – no OH \cdots N broad stretches near 2500 and 1900 cm^{-1} were observed in the IR; however; stretches corresponding to both the components were present with slight shifts for some stretches.)

6.2.3.5 C-pentyltetracarboxylic acid cavitand : 4,4'-bipyridine (1:2); 22a

C-pentyltetracarboxylic acid cavitand **22** (10 mg, 0.009 mmol) and 4,4'-bipyridine (3.0 mg, 0.02 mmol) were placed in a vial containing acetonitrile : methanol (1:1 mL) and heated until a clear homogeneous solution was obtained. After four days, transparent plate-shaped crystals were obtained. Dec. 250 °C; IR (neat) – ν 2471 and 1928 cm^{-1} (O-H \cdots N, br), 1713 cm^{-1} (C=O).

6.2.3.6 C-pentyltetracarboxylic acid cavitand : 2-amino-5-bromo-4-chloro-6-methylpyrimidine (1:3); 22b

C-pentyltetracarboxylic acid cavitand **22** (10 mg, 0.009 mmol) and 5-bromo-4-chloro-6-methylpyrimidin-2-amine (8.0 mg, 0.04 mmol) were placed in a vial containing acetonitrile (3 mL) and heated until a clear homogeneous solution was obtained. After four days, transparent block-shaped crystals were obtained. Dec. 220 °C; IR (neat) – ν 2533 and 1932 cm^{-1} (O-H \cdots N, br), 1722 cm^{-1} (C=O).

6.3 Results and discussion

6.3.1 Multi-component supramolecular assembly in solution

In solutions the characterization of supramolecular assemblies and patterns are not well established due to the dynamic equilibrium between different species existing in the solution. However, using the right concentration range we can analyze the thermodynamic data using ITC.

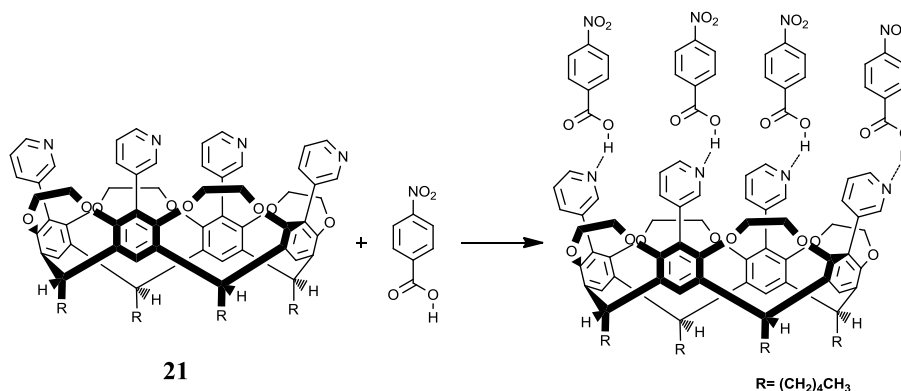


Figure 6.8 Proposed multi-component supramolecular assembly in solution.

We focused our work on ITC as a way of analyzing thermodynamic outputs when two or more molecules interact via non-covalent interactions. We titrated concentrated C-pentyltetra(3-pyridyl)cavitand **21** into a dilute solution of 4-nitrobenzoic acid, expecting a pentameric assembly, Figure 6.8. The initial injection of the **21** resulted in the binding of most of the **21** molecules, and hence maximum heat is generated in the process as seen by the exothermic nature of the curve. Upon subsequent addition of **21**, fewer and fewer acid molecules exist for binding with the injected ligand and thereby the amount of heat liberated is reduced substantially. Ultimately, with repetitive injection of the ligand no more acid molecules are available for

binding and no further heat release is observed. Moreover, an endothermic event was observed after 8-9 injections in both the replicate experiments, Figure 6.9 and Figure 6.11. The heat resulting from each individual injection is then integrated with respect to time and plotted against the molar ratio of the two components. These values are fitted using the independent model from the software *NanoAnalyze* to get output in terms of enthalpy change (ΔH), association constant (K_a), and stoichiometry (N). Since predicted N was 0.25, during plotting of the data, we fixed N in the range of (0.2 to 0.3). ΔH and K_a were not fixed to any range. The output of the thermodynamic parameters is given in Figure 6.9b.

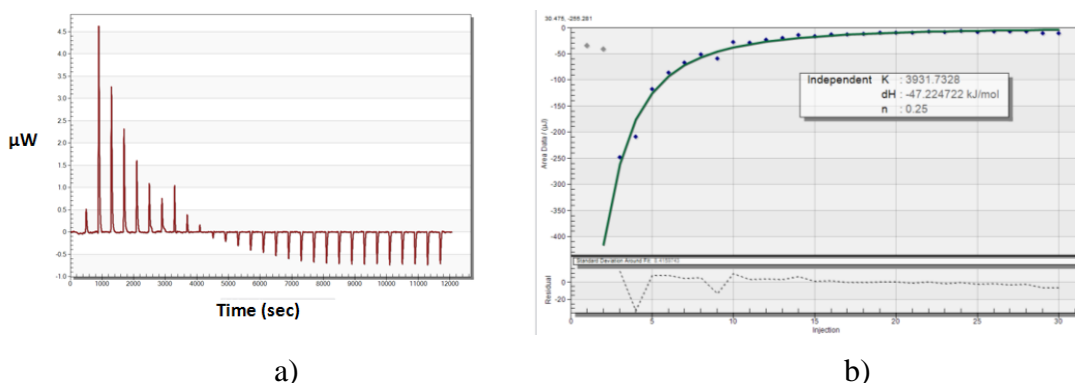


Figure 6.9 (a) ITC titration curve of C-pentyltetra(3-pyridyl)cavitand vs. 4-nitrobenzoic acid; (b) thermodynamic fit parameters.

A statistical analysis was performed on the thermodynamic parameter using *NanoAnalyze* to obtain the error values, Figure 6.11b.

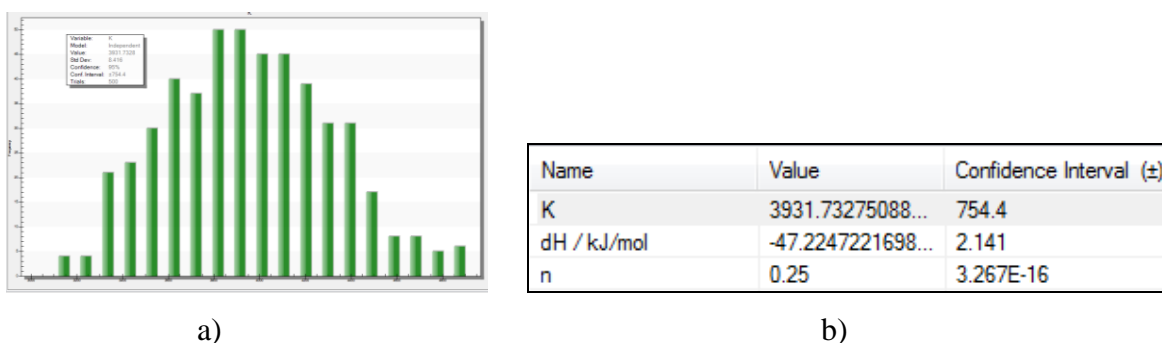


Figure 6.10 (a) Statistical data analysis of ITC experiment; (b) Output from *NanoAnalyze* software using an independent model.

The first experiment is repeated using identical conditions to test the consistency of the data. The data comparison for both the experiment unambiguously shows that similar thermodynamic parameters are obtained, Figure 6.11 and Figure 6.12.

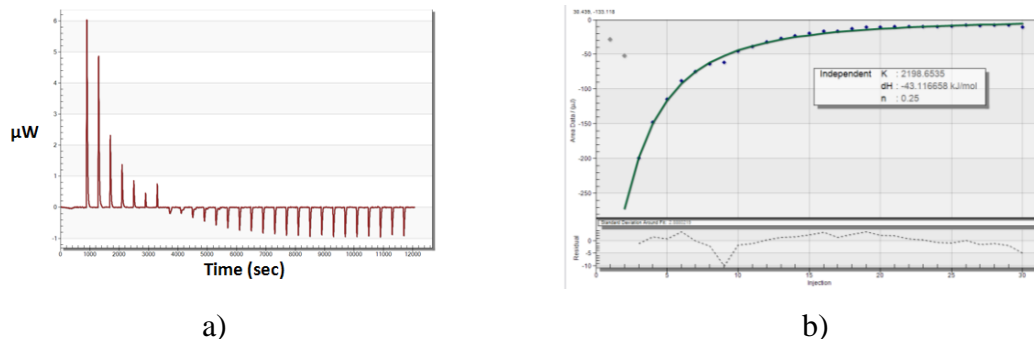


Figure 6.11 (a) Second ITC titration curve of C-pentyltetra(3-pyridyl)cavitand vs. 4-nitrobenzoic acid; (b) thermodynamic fit parameters.

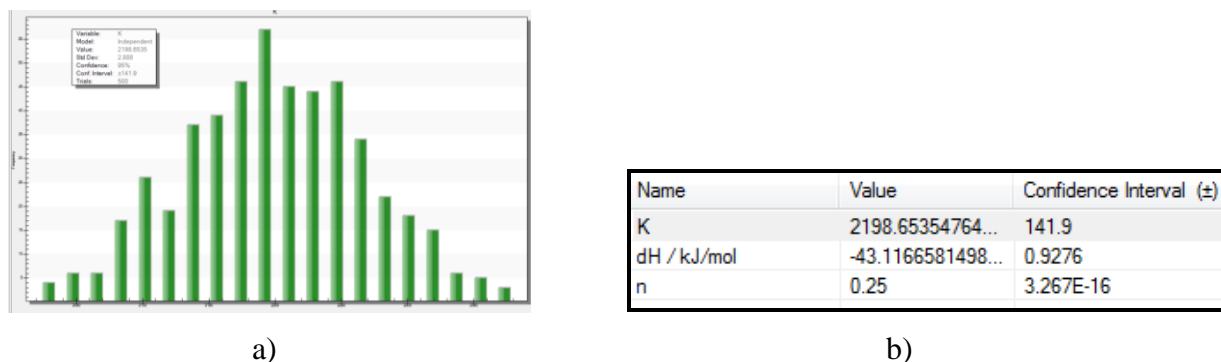


Figure 6.12 (a) Statistical data analysis of ITC experiment; (b) Output from *NanoAnalyze* software using independent model.

The equation, $\Delta G = -RT \ln K_a$ can be used to obtain the free energy change (ΔG). From the equation; $\Delta G = \Delta H - T\Delta S$; we can obtain ΔS .

Table 6.1 Comparison of thermodynamic parameters for the complexation of **21** with 4-nitrobenzoic acid.

	Experiment 1*	Experiment 2*
ΔH (kJ/mol)	-47.22 ± 2.14	-43.11 ± 0.92
ΔS (kJ/mol)	-0.066	-0.080

ΔG (kJ/mol)	-27.39	-19.06
K_a	3931 \pm 754	2198 \pm 141
N	0.25 \pm 3.26E-16	0.25 \pm 3.26E-16

* For note on errors see endnote.²²

Thermodynamic parameters for complexation of **21** with 4-nitrobenzoic acid are shown in Table 6.1. The experimental stoichiometry of **21** with 4-nitrobenzoic acid should be close to 0.25, due to four binding sites of C-pentyltetra(3-pyridyl)cavitand available to bind four 4-nitrobenzoic acids. As predicted, we obtained very close value of N = 0.25 based on the ITC titrations. The association constant (K_a) is around 3079, which is the important factor as other thermodynamic events such as, entropy and free energy are dependent on it.

There is not a single report which uses ITC as a way of determining thermodynamic parameters of hydrogen bonded multi-component system. However, there are reports which use IR spectroscopy to measure the enthalpy of pyridine and benzoic acid complexation.²³ Literature value for enthalpy of one hydrogen bond formation between pyridine and benzoic acid is -44.52 kJ/mol. For our experiment the expected enthalpy for formation of four hydrogen bonds ($\text{COOH}\cdots\text{N}_{\text{pyr}}$) should be ca. -180 kJ/mol; however, our experimental value of enthalpy is around -45 kJ/mol (average of the two experiments). This observed lower enthalpy value might be result of solution measurement of thermodynamic parameters (ITC) as compared to the literature measurement of complexes at 100% concentration (neat sample) using IR. In order to form a pentameric assembly in solution between **21** and 4-nitrobenzoic acid, the chloroform molecules surrounding the individual entities or dimers of 4-nitrobenzoic acids need to be removed and the dimer has to be broken down into monomers. Also, five molecular species (one cavitand and four carboxylic acids) should come together to form pentamer. This process makes the system more organized thereby reducing the entropy to some extent. Therefore, we observed entropy for pentameric supramolecular assembly as -0.073 kJ/mol. The free energy change for the supramolecular reaction is *c.a.* -20 kJ/mol.

In summary, we were able to successfully demonstrate pentameric supramolecular assembly formation of tetrapyridyl cavitand with 4-nitrobenzoic acid in chloroform. Although, there are many reports on host-guest studies of cavitand in solution using ITC and NMR

spectroscopy, no report involves hydrogen bonding.²⁴ Our work may be the very first report in investigating the solution stoichiometry of cavitand supramolecular assembly and obtaining thermodynamic data in organic solvents. More work in this area will help in designing variety of supramolecular capsules with different thermodynamic stability.

6.3.2 Solid-state structures of cavitands

6.3.2.1 Cavitand co-crystals

The crystal structure determination of the C-pentyltetrabromocavitand **20** shows a C_{2v} symmetric cavitand structure with ellipsoidal shape, Figure 6.13. The cavitand entrance has one long axis (9.48 Å) and one short axis (7.58 Å), Figure 6.13b. The previously reported methylene bridged cavitand is C_{4v} symmetric with axis dimension of 7.87 Å.²⁵ The incorporation of ethylene bridges in the cavitand imparts the asymmetry and expands the size of the cavitand along one axis as compared to symmetric methylene bridged cavitands, Figure 6.13a.

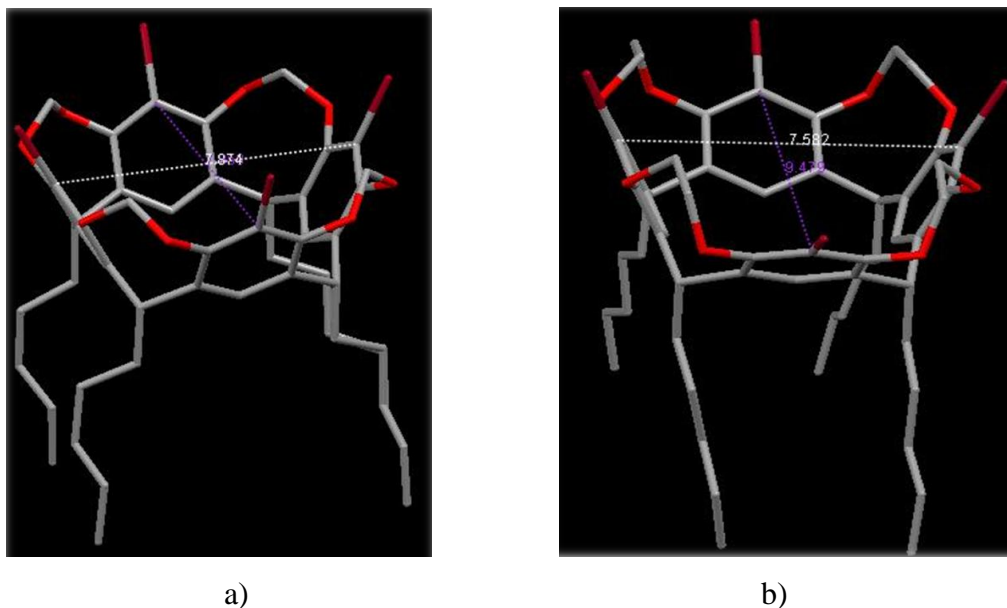


Figure 6.13 Comparison of (a) methylene bridged (7.87Å x 7.87Å)²⁵ and (b) ethylene bridged cavitand (9.48Å x 7.58Å) structures.

The crystal structure of **20** shows that one acetonitrile molecule resides between the pentyl feet of the cavitand and one acetonitrile encapsulated in the body and upper rim of cavitand, Figure 6.14. The orientation of the acetonitrile guest between the feet of cavitand (i.e.

nitrile group pointing towards the body of cavitand) is observed in eight out of eight structures analyzed from in house structural database of cavitand structures and reported structures.²⁶ This preferred orientation of acetonitrile guest could be attributed to $\text{CH}_3\text{CN}\cdots\text{H-C}$ (from cavitand body) interaction.

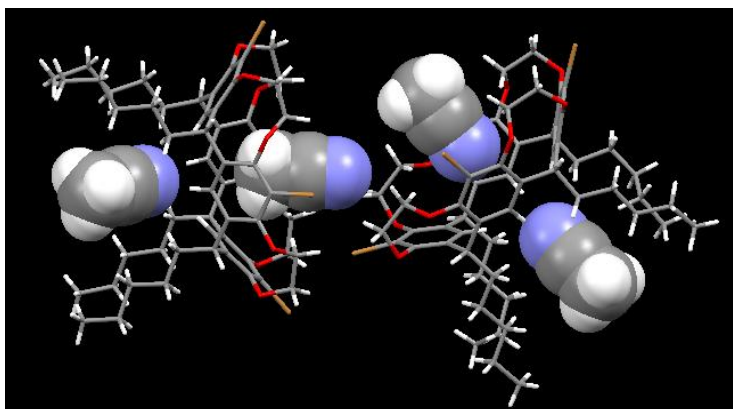


Figure 6.14 Crystal structure of **20** with acetonitrile molecules are shown in space filling.

The pyridyl functionalized cavitand **21** was synthesized using a Suzuki coupling reaction of tetrabromocavitand with 3-pyridyl boronic acid in moderate yield. The structure determination of **21** shows that the shape and size of the cavity remains unchanged with four pyridyl groups appended on the upper rim of the cavitand scaffold, Figure 6.15.

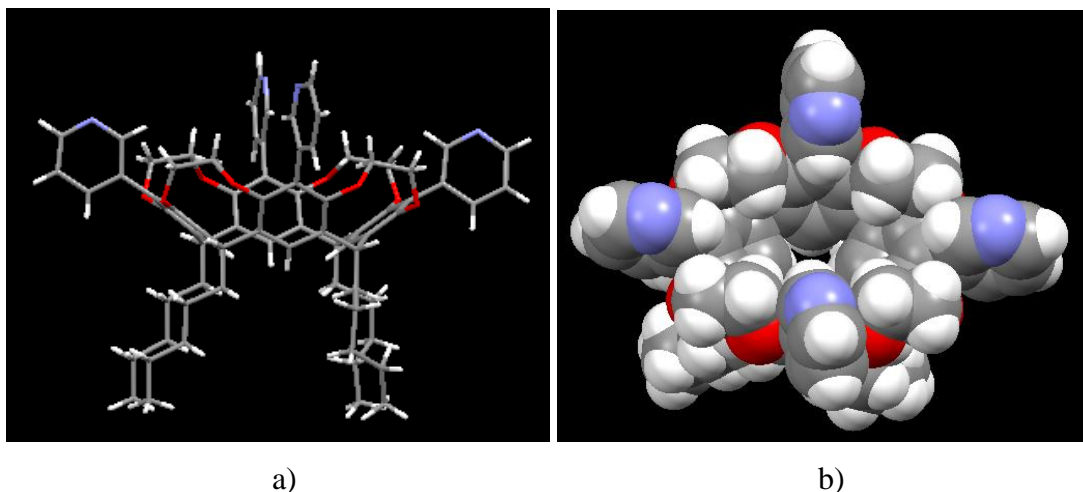


Figure 6.15 Crystal structure of **21** showing (a) horizontal view and (b) top view with space filling model (disordered ethanol and other solvent molecules were removed for clarity).

We tested the hydrogen-bond forming ability of **21** using ITC with 4-nitrobenzoic acid and we found 1:4 stoichiometry in solution. To analyze this assembly in solid-state single crystals of **21a** in nitrobenzene as a solvent were grown. We analyzed the crystals by IR spectroscopy for presence of hydrogen bonding stretches near 1900 and 2500 cm^{-1} (Figure 6.17).

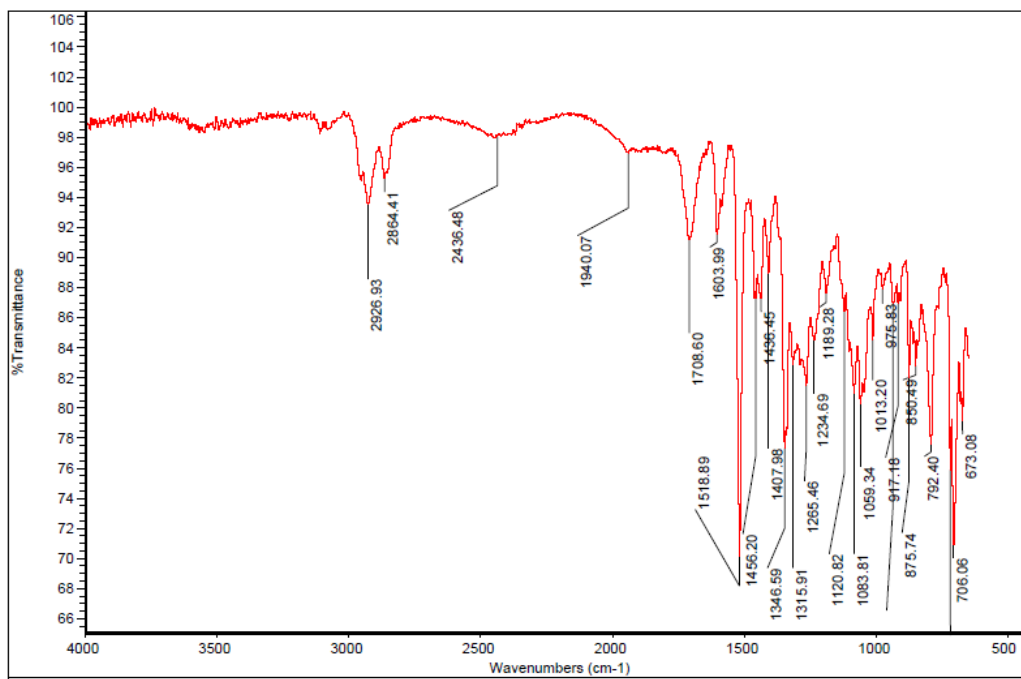


Figure 6.16 IR of single crystal of **21a**.

The structure determination of **21a** shows a pentameric co-crystal with one molecule of **21** binding to four molecules of 4-nitrobenzoic acid via hydrogen bonds. Moreover, nitrobenzene is encapsulated inside this assembly via weak van der Waals forces, Figure 6.17a. We also attempted to incorporate 2,6-dimethylnaphthalene; a C_{2v} symmetric guest inside the C_{2v} symmetric cavitand; however, the guest molecule resides outside the cavity, Figure 6.17b. The non-encapsulation of the guest molecule could be due to competing solvent molecules, which are present in large excess as compared to the number of guest molecules. This observation is evident from encapsulated solvent molecule inside the cavity cavitand. Moreover, the orientation of nitrobenzene molecule, with nitro group pointing towards body of cavitand, resembles the behaviour of the acetonitrile orientation in the crystal structure of **20**. The orientation of nitrobenzene is governed by $\text{NO}_2 \cdots \text{H-C}$ (from body of cavitand) hydrogen bonding. The

observations regarding alignment of guest molecule is of great interest for designing molecular capsules which can act as reaction chambers.²⁷

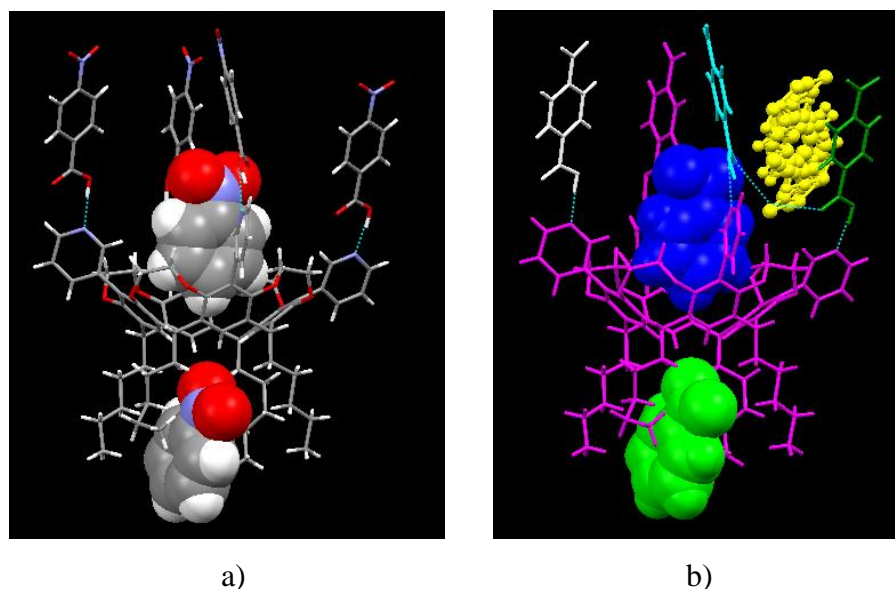


Figure 6.17 Crystal structure of **21a** showing (a) pentameric assembly with two nitrobenzene molecules in space filling and (b) **21a** colour coded for clarity (disordered 2,6-dimethyl naphthalene guest molecule is shown in yellow ball stick model).

We expanded the strategy of making pentameric assemblies using **21** with 3,5-dinitrobenzoic acid. The structure determination of **21b** shows that in the crystal lattice there are two unique supramolecular complexes; first with **21** hydrogen bonding to three molecules of 3,5-dinitrobenzoic acid (Figure 6.18a) and another one with **21** hydrogen bonding to one molecule of 3,5-dinitrobenzoic acid, Figure 6.18b. The detailed analysis of structure **21b** shows that this undesired stoichiometry in solid-state is due to competitive weak hydrogen bond donors (such as CH from the pentyl feet, CH from the aryl rings) interacting with acceptor site (pyridyl nitrogens). In this co-crystallization experiment, we also attempted to incorporate the 2,6-dimethylnaphthalene as a guest molecule; however, the guest resides outside the cavitand.

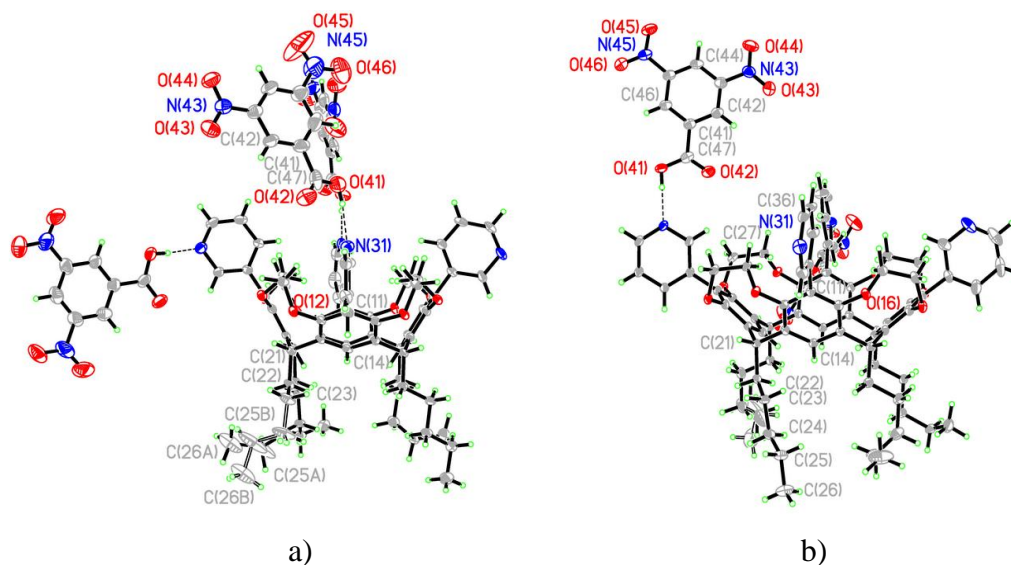
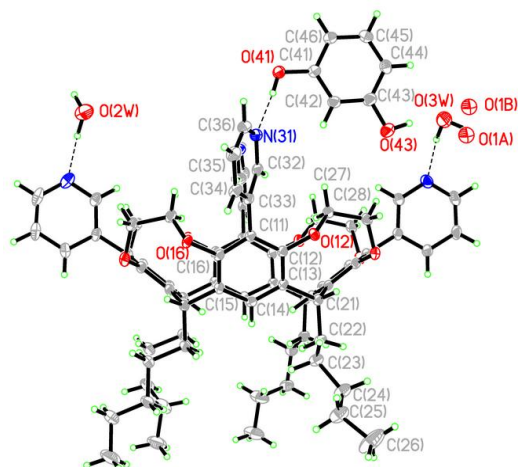


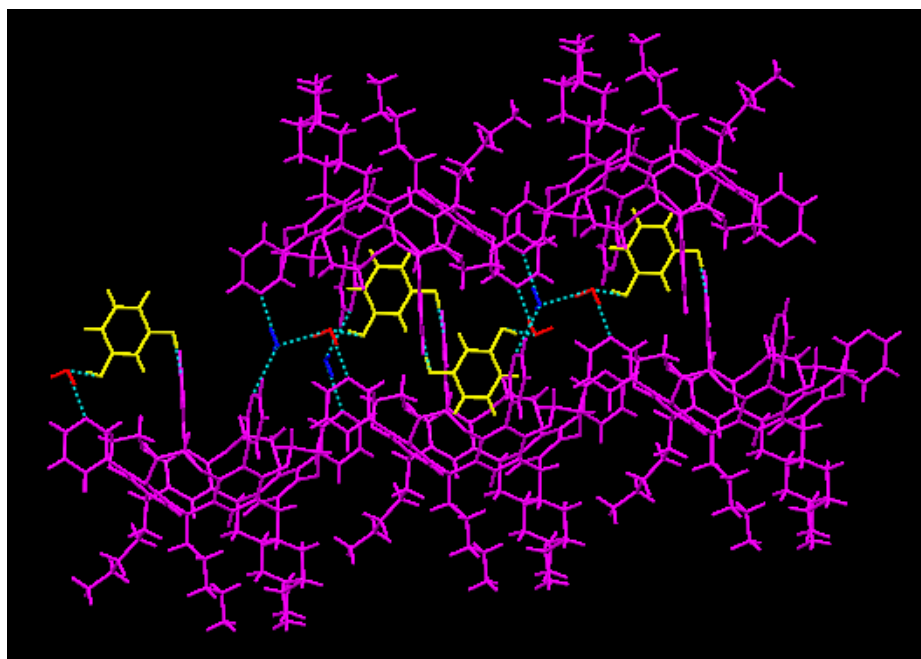
Figure 6.18 Molecular structure and labelled thermal ellipsoids (50%probability level) of **21b**. (a and b showing two unique molecular complexes present in crystalline lattice).

To obtain cavitand based capsules, we chose a design strategy using linker molecules to bring together two tetra(3-pyridyl)cavitands. For such a capsule we would need four linker molecules appended with ditopic hydrogen-bond donor groups. We chose resorcinol as a ditopic hydrogen bond donor linker due to its proven ability to form hydrogen bonds with pyridyl functionalities via $\text{OH}\cdots\text{N}$ interactions.¹⁷

Thus, cavitand **21** was allowed to co-crystallize with resorcinol. The crystal structure determination of **21c** shows that the product contains one resorcinol per cavitand **21** along with several water molecules. One pyridyl ring nitrogen of **21** is hydrogen bonding with resorcinol via $\text{OH}\cdots\text{N}$ interaction, two other pyridyl ring nitrogens are hydrogen bonding to water molecules and remaining nitrogen is not interacting with anything (the closest contact is OH from water at *c.a.* 2.98 Å).



(a)



(b)

Figure 6.19 a) Molecular structure of **21c** and (b) Extended structure of **21c** showing cavitated in purple, resorcinol molecule in yellow and water molecules in red/blue.

The desired supramolecular assembly of resorcinol with **21** is not formed, presumably due to the presence of water molecules disrupting the hydrogen-bond formation between resorcinol and tetrapyrrolyl cavitated **21**.

In order to place these results into broader context, we surveyed the crystallographic literature for relevant data. The CSD search was performed on calixarene co-crystals containing

pyridyl, -CCOH and -OH groups.²⁸ It turned out that eight out of twelve times unexpected stoichiometries were observed, Table 6.2. This clearly shows that achieving desired co-crystal stoichiometry in multidentate ligands is synthetically challenging.

Table 6.2 Table summarizing crystal structure data for calixarene co-crystals.²⁹

CSD code	Desired stoichiometry	Stoichiometry match	
		Yes	No (Exptl. stoichiometry)
AHUBUA	1:1	√	
MEXJII	1:4		1:2
QOQDIJ	1:2	√	
QOQDUV	1:4		1:2
RETKEG	1:12		1:8
VIKVAN	1:2		1:1
VIKVER	1:2		1:1
VIKVIV	1:2		1:1
VIKVOB	1:2	√	
WEMZEU	1:6		1:3
ELEMIS	1:3	√	
ELEMOY	1:4		1:1

6.3.3.2 Quest for molecular capsules

In our next attempt to design a molecular capsule, we used a tetracarboxylic acid cavitand **22**. To make a molecular capsule using **22**, homomeric interactions of carboxylic acids can be utilized (dimer formation). However, the carboxylic acids are not pointing ‘upward’; moreover, two of the carboxylic acid functional groups would be directed at *c.a.* 140° from the scaffold and other two at *c.a.* 120° (based on the crystal structure of the tetrabromocavitand **22**). However, a strategy of using linkers to assemble capsule could be applicable.

In the past, Atwood and coworkers utilized hydroxyl groups of calixarene to link two molecules in to a capsule using 4,4'-bipyridine as a linker, Figure 6.20. This multi-component system was found to bind two molecules of nitrobenzene simultaneously in the solid state.³⁰

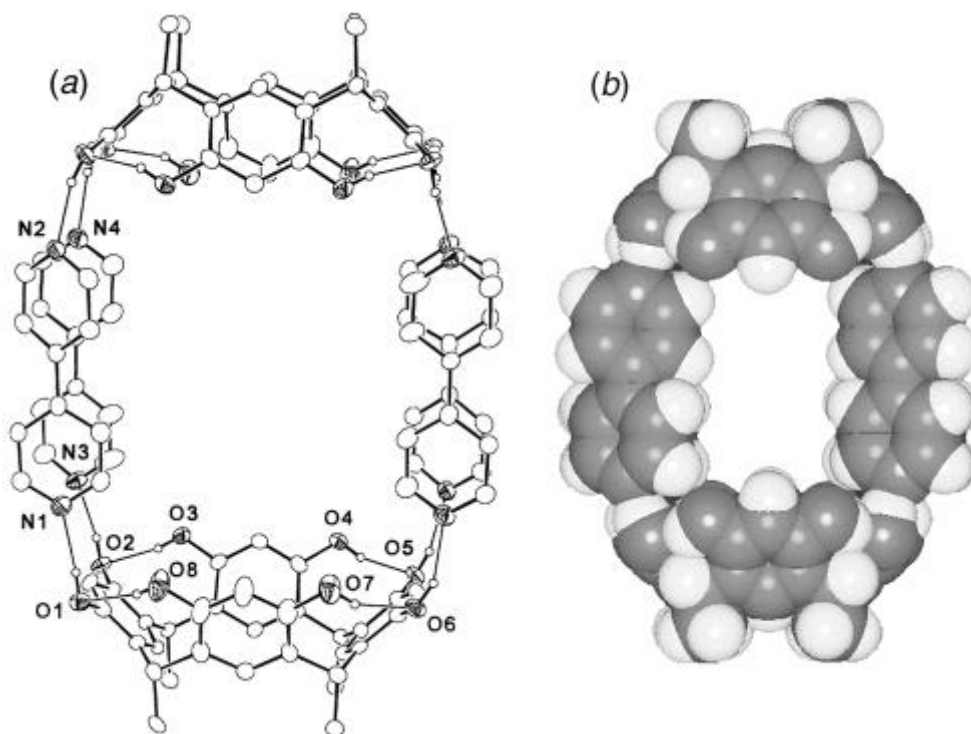


Figure 6.20 Molecular capsule formed via eight OH \cdots N hydrogen bonds; a) thermal ellipsoid plot of crystal structure and b) space filling model (solvent molecules are removed for clarity).^{30a}

We opted for 4,4'-bipyridine as a ditopic linker due to its proven ability to interact with carboxylic acids via OH \cdots N interactions.^{16,17} The cavitand **20** was allowed to co-crystallize with 4,4'-bipyridine to obtain single crystals of **22a**. The crystal structure determination of **22a** shows that two carboxylic acid groups are hydrogen bonding to methanol via OH \cdots N interaction to 4,4'-bipyridine, Figure 6.21. Another two carboxylic acid groups are linked to methanol via OH \cdots O interactions and hydroxyl groups of the methanol molecules bind (via OH \cdots N interaction) to one end of 4,4'-bipyridine, Figure 6.21.

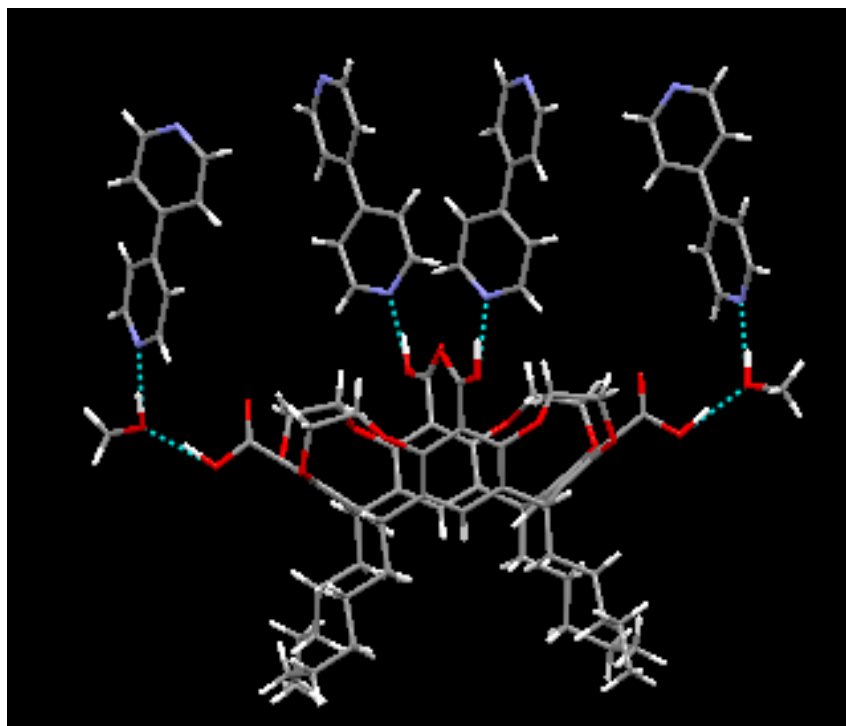


Figure 6.21 Molecular structure of **22a** showing co-crystal formation via OH \cdots N hydrogen bonding.

Upon extending the supramolecular assembly, shown in Figure 6.21, it was observed that each set of two adjacent 4,4'-bipyridine molecules are bonded to the neighboring tetracarboxylic acid cavitand (one acid group directly binds via OH \cdots N hydrogen bond to 4,4'-bipyridine and another acid group binds via the methanol-OH \cdots N interaction; which binds to another acid group). Therefore, the outcome of the reaction is not a discrete hexameric assembly, instead a 1D polymeric network is formed through multiple carboxylic acid \cdots pyridine hydrogen bonds, Figure 6.22.

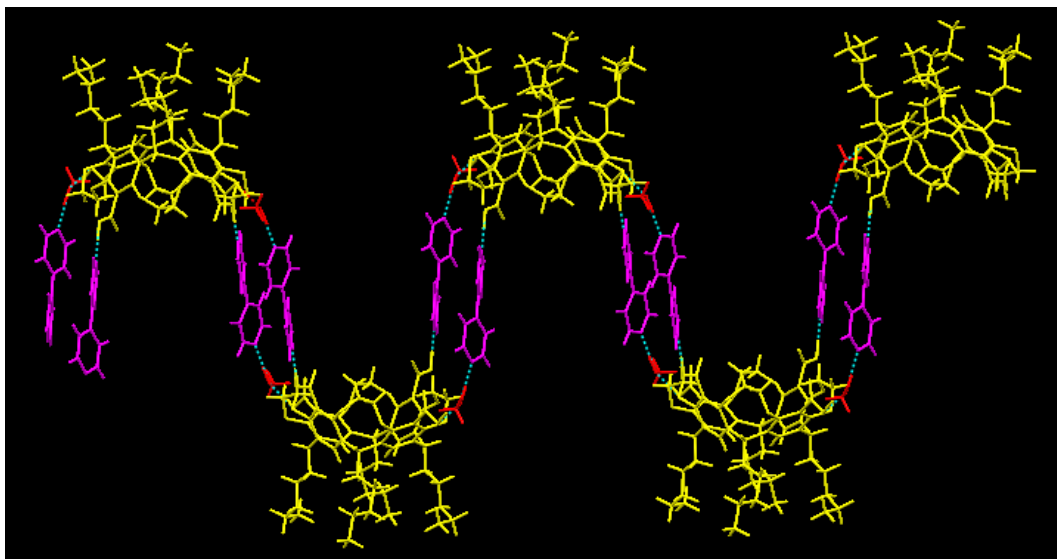


Figure 6.22 1D polymeric network formation in **22a** via acid $\text{OH}\cdots\text{N}(\text{bipy})$, $\text{OH}\cdots\text{O}(\text{methanol})$, methanol $\text{OH}\cdots\text{N}(\text{bipy})$. Acid cavitand **22** is shown in yellow, bipy molecules are shown in purple and methanol is shown in red.

In the crystal structure of **22a**, we were unable to obtain discrete capsule presumably due to a lack of an appropriate angle of the linker, thus favouring polymeric species formation over capsules. Another possible reason might be due to a lack of strong interactions to hold two cavitand molecules together in a capsular assembly. To address this commonly occurring polymeric network formation issue,³¹ we opted for different linker molecules to bring together two acid cavitand molecules. Kobayashi and co-workers utilized methylene bridged tetracarboxylic acid cavitands to obtain robust molecular capsules using 2-aminopyrimidine as a linker.³² The assembly was held together by sixteen hydrogen bonds.

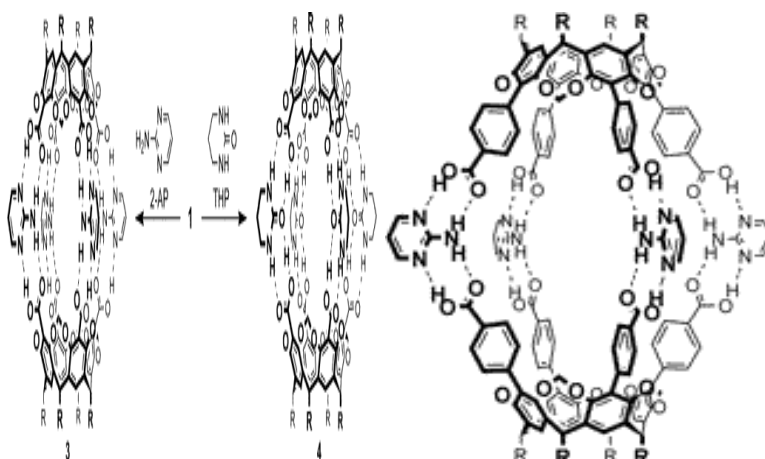


Figure 6.23 Self-assembly of tetracarboxylic acid cavitand (short and extended analogue) with 2-aminopyridine.³²

We chose 2-aminopyrimidine linker molecules, which should interact with carboxylic acid groups via two-point contact; moreover, the angle of binding should aid in bringing together two cavitands in discrete capsule. We co-crystallized **22** with variety of 2-aminopyrimidine derivatives and obtained single crystal of X-ray diffraction quality from the reaction of **22** with 2-amino-5-bromo-4-chloro-6-methylpyrimidine.

The structure determination of **22b** the linker forms hydrogen bonds via two-point contact with one carboxylic group of **22**. Another carboxylic acid group is hydrogen bonding to a 2-aminopyrimidine molecule via $C=O \cdots HN$ (of amino) and acid- $OH \cdots O$ (of water which hydrogen bonds to pyrimidine via $OH \cdots N$), Figure 6.24. The remaining two carboxylic groups of **22** hydrogen bond to an acid from another cavitand molecule via acid- $OH \cdots O=C$ and water- $OH \cdots O=C$ interactions.

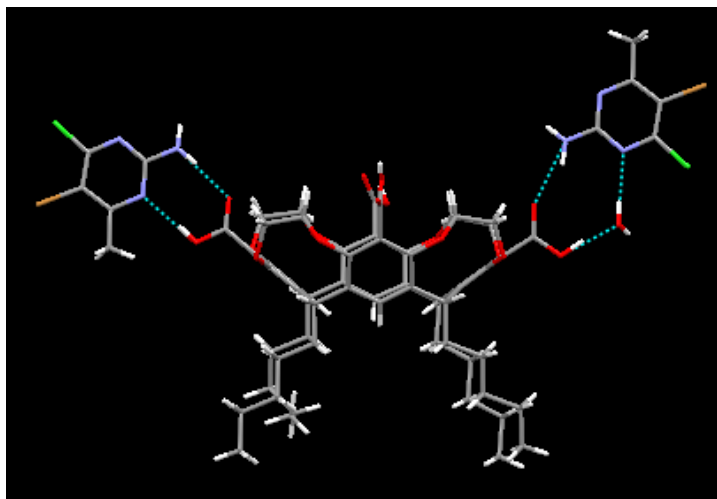


Figure 6.24 Molecular structure of **22b** showing hydrogen bonding interaction between carboxylic acid cavitand and 2-aminopyrimidine derivative.

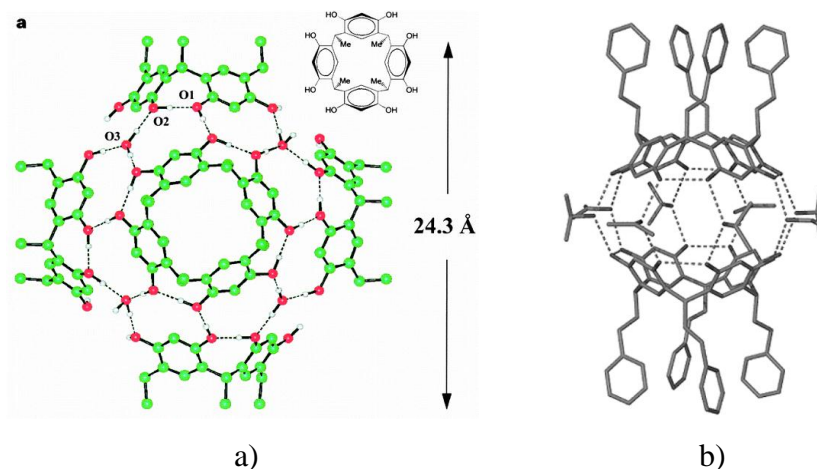


Figure 6.25 a) Hexameric capsule formed with the aid of eight water molecules. b) Dimeric capsule formed with eight *iso*-propanol molecules.

The extended structure of **22b** shows that discrete capsular assembly is formed via multiple OH \cdots N/ OH \cdots O hydrogen bonds, Figure 6.26. The capsule consists of two cavitands, two linker molecules and four water molecules. The water or solvent molecules hydrogen bonding to aid in capsule formation has been observed frequently in formation of hexameric,³³ dimeric³⁴ molecular capsules, Figure 6.25.

The dimensions of capsule **22b** are 13.2 Å x 15.2 Å x 0.75 Å. Due to the available space inside the capsule; it includes one molecule of 2-aminopyrimidine (used as a linker) as a guest, Figure 6.26. This example proves that molecular capsules of cavitands using linker molecules could be designed; provided appropriate linker molecule with desired angle of binding sites is used. Moreover, asymmetric guest encapsulation underscores the size and shape selectivity.

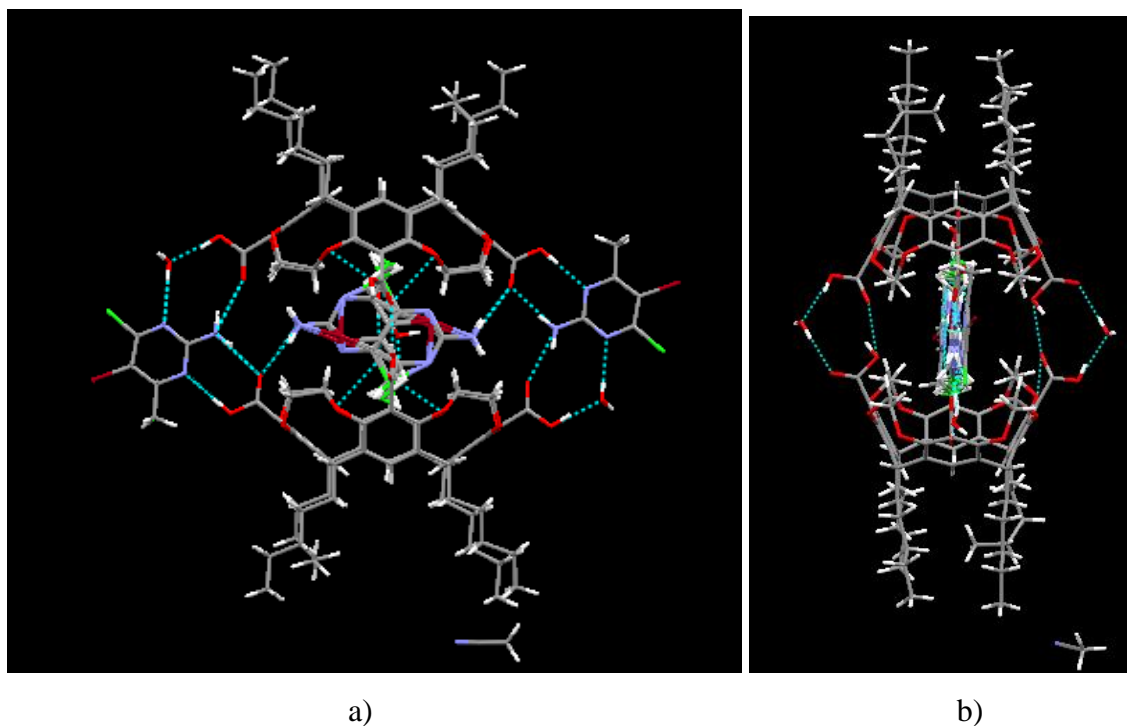


Figure 6.26 Extended structure of **22b** showing capsule formation via OH...N/ OH...O hydrogen bonding. (a) and (b) represents different views of capsule holding the guest inside the cavity. Encapsulated guest molecule is disordered.

6.3.3.3 Structural analysis of crystal structures

The structural analysis of our seven structures shows all include solvent molecules. There are three locations where these solvent molecules are found; body, feet and exo-host (i.e. outside the cavitand). A CSD analysis of cavitand-based structures shows that 17/17 times solvent molecules are incorporated, which highlights the importance of solvents in crystal structures of cavitand macromolecules which is in well agreement with our observation. The locations of solvents in these structures are summarized in Table 6.3, 15/17 times solvent molecules are found outside the cavitand and 9/17 times they incorporated inside the cavity.

Table 6.3 Table summarizing structural data for reported cavitands crystal structures. The locations of solvents were categorized.³⁵

CSD code	Body	Feet	Exo-host
FUDSIGIO	-	-	CH ₂ Cl ₂
FUDSOMIO	-	-	Ethanol

FUDSUSIO	-	-	CH ₂ Cl ₂
HANQOC	Water	-	Ethanol, water
ILIJOC	Xylene	-	Xylene, nitrobenzene
ILIJUI	-	-	Water, <i>p</i> -xylene
IWIWIU	Ethanol	-	-
NUFBIA	-	-	Chloroform, benzene
QADYEA	Acetonitrile	Acetonitrile	-
QUCWOA	Chloroform	-	Chloroform
QUCWUG	Chloroform	-	Chloroform
TOTCEK	-	-	Pentane
CUYZUS	-	-	CF ₃ CH ₂ OH
HUXJIU	-	-	Benzene
QAFBAC	Acetone	-	Acetone, CH ₂ Cl ₂
QAFBQQ	CH ₂ Cl ₂	-	CH ₂ Cl ₂
AVAFIN	Methanol, CH ₂ Cl ₂	-	Methanol, CH ₂ Cl ₂

We analysed locations of solvent molecules in the seven structures obtained in our work, Table 6.4. The observed solvent locations are; 4/7 times in the the body, 3/7 times around the feet and 5/7 times exo-host. Due to limited structural data (reported and obtained) on cavitands it is not possible to state unambiguously whether which solvent prefers which locations. However, additional structural data will ultimately help us to set guidelines for selective guest/solvent capture within cavitand structure.

Table 6.4 Table summarizing structural data for seven cavitand crystal structures obtained. The locations of solvents were categorized.

Label	Body	Feet	Crystal lattice
20	Acetonitrile	Acetonitrile	-
21	Ethanol	-	Ethanol
21a	Nitrobenzene	Nitrobenzene	-
21b	-	Nitromethane	Nitromethane
21c	-	-	Water
22a	Methanol	-	Methanol
22b	-	-	Water, acetonitrile

6.4 Conclusions

We incorporated ethylene bridges in cavitand scaffold, the crystal structure determination of all the cavitand derivatives clearly shows expanded cavity size and imparted asymmetry, Figure 6.27.

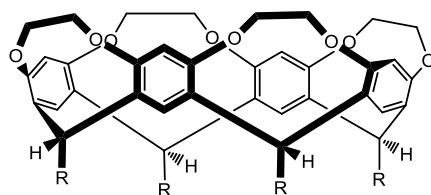


Figure 6.27 Ethylene bridged cavitand.

We have synthesized a pyridyl functionalized cavitand and studied supramolecular complex formation with carboxylic acid in solution (using ITC) and solid-state, Figure 6.28. The solution stoichiometry is further confirmed by solid-state structural data. This is the only study where multi-component supramolecular assembly of a cavitand is analyzed in solution (ITC) and supported by solid-state data.

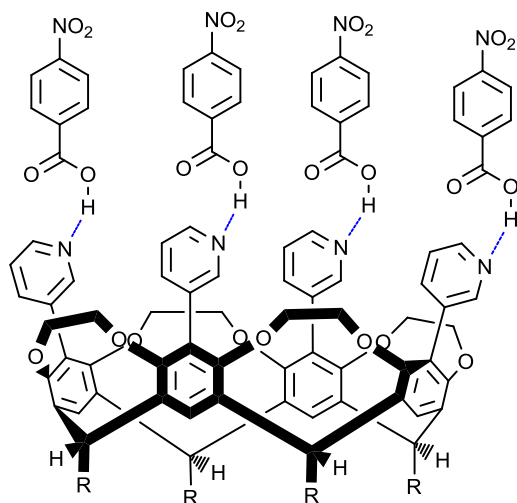


Figure 6.28 Pentameric supramolecular assembly analyzed in solution and solid-state.

We have successfully decorated cavitands with tetracarboxylic acid groups (Figure 6.29) and constructed a molecular capsule via use of stronger two-point contact. Moreover, this capsule encapsulated an asymmetric guest which demonstrates that multimeric capsular assembly can be achieved under suitable reaction conditions.

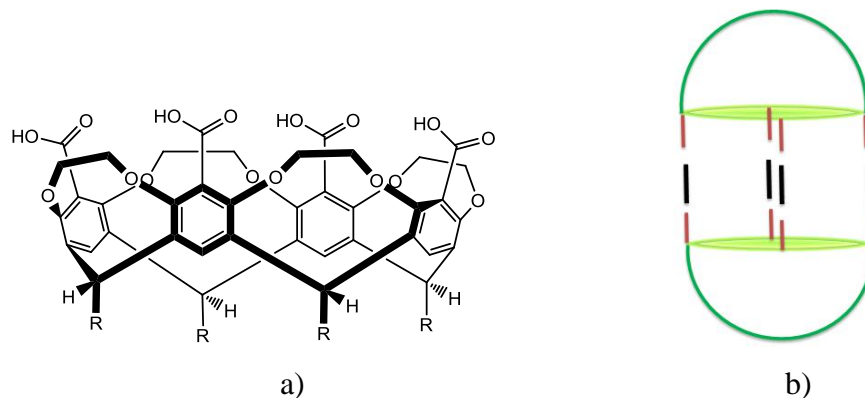


Figure 6.29 (a) Schematic of tetracarboxylic acid cavitand 22 and (b) Representation of capsule with linkers.

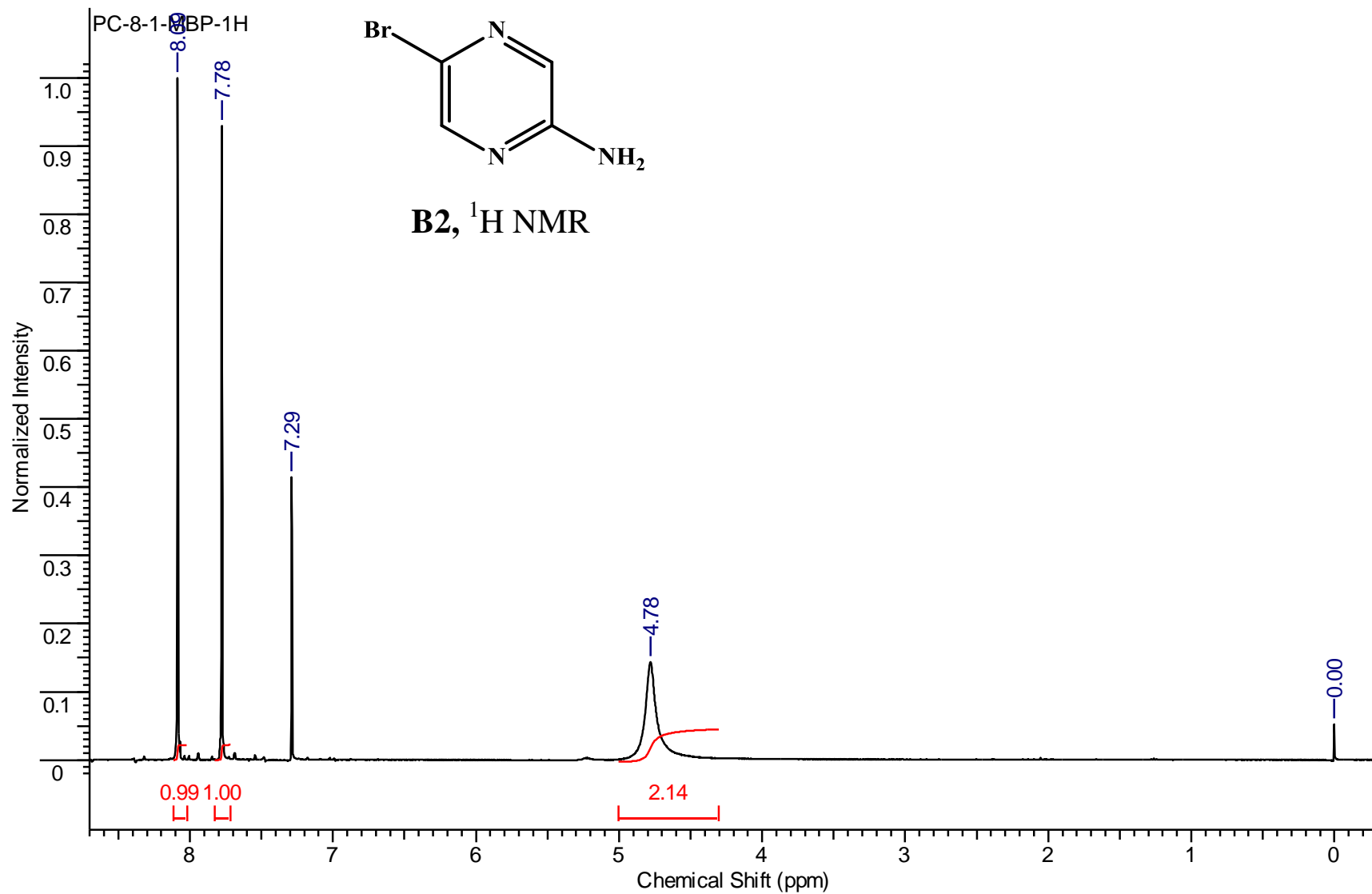
References

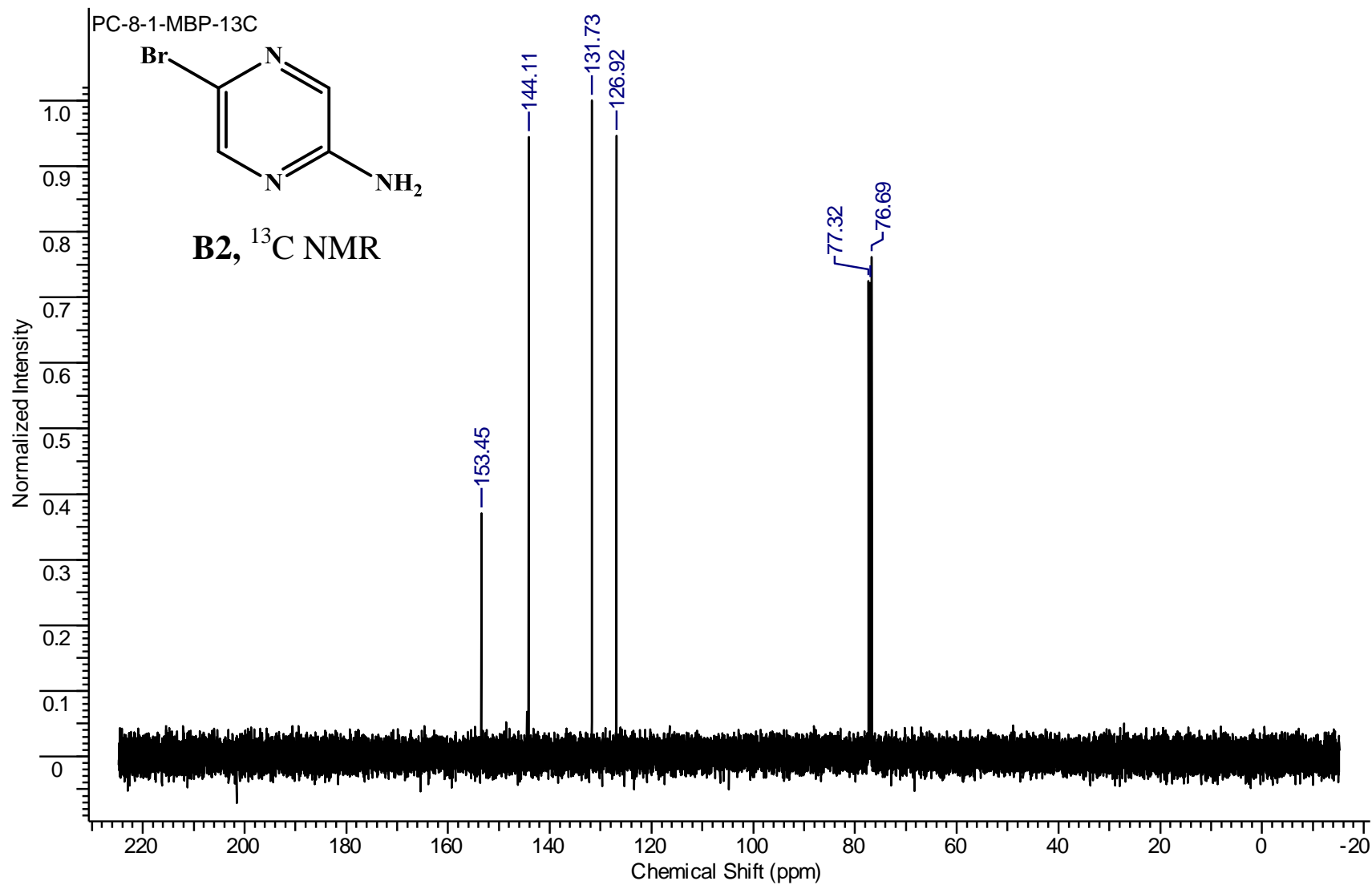
- ¹ (a) Moran, J. R.; Karbach, S.; Cram, D. J. *J. Am. Chem. Soc.* **1982**, *104*, 5826; (b) Cram, D. J. *Science* **1983**, *219*, 1177; (c) Cram, D.; Kim, H.; Knobler, C.; Maverick, E.; Ericson, J.; Helgeson, R. *J. Am. Chem. Soc.* **1988**, *110*, 2229.
- ² Nishimura, N.; Kobayashi, K. *J. Org. Chem.* **2010**, *75*, 6079.
- ³ (a) Fox, O. D.; Drew, M. G. B.; Beer, P. D. *Angew. Chem., Int. Ed.* **2000**, *39*, 135; (b) Pirondini, L.; Bertolini, F.; Cantadori, B.; Ugozzoli, F.; Massera, C.; Dalcanale, E. *Proc. Natl. Acad. Sci. USA* **2002**, *99*, 4911; (c) Yoshizawa, M.; Takeyama, Y.; Okano, T.; Fujita, M. *J. Am. Chem. Soc.* **2003**, *125*, 3243; (d) Yoshizawa, M.; Miyagi, S.; Kawano, M.; Ishiguro, K.; Fujita, M. *J. Am. Chem. Soc.* **2004**, *126*, 9172.
- ⁴ (a) Corbellini, F.; Fiammengo, R.; Timmerman, P.; Crego-Calama, M.; Versluis, K.; Heck, A. J. R.; Luyten, I.; Reinhoudt, D. N. *J. Am. Chem. Soc.* **2002**, *124*, 6569; (b) Oshovsky, G. V.; Reinhoudt, D. N.; Verboom, W. *J. Am. Chem. Soc.* **2006**, *128*, 5270.
- ⁵ (a) Chapman, R. G.; Sherman, J. C. *J. Am. Chem. Soc.* **1995**, *117*, 9081. (b) MacGillivray, L. R.; Atwood, J. L. *Nature* **1997**, *389*, 469–472. (c) Heinz, T.; Rudkevich, D. M.; Rebek, J., Jr. *Nature* **1998**, *394*, 764. (d) Shivanyuk, A.; Paulus, E. F.; Böhmer, V. *Angew. Chem., Int. Ed.* **1999**, *38*, 2906. (e) Kobayashi, K.; Shirasaka, T.; Yamaguchi, K.; Sakamoto, S.; Horn, E.; Furukawa, N. *Chem. Commun.* **2000**, 41. (f) Ebbing, M. H. K.; Villa, M.-J.; Valpuesta, J.-M.; Prados, P.; de Mendoza, J. *Proc. Natl. Acad. Sci. U.S.A.* **2002**, *99*, 4962. (g) Kobayashi, K.; Ishii, K.; Sakamoto, S.; Shirasaka, T.; Yamaguchi, K. *J. Am. Chem. Soc.* **2003**, *125*, 10615. (h) Sansone, F.; Baldini, L.; Casnati, A.; Chierici, E.; Faimani, G.; Ugozzoli, F.; Ungaro, R. *J. Am. Chem. Soc.* **2004**, *126*, 6204. (i) Ajami, D.; Rebek, J., Jr. *J. Am. Chem. Soc.* **2006**, *128*, 5314. (j) Yamanaka, M.; Ishii, K.; Yamada, Y.; Kobayashi, K. *J. Org. Chem.* **2006**, *71*, 8800. (k) Kitagawa, H.; Kobori, Y.; Yamanaka, M.; Yoza, K.; Kobayashi, K. *Proc. Natl. Acad. Sci. U.S.A.* **2009**, *106*, 10444.
- ⁶ Giles, M. D.; Liu, S.; Emanuel, R. L.; Gibb, B. C.; and Grayson, S. M. *J. Am. Chem. Soc.* **2008**, *130*, 14430

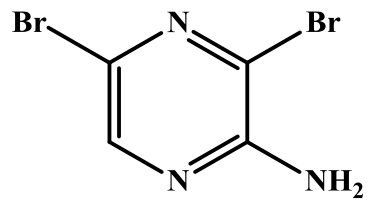
-
- ⁷ Hooley, R.; Rebek, J., Jr. *Org. Biomol. Chem.* **2007**, *5*, 3631.
- ⁸ (a) Zampolli, S.; Betti, P.; Elmi, I.; Dalcanale, E. *Chem. Commun.* **2007**, 2790. (b) Pirondini, L.; Dalcanale, E. *Chem. Soc. Rev.*, **2007**, *36*, 695. (c) Pinalli R., Suman M., Dalcanale E., *Eur. J. Org. Chem.* **2004**, 451.
- ⁹ Iwasawa, T.; Hooley, R.; Rebek J., Jr. *Science* **2007**, *317*, 493.
- ¹⁰ Nishimura, N.; Kobayashi, K.; *J. Org. Chem.* **2010**, *75*, 6079.
- ¹¹ (a) Chopra, N.; Sherman, J. C. *Angew. Chem., Int. Ed.* **1999**, *38*, 1955. (b) Green, J. O.; Bird, J.-H.; Gibb, B. C. *Org. Lett.* **2000**, *2*, 3845. (c) Wash, P. L.; Renslo, A. R.; Rebek, J., Jr. *Angew. Chem., Int. Ed.* **2001**, *40*, 1221. (d) Barrett, E. S.; Irwin, J. L.; Turner, P.; Sherburn, M. S. *J. Org. Chem.* **2001**, *66*, 8227–8229.
- ¹² Cram and co-workers first synthesized ethylene bridged cavitands and crystal structure of these cavitands showed C_{2v} symmetric structure. For details, see; Tucker, J. A.; Knobler, C. B.; Trueblood, K. N.; Cram, D. J. *J. Am. Chem. Soc.* **1989**, *111*, 3688.
- ¹³ Structures were minimized using molecular mechanics force field (MMFF) level of theory in Spartan'08 software.
- ¹⁴ Saboury, A. A. *J. Therm. Anal. Cal.* **2004**, *77*, 997.
- ¹⁵ (a) Aakeröy, C. B.; Beatty, A. M.; Helfrich, B. A. *J. Am. Chem. Soc.* **2002**, *124*, 14425. (b) Aakeröy, C. B.; Desper, J.; Urbina, J. F. *Chem. Commun.* **2005**, *22*, 2820. (c) Aakeröy, C. B.; Desper, J.; Elisabeth, E.; Helfrich, B. A.; Levin, B.; Urbina, J. F. *Zeit. Krist.* **2005**, *220*, 325. (d) Aakeröy, C. B.; Chopade, P. D.; Ganser, C.; Desper, J.; *Chem. Commun.*, **2011**, *47*, 4688.
- ¹⁶ Acid---N_{pyridine}: (a) Arora, K. K.; Pedireddi, V. R. *J. Org. Chem.* **2003**, *68*, 9177. (b) Shattock, T. R.; Vishweshwar, P.; Wang, Z.; Zaworotko, M. J. *Cryst. Growth Des.* **2005**, *5*, 2046. (c) Steiner, T. *Acta Crystallogr., Sect. B: Struct. Sci.* **2001**, *57*, 103. (d) Vishweshwar, P.; Nangia, A.; Lynch, V. M. *Cryst. Growth Des.* **2003**, *3*, 783. (e) Vishweshwar, P.; Nangia, A.; Lynch, V. M. *J. Org. Chem.* **2002**, *67*, 556. (f) Etter, M. C.; Adson, D. A. *J. Chem. Soc., Chem. Commun.* **1990**, 589. (g) Bhogala, B. R.; Vishweshwar, P.; Nangia, A. *Cryst. Growth Des.* **2002**, *2*, 325.
- ¹⁷ OH---N_{pyridine} (a) Bis, J. A.; Vishweshwar, P.; Weyna, D.; Zaworotko, M. J. *Mol. Pharm.* **2007**, *4*, 401. (b) Varughese, S.; Pedireddi, V. R. *Chem. Eur. J.* **2006**, *12*, 1597. (c) Vishweshwar, P.; Nangia, A.; Lynch, V. M. *CrystEngComm* **2003**, *5*, 164. (d) Papaefstathiou, G. S.; MacGillivray, L. R. *Org. Lett.* **2001**, *3*, 3835.
- ¹⁸ Helgeson, R. C., Paek, K., Knobler, C. B., Maverick, E. F. and Cram, D. J. *J. Am. Chem. Soc.* **1996**, *118*, 5590.
- ¹⁹ Kobayashi, K., Yamada, Y., Yamanaka, M., Sei, Y. and Yamaguchi, K. *J. Am. Chem. Soc.* **2004**, *126*, 13896.
- ²⁰ (a) Moran, J. R.; Karbach, S.; Cram, D. J. *J. Am. Chem. Soc.* **1982**, *104*, 5826. (b) Yamanaka, M.; Ishii, K.; Yamada, Y.; Kobayashi, K. *J. Org. Chem.* **2006**, *71*, 8800.
- ²¹ <http://www.tainstruments.com/product.aspx?id=261&n=1&siteid=11>
- ²² Errors on the thermodynamic parameters seems to larger; however, similar or even bigger errors are acceptable for ITC experiments. See; Sessler, J. L.; Gross, D. E.; Cho, W.-S.; Lynch, V. M.; Schmidtchen, F. P.; Bates, G. W.; Light, M. E.; Gale, P. A. *J. Am. Chem. Soc.* **2006**, *128*, 12281.
- ²³ Odinkov, S. E.; Iogansen, A. V. *J. Appl. Spectrosc.* **1961**, *14*, 1076.

-
- ²⁴ a) Gan, H.; Gibb, B. C. *Supramol. Chem.* **2010**, *22*, 808. b) Hornung, J., Fankhauser, D., Shirtcliff, L. D., Praetorius, A., Schweizer, W. B. and Diederich, F. *Chemistry - A European Journal* **2010**, *17*, 12362.
- ²⁵ Aakeröy, C. B.; Schultheiss, N. S.; Desper, J. *Org. Lett.* **2006**, *8*, 2607.
- ²⁶ CSD code for one reported structure is QADYEA.
- ²⁷ Amrhein, P.; Wash, P. L.; Shivanyuk, A.; Rebek, J. *Org. Lett.* **2002**, *4*, 319.
- ²⁸ Since there are very few number of cavitand co-crystals reported, we opted for calixarene co-crystals. The pyridyl, COOH and –OH groups were included in search due to use of same functional groups in current study.
- ²⁹ CSD search carried out on ConQuest Version 1.13 (updated until November 2011).
- ³⁰ a) MacGillivray, L.; Atwood, J. *Chem. Commun.* **1999**, 181. b) MacGillivray, L.; Atwood, J. *J. Am. Chem. Soc.* **1997**, *119*, 6931.
- ³¹ a) Kobayashi, K.; Shirasaka, T.; Horn, E.; Furukawa, N. *Tetrahedron Lett.* **1999**, *40*, 8883. b) Volkmer, D.; Fricke, M.; Vollhardt, D.; Siegel, S. *J. Chem. Soc., Dalton Trans.* **2002**, 4547. c) Lazar, A.; Danylyuk, O.; Suwinska, K.; Perret, F.; Coleman, A. N. *Chem. Commun.* **2006**, 903. d) Aakeröy, C.; Schultheiss, N.; Desper, J. *CrystEngComm* **2007**, *9*, 211. e) For example on bipy based 1D network structures see; MacGillivray, L. R.; Spinney, H. A.; Reid, J. L.; Ripmeester, J. A. *Chem. Commun.*, **2000**, 517.
- ³² a) Kobayashi, K.; Shirasaka, T.; Yamaguchi, K.; Sakamoto, S.; Horn, E.; Furukawa, N. *Chem. Commun.*, **2000**, 41. b) Yamanaka, M.; Ishii, K.; Yamada, Y.; Kobayashi, K. *J. Org. Chem.* **2006**, *71*, 8800.
- ³³ Shivanyuk, A.; Rebek, J. *Proc Nat Acad Sci USA*, **2001**, 98,766.
- ³⁴ Rose, K. N.; Barbour, L. J.; Orr, G. W.; Atwood, J. L. *Chem Commun* **1998**, 407.
- ³⁵ CSD search carried out on ConQuest Version 1.13 (updated until November 2011). The search was carried out on ‘cavitand’ as a class of molecules.

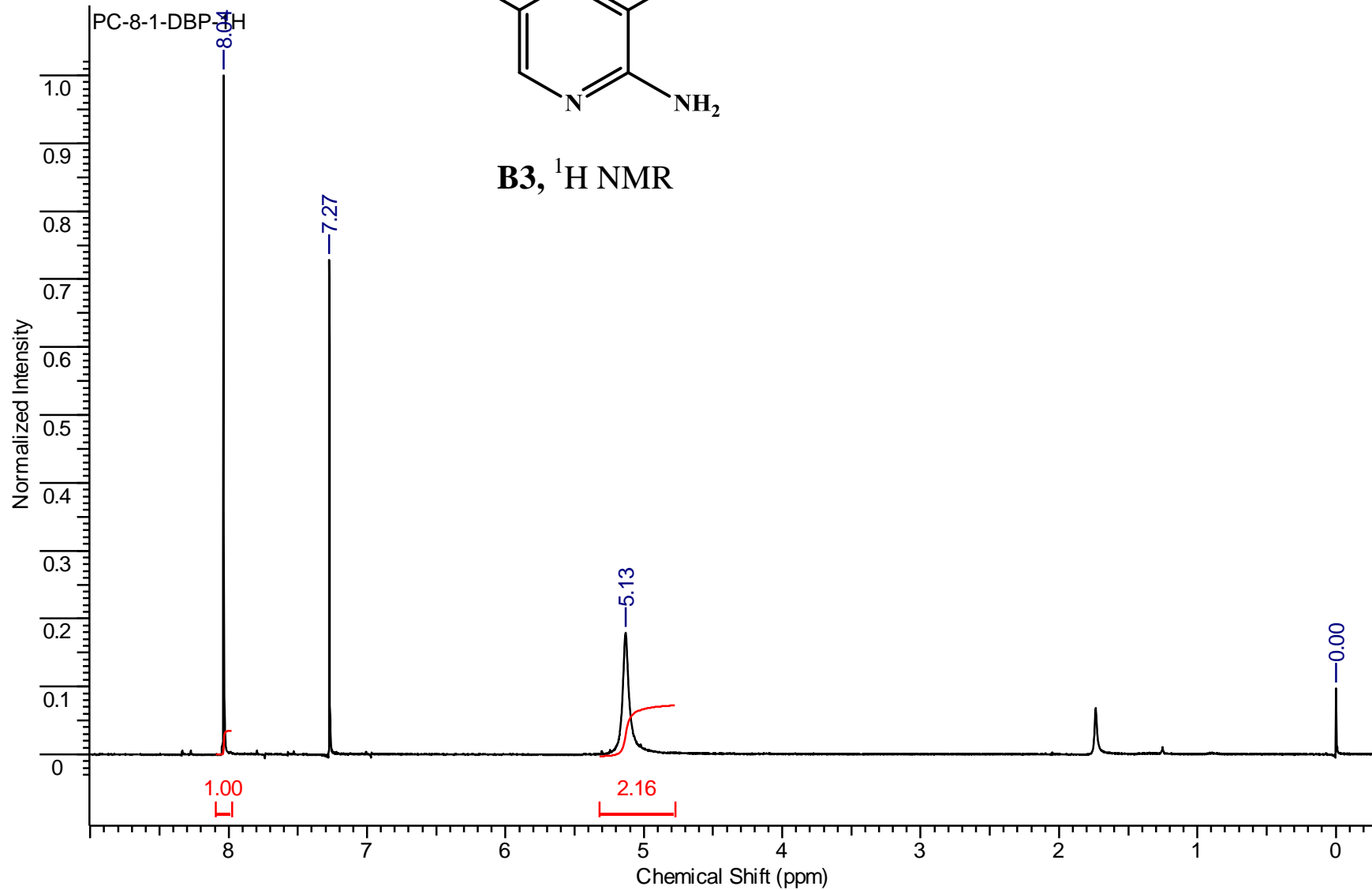
Appendix A – ^1H , ^{13}C NMR and HRMS

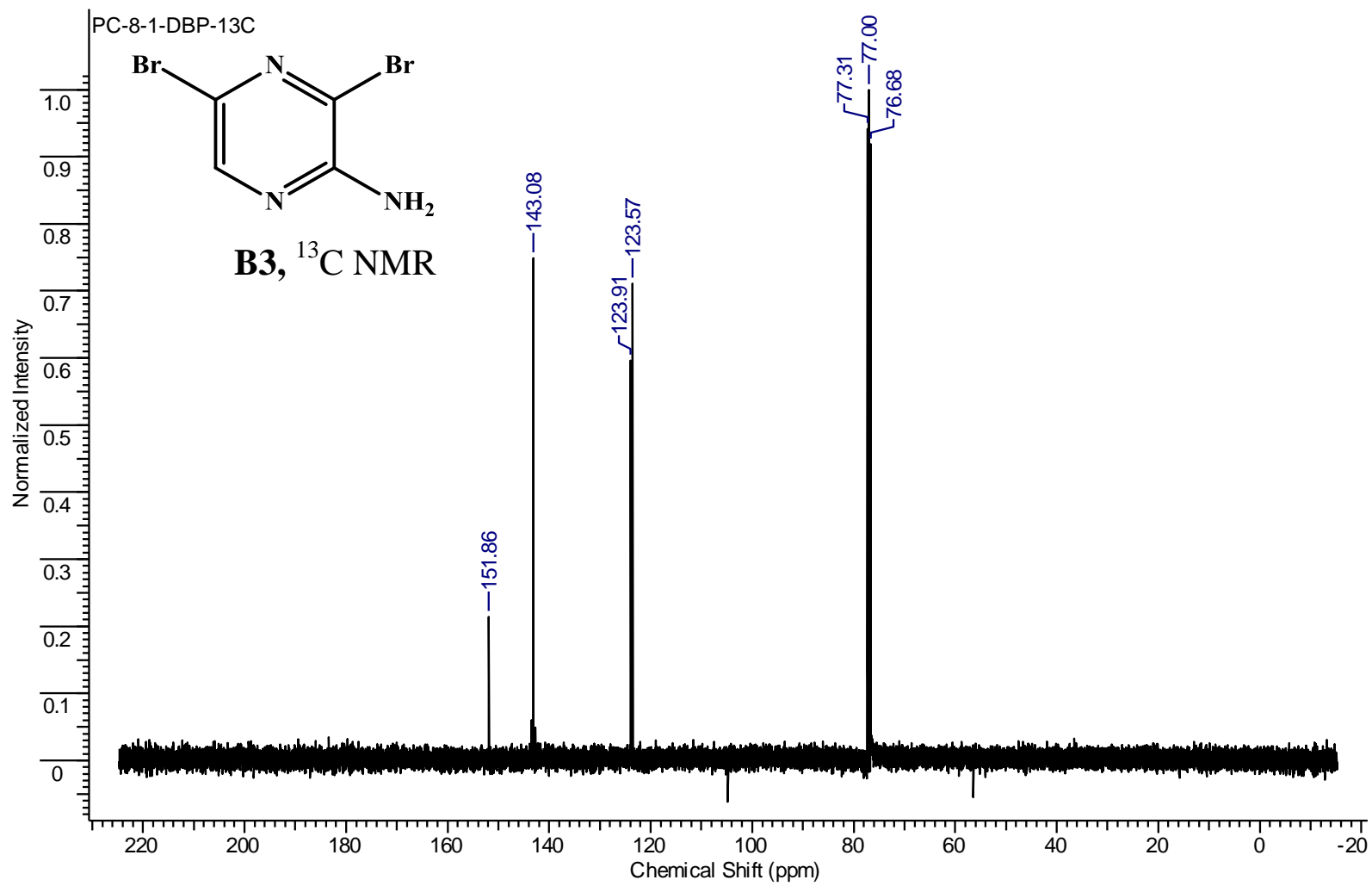


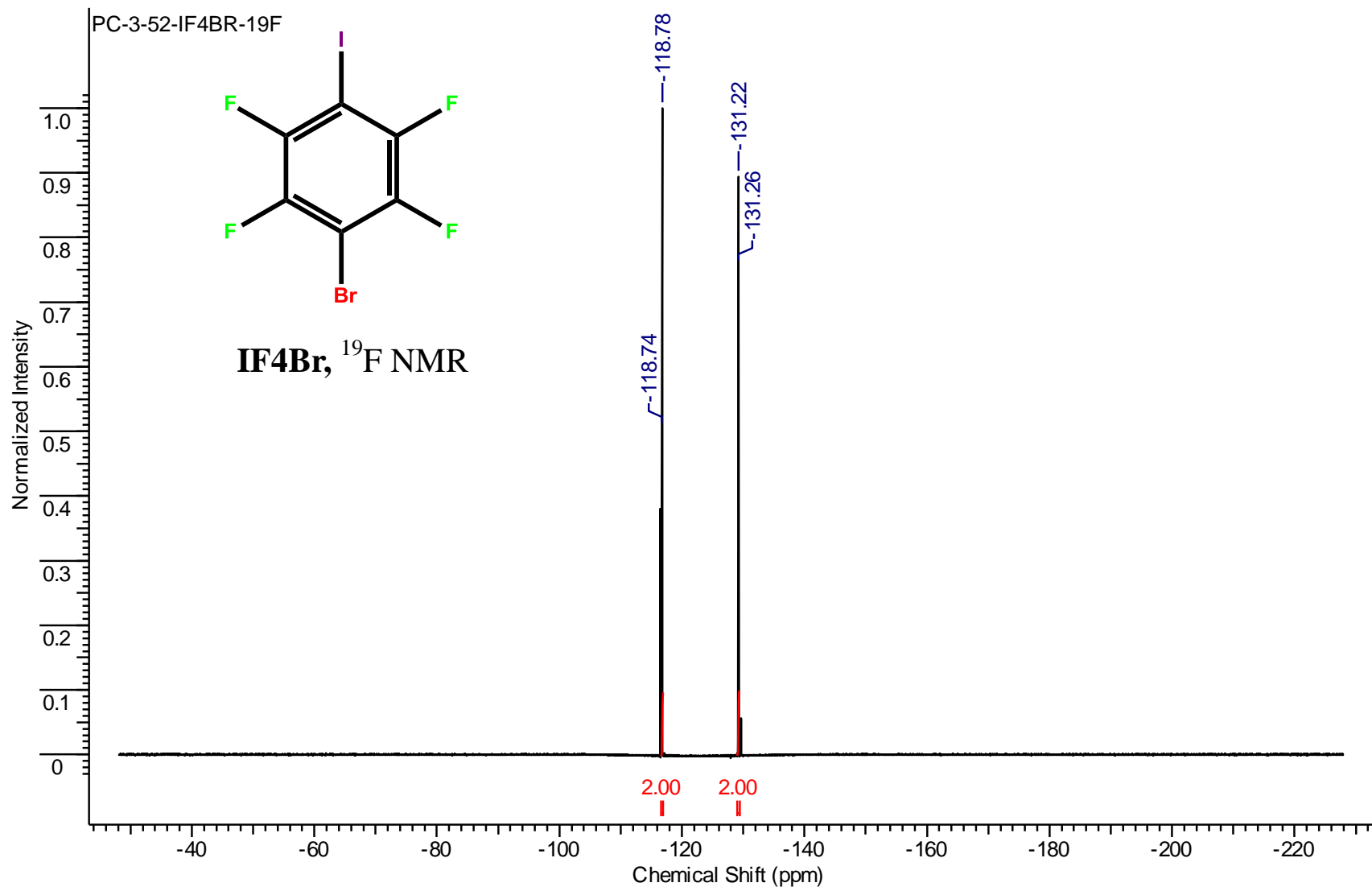


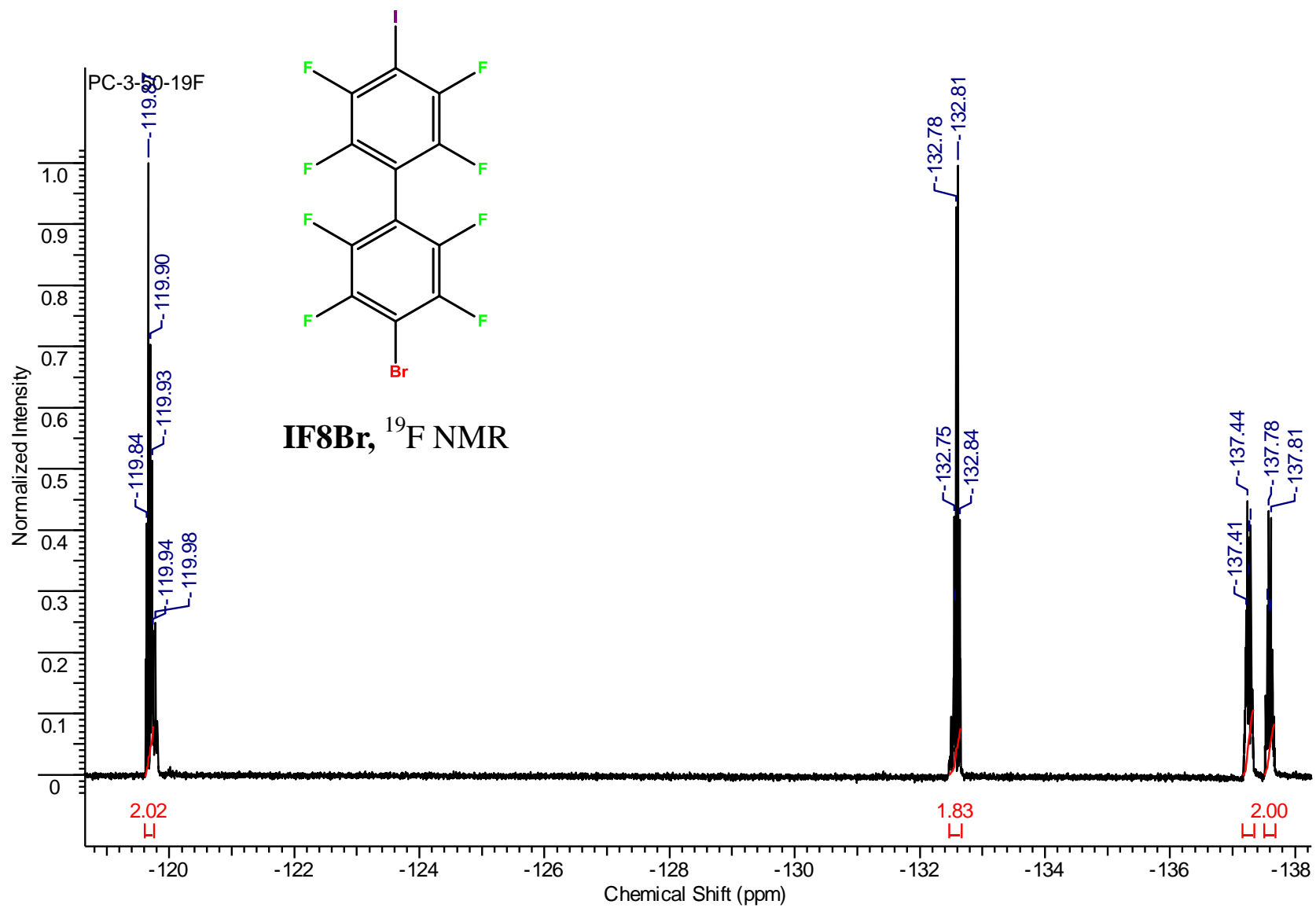


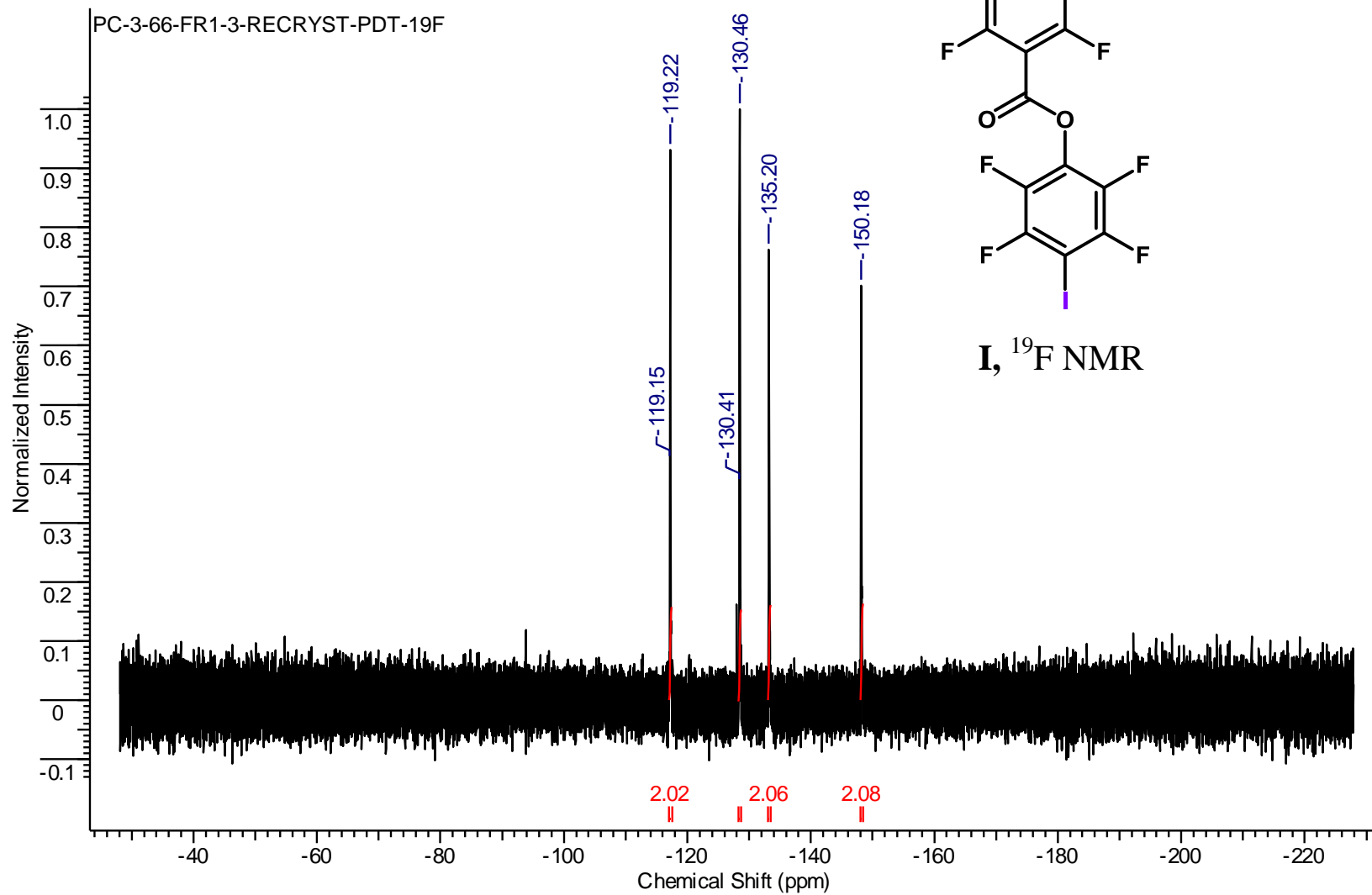
B3, ¹H NMR

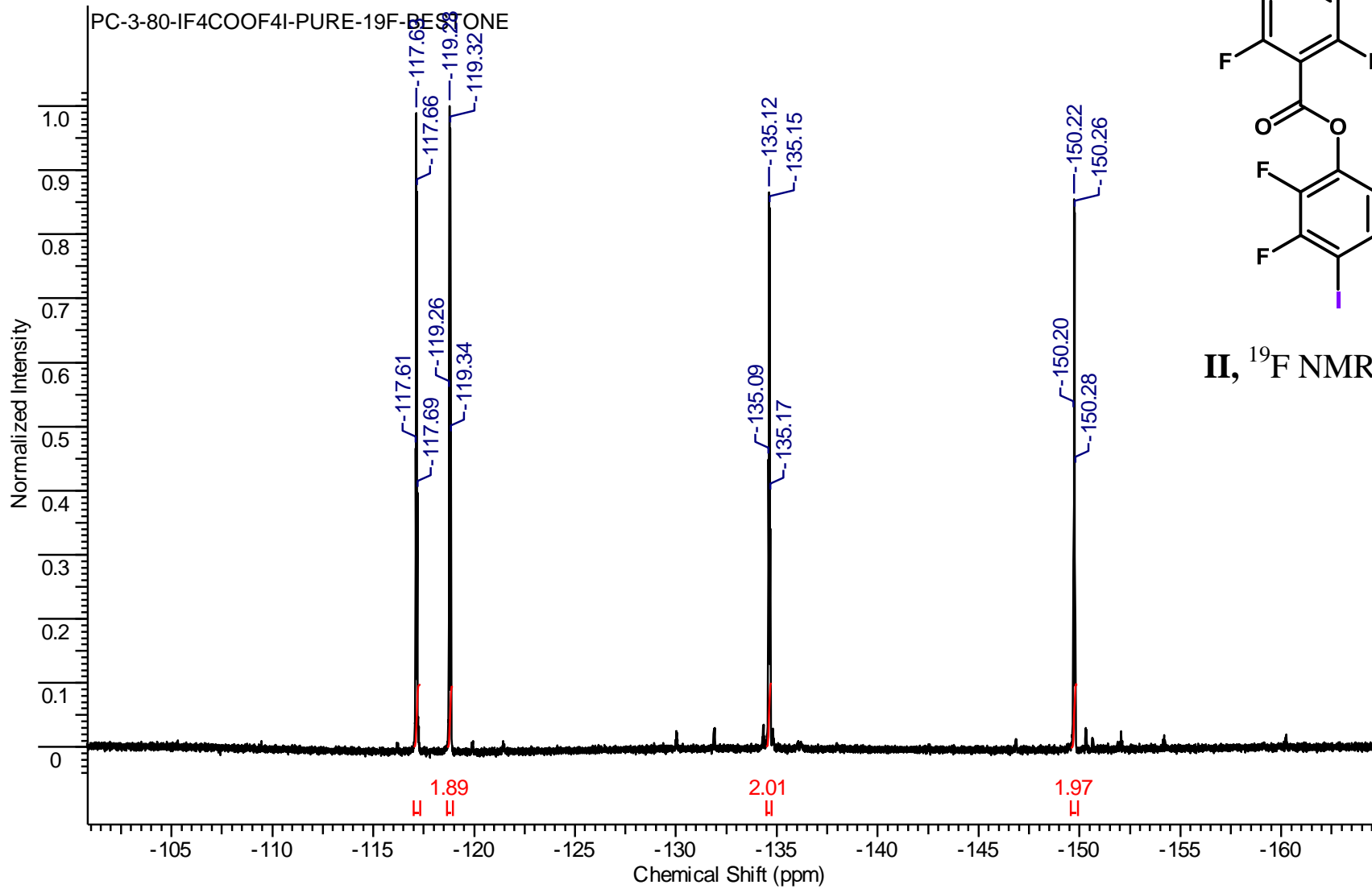


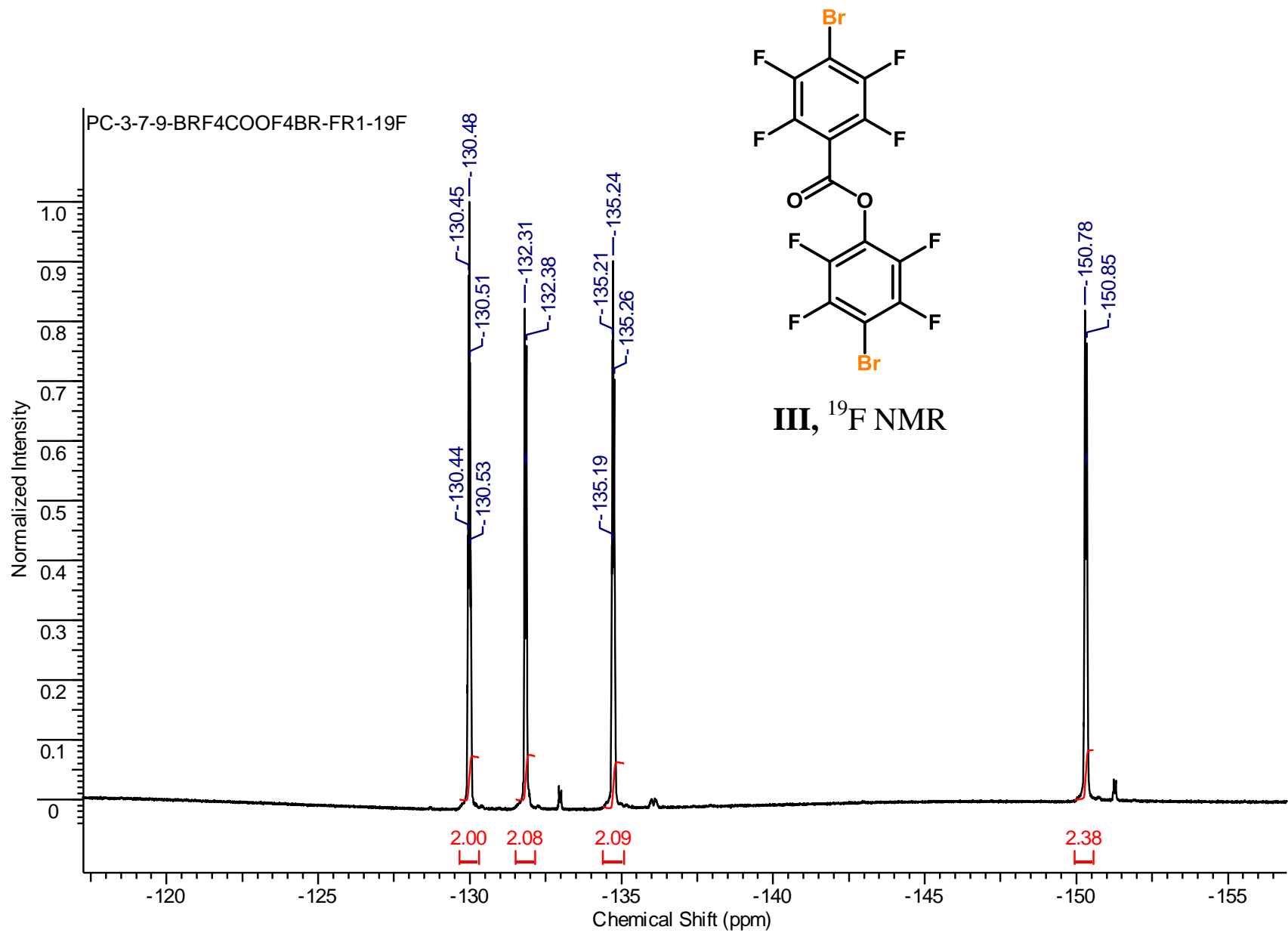


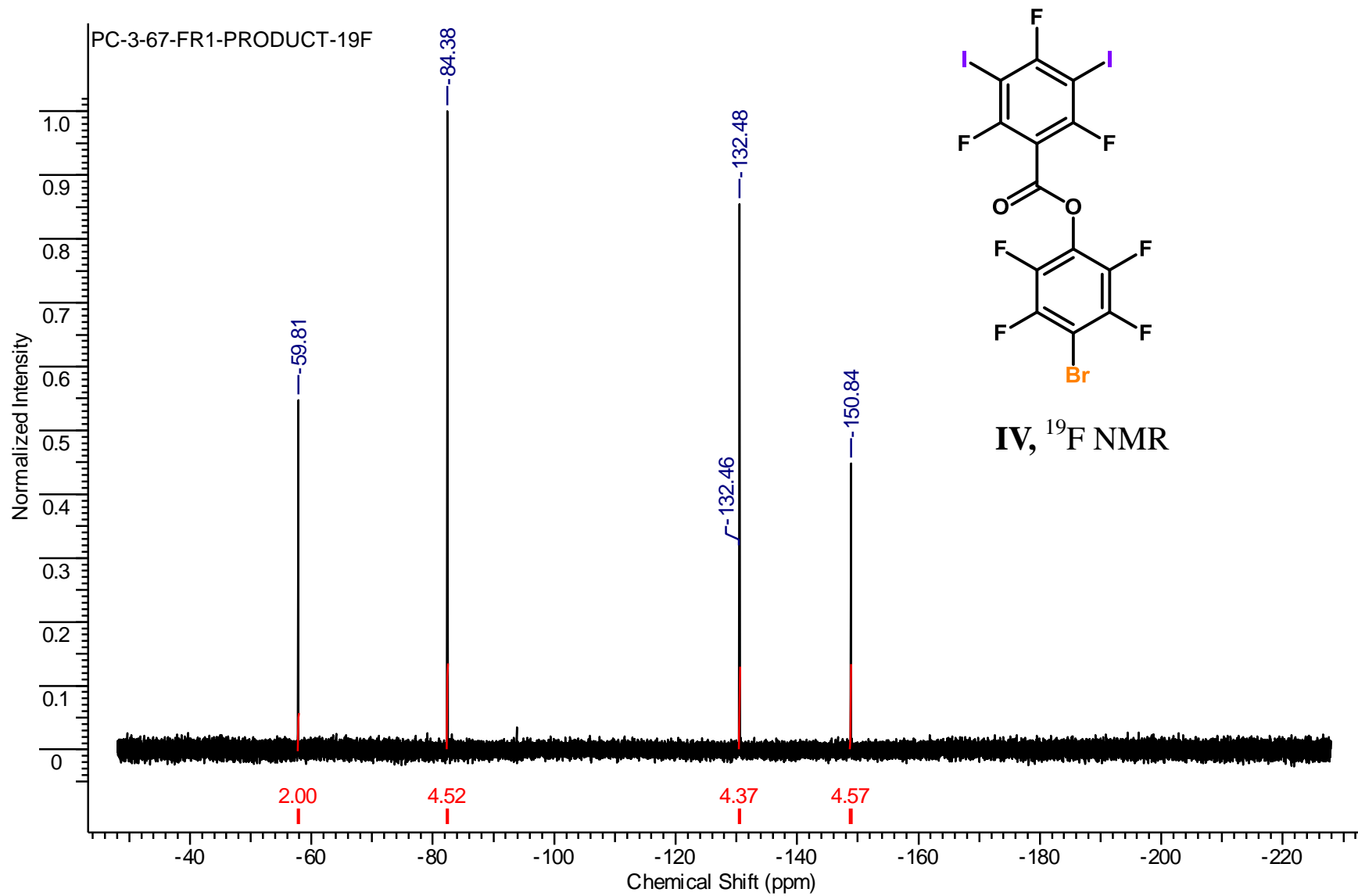


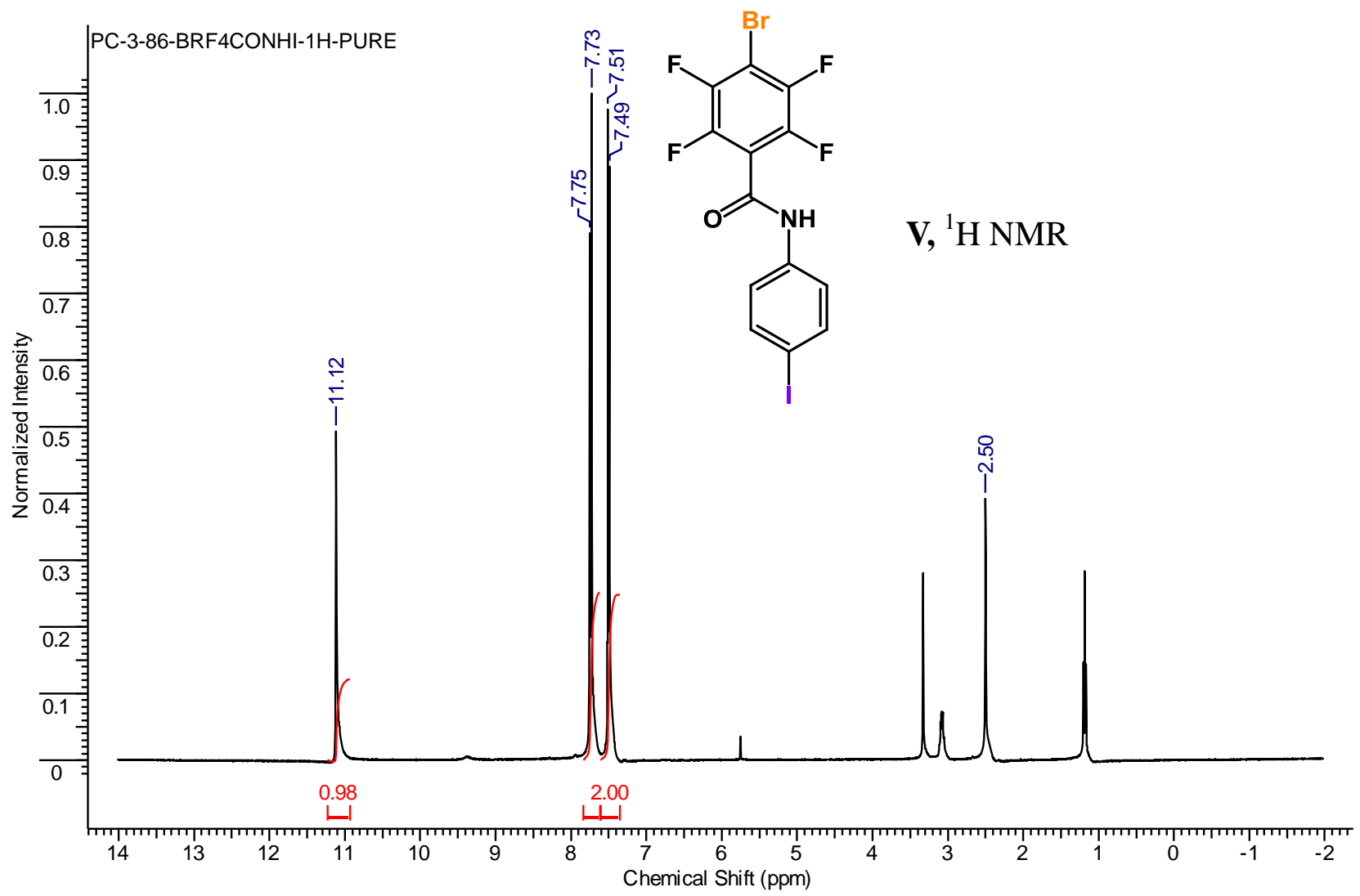




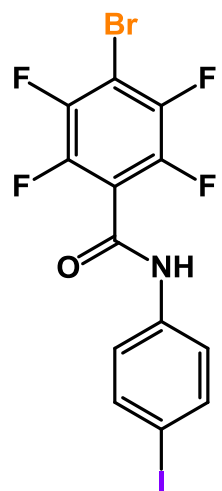




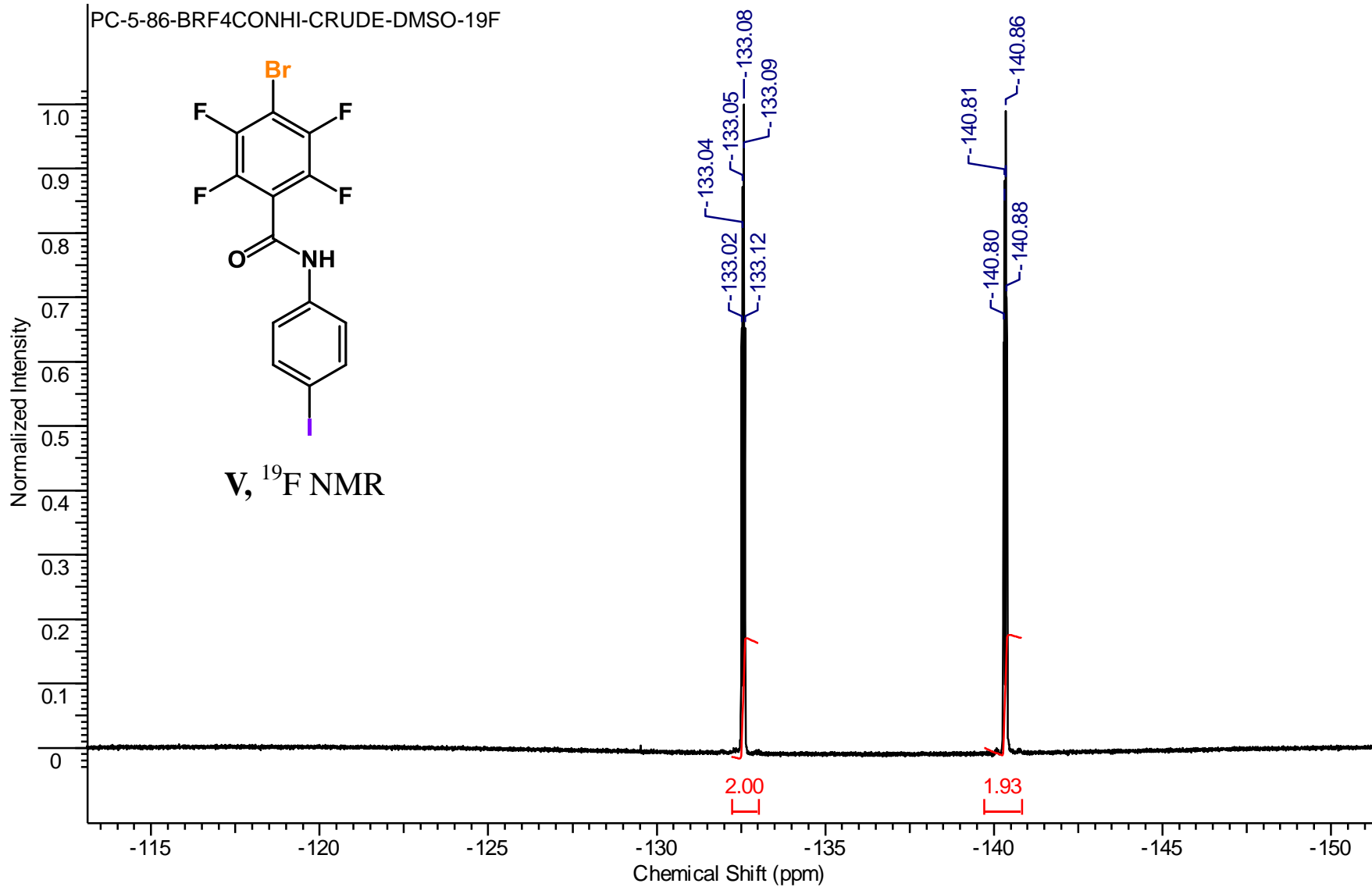


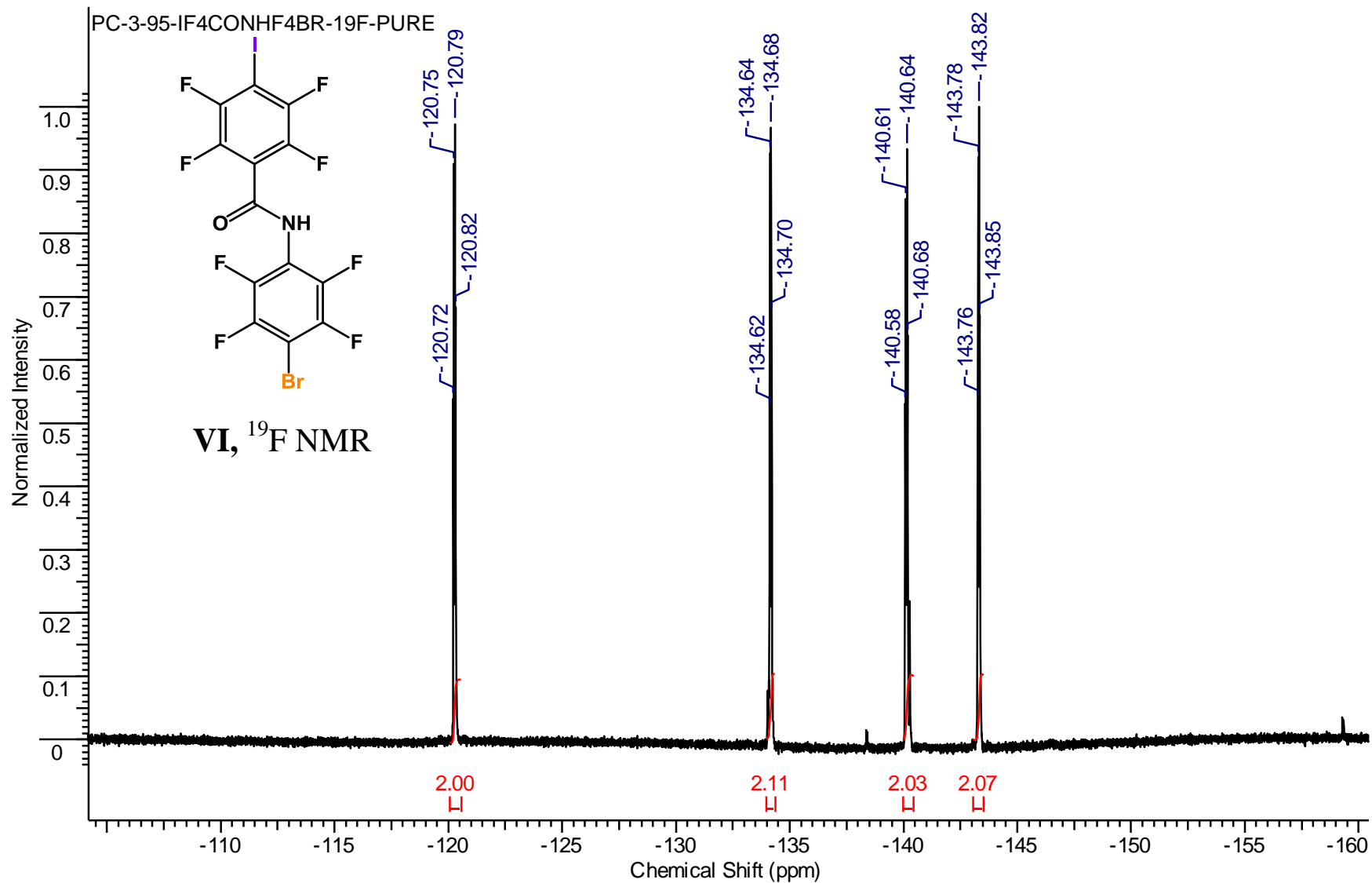


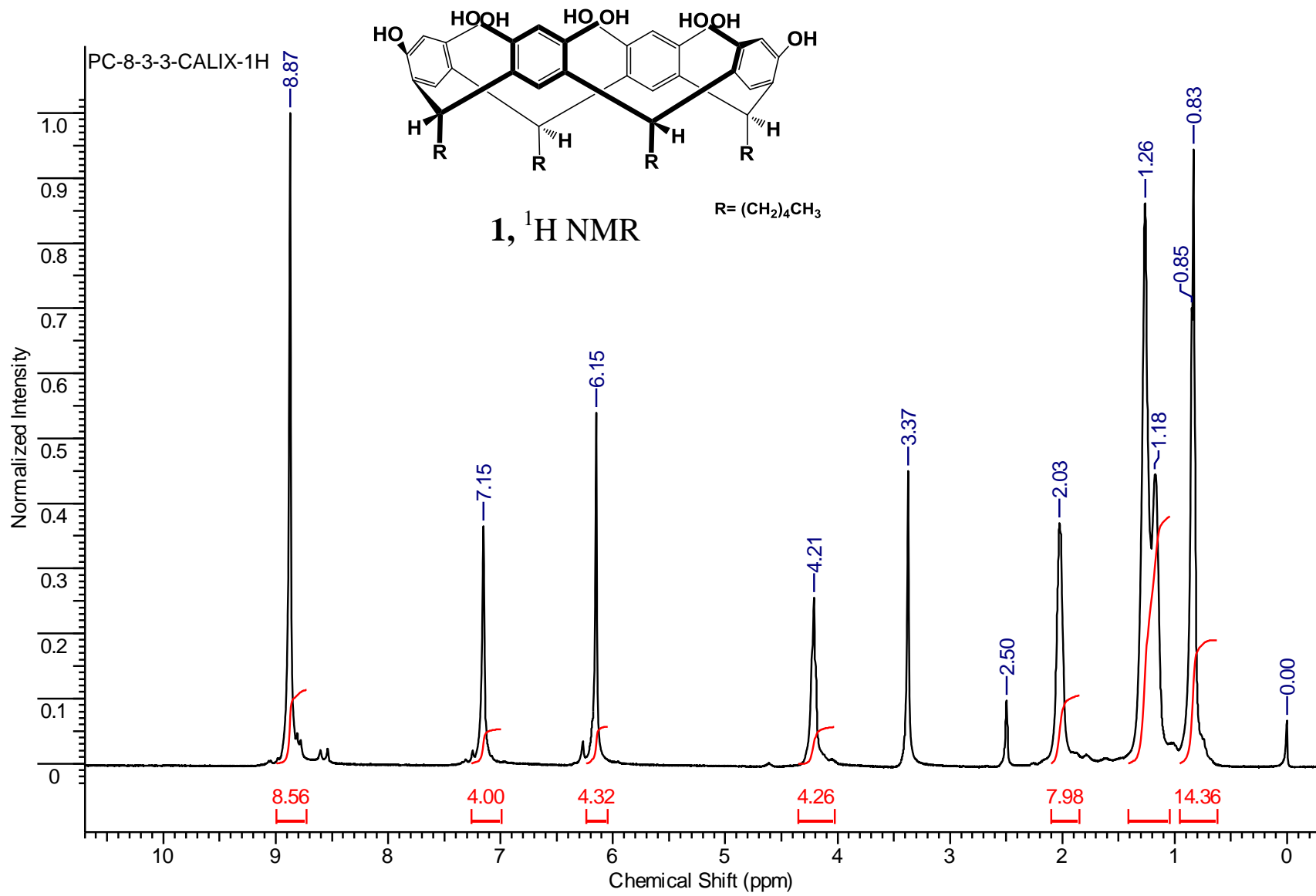
PC-5-86-BRF4CONHI-CRUDE-DMSO-19F

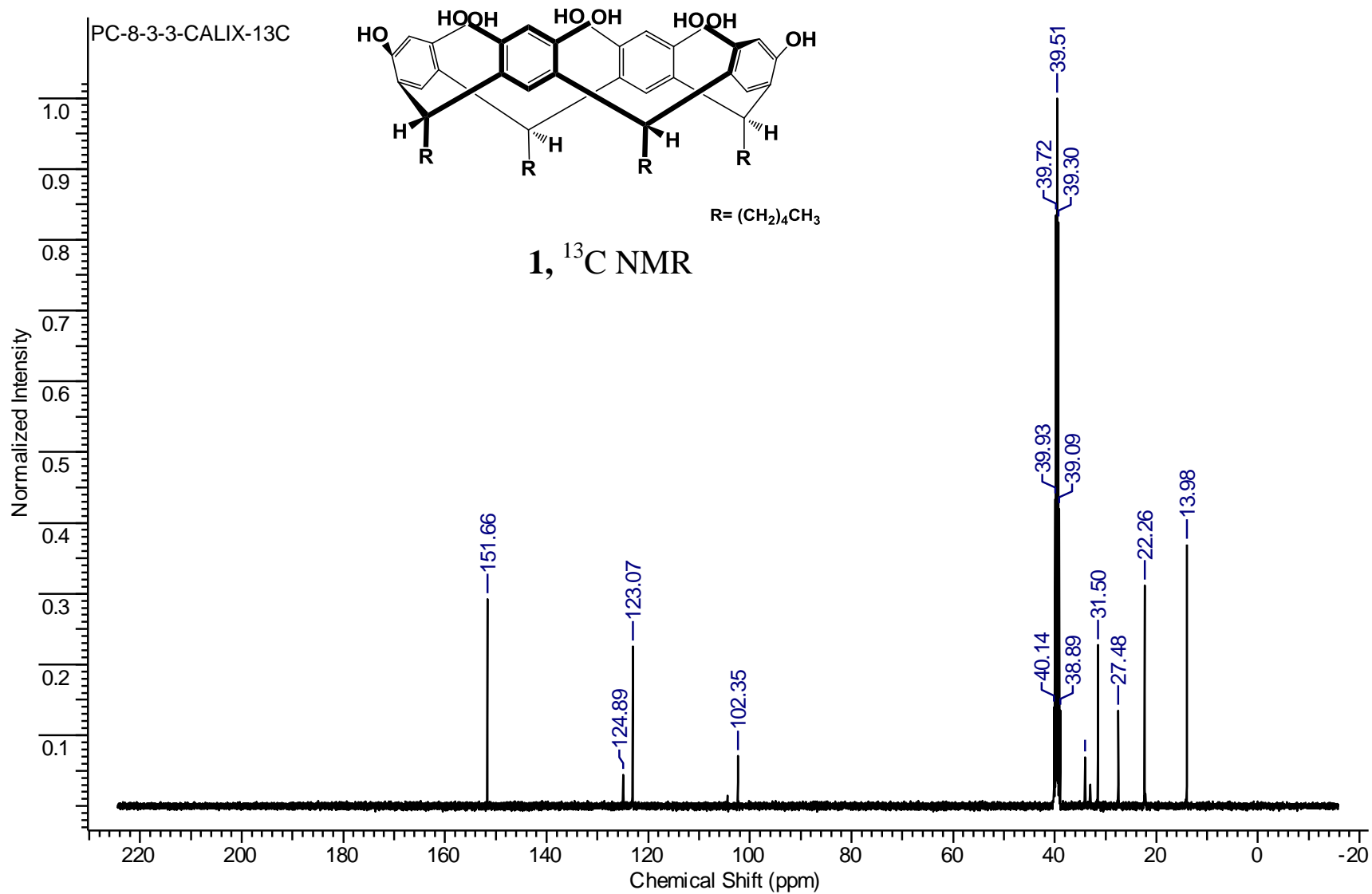


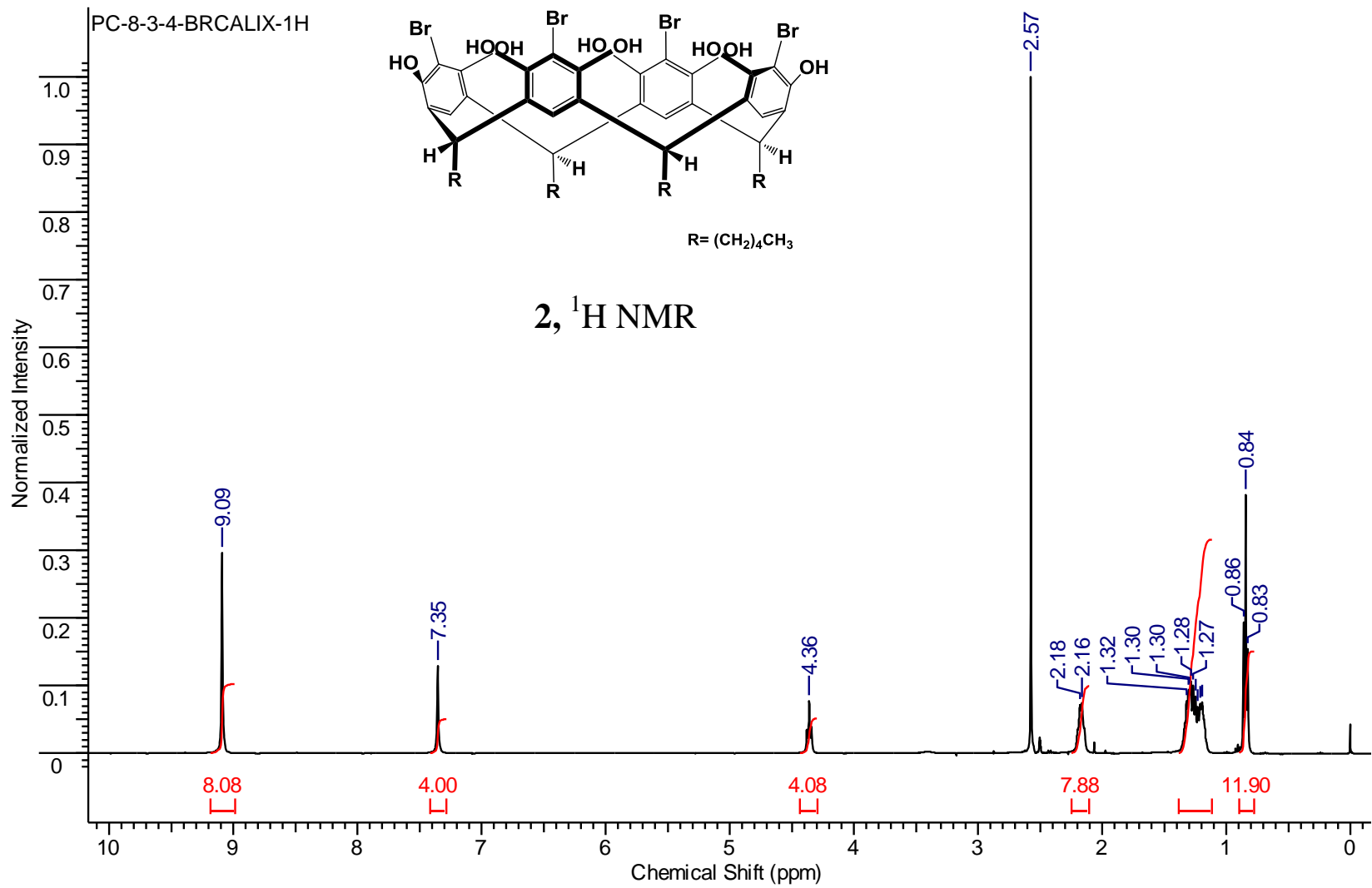
V, ¹⁹F NMR

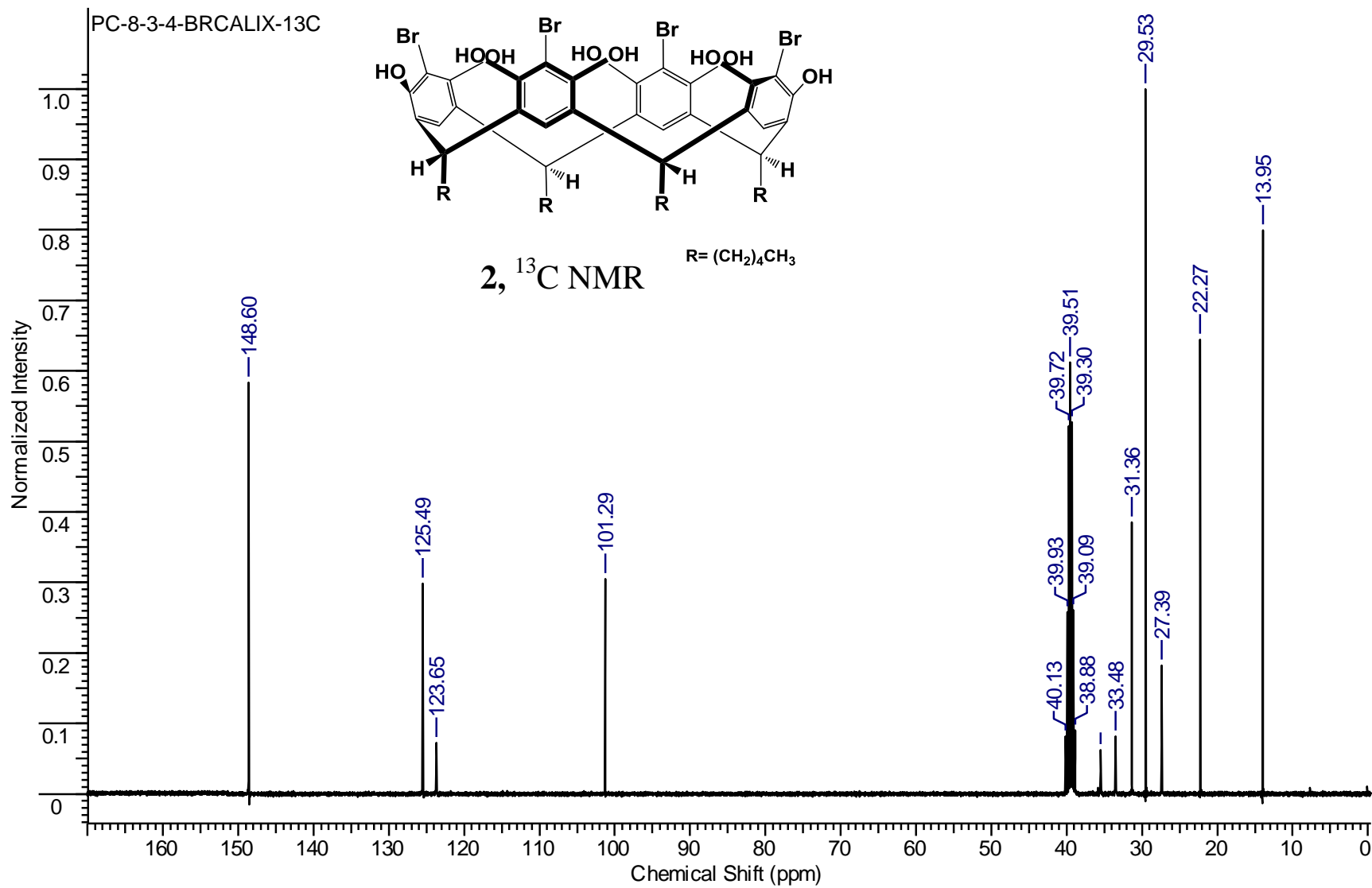


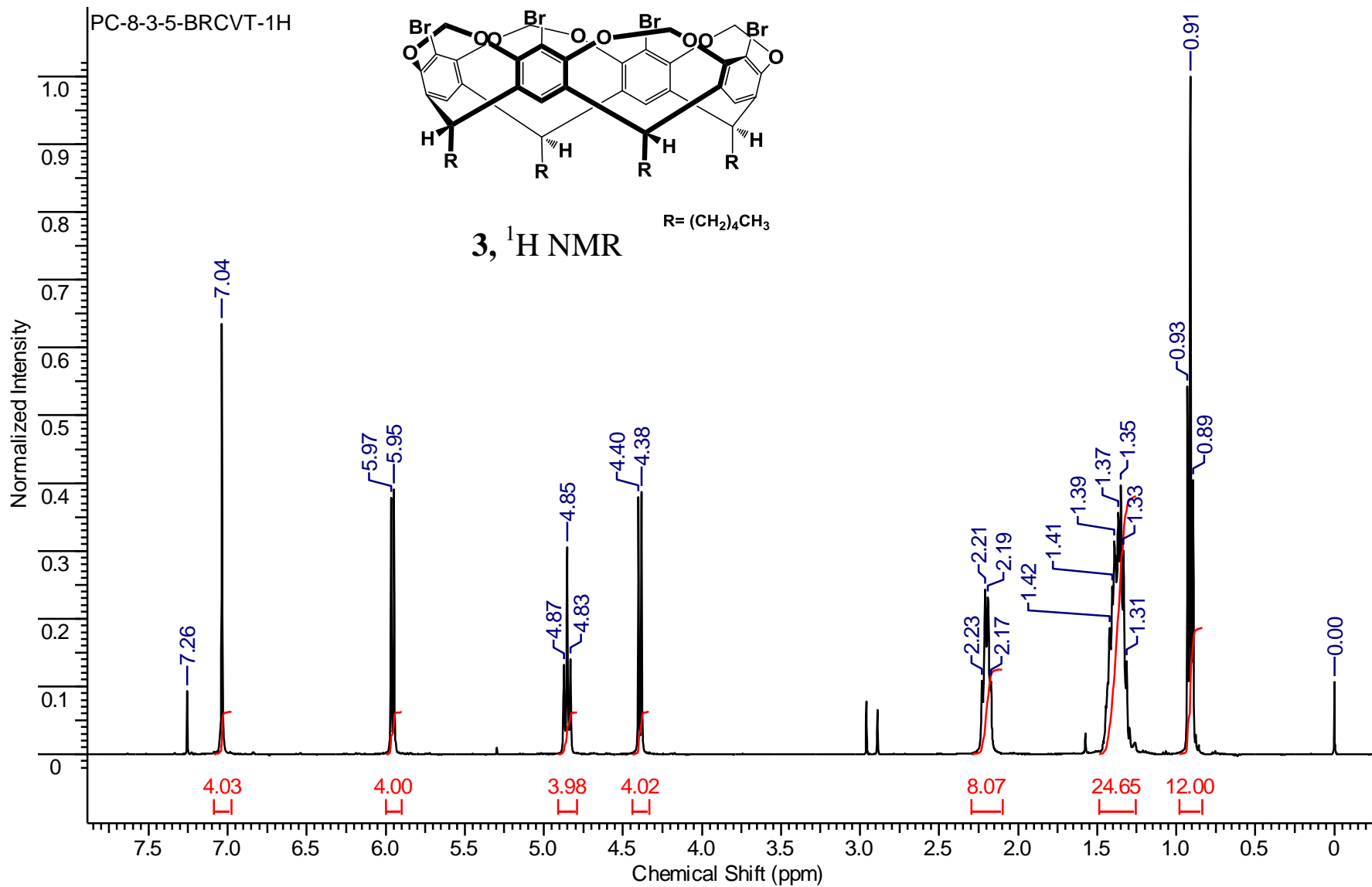


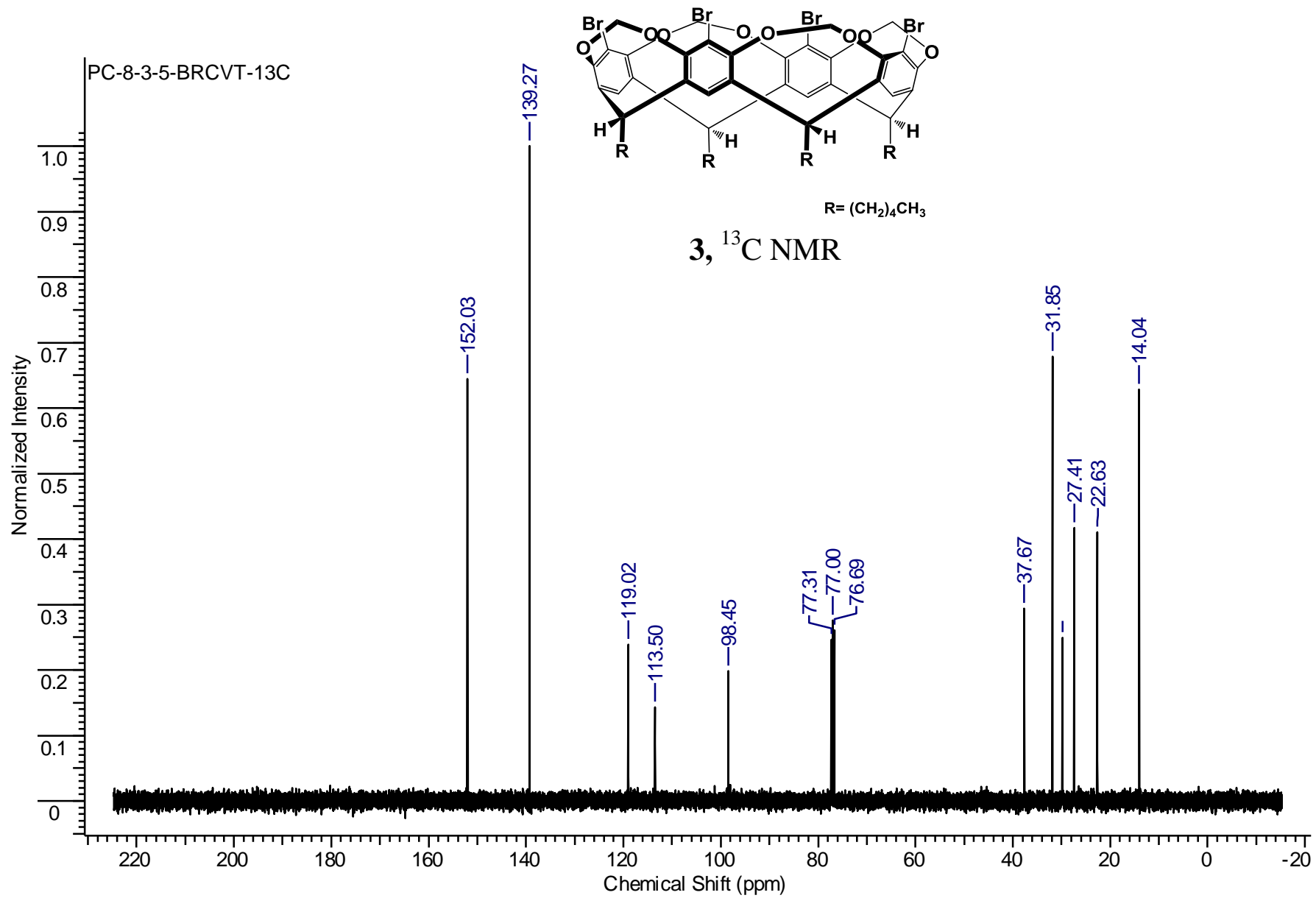


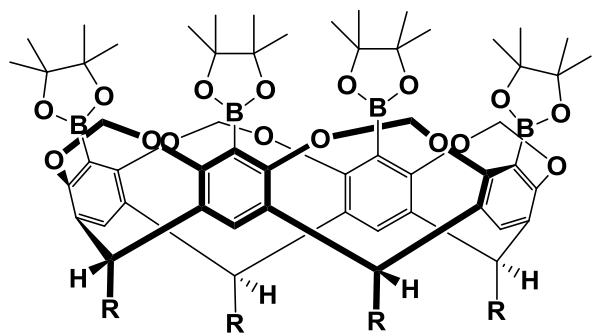




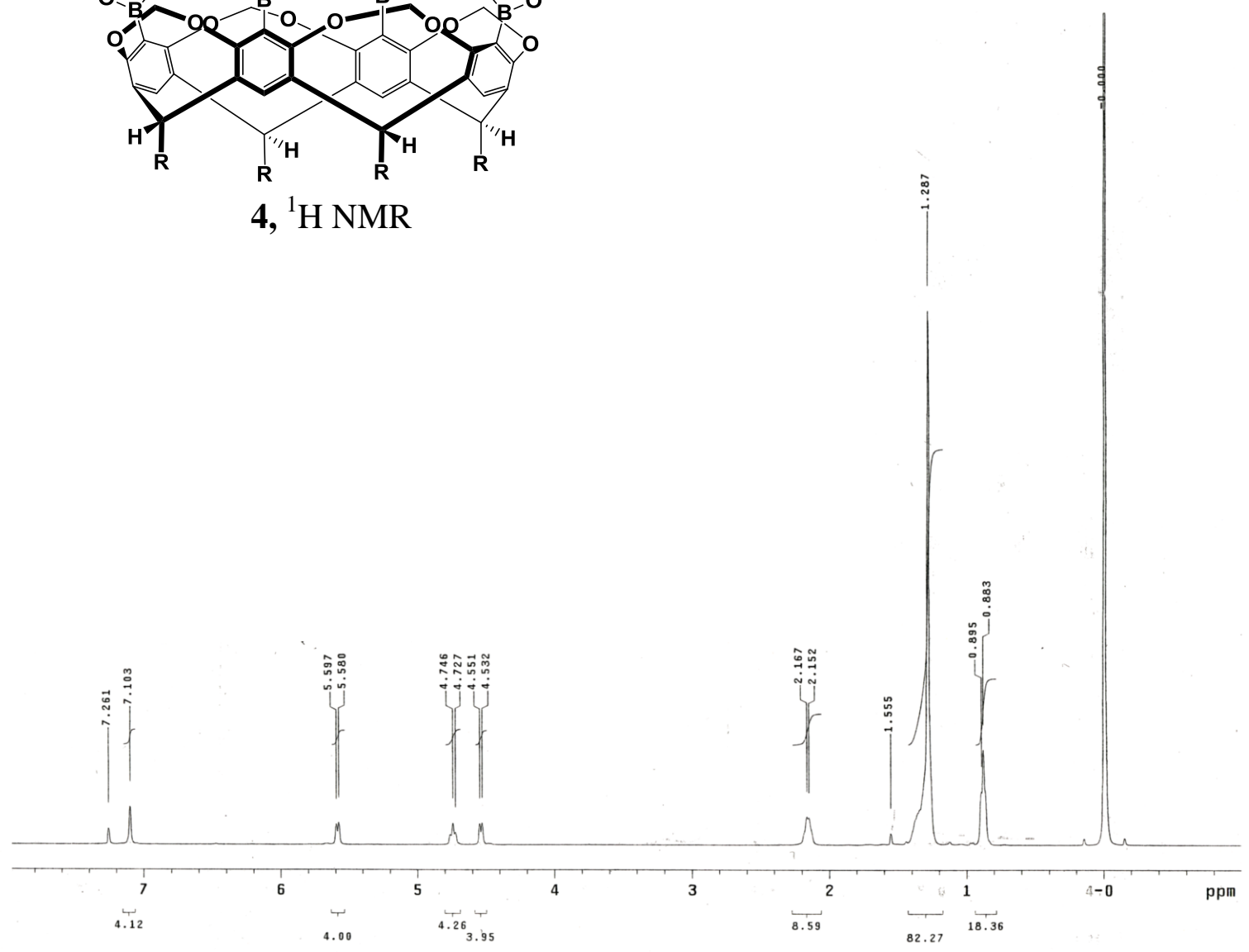


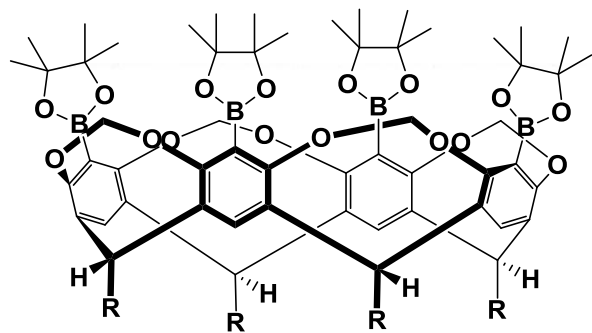




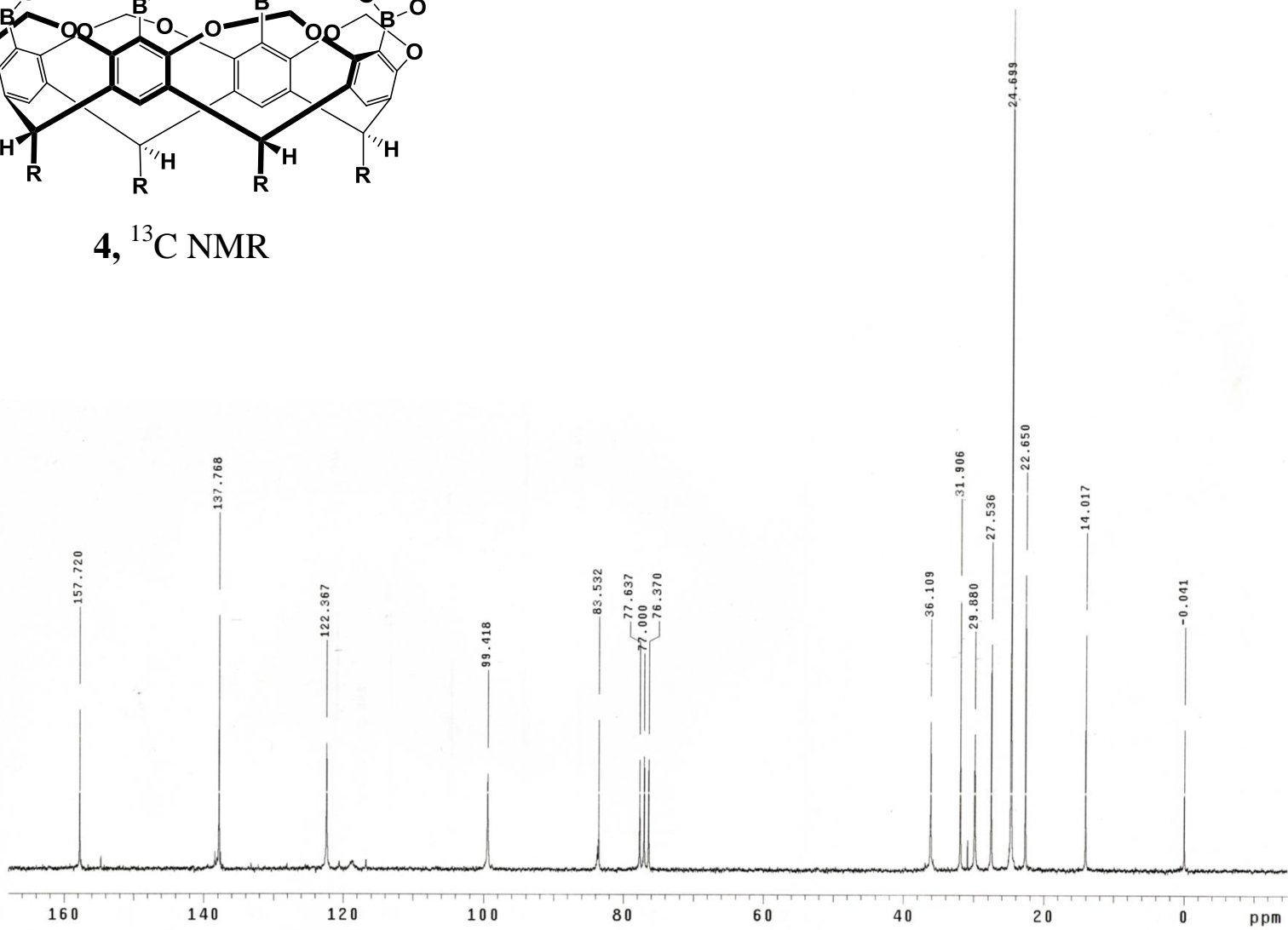


4, ^1H NMR

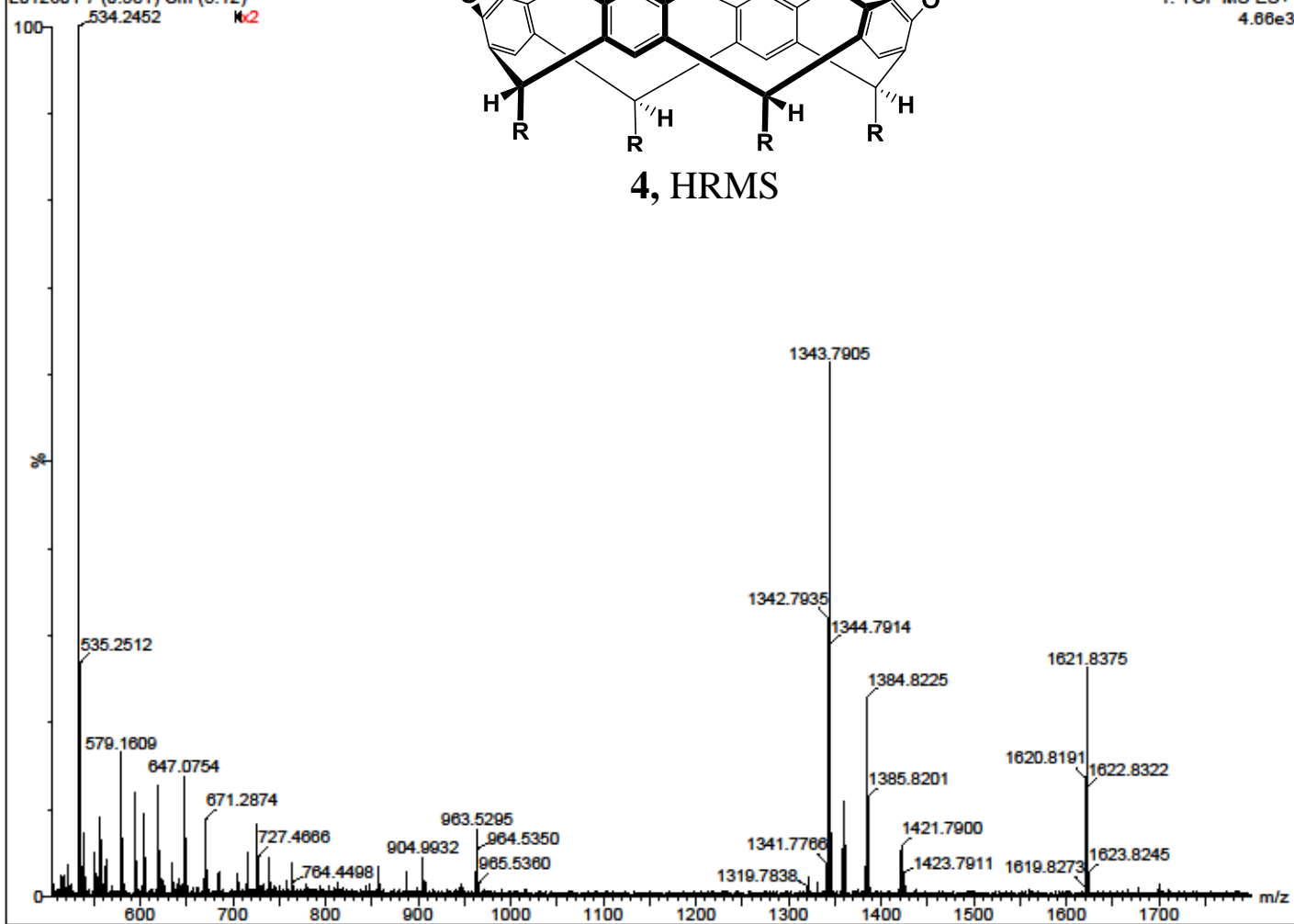




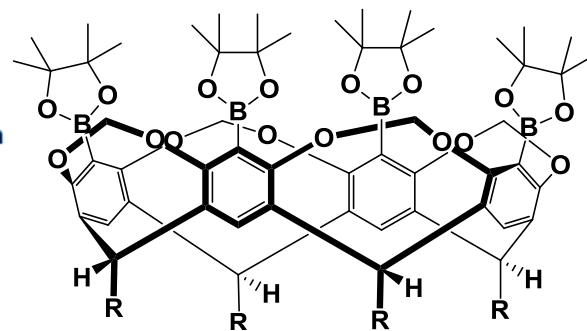
4, ^{13}C NMR



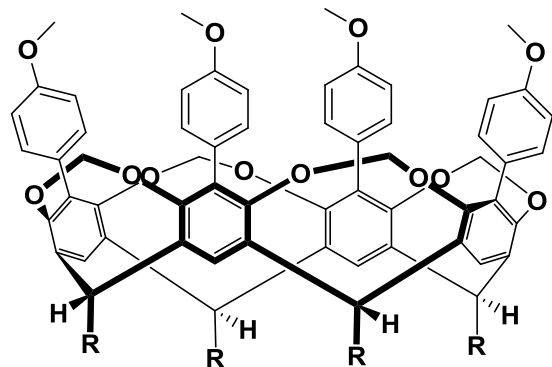
BAesterCVT, P. Chopade, direct injection
L012601 7 (0.381) Cm (5:12)



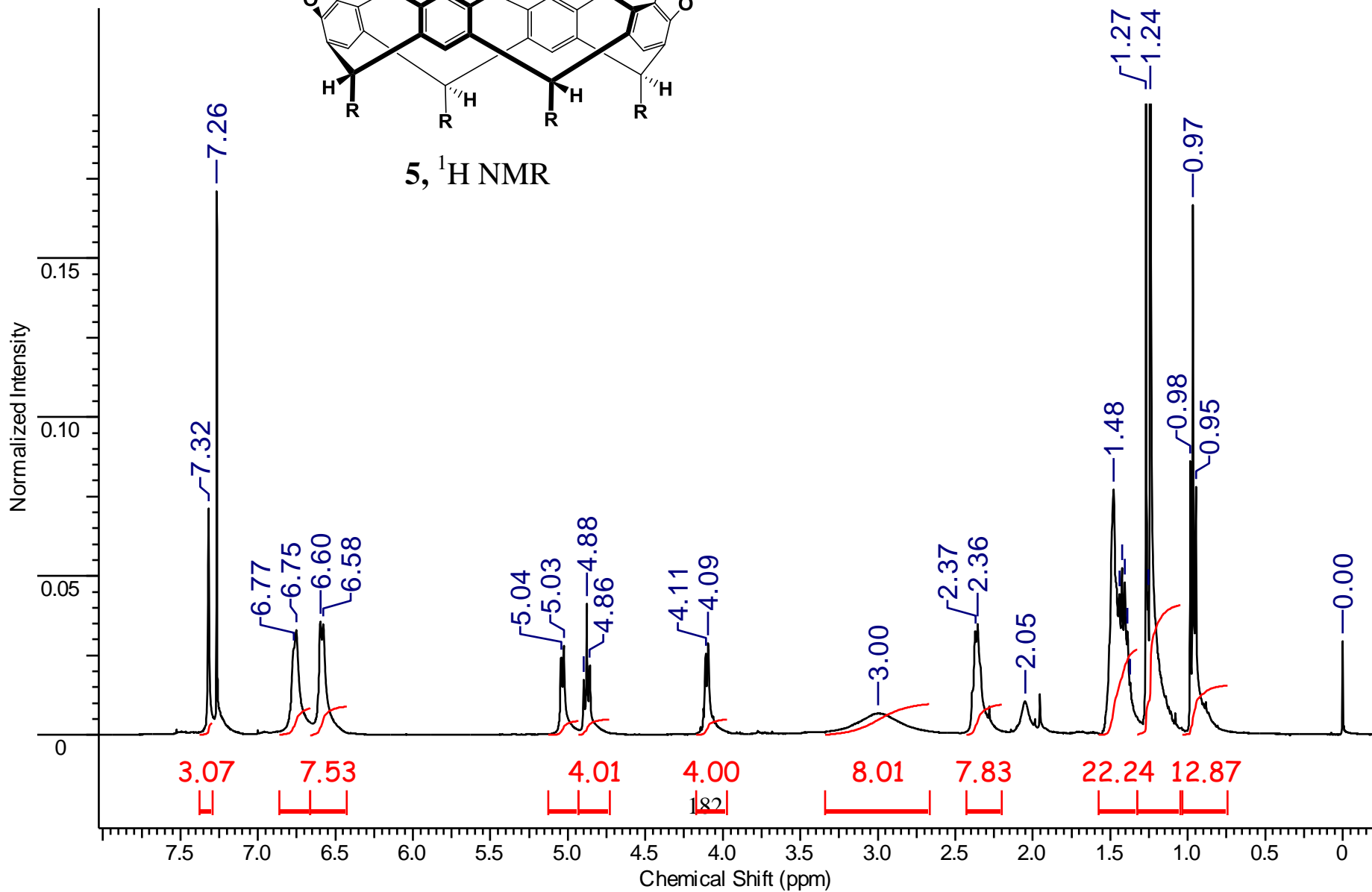
1: TOF MS ES+
4.66e3

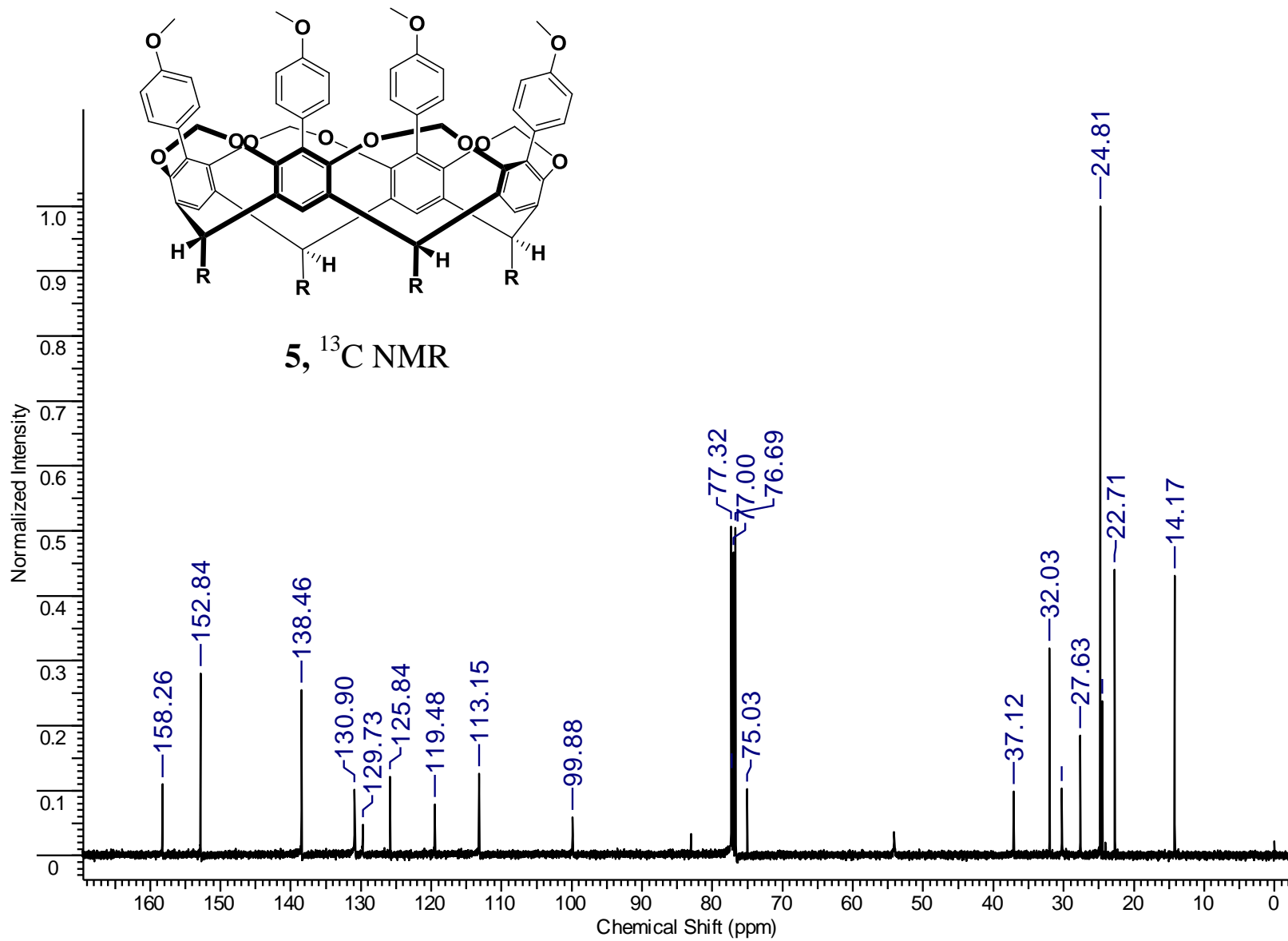


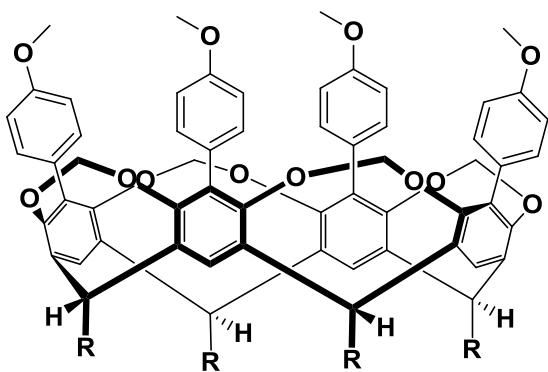
4, HRMS



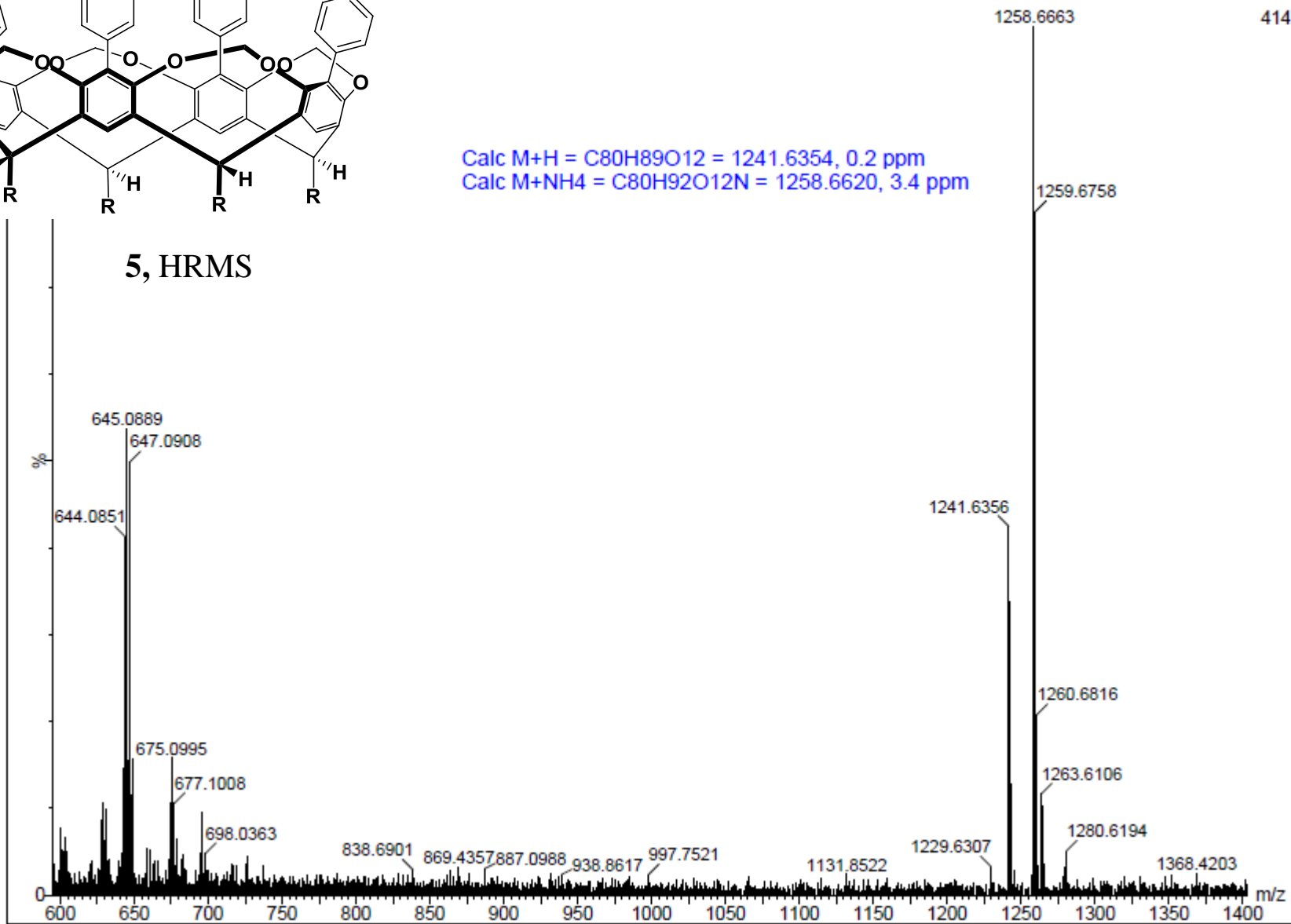
5, ^1H NMR



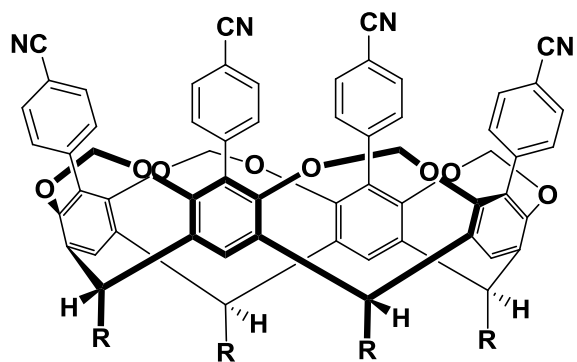




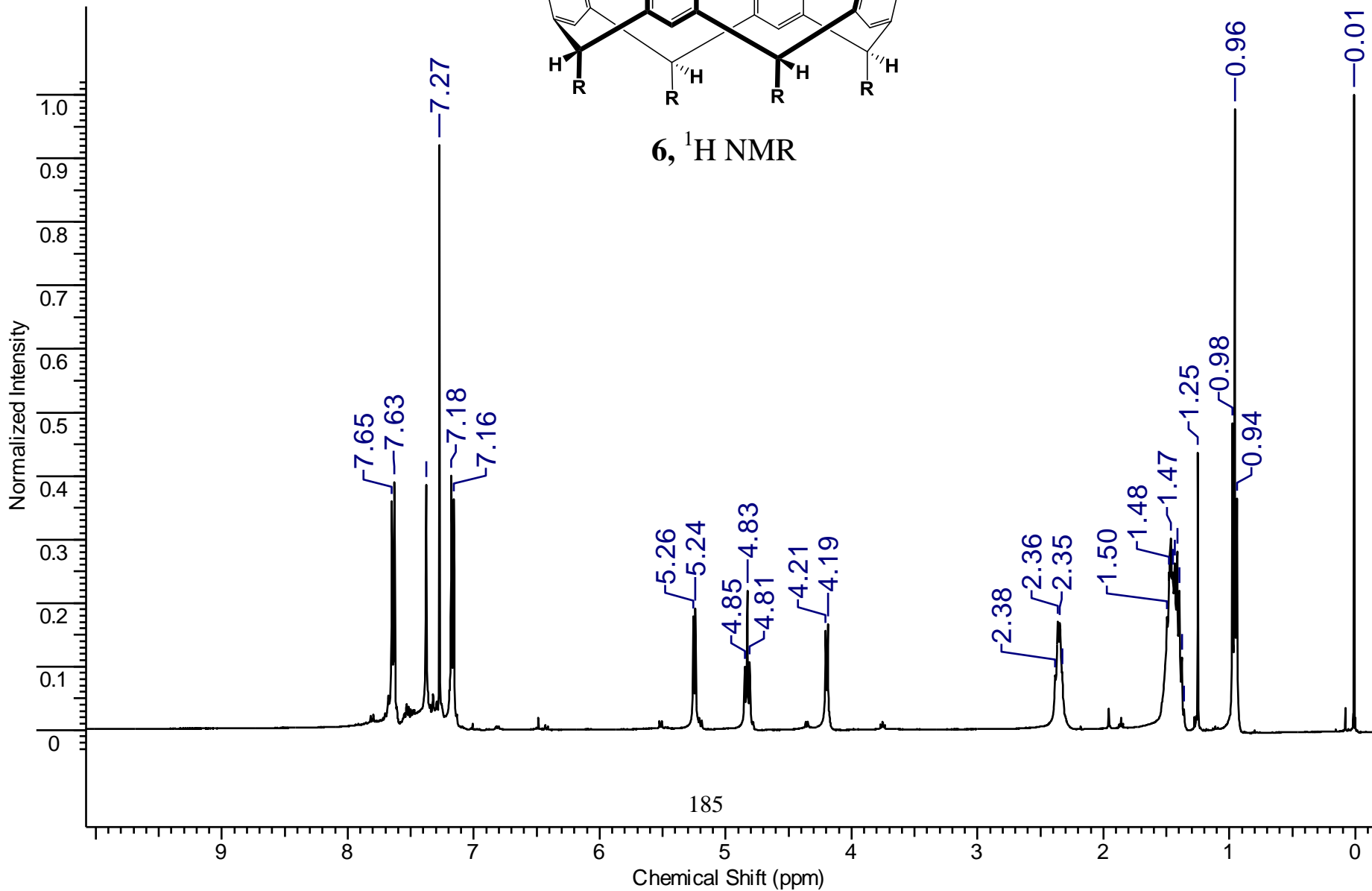
5, HRMS

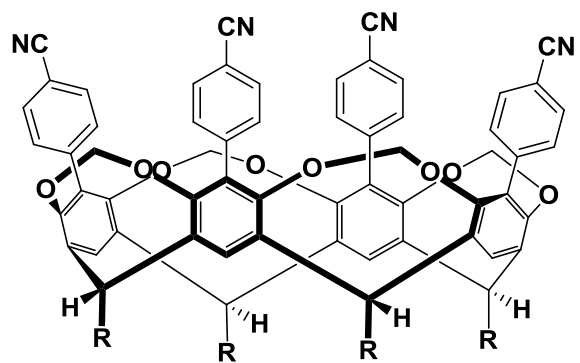


Calc M+H = C₈₀H₈₉O₁₂ = 1241.6354, 0.2 ppm
 Calc M+NH₄ = C₈₀H₉₂O₁₂N = 1258.6620, 3.4 ppm

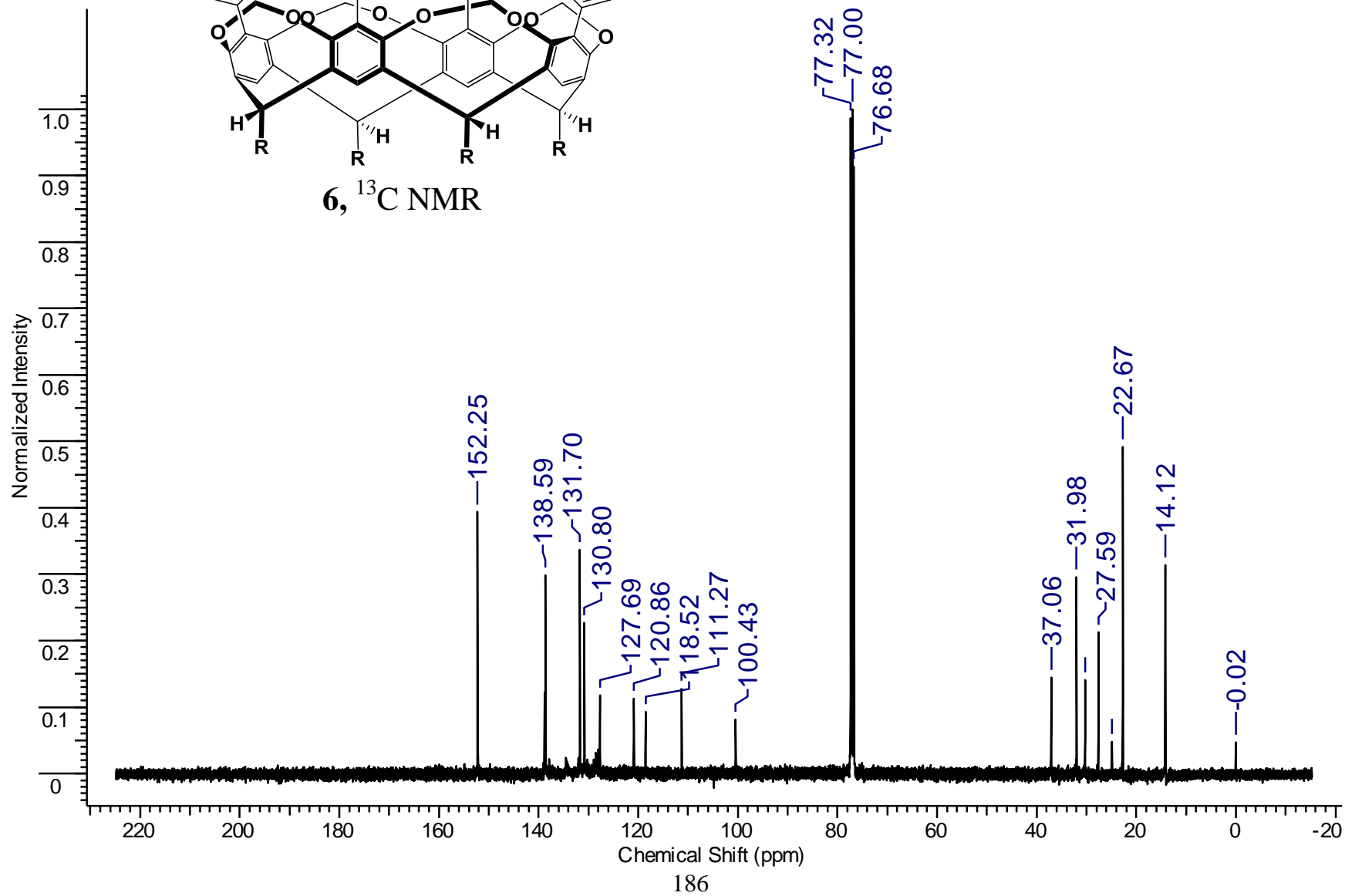


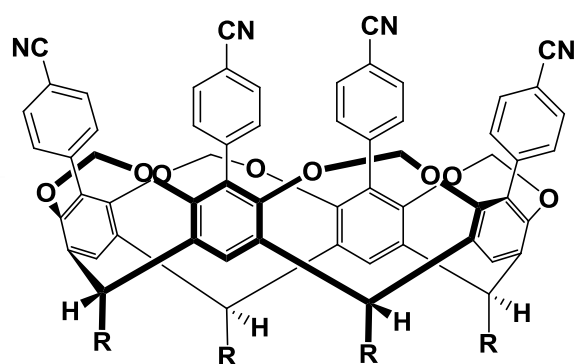
6, ^1H NMR



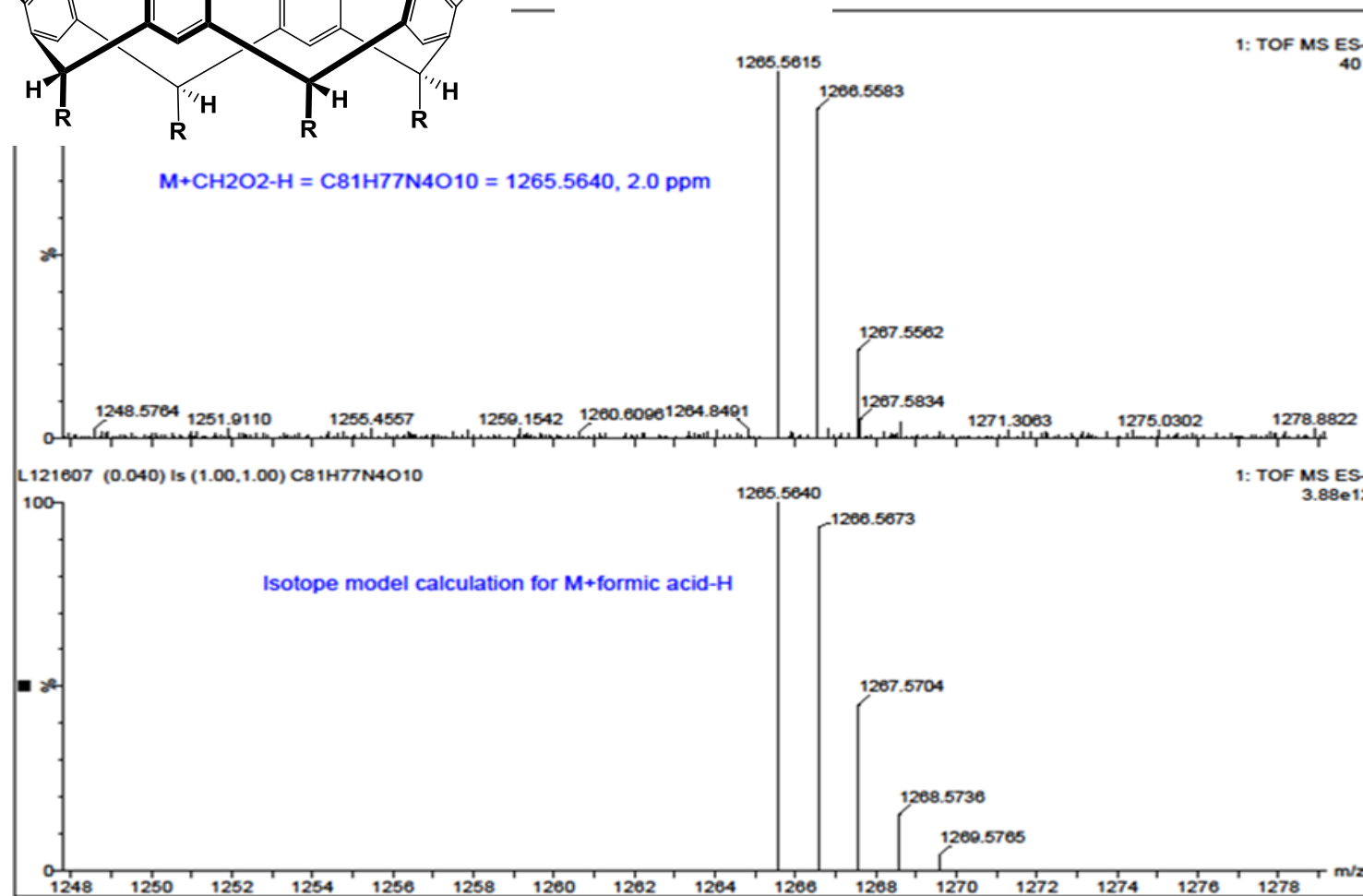


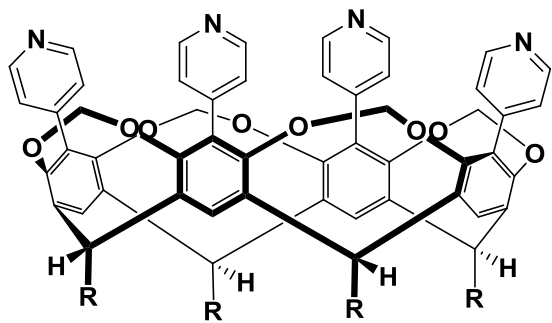
6, ^{13}C NMR



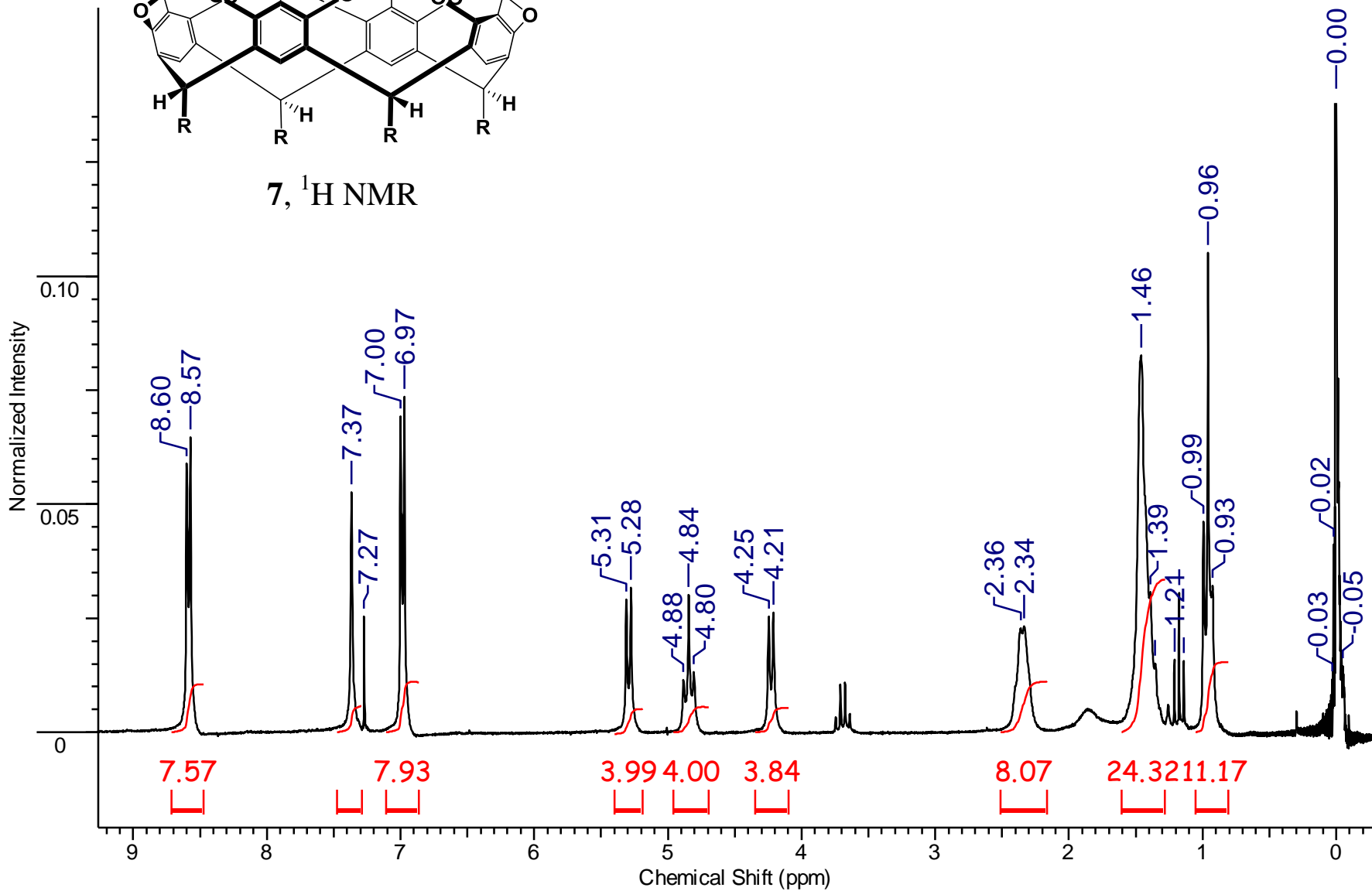


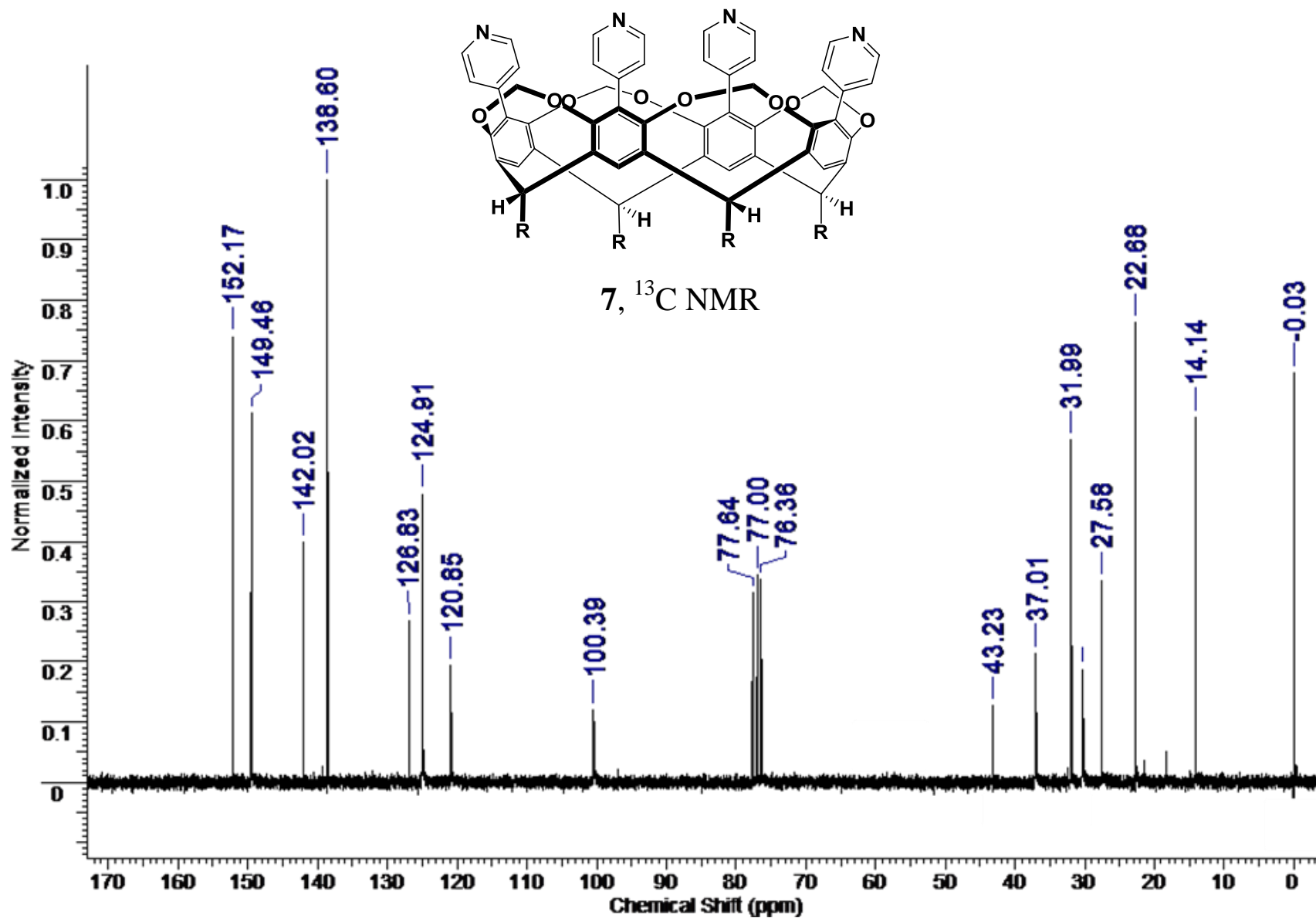
6, HRMS

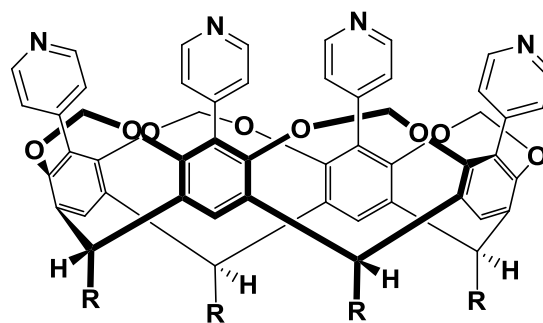




7, ^1H NMR

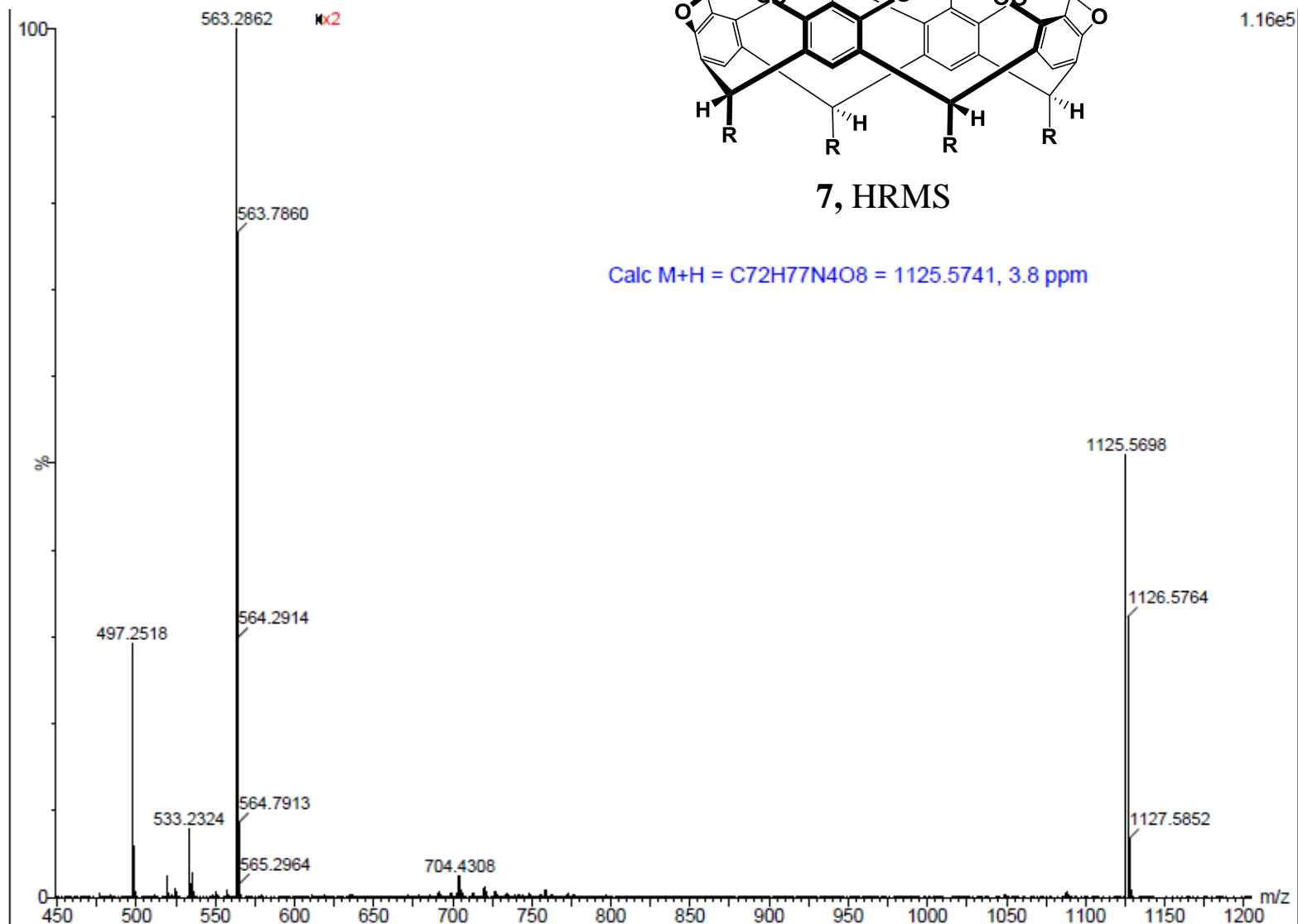


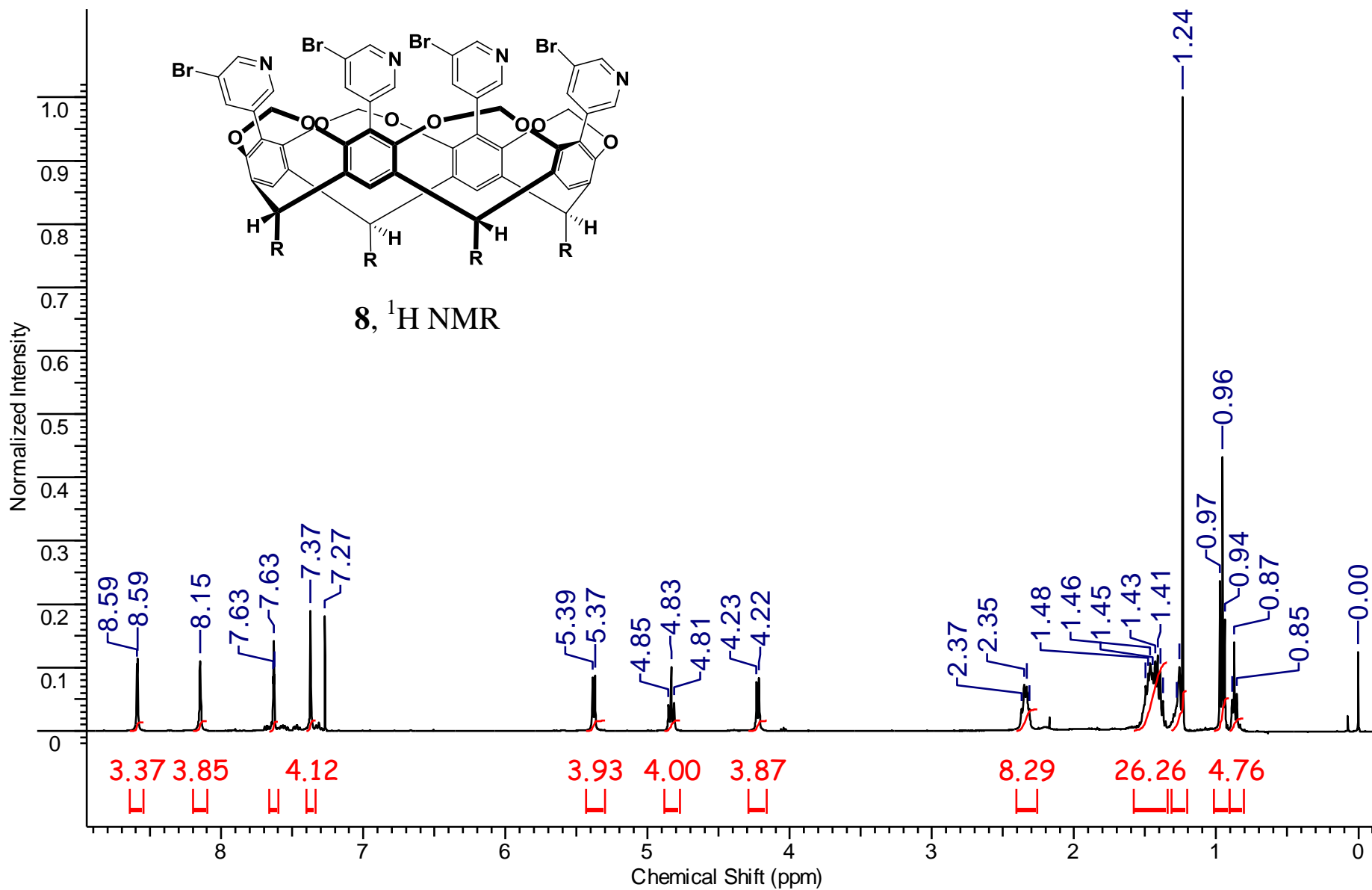


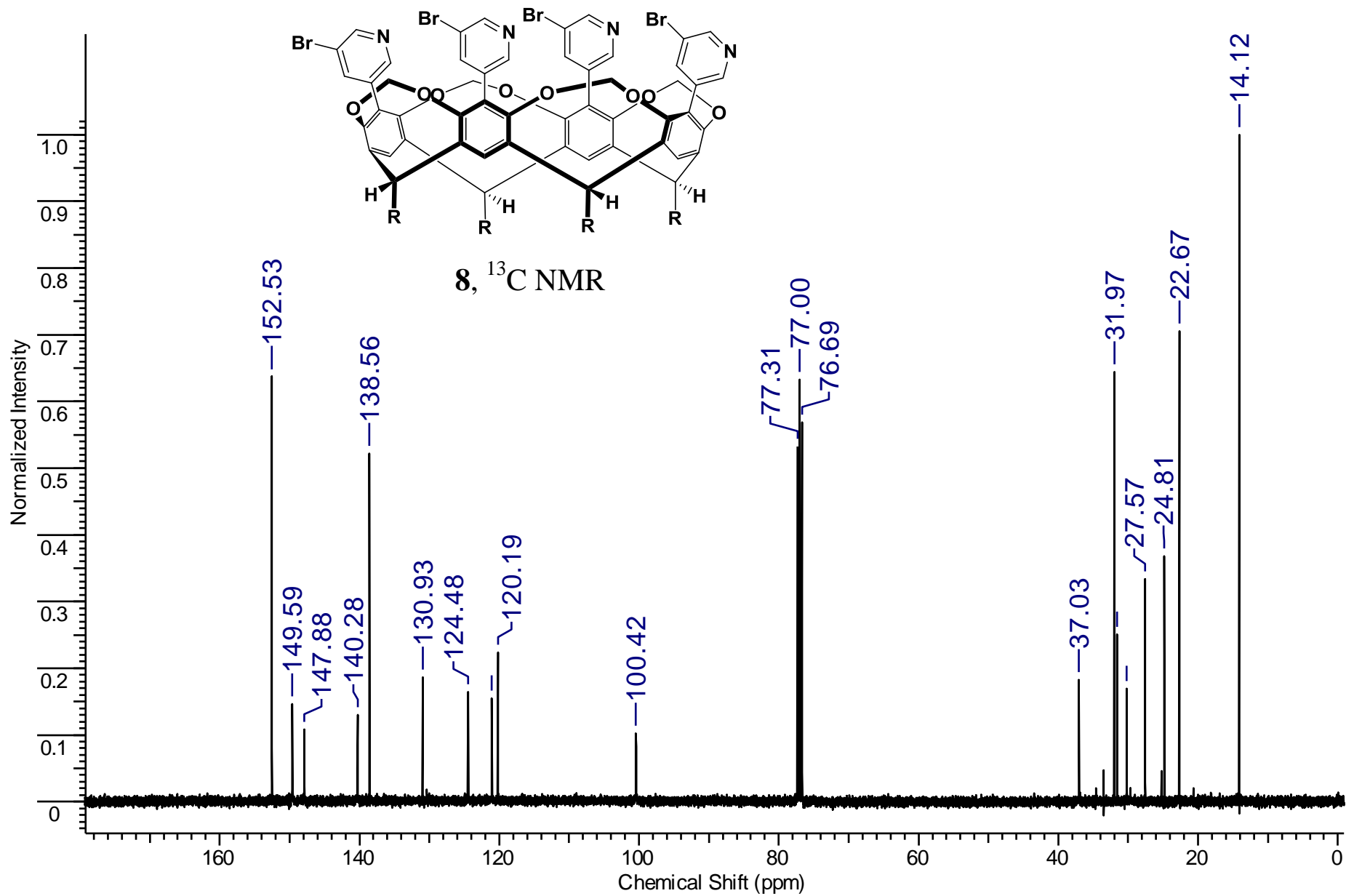


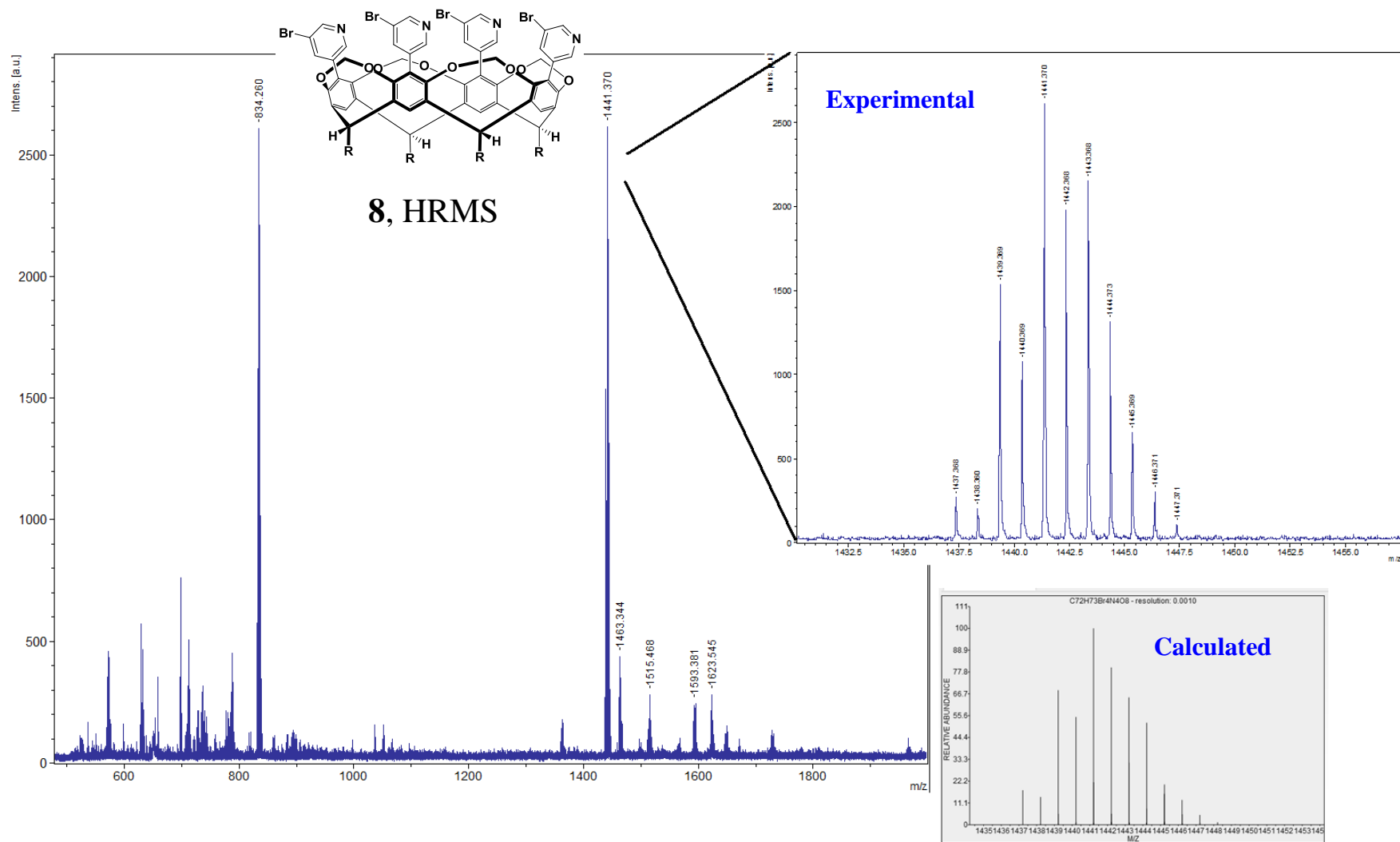
7, HRMS

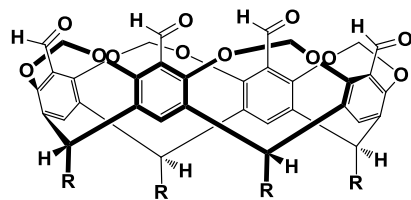
Calc M+H = C₇₂H₇₇N₄O₈ = 1125.5741, 3.8 ppm



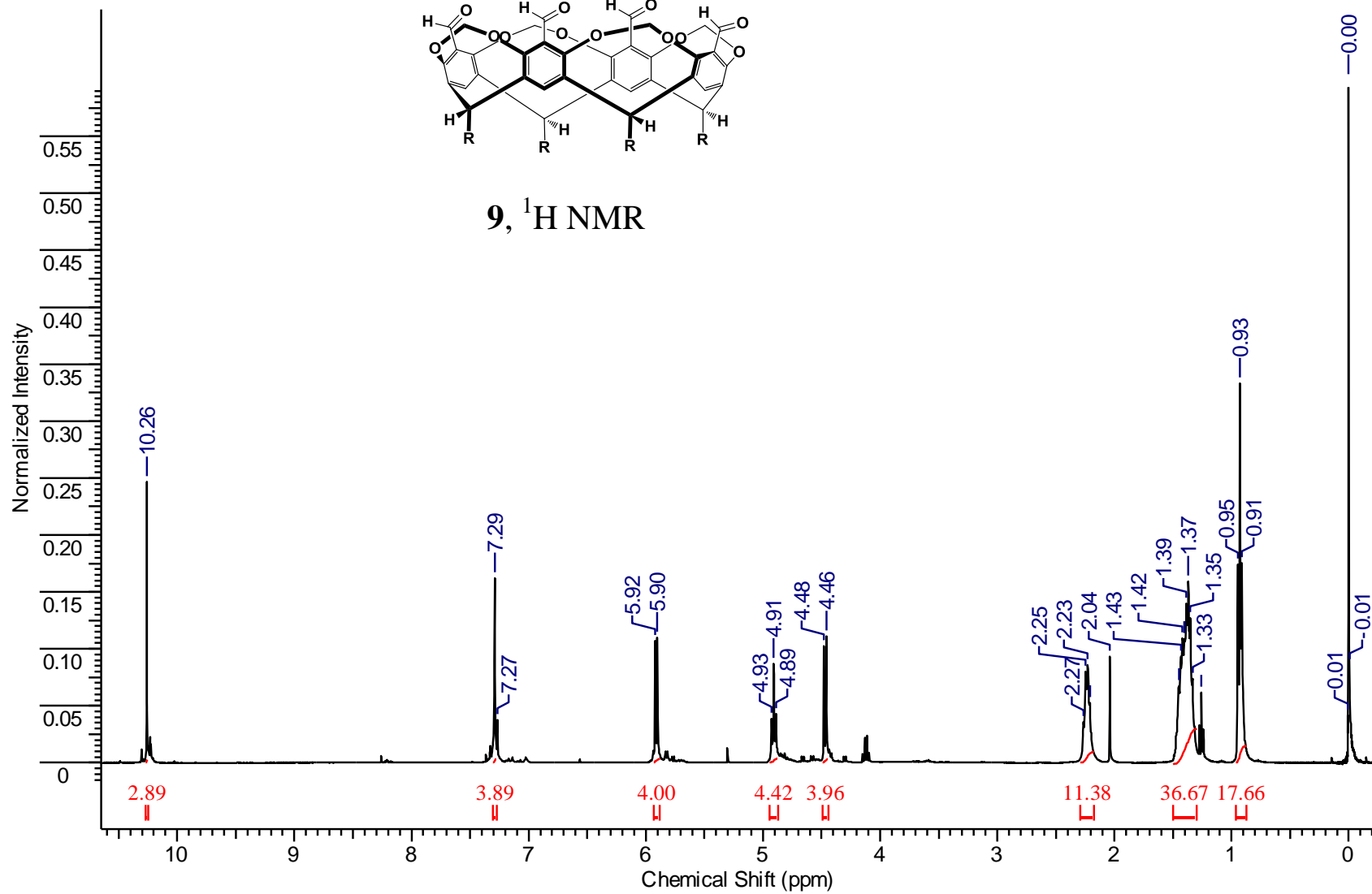


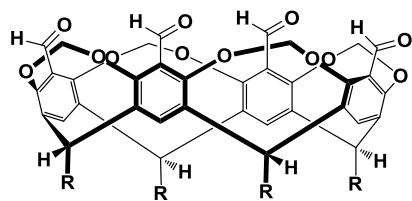




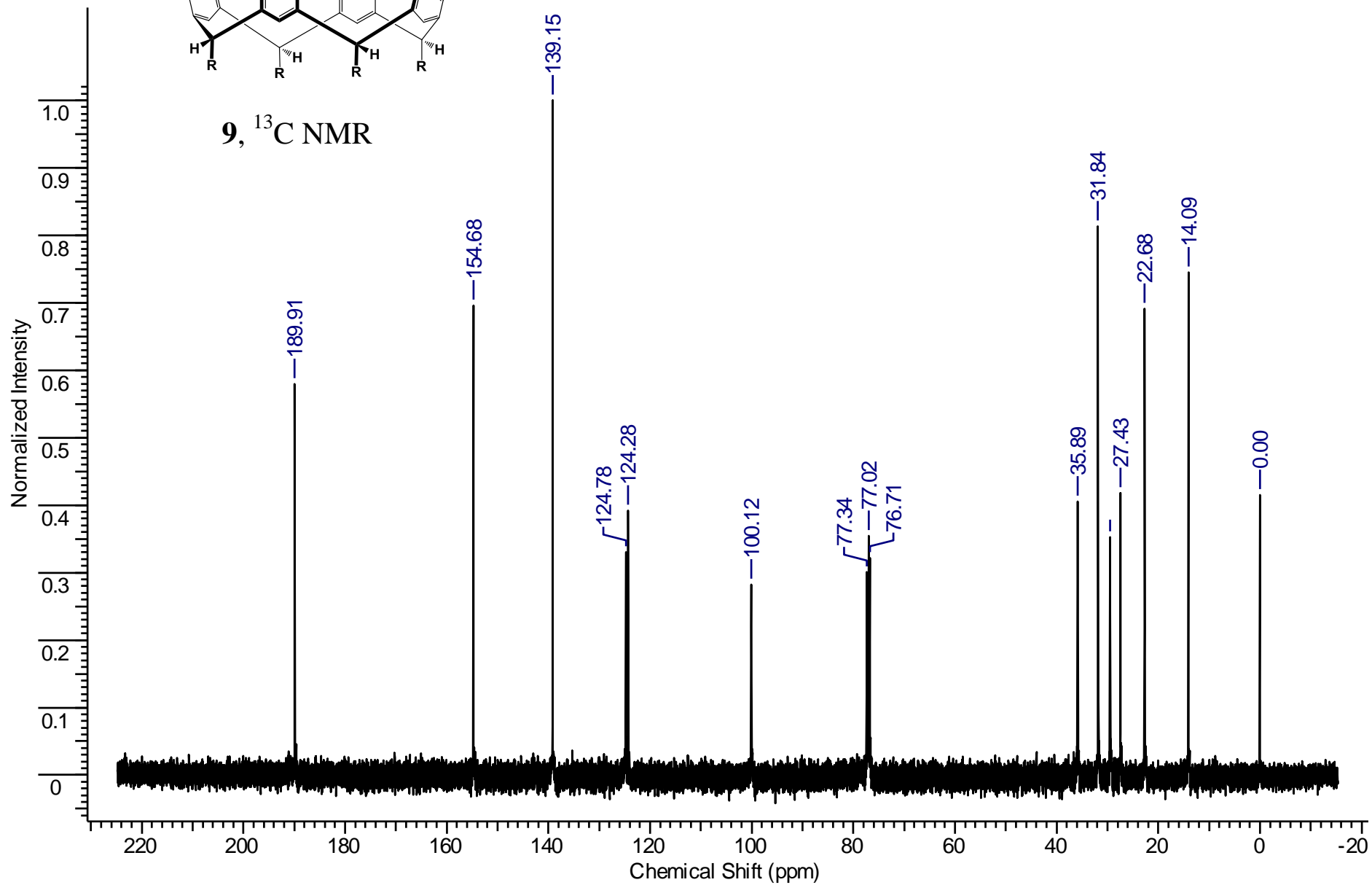


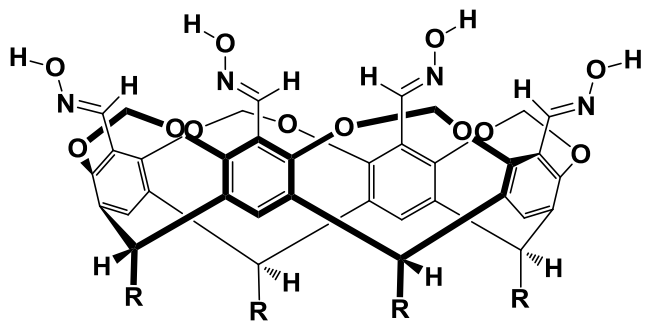
9, ^1H NMR



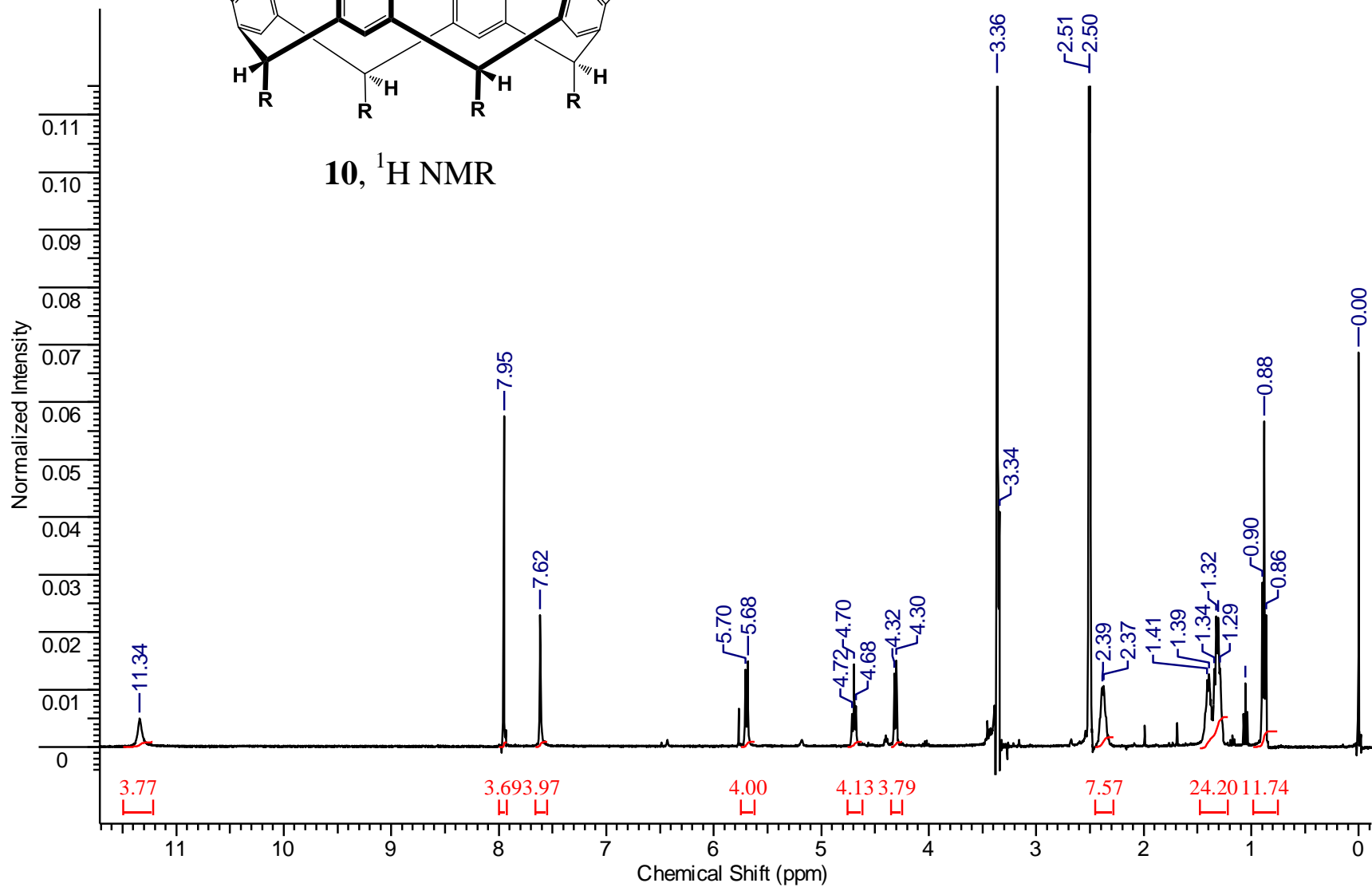


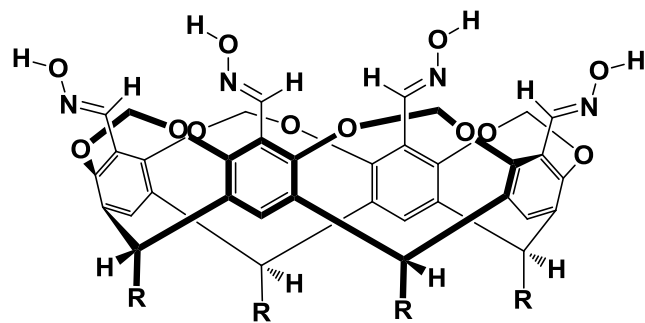
9, ^{13}C NMR



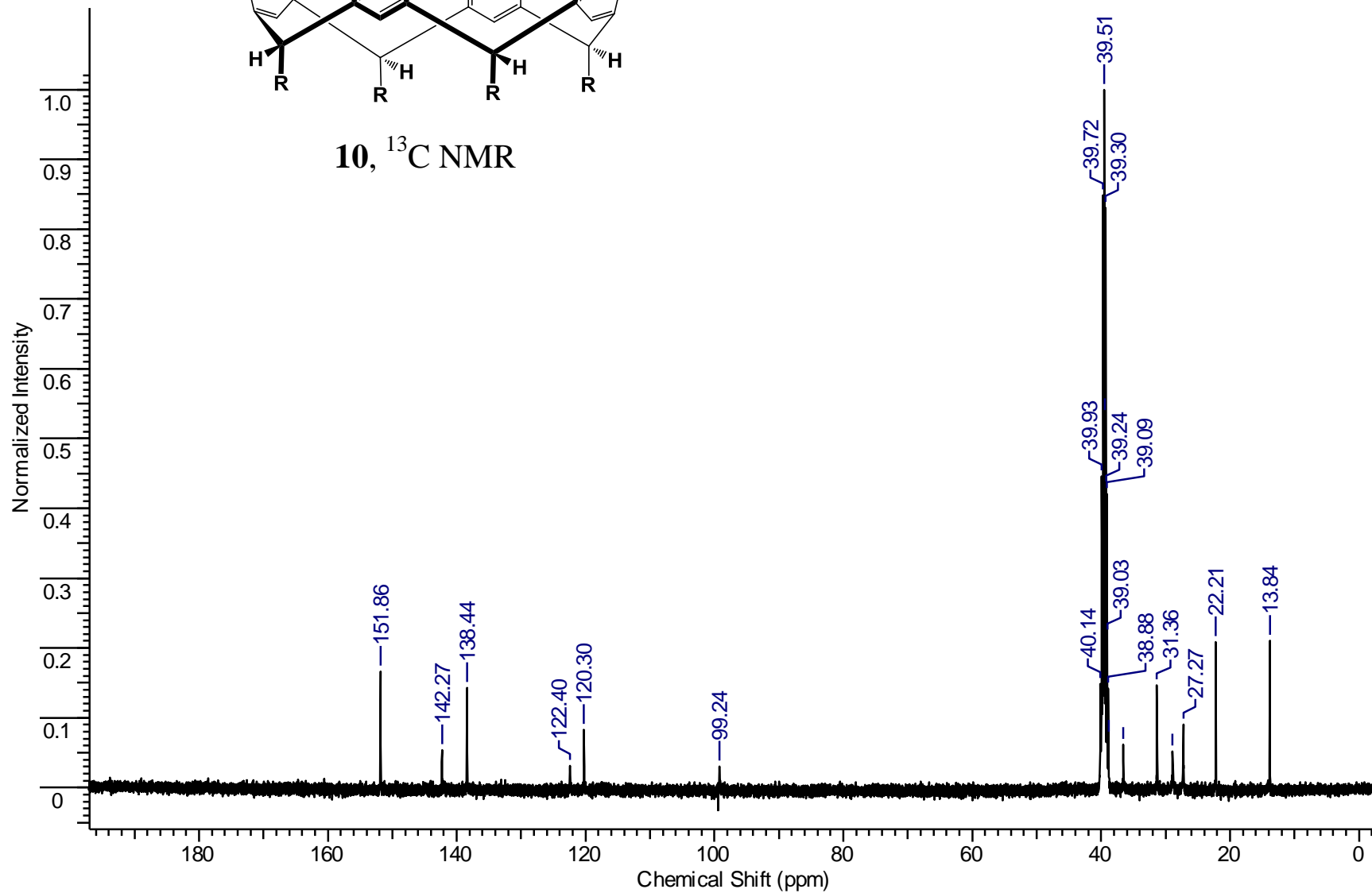


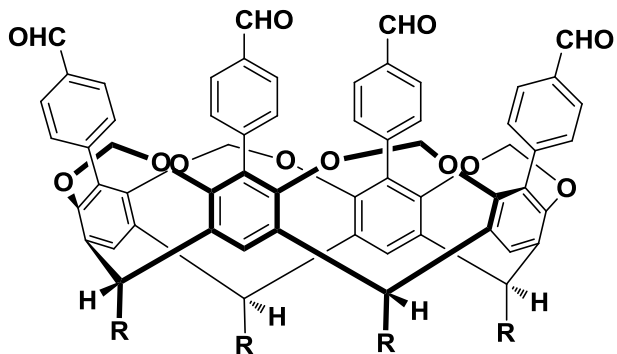
10, ^1H NMR



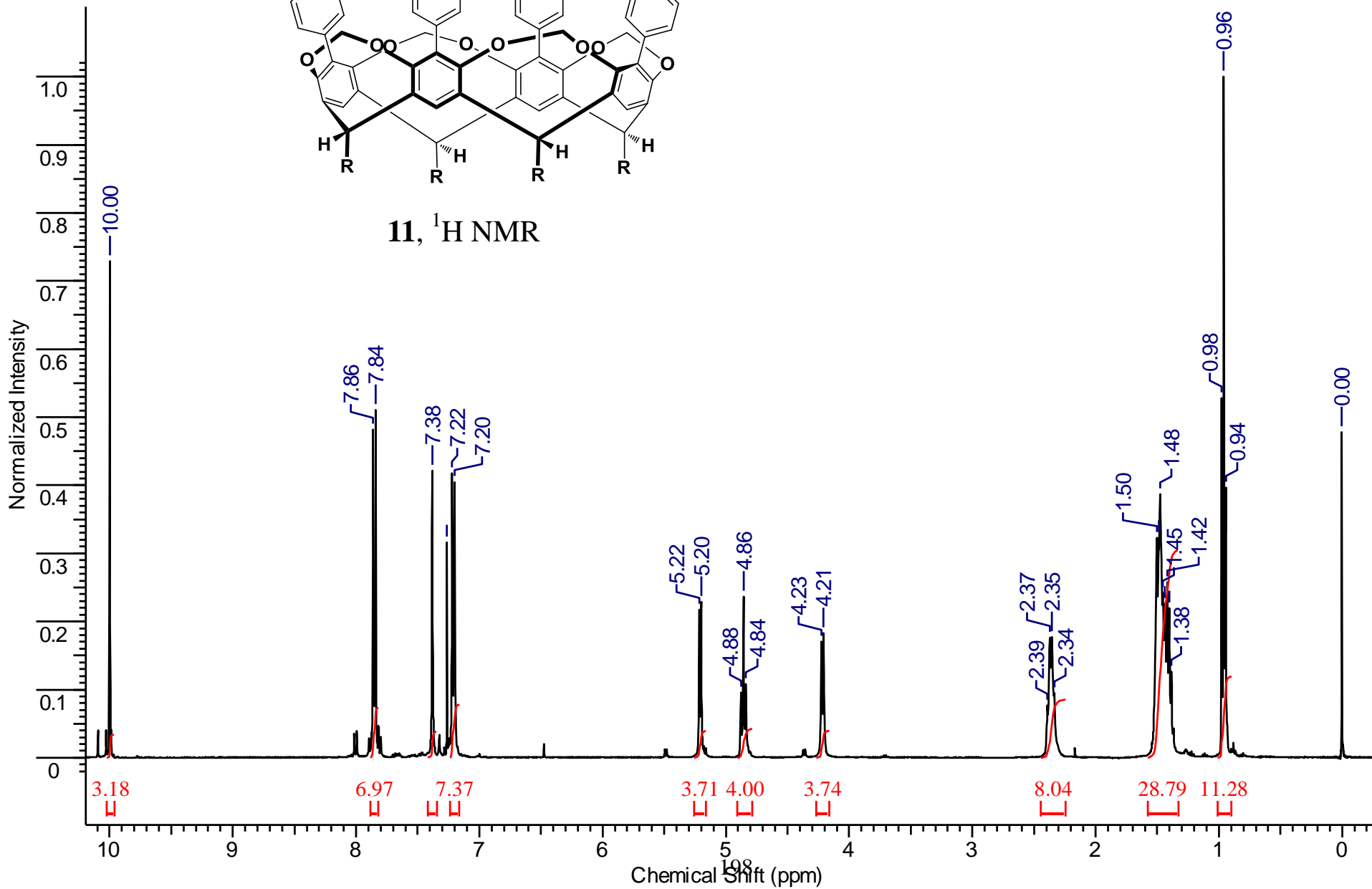


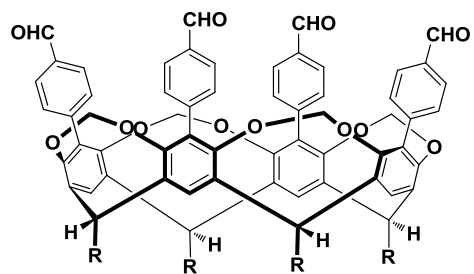
10, ^{13}C NMR



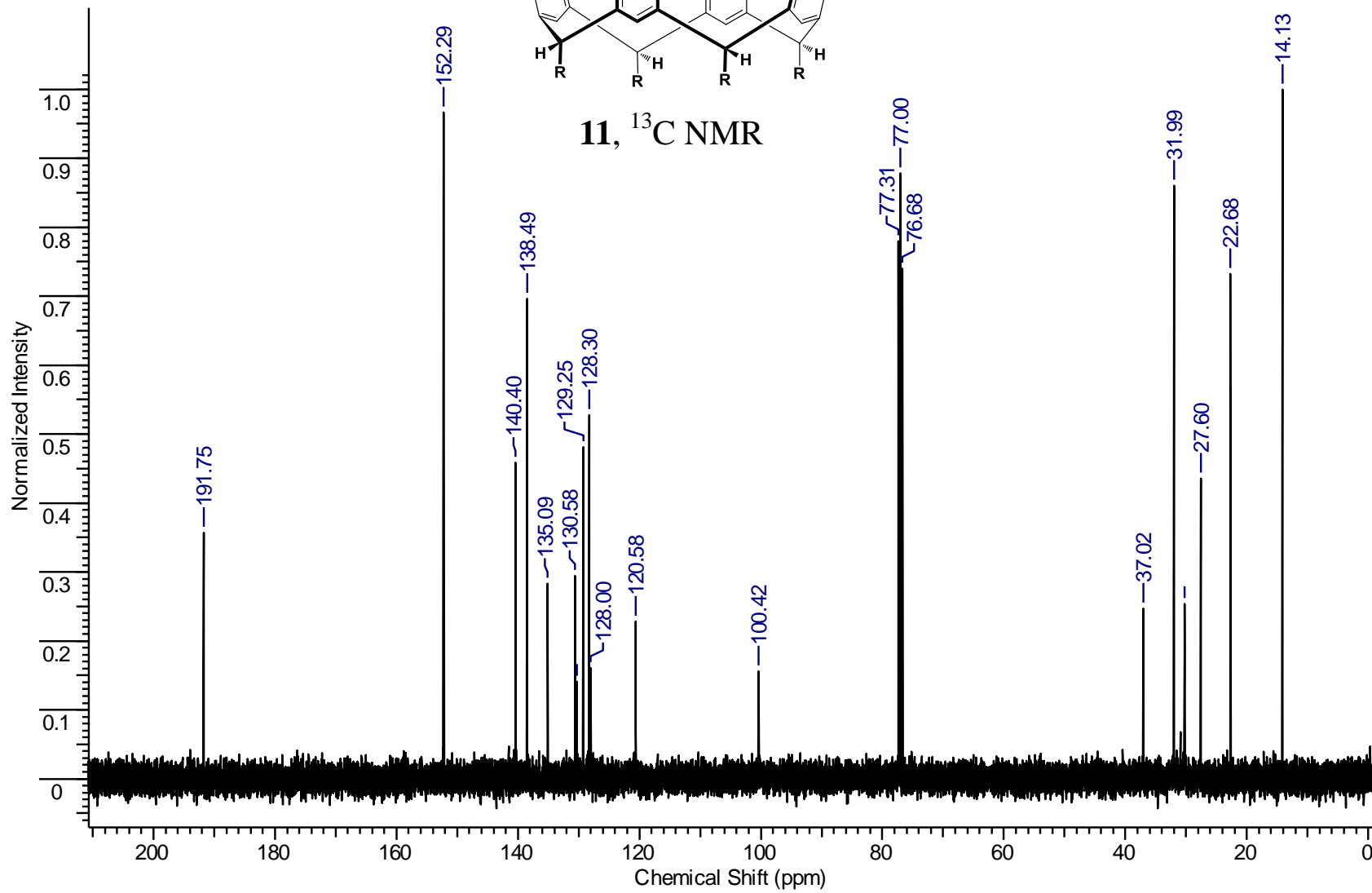


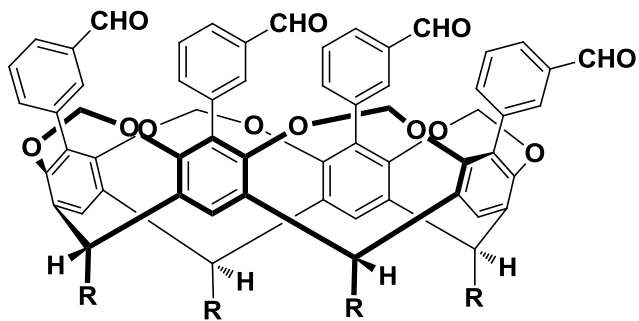
11, $^1\text{H NMR}$





11, ^{13}C NMR





13, ^1H NMR

